DEPARTMENT OF MECHANICAL ENGINEERING AND MECHANICS
COLLEGE OF ENGINEERING & TECHNOLOGY
OLD DOMINION UNIVERSITY
NORFOLK, VIRGINIA 23508

215P

TRANSIENT RADIATIVE ENERGY TRANSFER IN INCOMPRESSIBLE LAMINAR FLOWS

By

S. N. Tiwari, Principal Investigator

and

D. J. Singh, Graduate Research Assistant

Progress Report
For the period ended June 30, 1987

Prepared for the
National Aeronautics and Space Administration
Langley Research Center
Hampton, Virginia 23665

Under
Research Grant NAG-1-423
Drs. A. Kumar and J. P. Drummond, Technical Monitors
HSAD- Computational Methods Branch

June 1987

DEPARTMENT OF MECHANICAL ENGINEERING AND MECHANICS
COLLEGE OF ENGINEERING & TECHNOLOGY
OLD DOMINION UNIVERSITY
NORFOLK, VIRGINIA 23508

TRANSIENT RADIATIVE ENERGY TRANSFER IN INCOMPRESSIBLE LAMINAR FLOWS

By

S. N. Tiwari, Principal Investigator

and

D. J. Singh, Graduate Research Assistant

Progress Report
For the period ended June 30, 1987

Prepared for the
National Aeronautics and Space Administration
Langley Research Center
Hampton, Virginia 23665

Under
Research Grant NAG-1-423
Drs. A. Kumar and J. P. Drummond, Technical Monitors
HSAD- Computational Methods Branch

Submitted by the
Old Dominion University Research Foundation
P.O. Box 6369
Norfolk, Virginia 23508

June 1987

FOREWORD

This is a progress report on the research project entitled "Analysis and Computation of Internal Flow Field in a Scramjet Engine," for the period ended June 30, 1987. Specific attention has been directed to investigate "Transient Radiative Energy Transfer in Incompressible Laminar Flows." This work was supported by the NASA Langley Research Center (Computational Methods Branch of the High-Speed Aerodynamics Division) under research grant NAG-1-423. The grant was monitored by Drs. A. Kumar and J. P. Drummond of the High-Speed Aerodynamics Division.

TRANSIENT RADIATIVE ENERGY TRANSFER IN INCOMPRESSIBLE LAMINAR FLOWS

S. N. Tiwari[1] and D. J. Singh[2]
Old Dominion University, Norfolk, Virginia 23529-0247

ABSTRACT

Analysis and numerical procedures are presented to investigate the transient radiative interactions of nongray absorbing-emitting species in laminar fully-developed flows between two parallel plates. The particular species considered are OH, CO, CO_2, and H_2O and different mixtures of these species. Transient and steady-state results are obtained for the temperature distribution and bulk temperature for different plate spacings, wall temperatures, and pressures. Results, in general, indicate that the rate of radiative heating can be quite high during earlier times. This information is useful in designing thermal protection systems for transient operations.

---

[1]Eminent Professor, Dept. of Mechanical Engineering and Mechanics.

[2]Graduate Research Assistant, Dept. of Mechanical Engineering and Mechanics.

TABLE OF CONTENTS

LIST OF FIGURES

List of Figures (continued)

NOMENCLATURE

A	band absorptance = $A(u,\beta)$, cm^{-1}
A_o	band width parameter, cm^{-1}
C_o	correlation parameter, atm^{-1} - cm^{-1}
C_p	specific heat at constant pressure, kJ/kg-k = erg/gm-k
e_ω	Planck's function, $(W\text{-}cm^{-2})/cm^{-1}$
e_{ω_o}	Planck's function evaluated at wave number ω_o
e_1, e_2	emissive power of surfaces with temperatures T_1 and T_2, $W\text{-}cm^{-2}$
H_{1i}, H_1	gas property for the large path length limit
k	thermal conductivity, erg/cm-sec-K
K_1	gas property for the optically thin limit distance between plates
M	large path length parameter, nondimensional
N	optically thin parameter, nondimensional
P	pressure, atm
q_R	total radiative heat flux, W/cm^2
$q_{R\omega}$	spectral radiation heat flux, $(W\text{-}cm^{-2})/cm^{-1}$
q_ω	wall heat flux, W/cm^2
S	integrated intensity of a wide band, $atm^{-1}\text{-}cm^{-2}$
t	time, sec
T	temperature, K
T_1	wall temperature, K; $T_1 = T_w$
T_b	bulk temperature, K
u	nondimensional coordinate = SPy/A_o
u_o	nondimensional path length = SPL/A_o
y	transverse coordinate, cm
β	line structures parameter
θ	nondimensional temperature

θ_b	dimensionless bulk temperature
κ_ω	spectral absorptin coefficient, cm^{-1}
ξ	nondimensional coordinate = $y/L = u/u_o$
ρ	density, kg/m^3
τ	nondimensional time
ω	wave number, cm^{-1}
ω_o	wave number at the band center, cm^{-1}

INTRODUCTION

The radiative energy transfer in participating medium has received special attention in recent years because of its applications in the areas of the remote sensing, earth's radiation budget studies and climate modeling, fire and combustion research, entry and reentry phenomena, hypersonic propulsion and defense-oriented research. In most studies involving combined mass, momentum, and energy transfer, however, the radiative transfer formulation has been coupled mainly with the steady processes [1-20] and the interaction of radiation in transient processes has received very little attention. However, the transient approach appears to be the logical way of formulating a problem in general sense for elegant numerical and computational solutions. The steady-state solutions can be obtained as limiting solutions for large times.

The limited number of studies available on the transient radiative transfer in gaseous systems [21-31] are reviewed critically in [32-34]. The literature survey reveals that the transient behavior of a physical system can be influenced significantly in the presence of radiation.

The goal of this research is to include the nongray radiative formulation in the general governing equations and provide the step-by-step analysis and solution procedure for several realistic problems. The basic formulations are presented in [32] and the specific case of transient radiative exchange in nongray gases between two parallel plates is investigated in [33, 34]. The objective of this study is to investigate the interaction of transient radiation in fully-developed laminar flows between two parallel plates. Thus, special attention is directed to include the nonsteady phenomenon only in the energy equation. Homogeneous as well as nonhomogeneous mixtures of absorbing-

emitting species are considered. In subsequent studies, the present analysis and numerical techniques will be used to investigate the unsteady flow of compressible and chemically reacting species in one- and multi-dimensional systems.

BASIC FORMULATION

The physical system considered is the energy transfer in laminar, incompressible, constant properties, fully-developed flow of absorbing-emitting gases between parallel plates (Fig. 1). The condition of uniform surface heat flux for each plate is assumed such that the temperature of the plates varies in the axial direction. Extensive treatment of this problem is available in the literature under steady state conditions [8, 11]. The primary motivation of this study is to investigate the extent of transient radiative interaction for high temperature flow conditions.

For the physical problem considered, the energy equation can be expressed as [1]

$$\rho C_p \left(\frac{\partial T}{\partial t} + u \frac{\partial T}{\partial x} + v \frac{\partial T}{\partial y}\right) = k \frac{\partial^2 T}{\partial y^2} + \beta T u \frac{dp}{dx} + \mu\left(\frac{\partial u}{\partial y}\right)^2 - \mathrm{div} q_R \qquad (1)$$

where u and v denote x and y components of velocity, respectively. In deriving Eq. (1) it has been assumed that the net conduction heat transfer in the x direction is negligible compared with the net conduction in the y direction. This represents the physical condition of a large value of the Peclet number. By an analogous reasoning, the radiative heat transfer in the x direction can be neglected in comparison to that transferred in the y direction. If, in addition, it is assumed that the Eckert number of the flow is small, then Eq. (1) reduces to

$$\frac{\partial T}{\partial t} + u \frac{\partial T}{\partial x} + v \frac{\partial T}{\partial y} = \alpha \frac{\partial^2 T}{\partial y^2} - \frac{1}{\rho C_p} \frac{\partial q_R}{\partial y} \qquad (2)$$

where $\alpha = (k/\rho C_p)$ represents the thermal diffusivity of the fluid.

For a steady fully-developed flow, $v = 0$, and u is given by the well-known parabolic profile as

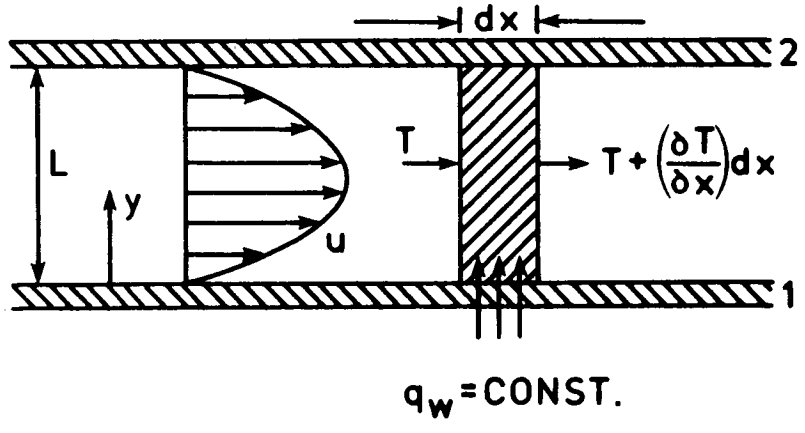

Figure 1. Physical model and coordinate systems for flow of radiating gases between parallel plates.

$$u = 6\, u_m\, (\xi - \xi^2);\ \xi = y/L \tag{3}$$

where u_m represents the mean fluid velocity. Also, for the flow of a perfect gas with uniform heat flux, $\partial T/\partial x$ is constant and is given by

$$\partial T/\partial x = (2\alpha q_w)/(u_m L/k) \tag{4}$$

Now, by combining Eqs. (2) - (4), the energy equation is expressed in nondimensional form as

$$\frac{\partial \theta}{\partial \tau} + 12\, (\xi - \xi^2) = \frac{\partial^2 \theta}{\partial \xi^2} - \frac{1}{q_w} \frac{\partial q_R}{\partial \xi} \tag{5}$$

where

$$\tau = \alpha t/L^2\ ;\ \theta = (T - T_1)/(q_w L/k)$$

By assuming that the initial temperature distribution in the gas is some uniform value $T_o = T_1$, the initial and boundary conditions for this problem can be expressed as

$$\theta(\xi, 0) = 0 \tag{6a}$$

$$\theta(0, \tau) = \theta\,(1, \tau) = 0 \tag{6b}$$

$$\theta_\xi(\xi = 1/2) = 0\ ;\ \theta_\xi(\xi = 0) = -\,\theta_\xi(\xi = 1) \tag{6c}$$

It should be noted that all the boundary conditions given in Eqs. (6) are not independent and any two convenient conditions can be used to obtain solutions. Also, the initial temperature distribution can be any specified or calculated value of $\theta(\xi, 0) = f(\xi)$.

As discussed in Refs. 32-34, the radiative transfer equations are formulated for one-dimensional planar systems for many engineering and astrophysical applications. For diffuse nonreflecting boundaries and in the

absence of scattering, the expression for the total radiative flux is given, for an n-band gaseous system, by [1, 8, 32]

$$q_R(y) = e_1 - e_2$$

$$+ \frac{3}{2} \sum_{i=1}^{n} \int_{\Delta\omega_i} \{ \int_o^y F_{1\omega_i}(z)\, \kappa_{\omega_i} \exp[-\frac{3}{2} \kappa_{\omega_i}(y-z)]dz$$

$$- \int_y^L F_{2\omega_i}(z)\, \kappa_{\omega_i} \exp\,[-\frac{3}{2} \kappa_{\omega_i}(z-y)]dz\}d\omega_i \qquad (7)$$

where

$$F_{1\omega_i}(z) = e_{\omega_i}(z) - e_{1\omega_i};\ F_{2\omega_i}(z) = e_{\omega_i}(z) - e_{2\omega_i}$$

Equation (7) is in proper form for obtaining the nongray solutions of molecular species. In fact, this is an ideal equation for the line-by-line and narrow-band model formulations. However, in order to be able to use the wide band models and correlations, Eq. (7) is transformed in terms of the correlation quantities as [1, 7-13, 32]

$$q_R\,(\xi) = e_1 - e_2$$

$$+ \frac{3}{2} \sum_{i=1}^{n} A_{oi}\, u_{oi} \{ \int_o^{\xi} F_{1\omega_i}(\xi')\, \bar{A}'_i\, [\frac{3}{2} u_{oi}\, (\xi-\xi')]d\xi'$$

$$- \int_{\xi}^{1} F_{2\omega_i}(\xi')\, \bar{A}'_i\, [\frac{3}{2} u_{oi}\, (\xi'-\xi)]d\xi'\} \qquad (8)$$

where

$$\xi = u/u_o = y/L;\ \xi' = u'/u_o = z/L;\ \bar{A} = A/A_o;$$

$$u = (S/A_o)\, py;\ u_o = (S/A_o)\, PL;\ PS = \int_{\Delta\omega} \kappa_\omega\, d\omega$$

It should be noted that $F_{1\omega_i}$ and $F_{2\omega_i}$ in Eq. (8) represent the values at the center of the ith band and $\bar{A}'(u)$ denotes the derivative of $\bar{A}(u)$ with respect to u. Upon performing the integration by parts, Eq. (8) can be expressed in an alternate form as [32]

$$q_R(\xi) = e_1 - e_2 + \sum_{i=1}^{n} A_{oi} \{\int_o^{\xi} [de_{\omega_i}(\xi')/d\xi'] \bar{A}_i [\tfrac{3}{2} u_{oi}(\xi-\xi')]d\xi' + \int_{\xi}^{1} [de_{\omega_1}(\xi')/d\xi'] \bar{A}_i [\tfrac{3}{2} u_{oi}(\xi'-\xi)]d\xi'\} \quad (9)$$

A direct differentiation of Eq. (9) provides the expression for the divergence of radiatve flux as

$$\frac{dq_R(\xi)}{d\xi} = \frac{3}{2} \sum_{i=1}^{n} A_{oi} u_{oi} \{\int_o^{\xi} [de_{\omega_i}(\xi')/d\xi'] x \bar{A}_i' [\tfrac{3}{2} u_{oi}(\xi-\xi')]d\xi' - \int_{\xi}^{1} [de_{\omega_i}(\xi')/d\xi'] x \bar{A}_i' [\tfrac{3}{2} u_{oi}(\xi'-\xi)]d\xi'\} \quad (10)$$

Equations (8) through (10) are the most convenient equations to use when employing the band-model correlations in radiative transfer analyses.

For the present physical problem, $e_1 = e_2$ and $F_{1\omega_i} = F_{2\omega_i}$. Thus, for the case of linearized radiation, a combination of Eqs. (5) and (8) results in [8, 32]

$$\theta_{\xi\xi} - \theta_{\tau} - 3N\theta - 12(\xi-\xi^2) = \frac{9}{4}(L/k) \sum_{i=1}^{n} H_{1i} u_{oi}^2 \{\int_o^{\xi} \theta(\xi', \tau) x \bar{A}_i'' [\tfrac{3}{2} u_{oi}(\xi-\xi')]d\xi' + \int_{\xi}^{1} \theta(\xi', \tau) x \bar{A}_i'' [\tfrac{3}{2} u_{oi}(\xi'-\xi)]d\xi'\} \quad (11a)$$

where

$$N = (PL^2/k)\, K_l = (PL^2/k) \sum_{i=1}^{n} S_i(T)\, (de_{\omega_i}/dT)_{T_l}$$

$$H_{li} = A_{oi}(T)\, (de_{\omega i}/dT)T_l \;,\; H_l = \sum_{i=1}^{n} H_{li}$$

The dimensionless gas property N characterizes the relative importance of radiation versus conduction within the gas under optically thin conditions. Also, by combining Eqs. (5) and (10) another form of the transient energy equation is obtained as

$$\theta_{\xi\xi} - \theta_\tau - 12\,(\xi-\xi^2) = \frac{3}{2}\,(L/k) \sum_{i=1}^{n} H_{li}\, u_{oi} \{\int_o^\xi (\partial\theta/\partial\xi')\, x$$

$$\bar{A}_i' \,[\tfrac{3}{2}\, u_{oi}(\xi-\xi')]d\xi' - \int_\xi^1 (\partial\theta/\partial\xi')\, x$$

$$\bar{A}_i' \,[\tfrac{3}{2}\, u_{oi}\,(\xi'-\xi)]d\xi'\} \qquad (11b)$$

Note again that Eq. (11b) can be obtained directly by integrating the right-hand side of Eq (11a) by parts. Quite often, Eq. (11b) is the convenient form to use in radiative transfer analyses.

For flow problems, the quantity of primary interest is the bulk temperature of the gas, which may be expressed as [11]

$$\theta_b = (T_b-T_l)/(q_w L/k) = 6 \int_0^1 \theta(\xi,\tau)(\xi-\xi^2)d\xi \qquad (12)$$

The heat transfer q_w is given by the expression, $q_w = h_c\,(T_l-T_b)$, where h_c is the convective heat transfer coefficient (W/cm^2-K). In general, the heat transfer results are expressed in terms of the Nusselt number $Nu = h_c\, D_h/k$. Here, D_h represents the hydraulic diameter, and for the parallel plate geometry it equals twice the plate separation, i.e., $D_h = 2L$. Upon

eliminating the convective heat transfer coefficient h_c from the expressions for q_w and Nu, a relation between the Nusselt number and the bulk temperature is obtained as

$$Nu = 2\,Lq_w/k(T_1-T_b) = -2/\theta_b \tag{13}$$

The heat transfer results, therefore, can be expressed either in terms of Nu or θ_b.

LIMITING CASES AND SOLUTIONS

Before discussing the method of solution for the general case, it is advisable to explore the various limiting cases. Quite often, closed form solutions can be obtained for some of these cases. Specifically four limiting cases are considered here and these are the steady laminar flows, the case of negligible radiation, the optically thin limit, and the large path length limit.

Steady Laminar Flow

For steady-state conditions $\partial\theta/\partial\tau = 0$ and Eqs. (11) provide two forms of the energy equation for this case. Another convenient form is obtained by letting $\partial\theta/\partial\tau = 0$ in Eq. (5) such that

$$\theta'' - 12\,(\xi-\xi^2) = (1/q_w)\,dq_R/d\xi \tag{14}$$

By integrating Eq. (14) once and using the conditions that at $\xi = 1/2$, $q_R(\xi)$ and $(d\theta/d\xi)$ are equal to zero, one obtains

$$\theta' - 2(3\xi^2 - 2\xi^3) + 1 = q_R(\xi)/q_w \tag{15}$$

A combination of Eqs. (8) and (15) results in

$$\theta' - 2(3\xi^2 - 2\xi^3) + 1 = \frac{3}{2}\,(L/k) \sum_{i=1}^{n} H_{1i}\,u_{oi}\,\{\int_0^{\xi} \theta(\xi')\ x$$

$$\bar{A}_i' \left[\frac{3}{2} u_{oi}(\xi-\xi')\right]d\xi' - \int_{\xi}^{1} \theta(\xi') \times$$

$$\bar{A}_i' \left[\frac{3}{2} u_{oi}(\xi'-\xi)\right]d\xi'\} \qquad (16)$$

It should be pointed out that by combining Eqs. (9) and (15) another useful form of the energy equation can be obtained for the steady case.

For the case of negligible radiation, Eq. (16) reduces to a very simple form and utilizing the boundary condition $\theta(0) = 0$, the solution of the resulting equation is found to be

$$\theta(\xi) = \xi(2\,\xi^2 - \xi^3 - 1) \qquad (17a)$$

The result for the bulk temperature is found by combining Eqs. (12) and (17a) as

$$-\theta_b = 17/70 \qquad (17b)$$

The results provided by Eqs. (17) are useful in determining the extent of radiatve contributions.

Negligible Radiation

For the case of negligible radiation, N = 0 and both forms of Eq. (11) reduce to

$$\theta_{\xi\xi} - \theta_{\tau} = 12\,(\xi-\xi^2) \qquad (18)$$

By employing the product solution procedure, the solution of Eq. (18) can be obtained and the result can be expressed in terms of the bulk temperature through use of Eq. (12). Alternately, the solution of Eq. (18) is assumed to be of the form

$$\theta(\xi,\tau) = g(\xi) + h(\xi,\tau) \qquad (19)$$

From Eqs. (18) and (19), there is obtained two separate equations as

$$g'' = 12(\xi - \xi^2) \tag{20}$$

$$h_{\xi\xi} - h_{\tau} = 0 \tag{21}$$

Solutions of Eqs. (20) and (21) are found separately from which the complete solution for the temperature distribution is obtained as [32]

$$\theta(\xi,\tau) = \xi(2\,\xi^2 - \xi^3 - 1) + \sum_{n=1}^{\infty} C_n \sin(a\,\xi) \exp(-a\ \tau);\ a^2 = n\pi \tag{22a}$$

where

$$C_n = (4/a^5)[(12 - 12a^2 + a^4)\cos(a) - 24],\ n = 1, 2, \ldots$$

Finally, the expression for the bulk temperature is found by using Eq. (12) as

$$\theta_b = -17/70 + 6 \sum_{n=1}^{\infty} C_n [(1/a) + (4/a^3)] \exp(-a^2\tau) \tag{22b}$$

Equations (22) are useful in determining the extent of radiative contributions for the transient case.

Optically Thin Limit

In the optically thin limit, the expression for the bulk temperature for the steady case is found to be [11, 32]

$$\theta_b = [1/(3N)^3]\ \{576(3N)^{-1/2}(NEXP) - 21.6N^2 + 72N - 288\} \tag{23}$$

where

$$NEXP = \{1-\exp[-(3N^{1/2}]\}/\{1 + \exp[-(3N)^{1/2}]\}$$

Both forms of the transient energy equation, Eqs. (11a) and (11b), reduce to a simplified form in the optically thin limit as [32]

$$\theta_{\xi\xi} - \theta_{\tau} - 3N\theta = 12(\xi-\xi^2) \tag{24}$$

Assuming a solution of the form given by Eq. (19), Eq. (24) is written as

$$h_{\xi\xi} - h_{\tau} - 3Nh = - g_{\xi\xi} + 3Ng + 12(\xi - \xi^2) \tag{25}$$

Consequently,

$$g'' - 3Ng = 12(\xi - \xi^2) \tag{26}$$

and

$$h_{\xi\xi} - h_{\tau} - 3Nh = 0 \tag{27}$$

From the solution of Eqs. (26) and (27), the solution for Eq. (24) is obtained as

$$\theta(\xi,\tau) = (16/3N^2)\,[\sinh(-\sqrt{3N}/2)/\sinh(\sqrt{3N})]$$

$$\cosh[\sqrt{3N}\,(\xi-1/2)] + (4/N)(\xi^2 - \xi + 2/3N)$$

$$+ \sum_{n=1}^{\infty} C_n \sin(a\xi) \exp[-(3N + a^2)\,\tau];\ a = n\pi \tag{28a}$$

where

$$C_n = 0 \qquad \text{, for n even} \tag{28b}$$

$$= 32\,(3N + a^2)/(3N^2\,a^3)$$

$$+ 2a/[3N^2(3N + a^2)] \qquad \text{, for n odd} \tag{28c}$$

By combining Eqs. (12) and (28), the expression for the bulk temperature is obtained as

$$\theta_b = 6\,\{(16/3N^2)[\sinh(-\sqrt{3N}/2)/\sinh(\sqrt{3N})]\ x$$

$$[(1/3N)\cosh(\sqrt{3N}/2) - (4 + \sqrt{3N})\,(3N)^{-3/2}\ x$$

$$\sinh(\sqrt{3N}/2)] + (4/N)\,[-1/30 + 1/(9N)]$$

$$+ \sum_{n=1}^{\infty} C_n(1/a + 4/a^3)\exp[-(3N + a^2)\tau]\} \tag{29}$$

Large Path Length Limit

In this limit, the steady-state energy equation, Eq. (16), reduces to [8, 11, 32]

$$\theta' - 2(3\xi^2 - 2\xi^3) + 1 = M\int_0^1 \theta(\xi')\,d\xi'/(\xi - \xi') \tag{30}$$

where

$$M = H_1\,L/k = (L/k)\sum_{i=1}^{n} A_{oi}\,(de_{\omega i}/dT)_{T_1}$$

The nondimensional parameter M constitutes the radiation-conduction interaction parameter for the large path length limit. Equation (30) does not appear to possess a closed form solution; a numerical solution, however, can be obtained easily.

In the large path length limit, the transient energy equations, Eqs. (11a) and (11b), reduce to

$$\theta_{\xi\xi} - \theta_\tau - 3N\theta - 12(\xi - \xi^2) = -M\left[\int_0^{\xi} \theta(\xi',\tau)\,d\xi'/(\xi - \xi')^2 + \int_{\xi}^{1} \theta(\xi',\tau)d\xi'/(\xi'-\xi)^2\right] \tag{31a}$$

$$\theta_{\xi\xi} - \theta_\tau - 12\,(\xi - \xi^2) = M\int_0^1 (\partial\theta/\partial\xi')d\xi'/(\xi-\xi') \tag{31b}$$

Since $|(\xi-\xi')^2| = |(\xi'-\xi)^2|$, Eq. (31a) can be written as

$$\theta_{\xi\xi} - \theta_\tau - 3N\theta - 12(\xi - \xi^2) = -M\int_0^1 \theta(\xi',\tau)\,d\xi'/(\xi - \xi')^2 \tag{31c}$$

Through integration by parts, Eq. (31c) can be expressed as

$$\theta_{\xi\xi} - \theta_{\tau} - 3N\theta - 12(\xi - \xi^2) = M \int_0^1 (\partial\theta/\partial\xi')d\xi'/(\xi-\xi') \qquad (31d)$$

Equations (31a) - (31d) represent different forms of the governing equations in the large path length limit. With the exception of the term $(-3N\theta)$ on the left-hand side, Eq. (31d) is identical to Eq. (31b). Since N represents the radiation-conduction interaction parameter only in the optically thin limit [8], it should not appear in the governing equation for the large path length limit. Thus, Eq. (31b) is the correct equation to use for solution in the large path length limit; the solution of this equation is obtained by numerical techniques.

METHOD OF SOLUTION

The solution procedures for both steady and unsteady cases are presented in this section. In principle, the same numerical procedure applies to both the general and large path length limit cases.

Steady-State Solutions

The general solution of Eq. (16) is obtained numerically by employing the method of variation of parameters. For this, a polynomial form for $\theta(\xi)$ is assumed in powers of ξ as

$$\theta(\xi) = \sum_{m=0}^{n} a_m \xi^m \qquad (32)$$

By considering a five term series solution (a quartic solution in ξ) and satisfying the boundary conditions $\theta(0) = \theta'(1/2) = 0$ and $\theta'(0) = -\theta'(1)$, one obtains

$$\theta(\xi) = a_1(\xi - 2\xi^3 + \xi^4) + a_2(\xi^2 - 2\xi^3 + \xi^4) \qquad (33)$$

$$\theta'(\xi) = a_1(1 - 6\xi^2 + 4\xi^3) + a_2(2\xi - 6\xi^2 + 4\xi^3) \tag{34}$$

A substitution of Eq. (34) in Eq. (16) results in

$$a_1(1 - 6\xi^2 + 4\xi^3) + a_2(2\xi - 6\xi^2 + 4\xi^3)$$

$$- 2(3\xi^2 - 2\xi^3) + 1 = \frac{3}{2}(L/k) \sum_{n=1}^{n} H_{1i}\, u_{oi}\, x$$

$$\{\int_0^{\xi} \theta(\xi')\, \bar{A}_i' \left[\frac{3}{2} u_{oi}(\xi - \xi')\right] d\xi'$$

$$- \int_{\xi}^{1} \theta(\xi')\, \bar{A}_i' \left[\frac{3}{2} u_{oi}(\xi' - \xi)\right] d\xi'\} \tag{35}$$

where expressions for $\theta(\xi')$ are obtained from Eq. (33).

The two unknown constants a_1 and a_2 in Eq. (35) are evaluated by satisfying the integral equation at two convenient locations (ξ=0 and ξ=1/4 in the present case). The entire procedure for obtaining a_1 and a_2 is described in [32]. With known values of a_1 and a_2, Eq. (33) provides the general solution for $\theta(\xi)$. The expression for the bulk temperature is obtained by combining Eqs. (12) and (33) as

$$\theta_b = (1/70)\,(17a_1 + 3a_2) \tag{36}$$

It should be noted that for the case of no radiative interaction $a_2 = 0$ and $a_1 = -1$, and Eq. (36) gives the result of Eq. (17).

The governing equation for the large path length limit is Eq. (30). For this equation also the solution is given by Eqs. (33) and (36) but the values of a's are completely different in this case [32].

Transient Solutions

The governing energy equations for the transient case are Eqs. (11a) and (11b). General solutions of these equations are obtained also numerically by employing the method of variation of parameters. For the present problem, a polynomial form for $\theta(\xi,t)$ is assumed as

$$\theta(\xi,\tau) = \sum_{m=0}^{n} a_m(\tau)\ \xi^m \tag{37}$$

For a quadratic temperature distribution in ξ (with time dependent coefficients), Eq. (37) is written as

$$\theta(\xi,\tau) = a_0(\tau) + a_1(\tau)\ \xi + a_2(\tau)\ \xi^2 \tag{38a}$$

By using the boundary conditions $\theta(0,\tau) = 0$ and $\theta_\xi(\xi=1/2) = 0$, this reduces to

$$\theta(\xi,\tau) = g(\tau)\ (\xi-\xi^2) \tag{38b}$$

where g(t) represents the time dependent coefficient. Consequently,

$$\theta_\xi(\xi,\tau) = g(\tau)\ (1-2\xi);\ \theta_{\xi\xi}(\xi,\tau) = -2g(\tau);\ \theta_\tau(\xi,\tau) = (\xi-\xi^2)\ g'(\tau) \tag{39}$$

Also, a combination of Eq. (6a) and (38b) yields the initial condition

$$\theta(\xi,0) = g(0) = 0 \tag{40}$$

Note that essential boundary conditions are used already in obtaining the solution represented by Eq. (38b).

By employing Eqs. (38b) and (39), Eqs. (11a) and (11b) are transformed in alternate forms which are expressed in a compact form as

$$g'(\tau) + \begin{bmatrix} J_1(\xi), \\ J_2(\xi) \end{bmatrix}\ g(\tau) + 12 = 0 \tag{41}$$

where $J_1(\xi)$ and $J_2(\xi)$ are defined in [32]. The function $J_1(\xi)$ is used for solution of Eq. (11a) and $J_2(\xi)$ is used for solution of Eq. (11b). The solution of Eq. (41) satisfying the initial conditions of Eq. (40) is given by

$$g(\tau) = \frac{12}{J(\xi)} \{\exp [-J(\xi)\tau]-1\} \tag{42}$$

The temperature distribution given by Eq. (38b) can be expressed now as

$$\theta(\xi,\tau) = \frac{12}{J(\xi)} \{\exp[-J(\xi)\tau]-1\}(\xi-\xi^2) \tag{43}$$

The expression for the bulk temperature is obtained through use of Eq. (12) as

$$\theta_b = 72 \int_0^1 [(\xi-\xi^2)^2/J(\xi)]\{\exp[-J(\xi)\tau]-1\} \tag{44}$$

Note that in Eqs. (42)-(44), $J(\xi)$ becomes $J_1(\xi)$ for solution of Eq. (11a) and $J_2(\xi)$ for solution of Eq. (11b).

For a quartic solution in ξ, Eq. (37) gives the result similar to Eq. (33) which for the transient case is expressed as

$$\theta(\xi,\tau) = g(\tau)\ (\xi - 2\xi^3 + \xi^4) + h(\tau)\ (\xi^2 - 2\xi^3 + \xi^4) \tag{45}$$

By substituting Eq. (45) into Eq. (11a), one obtains

$$x\ g'(\tau) + J_3(\xi)\ g(\tau) + yh'(\tau) + J_4(\xi)\ h(\tau) = -\ z \tag{46}$$

where

$$x = (\xi - 2\xi^3 + \xi^4);\ y = (\xi^2 - 2\xi^3 + \xi^4);$$

$$z = 12(\xi - \xi^2)$$

and functions $J_3(\xi)$ and $J_4(\xi)$ are defined in [32]. Equation (46) constitutes one equation in two unknowns, namely $g(\tau)$ and $h(\tau)$. However, since the equation is linear in τ, the principle of superposition can be used

to split the solution into two equations as

$$x\, g'(\tau) + J_3(\xi)\, g(\tau) = -z/2 \tag{47}$$

$$y h'(\tau) + J_4(\xi)\, h(\tau) = -z/2 \tag{48}$$

The initial condition for this case can be written as

$$\theta(\xi,0) = g(0)\,(\xi - 2\xi + \xi^3) + h(0)\,(\xi^2 - 2\xi^3 + \xi^4) = 0 \tag{49a}$$

Consequently,

$$g(0) = 0;\ h(0) = 0 \tag{49b}$$

The solution of Eqs. (47) and (48) satisfying the appropriate initial condition of Eq. (49b) is given respectively as

$$g(\tau) = [z(\xi)/2J_3(\xi)]\ \{\exp[-J_3(\xi)\tau/x(\xi)]-1\} \tag{50}$$

$$h(\tau) = [z(\xi)/2J_4(\xi)]\ \{\exp[-J_4(\xi)\tau/y(\xi)]-1\} \tag{51}$$

By substituting Eqs. (50) and (51) into Eq. (45), the expression for the temperature distribution is obtained as

$$\theta(\xi,\tau) = [6(\xi-\xi^2)(\xi-2\xi^3+\xi^4)/J_3(\xi)]\ x\ \{\exp[-J_3(\xi)\tau/x(\xi)]-1\} + [6(\xi-\xi^2)\ x\ (\xi^2-2\xi^3+\xi^4)/J_4(\xi)]\ \{\exp[-J_4(\xi)\tau/y(\xi)]-1\} \tag{52}$$

The bulk temperature in this case is given by

$$\theta_b = 36 \int_0^1 [(\xi-\xi^2)(\xi-2\xi^3+\xi^4)/J_3(\xi)]\ x$$

$$\{\exp[-J_3(\xi)\tau/x(\xi)]-1\}d\xi + 36\int_0^1 [(\xi-\xi^2)\ x$$

$$(\xi^2-2\xi^3+\xi^4)/J_4(\xi)]\{\exp[-J_4(\xi)\tau/y(\xi)]-1\}d\xi. \qquad (53)$$

where x and y are defined in Eq. (46).

By substituting Eq. (45) into Eq. (11b), there is obtained

$$xg' + J_5(\xi)\ g(\tau) + yh + J_6(\xi)\ h(\tau) = -z \qquad (54)$$

where again x,y,z are defined in Eq. (46) and functions $J_5(\xi)$ and $J_6(\xi)$ are defined in [32]. The solution procedure for this equation is identical to that for Eq. (46) and the results for temperature distribution and bulk temperature are given respectively by Eqs. (52) and (53) with J_3 replaced by J_5 and J_4 by J_6.

In the large path length limit, the two applicable governing equations are Eqs. (31b) and (31d). The solutions of these equations can be obtained from the general solutions by evaluating the integrals in J function in the large path length limit [32].

PHYSICAL CONDITIONS AND DATA SOURCE

As discussed in [32-34], four specific absorbing emitting species were selected for an extensive study; these are CO, CO_2, OH and H_2O. The species CO was selected because it contains only one fundamental vibration-rotation (VR) band and all spectral information are easily available in the literature. It is a very convenient gas to test the numerical procedure without requiring excessive computatinal resources. Species OH and H_2O are the primary radiation participating species for the pressure and temperature range anticipated in the combustor of the scramjet engine. Species CO_2, and combinations of CO_2 and H_2O are important absorbing-emitting species in many

other combustion processes. Different mixtures of various species (such as CO_2 + H_2O, OH + H_2O, and CO^2 + H_2O + OH) were selected for parametric studies. Thermophysical properties of these species are given in [33] for different temperatures.

In radiative transfer analyses, it is essential to employ a suitable model to represent the absorption-emission characteristics of specific species under investigation. Several line-by-line (LBL), narrow-band, and wide-band models are available to model the absorption of a VR band [7-12]. However, it is often desirable to use a simple correlation to represent the total absorption of a wide band. Several such correlations are available in the literature [7-12]. The relative merits of these correlations are discussed in [12]. In this study, the correlation proposed by Tien and Lowder [7] is employed and this is given by

$$\bar{A}(u) = \ln \{uf(\beta) [\frac{u + 2}{u + 2f(\beta)}] + 1\} \qquad (55)$$

where

$$f(\beta) = 2.94[1 - \exp(- 2.60\ \beta)]$$

and β represents the line structure parameter.

The spectral information and correlation quantities and thermodynamic and transport properties needed for different species were obtained from Refs. 7-9 and 33. Spectral information and correlation quantities for important infrared bands are provided in Appendix A. The specific VR bands considered for each species are: CO (4.7μ fundamental), OH (2.8μ fundamental), CO_2 (15μ, 4.3μ and 2.7μ), and H_2O (20μ, 6.3μ, 2.7μ, 1.87μ, and 1.38μ).

In a mixture of several species, spectral lines and bands overlap in certain spectral regions. The total absorptance in such regions cannot be

calculated simply by adding the contributions of different bands and corrections should be made to account for the partial overlapping. If line-by-line or narrow band models are employed in the general formulation of the physical problem, then there is no need for such corrections [12, 35, 36]. The solution of LBL formulation, however, requires considerably large computational resources. Use of narrow band models offers some computational relief but certain spectral information needed are not available for many species for temperatures higher than about 600 K. A relatively easier procedure (called the block method) is suggested by Edwards [13] and is useful in calculating the total emissivity of a mixture of several species. Another method suggested by Penner and Varanasi [37] is probably the most convenient method to use in the frame work of the radiative flux formulatin expressed in terms of the wide-band model absorptance and correlations.

For a homogeneous path, the total absorptance of a band is given by

$$A(y) = \int_0^\infty [1 - \exp(-\kappa_\omega y)] \, d\omega \tag{56}$$

where both κ_ω and ω have units of cm^{-1}. If in a spectral range $\Delta\omega_i$, there are contributions from bands of different species, then for a homogeneous path the transmittance is given by

$$\tau_{\Delta\omega_i} = \exp\left(-\sum_{j=1}^{N} \kappa_{\omega_{ij}} y\right) \tag{57}$$

where N represents the number of participating species in the gaseous mixture. Consequently, Eq. (56) can be expressed as

$$A_i = \int_{\Delta\omega_i} \left[1 - \exp\left(-\sum_{j=1}^{N} \kappa_{\omega_{ij}} y\right)\right] d\omega \tag{58}$$

If two bands of different (or same) species are occupying approximately the same spectral range $\Delta\omega_i$, then Eq. (58) reduces to

$$A_i = \int_{\Delta\omega_i} \{1 - \exp(\kappa_{\omega_{i1}} + \kappa_{\omega_{i2}})y]\} \, d\omega \tag{59}$$

By employing the relations for the exponentials, Eqs. (59) can be expressed as [37]

$$A_i = \int_{\Delta\omega_i} [1 - \exp(-\kappa_{\omega_{i1}} y)] \, d\omega + \int_{\Delta\omega_i} [1 - \exp(-\kappa_{\omega_{i2}})] \, d\omega - \Delta A \tag{60a}$$

or

$$A = A_1 + A_2 - \Delta A \tag{60b}$$

where

$$\Delta A = \int_{\Delta\omega_i} \{[1 - \exp(-\kappa_{\omega_{i1}} y)] \times$$

$$[1 - \exp(-\kappa_{\omega_{i2}} y)]\} \, d\omega \tag{60c}$$

Use of Eqs. (60) has been made by Felske and Tien [38] and Tien and Lee [39] to calculate absorptances of homogeneous and nonhomogeneous mixtures of CO_2 and H_2O in the 2.7 μ region for different pressure and temperature conditions. A similar procedure is used in this study to account for the overlapping effects of different species.

For the physical problem considered, the dependent variables are θ and θ_b (or Nu) and independent variables are τ and ξ. The parameters, in general, are T_w, P, and L. The large path length and optically thin limits are characterized respectively by parameters M and N. Radiative and thermophysical properties of participating species are evaluated at different specified pressures and temperatures.

RESULTS AND DISCUSSIONS

Extensive results have been obtained for variation of θ and θ_b for different conditions and most of these are available in Appendix B. The computer program used for numerical solutions is provided in Appendix C. Selected results are presented here to compare solutions of quadratic and quartic formulations and demonstrate the variation of θ with τ and ξ and of θ_b with L for single component systems and homogeneous mixtures. For all results presented here, a lower value of θ (or θ_b) in the figures indicates a higher value of temperature in the medium; this, in turn, implies a relatively higher ability of the gas to transfer radiative energy.

Results of quadratic and quartic formulations are compared in Figs. 2-5 for different species. The centerline temperature variations with nondimensional time are compared in Fig. 2 for P = 1 atm, T_w = 500 K, and L = 5 cm. The results show that the steady-state conditions are reached at an eariler time for H_2O; and this is followed respectively by CO_2, CO, and OH. Significant differences are noted between the quadratic and quartic solutions for larger times. For the conditions of results presented in the figure, the difference are found to be greatest for OH and lowest for H_2O. The results for θ versus ξ are compared for P = 1 atm, L = 10 cm, and T_w = 500 K in Fig. 3 and T_w = 1,000 K in Fig. 4. The results demonstrate that considerable differences in solutions can occur at different locations in the channel and that the differences are larger for the lower wall temperature. Results for θ_b versus L presented in Fig. 5 show that the differences in two solutions are relatively larger at lower plate spacings and that quartic results approach the correct limiting solution for the case of no radiative interaction (θ_b = -0.243). From the results presented in Figs. 2-5 and in Refs. 33 and 34 it is concluded that while quadratic and quartic solutions are

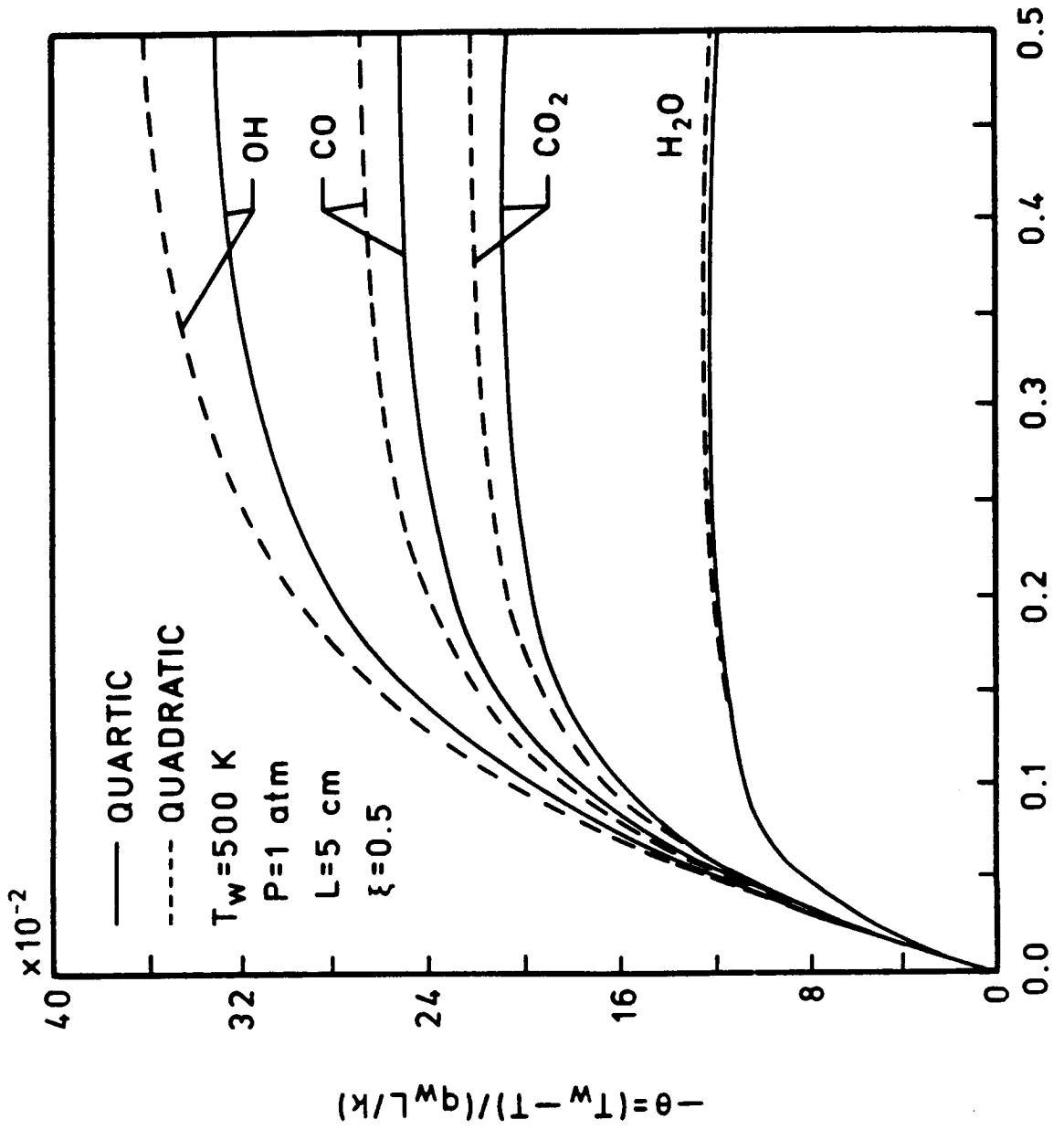

Figure 2. Comparison of quadratic and quartic results for the centerline temperature variations with time; T_w = 500 K, P = 1 atm, and L = 5 cm.

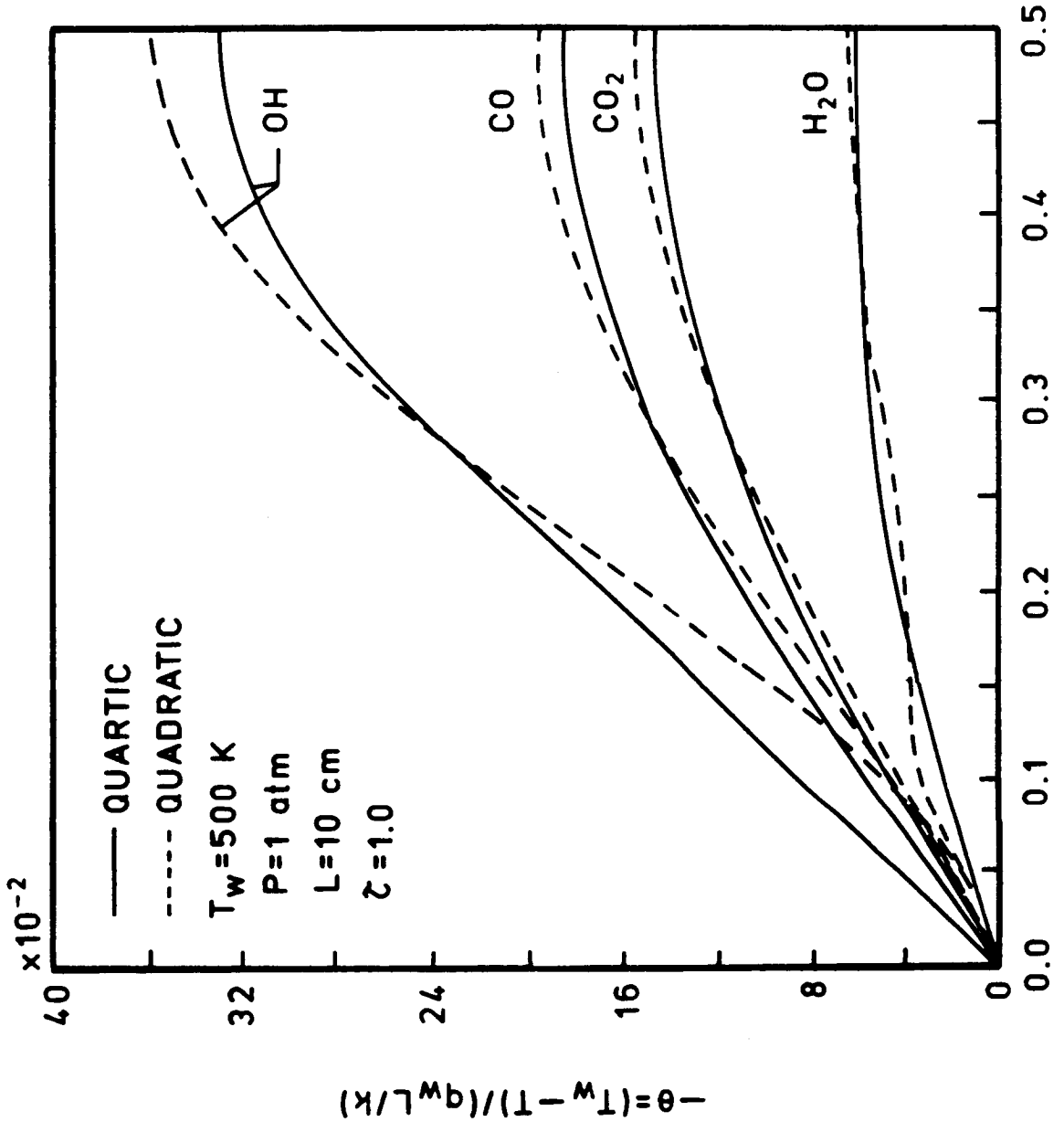

Figure 3. Comparison of quadratic and quartic results for temperature variations across the duct; P = 1 atm, L = 10 cm, and T_w = 500 K.

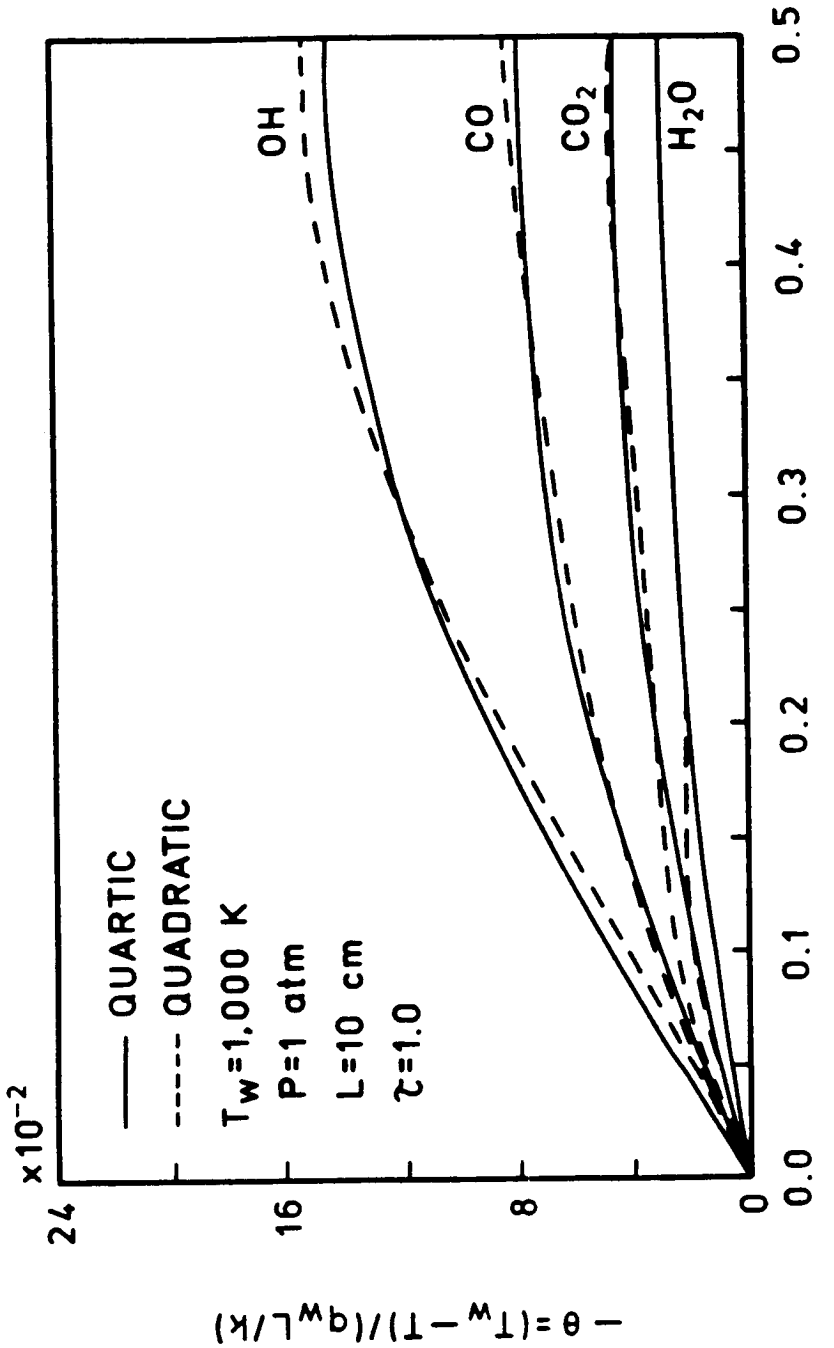

Figure 4. Comparison of quadratic and quartic results for temperature variations across the duct; P = 1 atm, L = 10 cm, and T_w = 1,000 K.

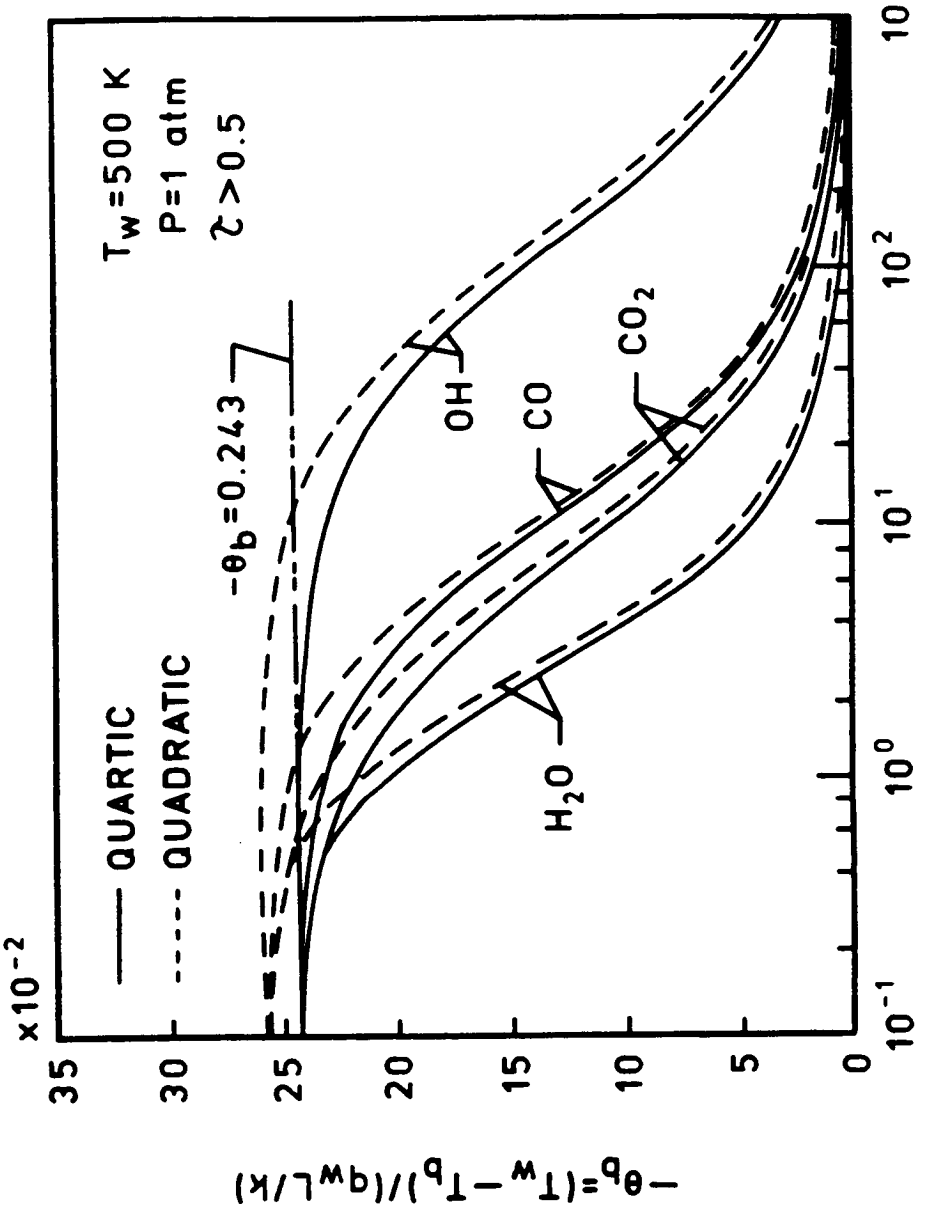

Figure 5. Comparison of quadratic and quartic results for the bulk temperature; P = 1 atm and T_w = 500 K.

identical for radiative equilibrium and radiation with conduction cases, they differ significantly for the case of combined conduction, convection and radiation. As such, all other results for this study were obtained by using the quartic formulation.

The results for temperature variations with nondimensional time are presented in Figs. 6-9 for various species and for different physical conditions. The centerline temperature distribution for general and limiting cases are illustrated in Fig. 6 for T_w = 500 K, P = 1 atm, and L = 5 cm. The results show that the steady-state conditions are reached at about τ = 0.5 for all species. As noted earlier, these results also demonstrate that H_2O is a highly radiation participating gas as compared to CO_2, CO, and OH. In comparison to other species considered, OH takes relatively longer times to reach the steady state and is least effective in transferring the radiative energy. For the specified physical conditions, the large path length solutions are closer to the general solutions and optically thin solutions provide higher rate of energy transfer. For all species, optically thin solutions reach the steady state faster than other solutions. Also, in the optically thin limit, CO_2 is more effective in the radiative transfer process than other species. The reasons for such trends are given in [8, 33, 34]. The results for T_w = 500 K and 1,000 K are compared in Fig. 7, and they simply indicate that the rate of energy transfer is higher at the higher temperature. The results for ξ = 0.25 and 0.5 are compared in Fig. 8 for T_w = 1,000 K, P = 1 atm, and L = 5 cm. It is noted that the rate of energy transfer is higher at earlier times and at locations closer to the wall. The centerline temperature variations for L = 5 cm and 10 cm are illustrated in Fig. 9 for T_w = 1,000 K and P = 1 atm. As would be expected, the rate of energy transfer is seen to increase with the increasing path length.

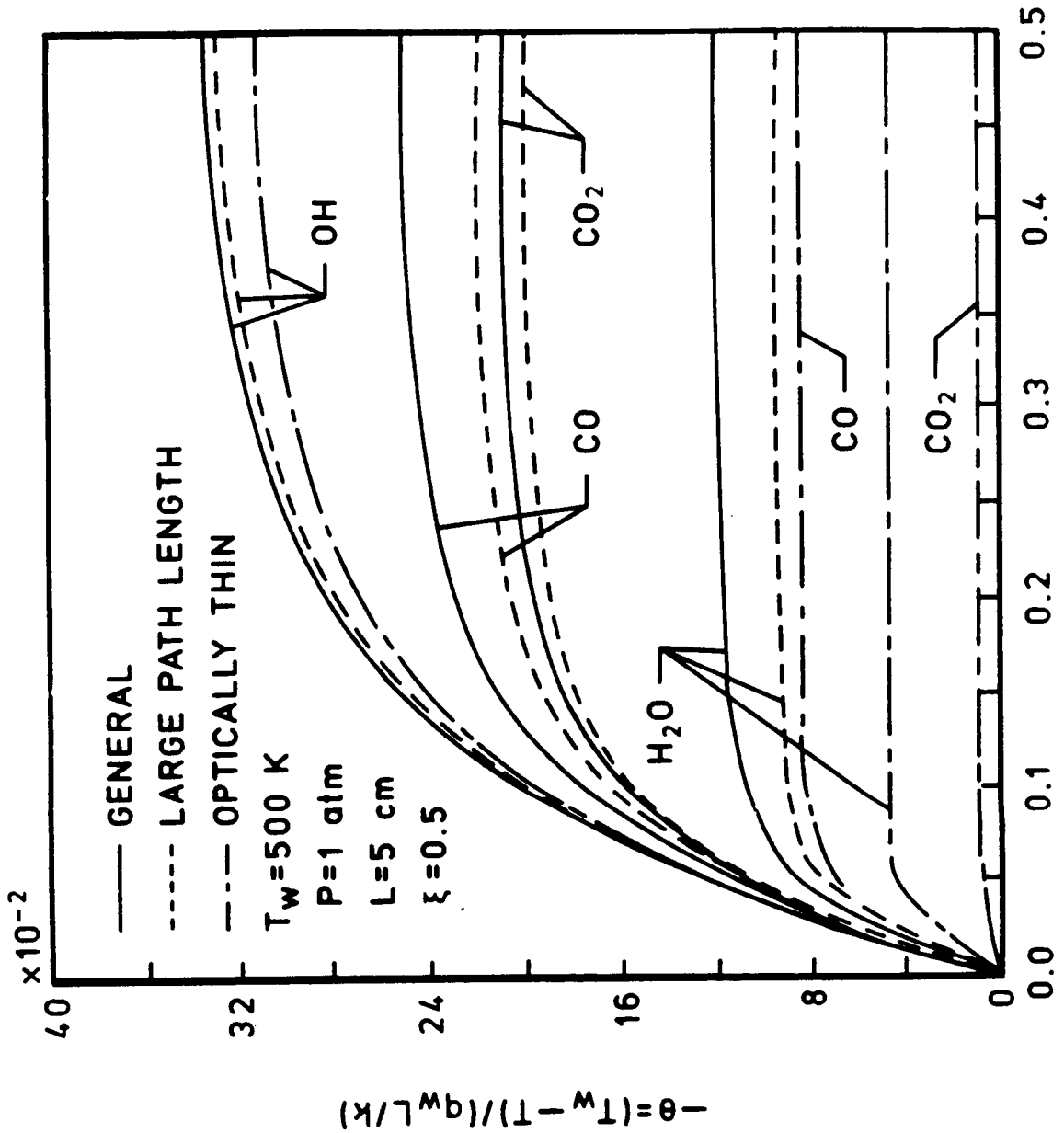

Figure 6. Comparison of general and limiting results for the centerline temperature variations with time; T_w = 500 K, P = 1 atm, and L = 5 cm.

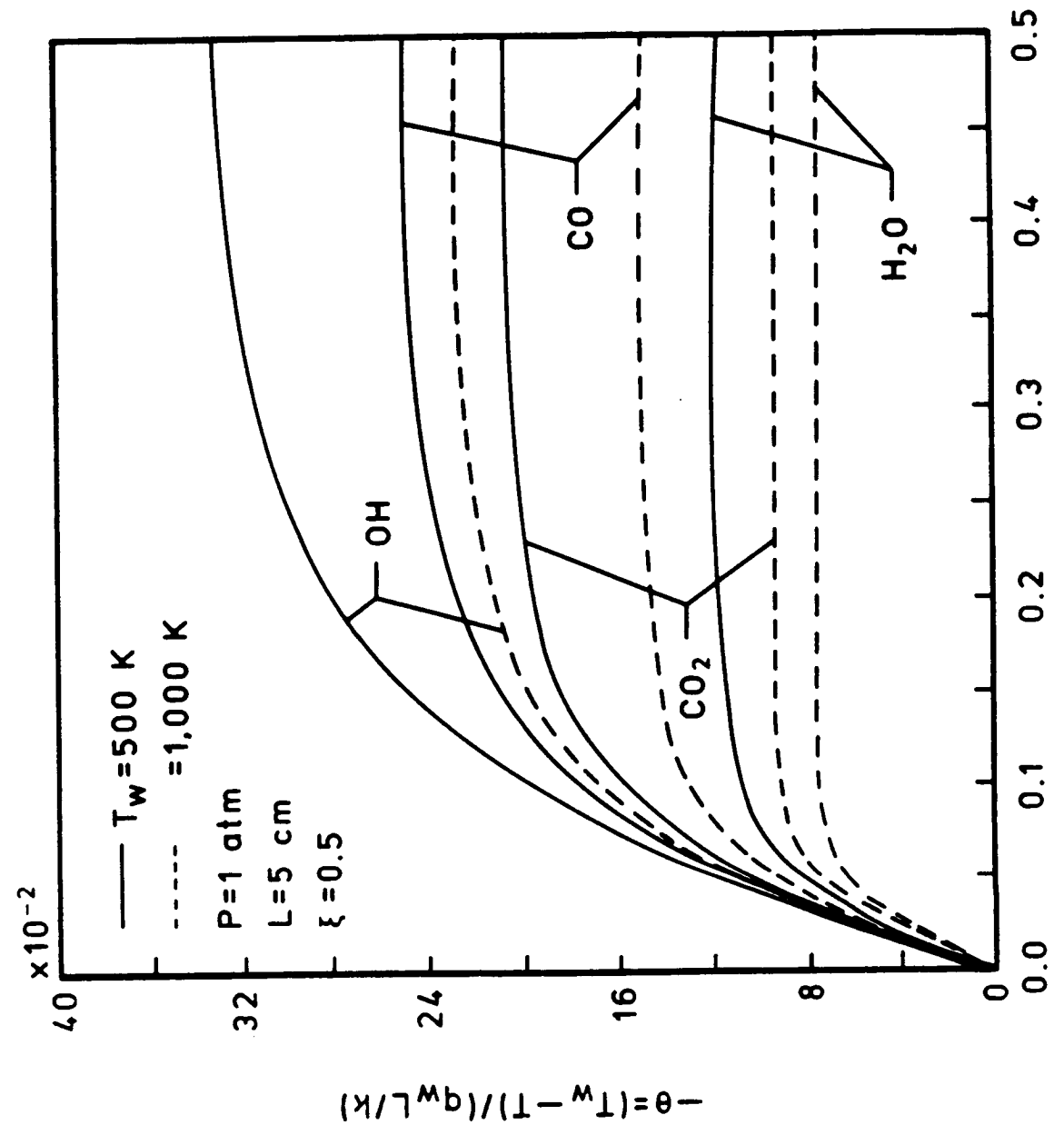

Figure 7. Comparison of centerline temperature variations with time for T_w = 500 K and 1,000 K; P = 1 atm and L = 5 cm.

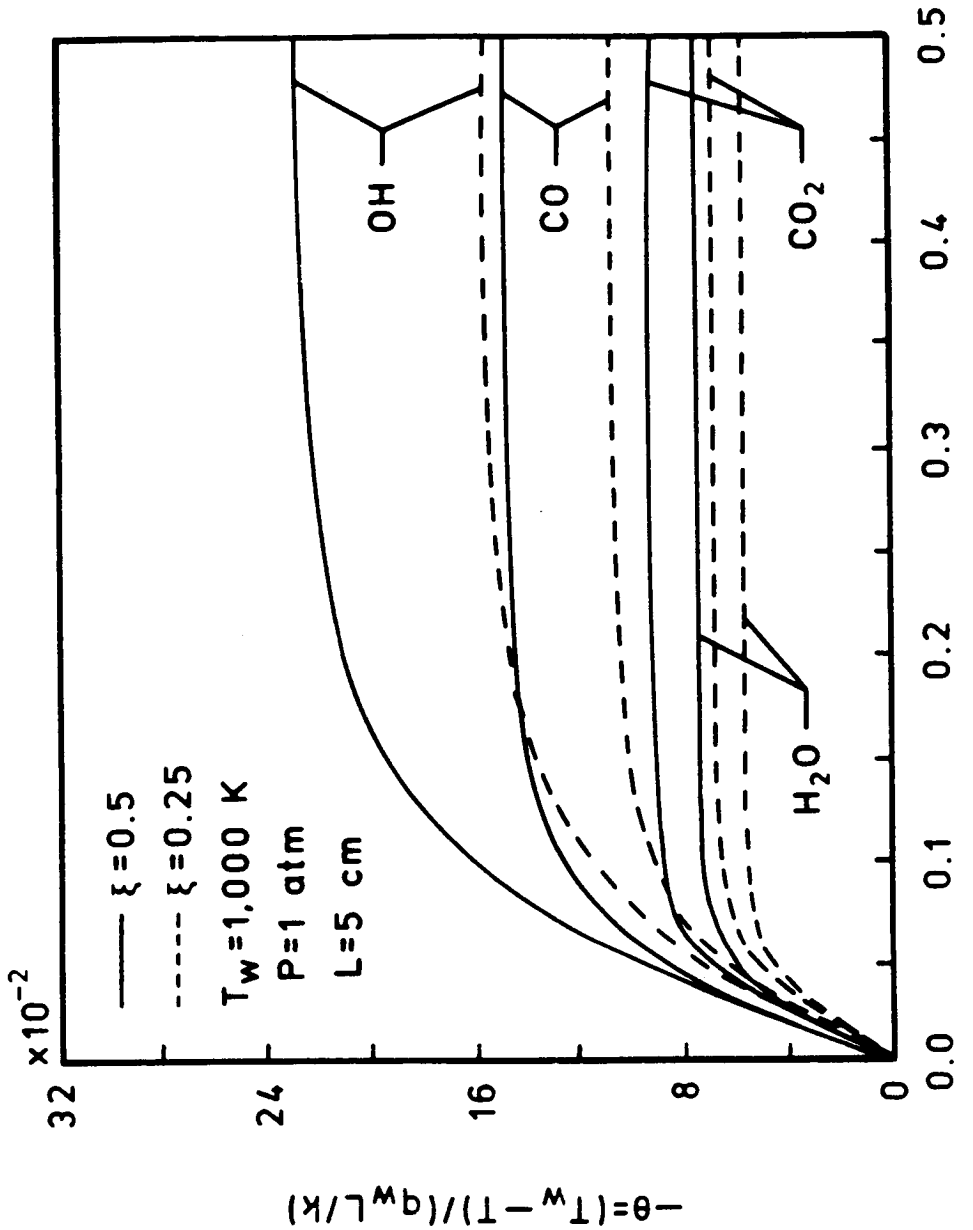

Figure 8. Comparison of temperature variations with time for ξ = 0.25 and 0.5; T_w = 1,000 K, P = 1 atm, and L = 5 cm.

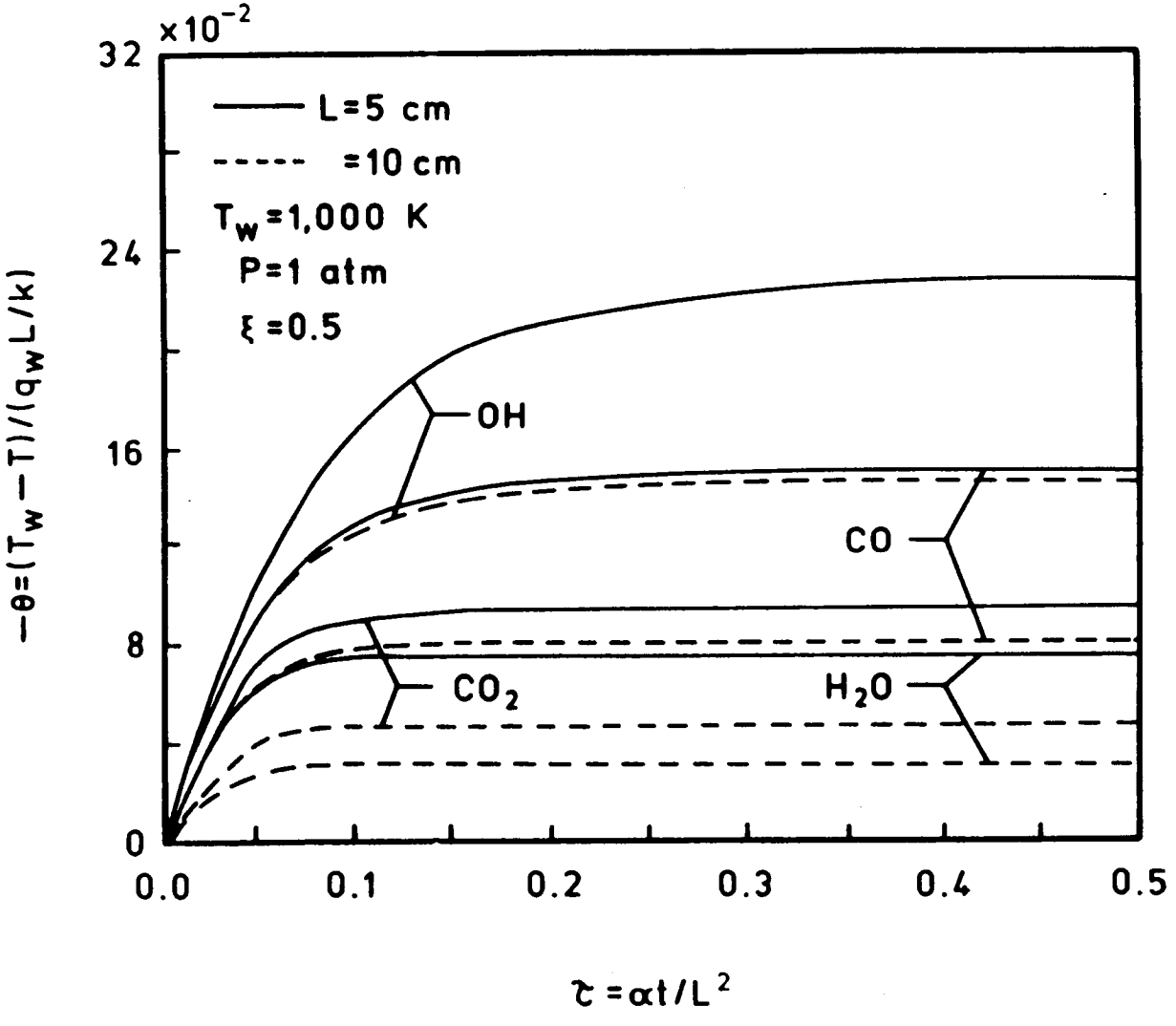

Figure 9. Comparison of centerline temperature variations with time for L = 5 cm and 10 cm; T_w = 1,000 K and P = 1 atm.

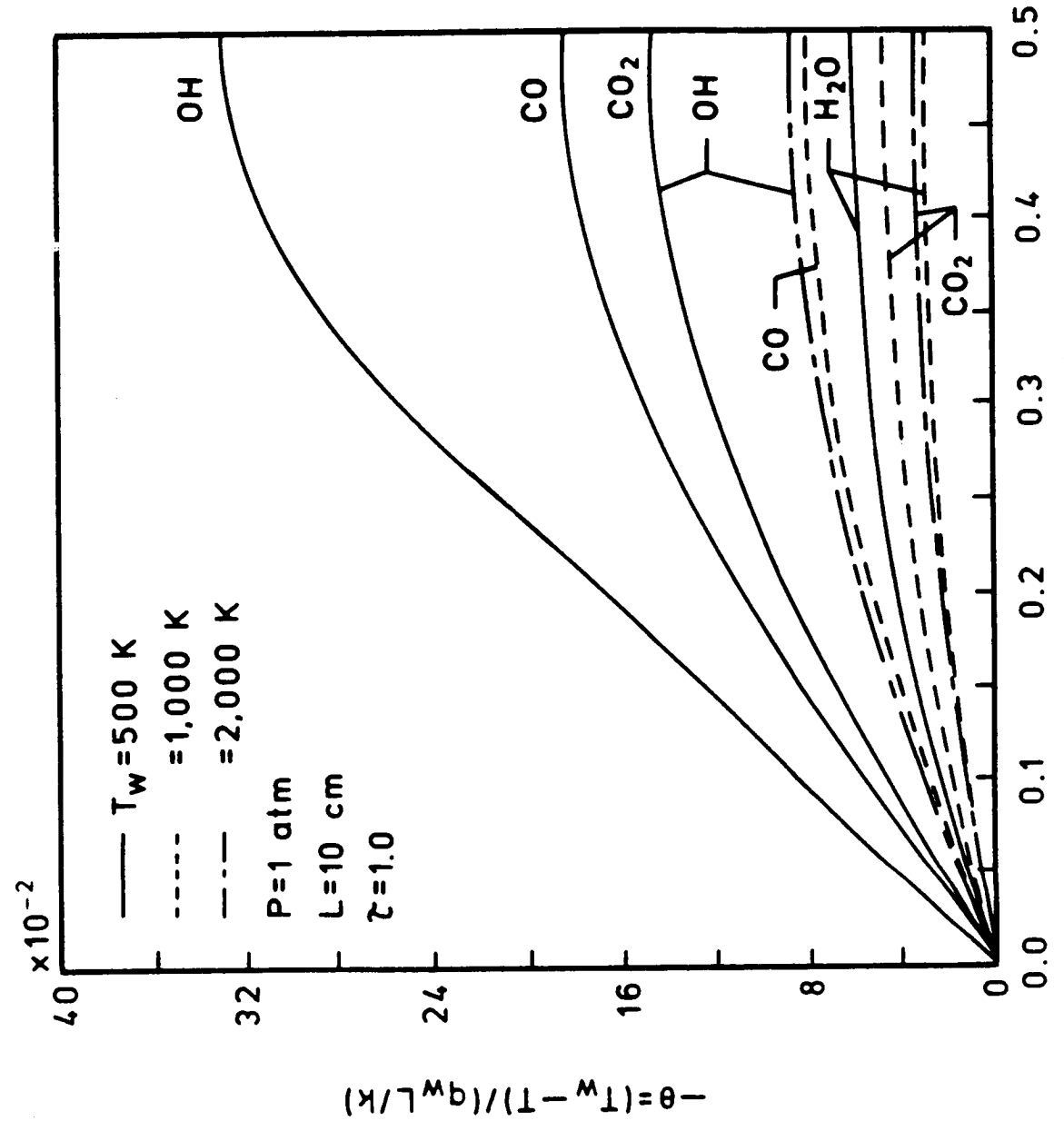

Figure 10. Comparison of temperature variations across the duct for T_w = 500 K, 1,000 K, and 2,000 K; P = 1 atm and L = 10 cm.

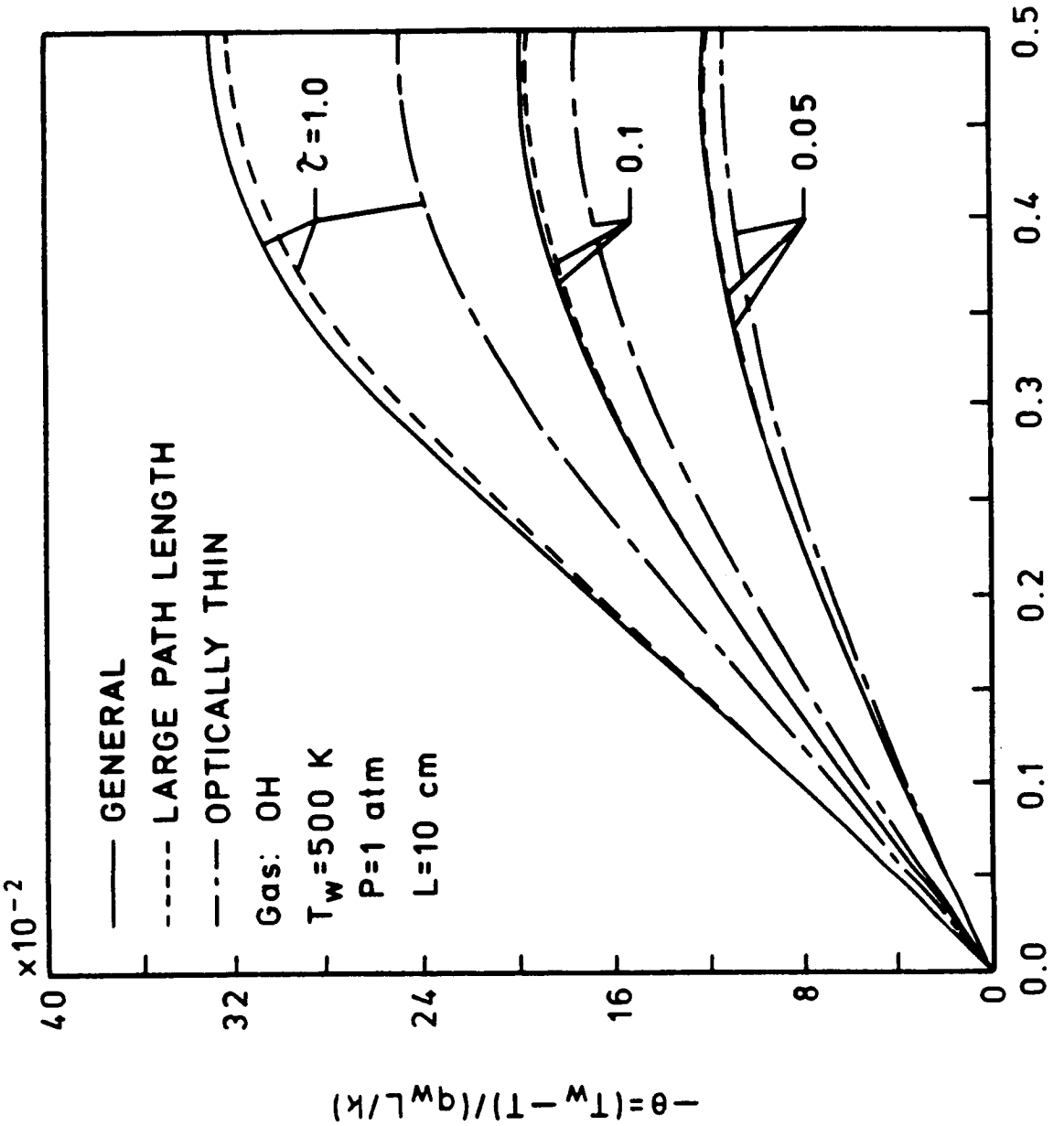

Figure 11. Comparison of temperature variations across the duct for OH; T_w = 500 K, P = 1 atm, and L = 10 cm.

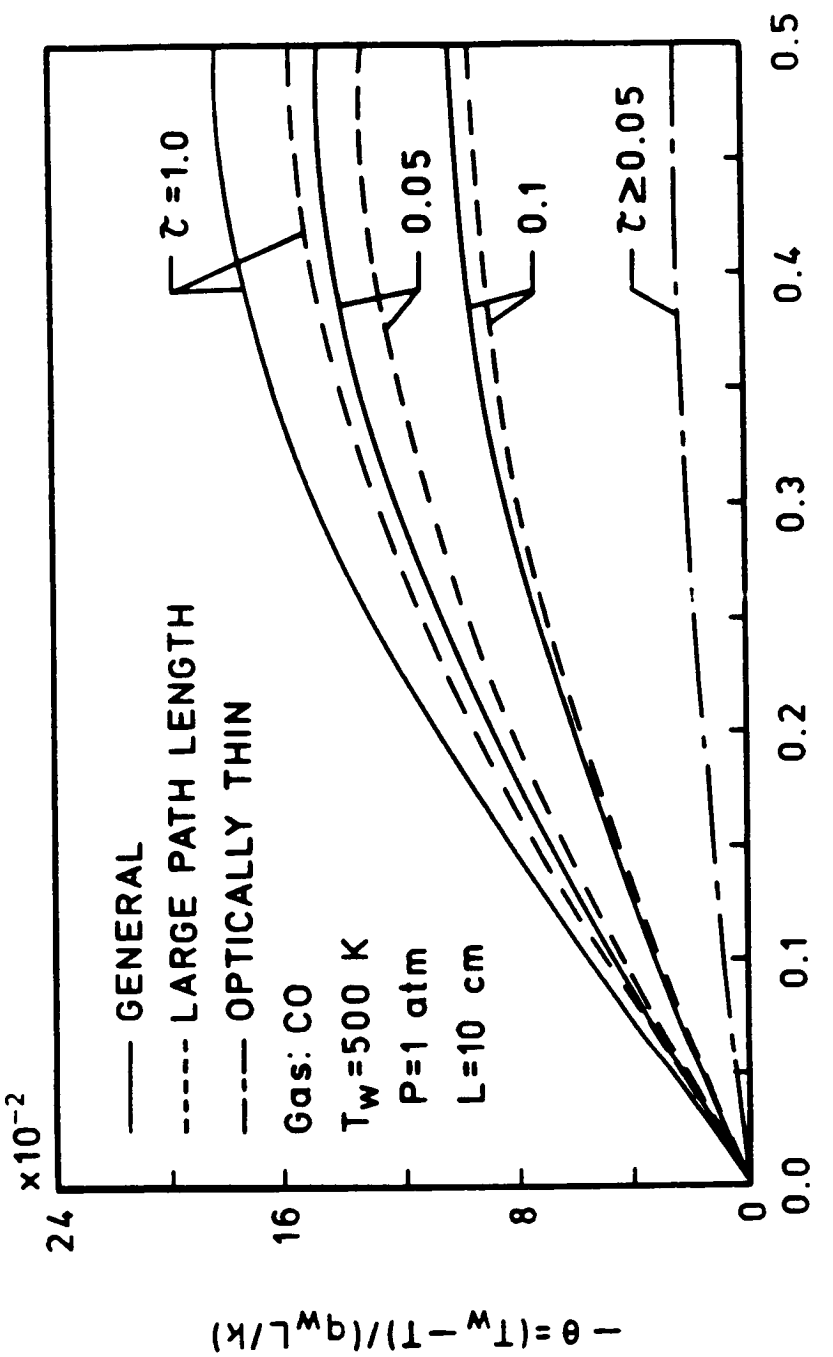

Figure 12. Comparison of temperature variations across the duct for CO; T_w= 500 K, P = 1 atm, and L = 10 cm.

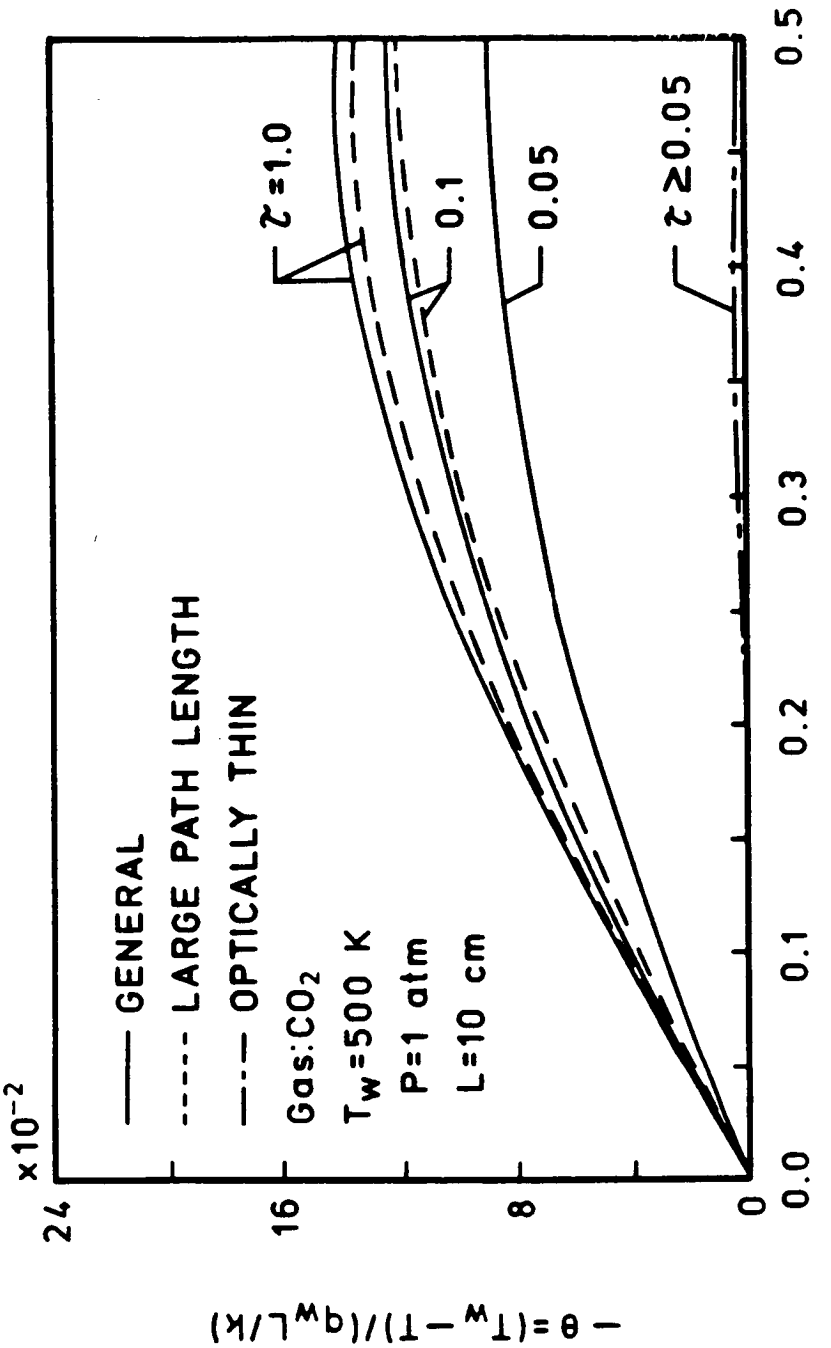

Figure 13. Comparison of temperature variations across the duct for CO_2; T_w = 500 K, P = 1 atm, and L = 10 cm.

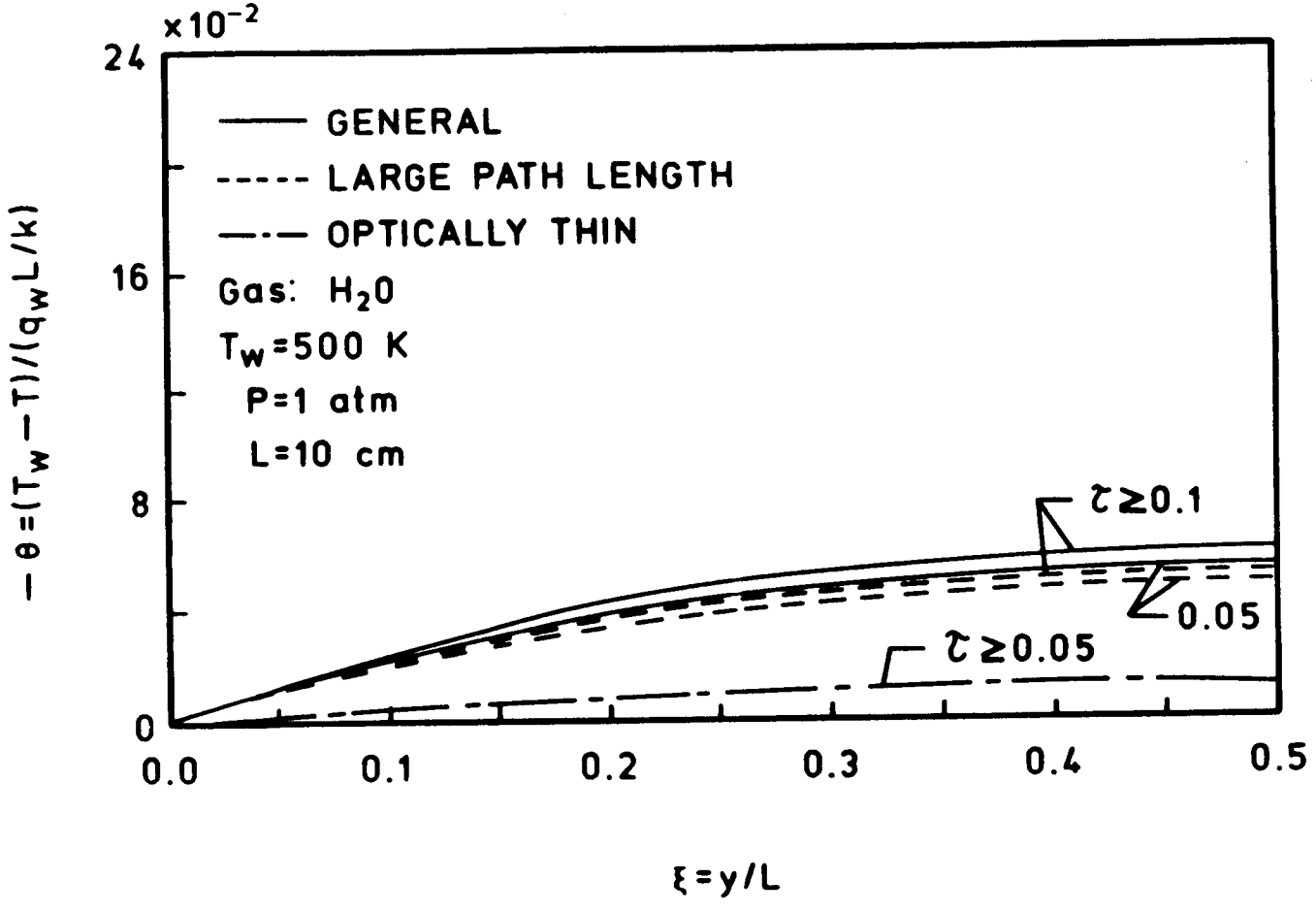

Figure 14a. Comparison of temperature variations across the duct for H_2O; T_w = 500 K, P = 1 atm.

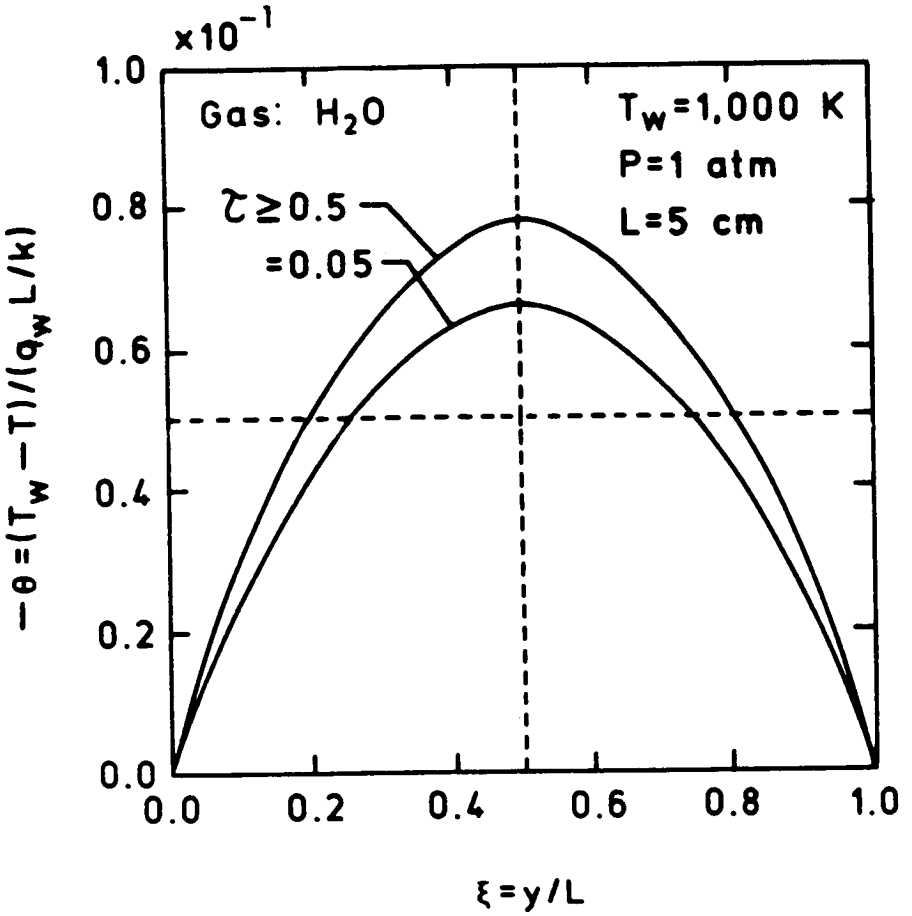

Figure 14b. Comparison of temperature variations across the duct for H_2O; T_W = 1,000 K, P = 1 atm, and L = 5 cm.

The bulk temperature results as a function of the distance between the plates are presented in Figs. 15-19 for different times. General as well as limiting solutions are illustrated in these figures. As mentioned earlier, the limiting value of $\theta_b = -0.243$ corresponds to negligible radiation. For all species, the results presented in the figures are for a pressure of one atmosphere. However, for any particular L, the large path length results essentially represent the limiting solutions for high pressures. The results, in general, demonstrate that the rate of energy transfer is higher at earlier times, the effect of radiation increases with increasing plate spacing, and the radiative transfer is more pronounced at the higher wall temperature.

General as well as limiting solutions for the bulk temperature are illustrated in Figs. 15-18 for individual species. It is seen that for all species the general solutions for $\tau = 0.5$ and 1.0 are essentially the same for all plate spacings, and the large path length results are valid for spacings greater than L = 10 cm for all times. The results for OH are presented in Figs. 15a and 15b for T_w = 500 K and 1,000 K, respectively. It is noted that optically thin results provide the correct limiting solutions for plate spacings upto L = 3 cm for all times. The results for T_w = 500 K show only slight difference between general and large path length solutions for $\tau = 0.5$, and no significant difference was noted at earlier times (Fig. 15a). This, however, is not the case for the results presented in Fig. 15b at T_w = 1,000 K. This trend in results for OH was noted also in [33, 34]. The results for CO are illustrated in Fig. 16 for T_w = 500 K and P = 1 atm. In this case, the optically thin solutions are seen to be valid only upto L = 1.5 cm. For T_w = 1,000 K and P = 1 atm, the results presented in Fig. 17 for CO_2 and in Fig. 18 for H_2O show the same general trend but the extent of radiative interaction is entirely different. For CO_2, there is a considerable

difference in general and optically thin solutions for all times. For H_2O, however, the optically thin results are closer to the general solutions for spacings upto L = 2.5 cm. The results presented in Figs. 15-18 clearly reveal that for a fixed spacing between the plates the rate of radiative heating will be considerably higher at earlier times than at the steady state. Thus, in a particular physical system, the extent of radiative heating can be very intense during the initial stages of operation. It is also important to note that both the optically thin and large path length results overestimate the influence of radiation. Since these solutions can be obtained with less numerical complications, they can be utilized to assess whether or not, for a given gas, the interaction of radiation is going to be important.

A comparison of the general band absorptance results for the four gases is shown in Figs. 19a and 19b for a pressure of one atmosphere. The results clearly demonstrate the relative ability of the four species for radiative transfer at different path lengths. For a plate spacing of greater than L = 3.0 cm, the results show the same trend as noted in Figs. 2-10. For lower plate spacings and relatively higher temperatures, however, CO_2 shows a significantly higher ability for radiative transfer than other species. This is a typical distinguishing feature of the CO_2 under optically thin conditions [8, 33, 34].

For steady-state conditions, bulk temperature results were obtained for mixtures of different absorbing-emitting species under various conditions and some of these are presented in Figs. 20-27. The relative amount of each species in the mixture and the relative ability of the species for radiative transfer in a given physical condition determine the extent of radiative interaction.

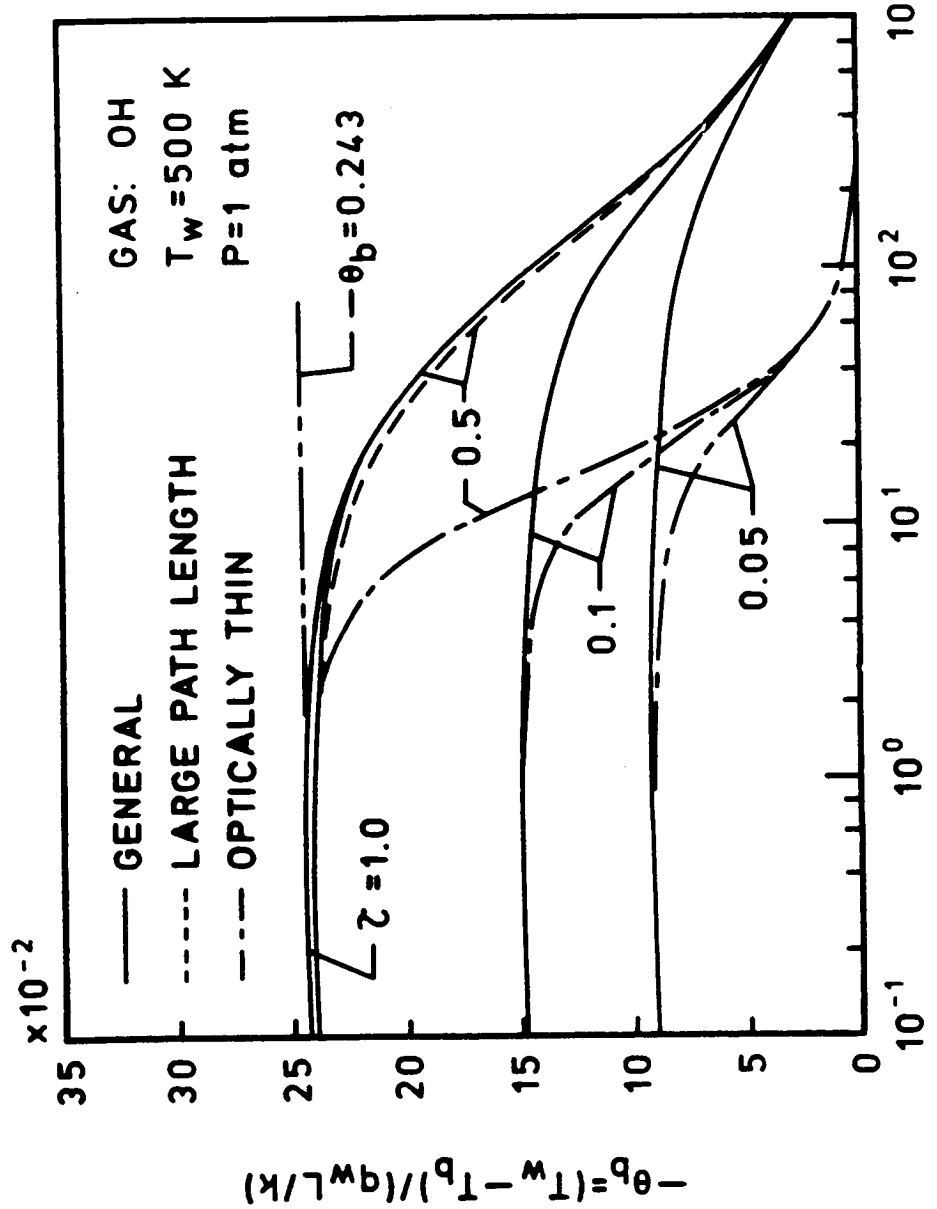

Figure 15a. Variation of bulk temperature with plate spacing for OH; T_w = 500 K and P = 1 atm.

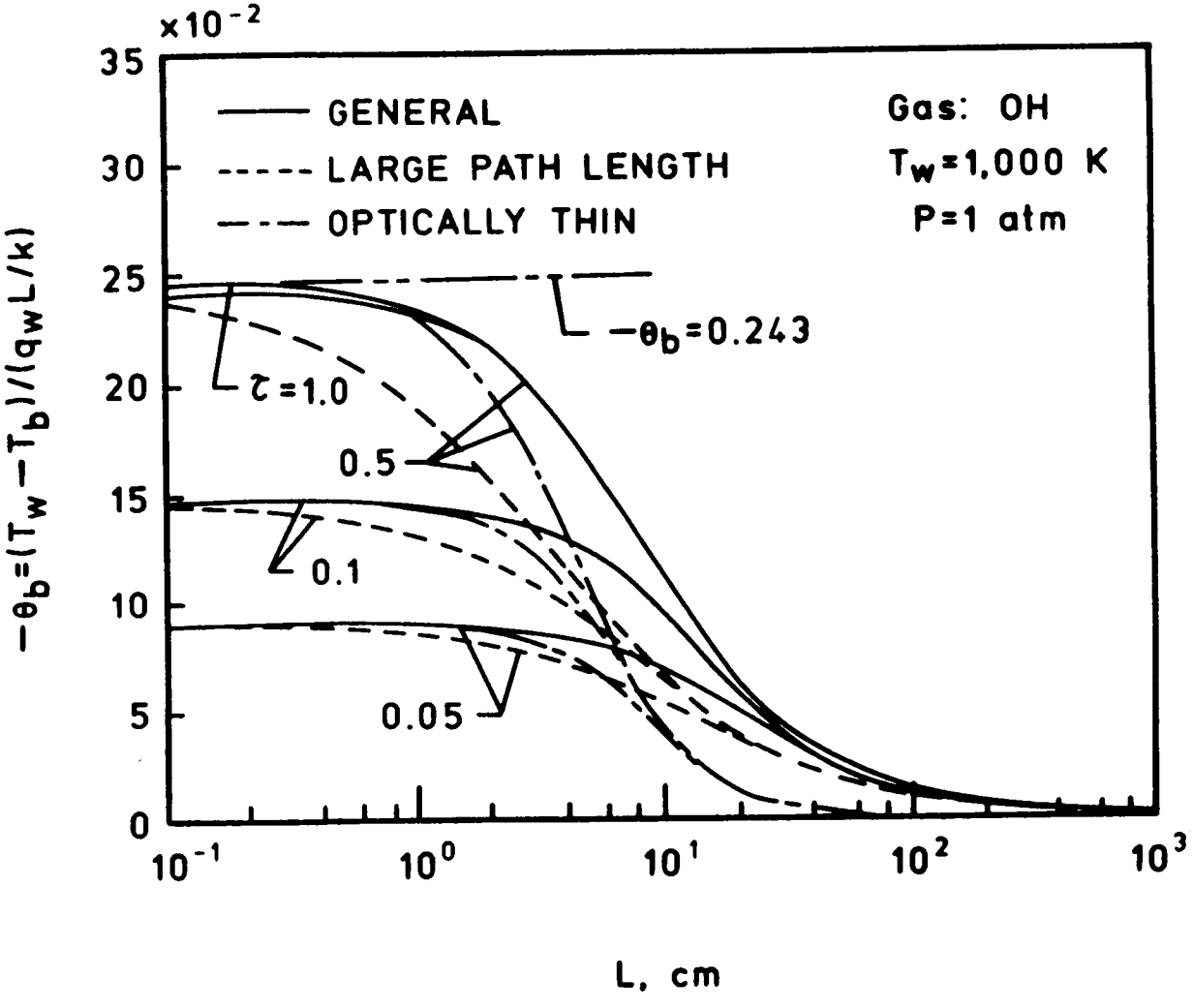

Figure 15b. Variation of bulk temperature with plate spacing for OH; T_w = 1,000 K and P = 1 atm.

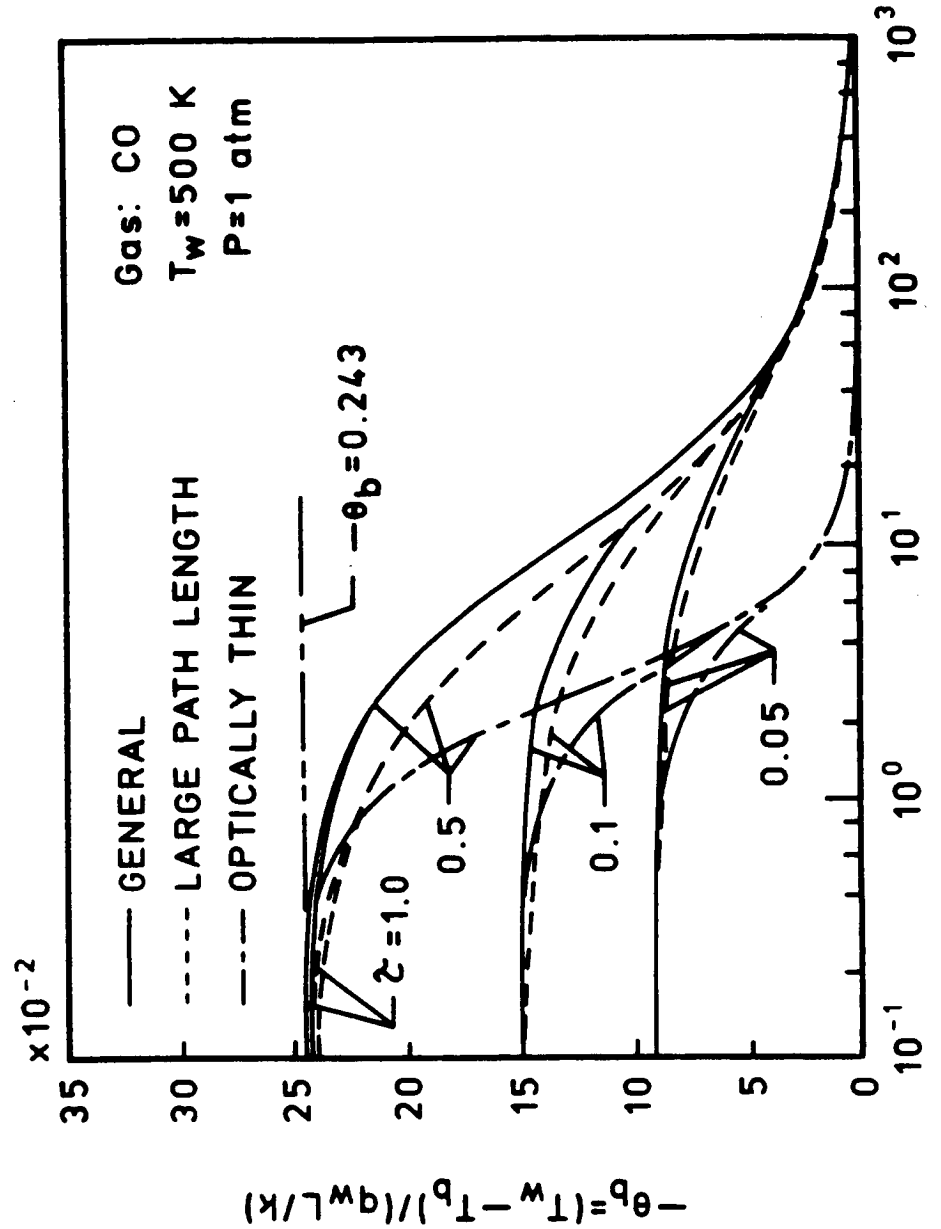

Figure 16. Variation of bulk temperature with plate spacing for CO; T_w = 500 K and P = 1 atm.

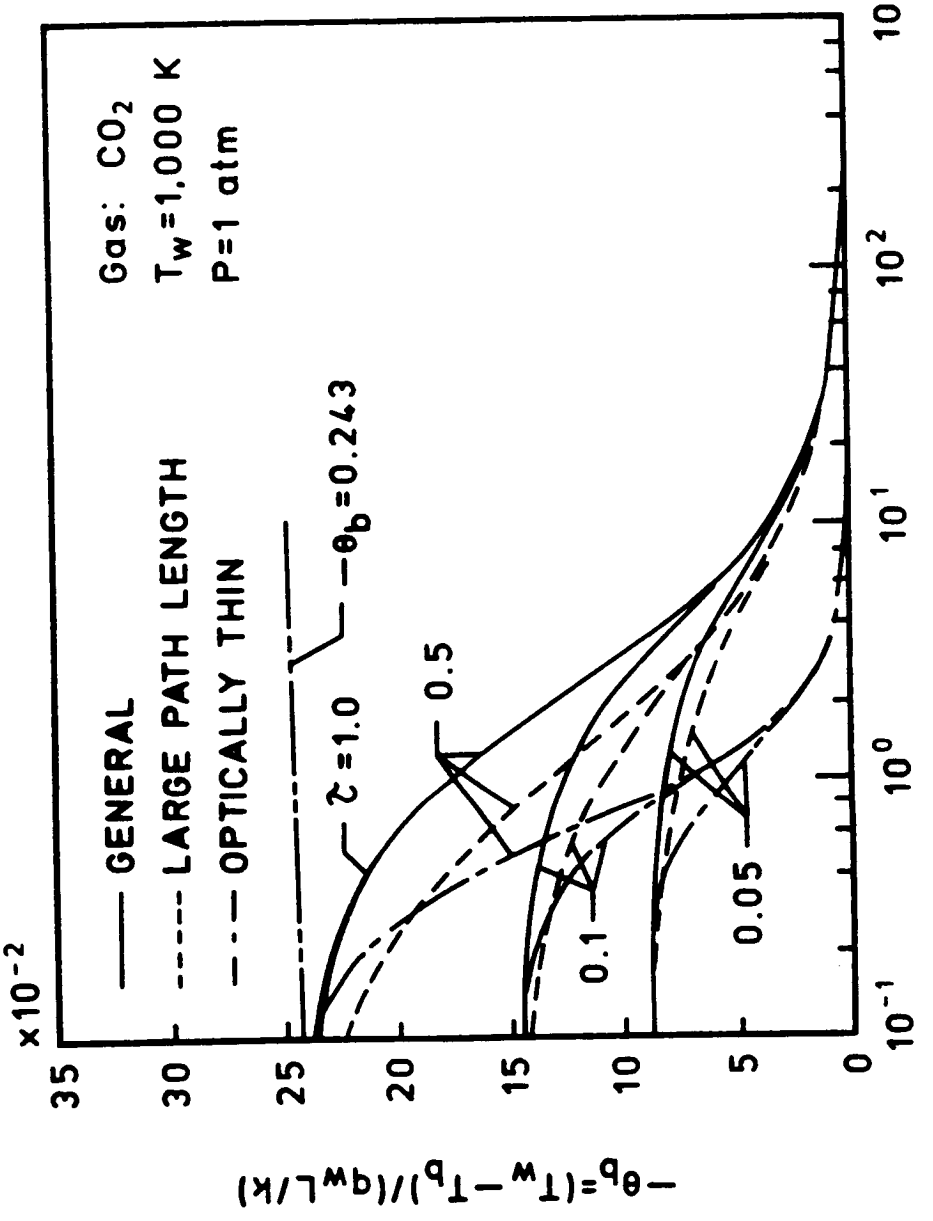

Figure 17. Variation of bulk temperature with plate spacing for CO_2; T_w = 1,000 K and P = 1 atm.

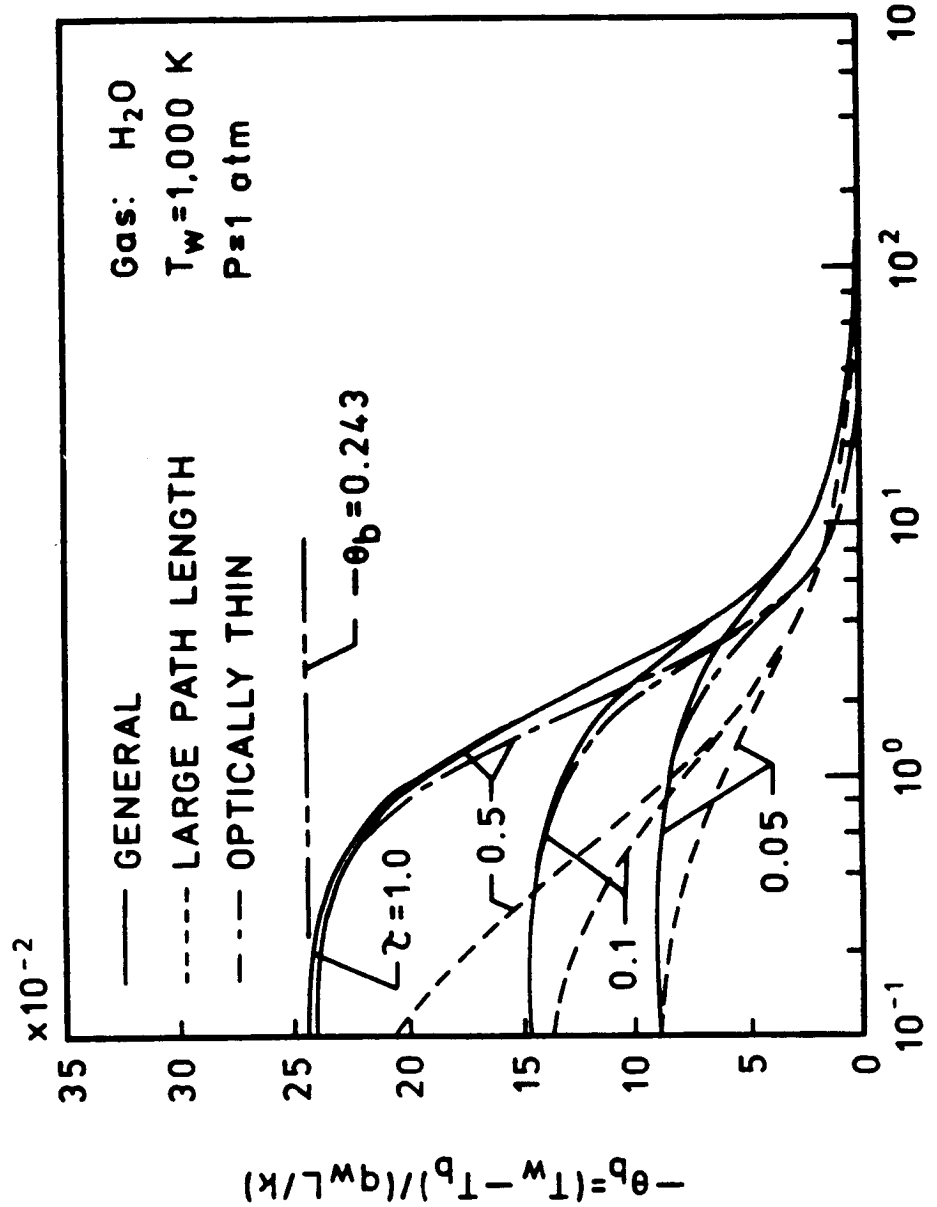

Figure 18. Variation of bulk temperature with plate spacing for H_2O; T_w = 1,000 K and P = 1 atm.

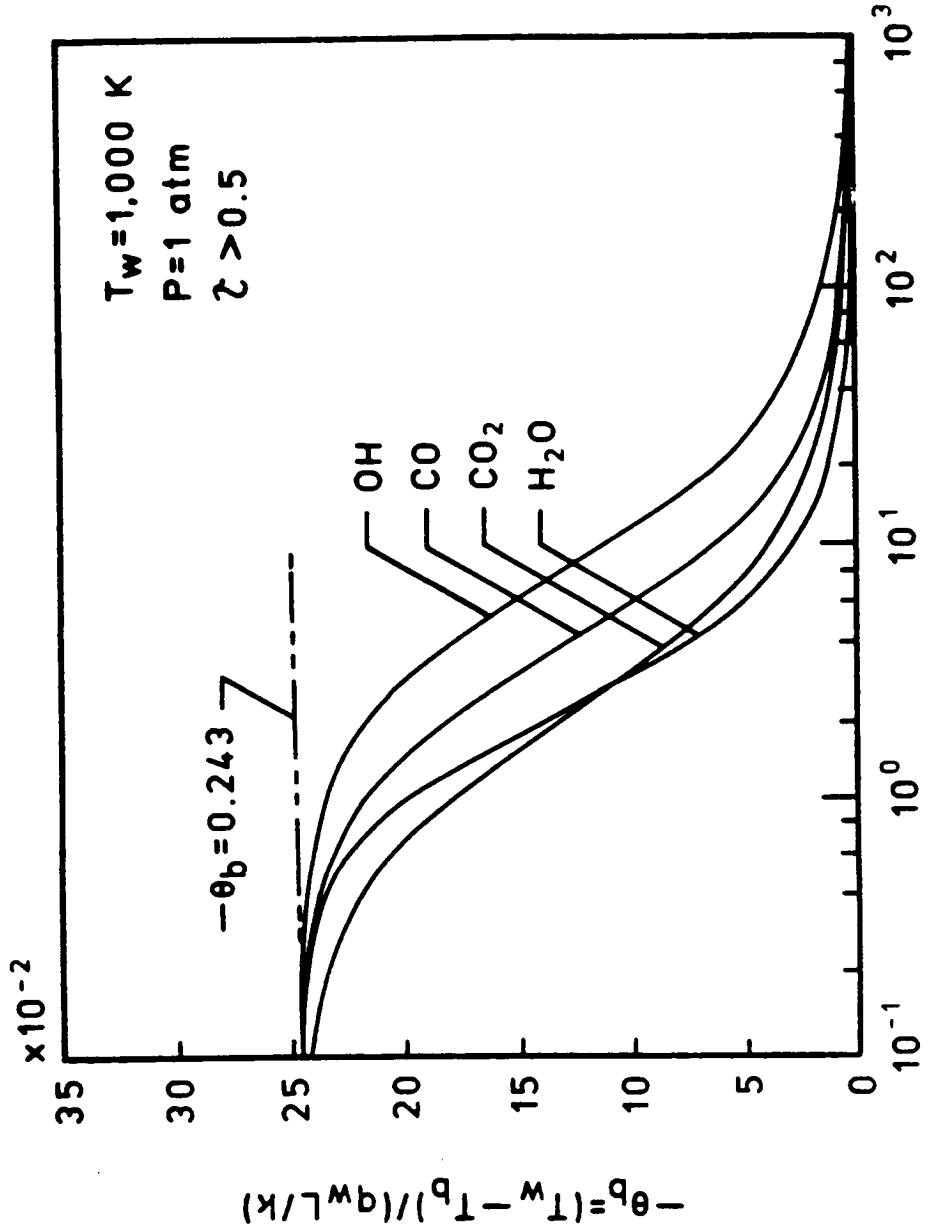

Figure 19a. Comparison of bulk temperature results for T_w = 1,000 K and P = 1 atm.

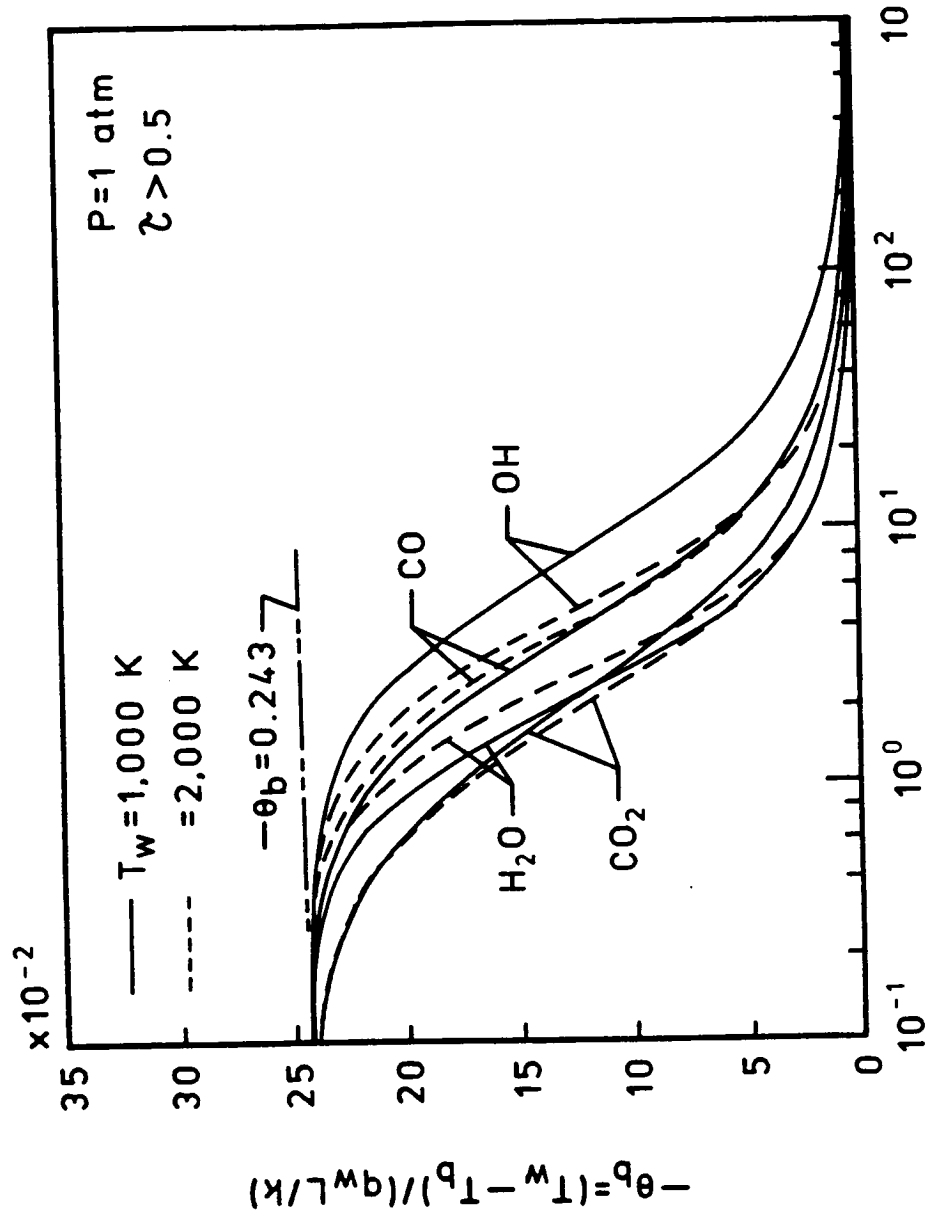

Figure 19b. Comparison of bulk temperature results for P = 1 atm.

As mentioned before, in many combustion processes involving fossil fuels, the predominant products of combustion are carbon dioxide and water vapor. Extensive studies have been conducted in the literature to determine the total emissivity of CO_2 and H_2O for homogeneous and nonhomogeneous conditions. However, only limited studies are available involving mixtures of CO_2 and H_2O for realistic and important physical conditions. The bulk temperature results for three different mixtures of CO_2 + H_2O are presented in Figs. 20-23 for different temperatures and pressures. As would be expected, the results, in general, show that the extent of radiative interaction increases with increasing temperature, pressure, and path length. It is seen that the radiative interaction is stronger for higher amount of H_2O in the mixture. However, for the optically thin conditions, the radiative contribution is seen to increase with increasing amount of CO_2 at relatively higher temperatures.

The bulk temperatures results for mixtures of OH and H_2O are illustrated in Figs. 24-26 and for mixtures of CO_2, H_2O, and OH in Fig. 27 for different pressures and temperatures. All these results clearly demonstrate that the radiative ability of a gaseous mixture essentially depends on the amount of highly radiation participating species in the mixture. For example, a comparison of results presented in Figs. 24 and 27 for P = 1 atm indicates that the rate of radiative transfer is significantly higher with the inclusion of 20% CO_2 in the mixture of OH and H_2O. It is further noted that OH becomes a highly radiation participating species at higher temperatures and pressures.

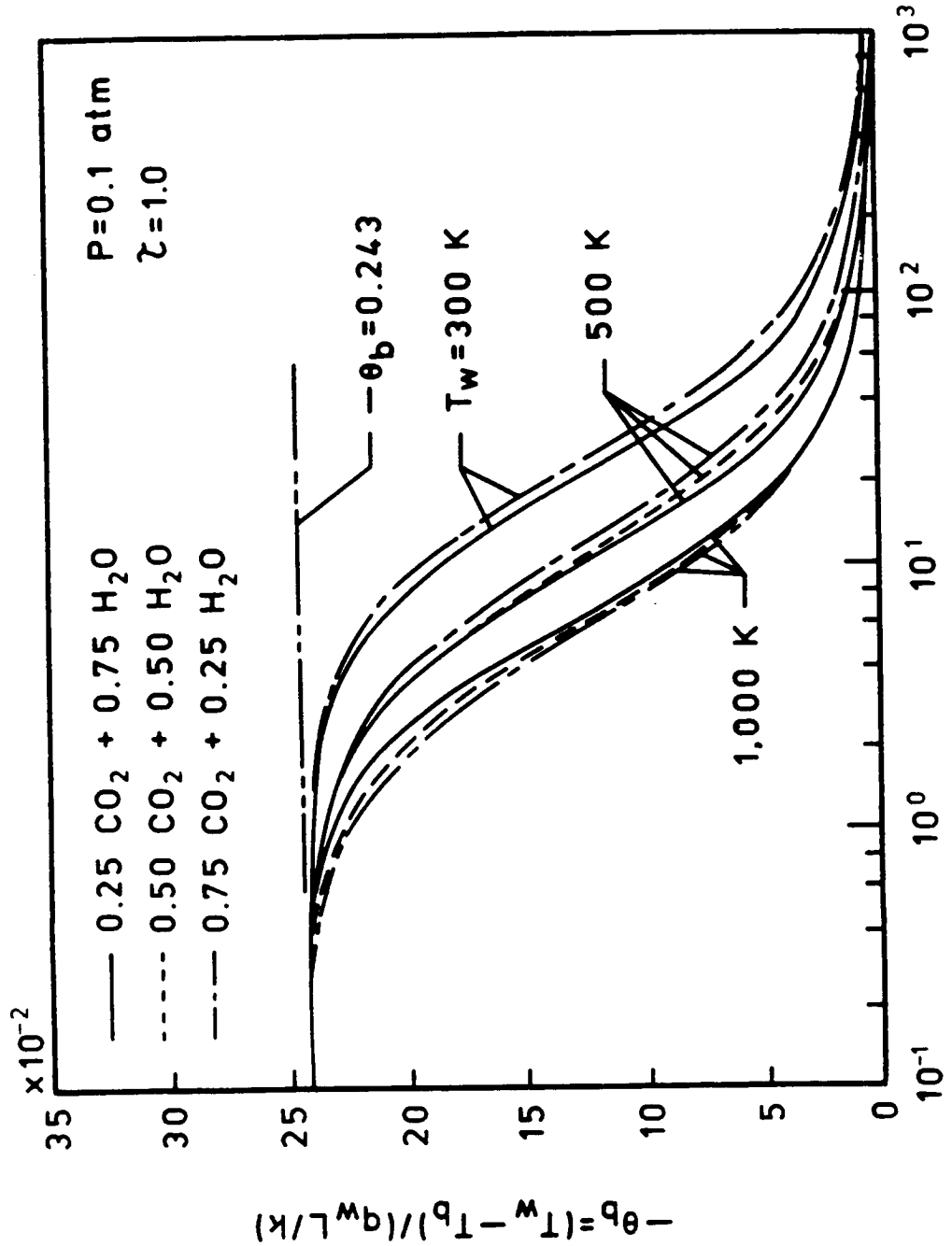

Figure 20. Bulk temperature results for CO_2 + H_2O for P = 0.1 atm.

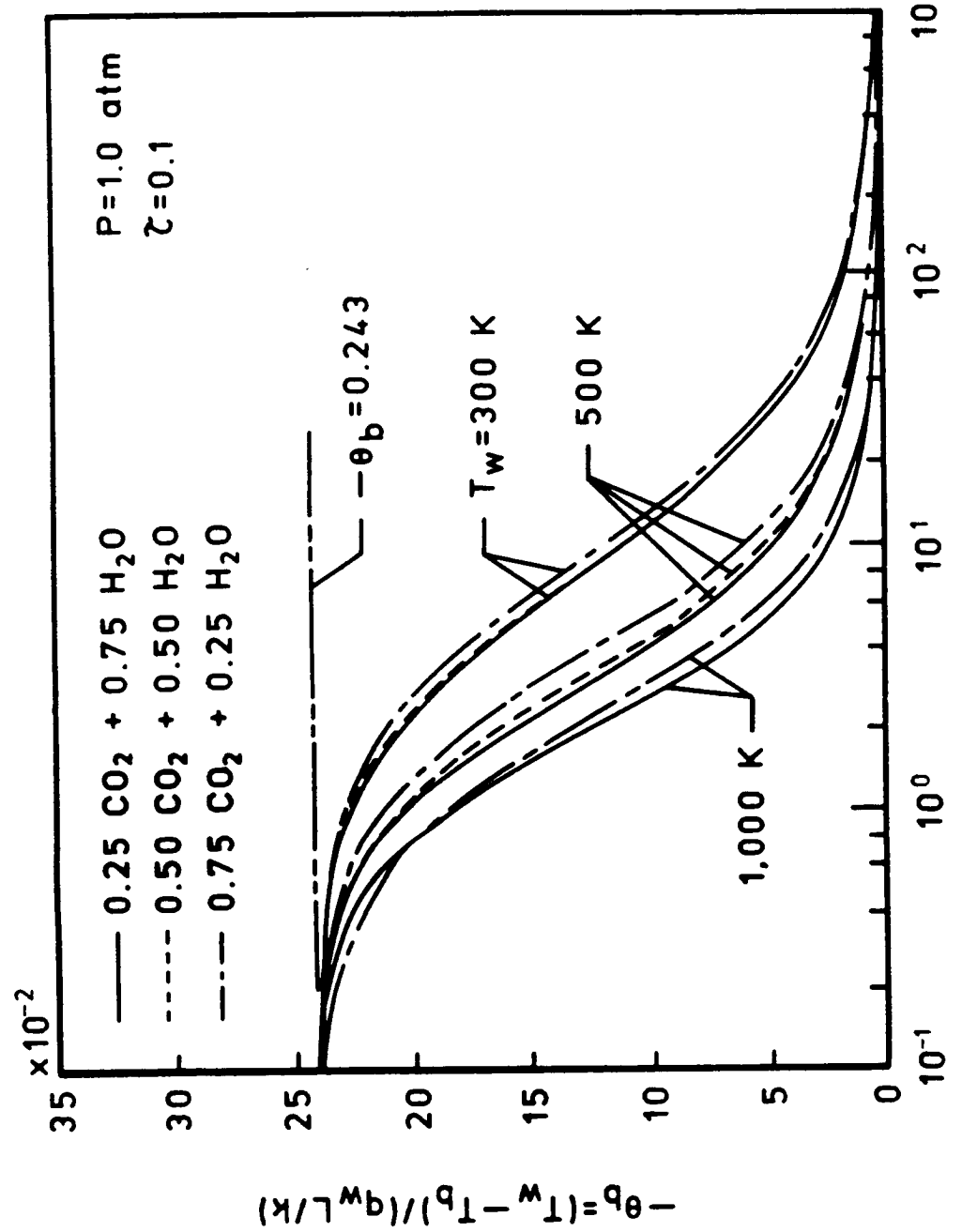

Figure 21. Bulk temperature results for CO_2 + H_2O for P = 1 atm.

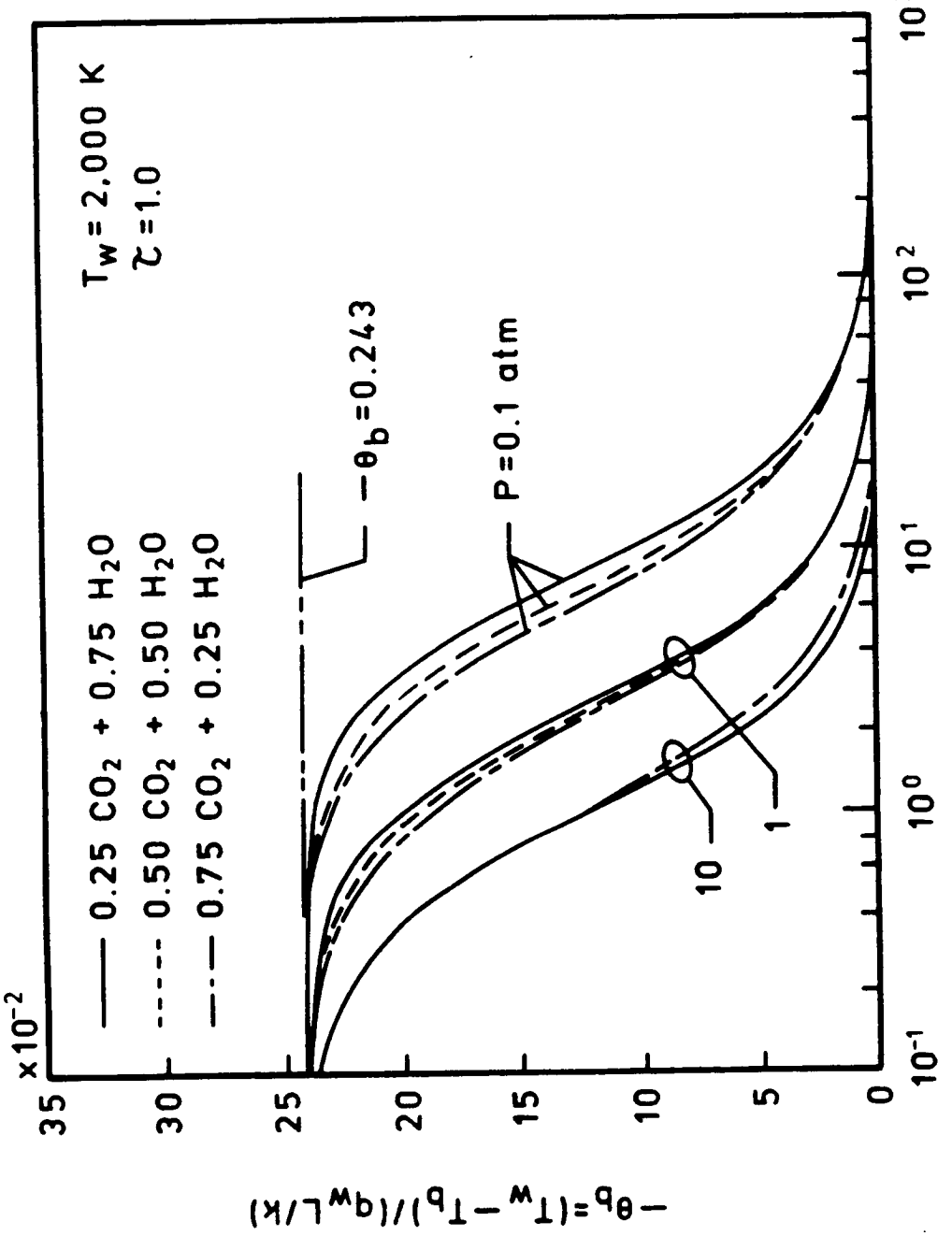

Figure 23. Bulk temperature results for CO_2 + H_2O for T_w = 2,000 K.

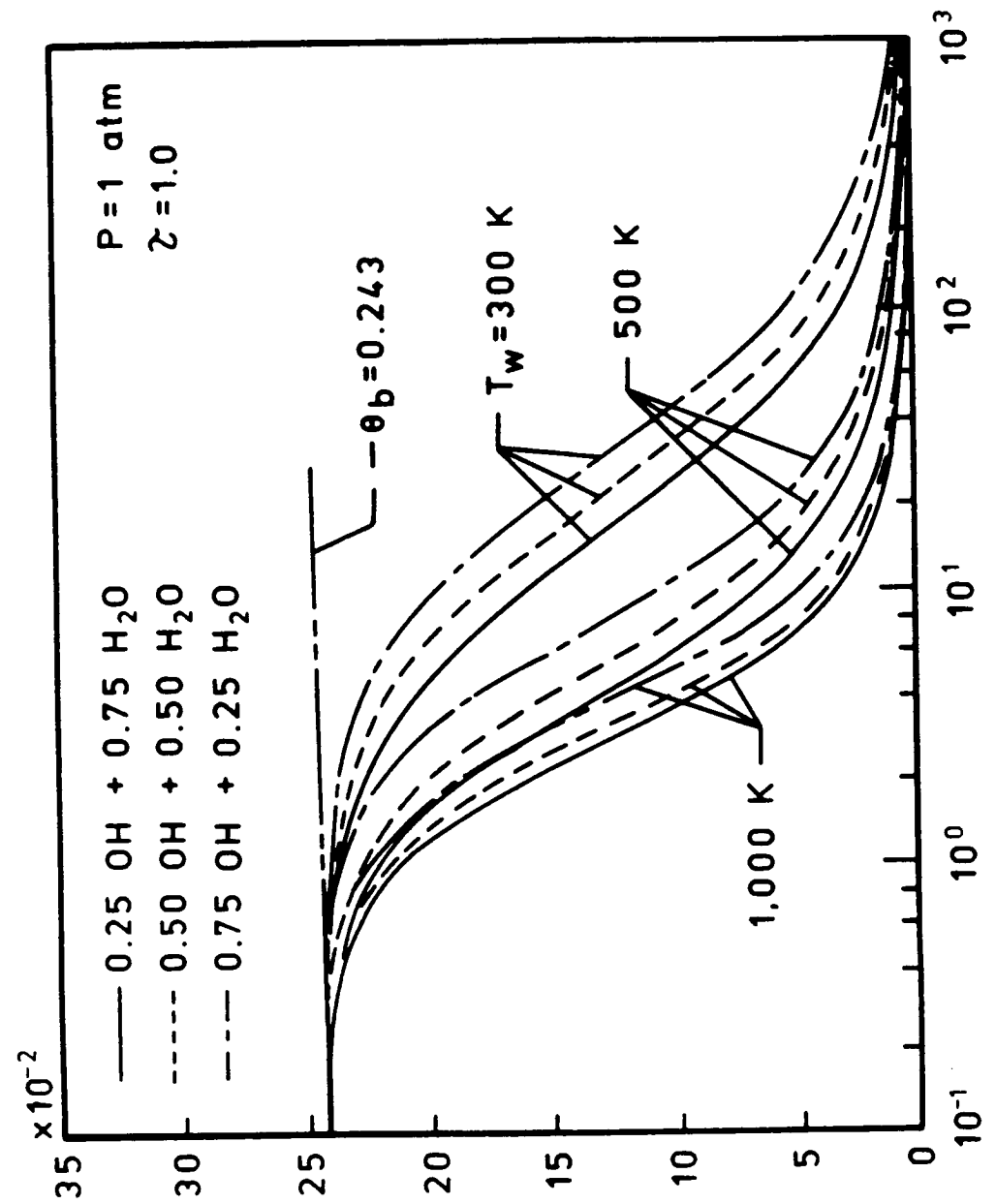

Figure 24. Bulk temperature results for OH and H_2O for P = 1 atm.

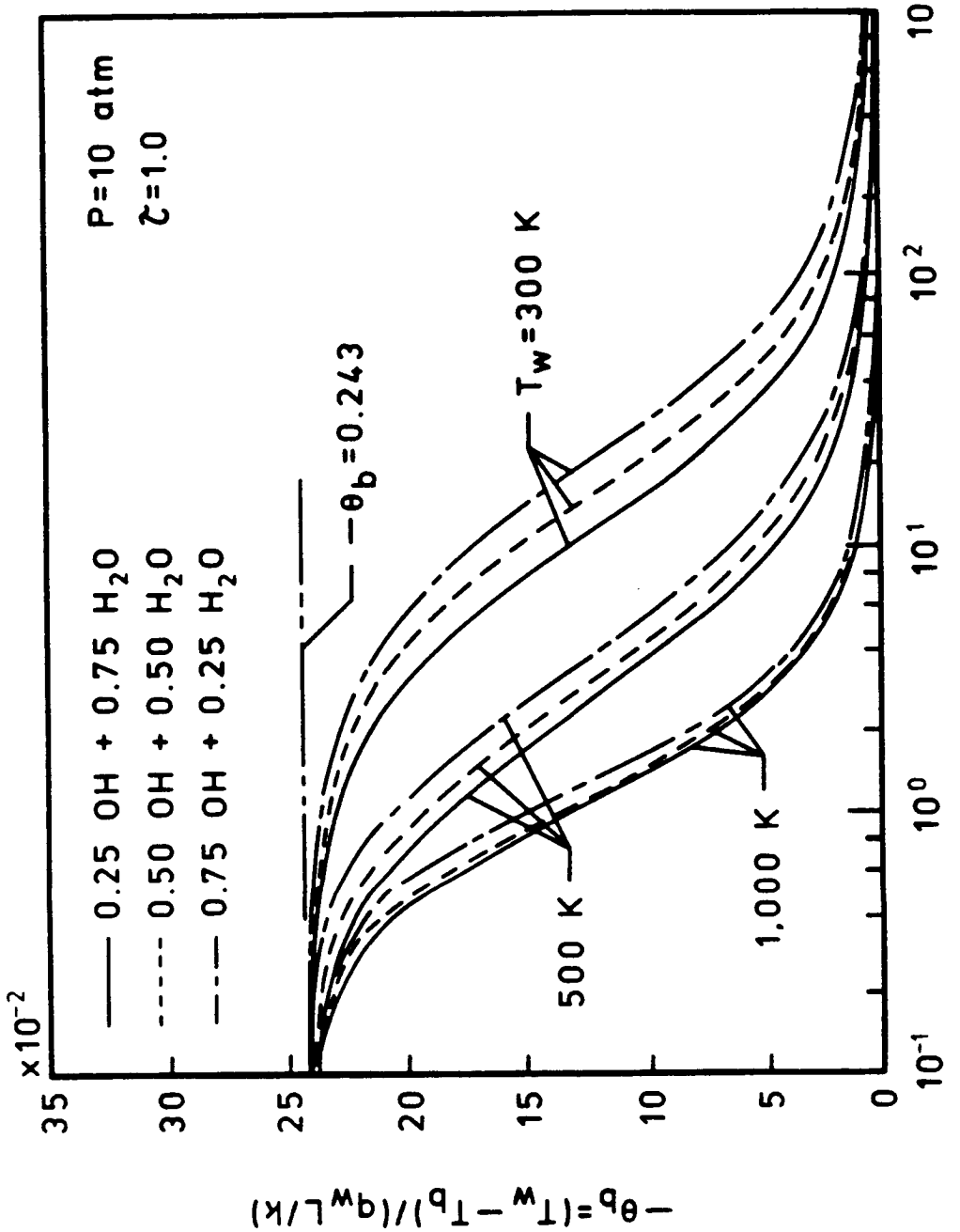

Figure 25. Bulk temperature results for OH and H_2O for P = 10 atm.

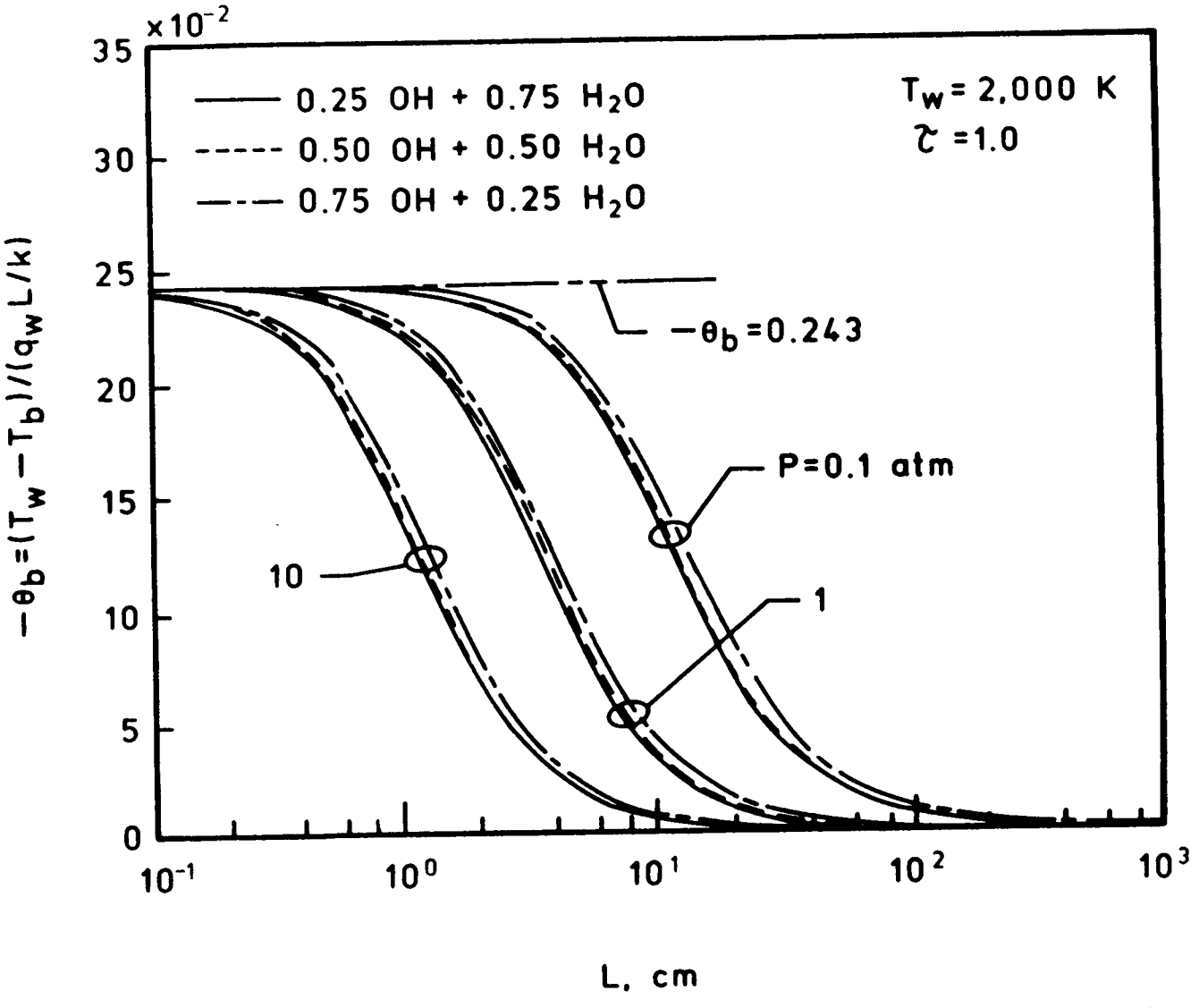

Figure 26. Bulk temperature results for OH and H_2O for T_w = 2,000 K.

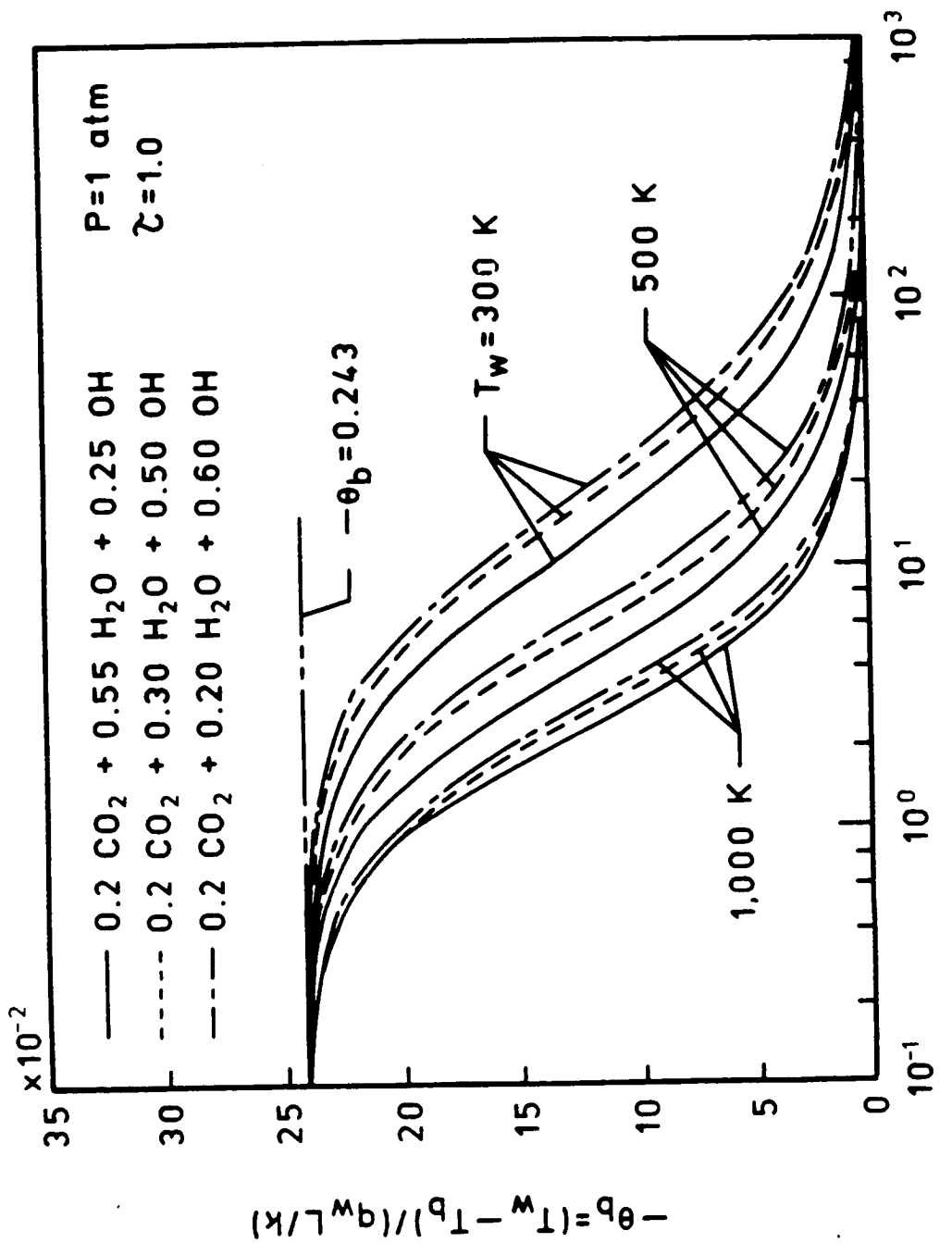

Figure 27. Bulk temperature results for CO_2 + H_2O + OH for P = 1 atm.

CONCLUDING REMARKS

Analytical formulations and numerical procedures have been developed to investigate the transient radiative interaction of absorbing-emitting species in laminar fully-developed flows. Extensive results have been obtained for OH, CO, CO_2 and H_2O for different physical conditions. Illustrative results for the temperature distribution and bulk temperature are presented for different pressures and wall temperatures. In these results, a lower value of temperature implies a relatively higher ability of the gas to transfer radiative energy.

Comparative results of quadratic and quartic formulations confirm the need to use the quartic formulation in the numerical procedures for the case of combined conduction, convection, and radiation. The results, in general, demonstrate that the steady-state conditions are reached at about $\tau = 0.5$ for all species, H_2O is a highly radiation participating species (as compared to CO_2, CO, and OH), the rate of energy transfer is higher at earlier times and at locations closer to the wall, differences between the limiting and general solutions are small at earlier times, the effect of radiation increases with increasing plate spacing, and the radiative transfer is more prounounced at higher wall temperature and pressure. Similar conclusions can be drawn from the results presented for various mixtures. The results clearly show that for a given physical condition the radiative ability of a gaseous mixture depends essentially on the amount of highly radiating species in the mixture. From the results presented in this study, the extent of total heating can be determined for different times. This information is essential in designing thermal protection systems for operations during the initial stages of intense heating.

REFERENCES

1. Sparrow, E. M. and Cess, R. D., Radiation Heat Transfer, Brooks/Cole, Belmont, Calif., 1966 and 1970. New Augmented Edition, Hemisphere Publishing Corp., Washington, D.C., 1978.

2. Hottel, H. C. and Sarofim, A. F., Radiative Transfer, McGraw-Hill Book Co., New York, 1967.

3. Siegel, R. and Howell, J. R., Thermal Radiation Heat Transfer, McGraw-Hill Book Co., New York, 1971; Second Edition, 1981.

4. Cess, R. D., "The Interaction of Thermal Radiation with Conduction and Convection Heat Transfer," Advances in Heat Transfer, Vol. 3, Academic Press, New York, 1966.

5. Sparrow, E. M., "Radiation Heat Transfer between Surfaces," Advances in Heat Transfer, Vol. 2, Academic Press, New York, 1965.

6. Viskanta, R., "Radiation Transfer and Interaction of Convection with Radiation Heat Transfer," Advances in Heat Transfer, Vol. 3, Academic Press, New York, 1966.

7. Tien, C. L., "Thermal Radiation Properties of Gases," Advances in Heat Transfer, Vol. 5, Academic Press, New York, 1968.

8. Cess, R. D. and Tiwari, S. N., "Infrared Radiative Energy Transfer in Gases," Advances in Heat Transfer, Vol. 8, Academic Press, New York, 1972.

9. Edwards, D. K., "Molecular Gas Band Radiation," Advances in Heat Transfer, Vol. 12, Academic Press, New York, 1976.

10. Tiwari, S. N. "Band Models and Correlations for Infrared Radiation," Radiative Transfer and Thermal Control (Progress in Astronautics and Aeronautics), Vol. 49, American Institute of Aeronautics and Astronautics, New York, 1976.

11. Tiwari, S. N., "Applications of Infrared Band Model Correlations to Nongray Radiation," International Journal of Heat and Mass Transfer, Vol. 20, No. 7, July 1977, pp. 741-751.

12. Tiwari, S. N., "Models for Atmospheric Radiation," Advances in Geophysics, Vol. 20, Academic Press, New York, 1978.

13. Edwards, D. K., Radiation Heat Transfer Notes, Hemisphere Publishing Corporation, Washington, D.C., 1981.

14. Kuroksi, Y., "Heat Transfer by Simultaneous Radiation and Convention in an Absorbing and Emitting Medium in a Flow Between Parallel Plates," Fourth International Heat Tranfer Conference, Vol. II, Paper R2.5, Paris-Versailles, 1970.

15. Larsen, P. A. and Lord, H. A., "Convention and Radiative Heat Transfer to Water Vapor in Uniformly Heated Tubes," Fourth International Heat Transfer Conference, Vol. III, Paper, R2.6, Paris-Versailles, 1970.

16. Martin, J. K. and Hwang, C. C. and "Combined Radiant and Convective Heat Transfer in Laminar Steam Flow Between Gray Parallel Plates with Uniform Heat Flux," Journal of Quantitative Spectroscopy and Radiative Transfer, Vol. 15, December 1975, pp. 1071-1081.

17. Jeng, D. R., Lee, E. J. and DeWitt, K. J., "A Study of Two Limiting Cases in Convective and Radiative Heat Transfer with Nongray Gases," International Journal of Heat and Mass Transfer, Vol. 19, June 1979, pp. 589-596.

18. Greif, R., "Laminar Convection with Radiation: Experimental and Theoretical Results," International Journal of Heat and Mass Transfer, Vol. 21, April 1978, pp. 477-480.

19. Kobiyama, M., Taniguchi, H. and Saita, T., "The Numerical Analyses of Heat Transfer Combined with Radiation and Convection," Bulletin of the Japanese Society of Mechanical Engineering, Vol. 22, No. 167, May 1979, pp. 707-714.

20. Im, K. H. and Ahluwalia, R. K., "Combined Convection and Radiation in Rectangular Ducts," International Journal of Heat and Mass Transfer, Vol. 27, No. 2, February 1984, pp. 221-231.

21. Lick, W., "Transient Energy Transfer by Radiation and Conduction," International Journal of Heat and Mass Transfer, Vol. 8, 1965, pp. 119-127.

22. Chang, Y. P. and Kang, C. S., "Transient and Steady Heat Transfer in a Conducting and Radiating Medium," AIAA Journal, Vol. 8, No. 4, April 1970, pp. 609-614.

23. Chang, Y. P. and Smith, R. C., Jr., "Steady and Transient Heat Transfer by Radiative and Conduction in a Medium Bounded by Two Coaxial Cylindrical Surfaces," International Journal of Heat and Mass Transfer, Vol. 13, 1970, pp. 69-80.

24. Doornink, D. G. and Hering, R. G., "Transient Radiative Heat Transfer in a Nongray Medium," Journal of the Quantitative Spectroscopy and Radiative Transfer, Vol. 12, 1972, pp. 1161-1174.

25. Larson, D. W. and Vikanta, R., "Transient Combined Laminar Free Convection and Radiation in a Rectangular Enclosure," Journal of Fluid Mechanics, Vol. 78, Part 1, 1976, pp. 65-85.

26. Melnikov, V. I. and Sukhovich, E. P., "Transient Heat Exchange Between a Radiating Plate and a High-Temperature Gas Flow," Heat Transfer-Soviet Research, Vol. 10, No. 3, May-June 1978, pp. 11-20 (Translation).

27. Heinisch, R. P. and Viskanta, R., "Transient Combined Conduction-Radiation in an Optically Thick Semi-Infinite Medium, AIAA Journal, Vol. 6, 1968, pp. 1409-1411.

28. Hazzah, A. S. and Beck, J. V., "Unsteady Combined Conduction-Radiation Energy Transfer Using a Rigorous Differential Method," Internatinal Journal of Heat and Mass Transfer, Vol. 13, March 1970, pp. 517-522.

29. Lii, C. C. and Özisik, M. N., "Transient Radiation and Conduction in an Absorbing, Emitting and Scattering Slab with Reflecting Boundaries," International Journal of Heat and Mass Transfer, Vol. 15, May 1972, pp. 1175-1179.

30. Weston, K. C. and Hauth, J. L., "Unsteady, Combined Radiation and Conduction in an Absorbing, Scattering and Emitting Medium," Journal of Heat Transfer, Vol. 95, August 1973, pp. 357-364.

31. Sutton, W. H., "A Short Time Solution for Coupled Conduction and Radiation in a Participating Slab Geometry," ASME Paper No. 84-HT-34, 1984.

32. Tiwari, S. N., "Radiative Interactions in Transient Energy Transfer in Gaseous Systems," Progress Report NAG-1-423, Dept. of Mechanical Engineering and Mechanics, College Engineering and Technology, Old Dominion University, Norfolk, VA, December 1985; also NASA-CR-176644 NAS 1.26:176644, December 1985.

33. Tiwari, S. N. and Singh, D. J., "Interaction of Transient Radiation in Nongray Gaseous Systems," Progress Report NAG-1-423, Dept. of Mechanical Engineering and Mechanics, College of Engineering and Technology, Old Dominion University, Norfolk, VA, January 1987; also NASA-CR-181389 NAS 1.26:181389, January 1987.

34. Tiwari, S. N., Singh, D. J. and Kumar, A., "Transient Radiative Energy Transfer in Nongray Gases," AIAA Paper 87-0323, January 1987.

35. Soufiani, A., Hartmann, J. M., and Taine, J., "Validity of Band-Model Calculations for CO_2 and H_2O Applied to Radiative Properties and Conductive-Radiative Transfer," Journal of Quantitative Spectroscopy and Radiative Transfer, Vol. 33, No. 3, March 1985, pp. 243-257.

36. Soufiani, A. and Taine, J., "Application of Statistical Narrow-Band Model to Coupled Radiation and Convection at High Temperature," International Journal of Heat and Mass Transfer, Vol. 30, No. 3, March 1987, pp. 437-447.

37. Penner, S. S. and Varanasi, P., "Effect of (Partial) Overlapping of Spectral Lines on the Total Emissivity of H_2O-CO_2 Mixtures ($T \gtrsim 800$ K)," Journal of Quantitative Spectroscopy and Radiative Transfer, Vol. 6, No. 2, March/April 1966, pp. 181-192.

38. Felske, J. D. and Tien, C. L., "Wide Band Characterization of the Total Band Absorptance of Overlapping Infrared Gas Bands," Combustion Science and Technology, Vol. 11, 1975, pp. 111-117.

39. Tien, C. L. and Lee, S. C., "Flame Radiation," Progress in Energy and Combustion Science, Vol. 8, No. 1, 1982, pp. 41-59.

APPENDIX A

SPECTRAL INFORMATION AND CORRELATION QUANTITIES FOR IMPORTANT INFRARED BANDS

Spectral information and correlation quantities for important infrared bands are available in [7-9]. The exponential band model correlation quantities for important bands of CO, CO_2, H_2O, and CH_4 are given in Table A.1. For some species, revised data are now available in [13].

In developing correlation quantities for different bands, it is important to have information on the integrated band intensity $S(T_0)$ and the band width parameter $A_0(T)$. The band intensities of many molecular bands are available in the literature [7-9, 13, 33] but this is not the case with the band width parameter. Different relations for $A_0(T)$ are proposed by Edwards et al. in references cited in [9]. From a critical evaluation of different relations available in the literature for $A_0(T)$ and after personal communications with Dr. D.K. Edwards, it was decided to adopt the following two relations:

$$A_0(T) = \frac{1}{2}\,\Gamma^2\,\left(\frac{3}{4}\right)\,\left(\frac{4kTB}{hc}\right)^{1/2} \qquad (A.1)$$

$$A_0(T) = 0.9\,\Gamma^2\,\left(\frac{3}{4}\right)\,\left(\frac{2kTB}{hc}\right)^{1/2} \qquad (A.2)$$

where B is the rotational constant of lower level, c is the speed of light, h is the Planck's constant and k is the Boltzmann's constant. The value of B is different for different molecules. Equations (A.1) and (A.2) are

essentially the same except Eq. (A.1) will result in a coefficient of 0.707 instead of 0.9. It is suggested to use Eq. (A.2) in determining approximate relations for $A_o(T)$ for all molecules whose values are not available in the literature. Information on the rotational constants for different molecules is available in the literature (for example, see Ref. 33). It is suggested to use the equivalent value for the rotational constant of polyatomic molecules.

It should be noted that in Eqs. (A.1) and (A.2), B, c, h, and k are constants and do not depend on the temperature. Thus, Eq. (A.2) may be expressed as:

$$A_o(T) = \text{CONST } (T)^{1/2} \tag{A.3a}$$

where

$$\text{CONST} = 0.9\, \Gamma^2 \left(\frac{3}{4}\right) \left(\frac{2kBe}{hc}\right)^{1/2} \tag{A.3b}$$

and B_e represents the equivalent rotational constant. By evaluating Eq. (A.3a) at a reference temperature T_{ref}, the value of $A_o(T_{ref})$ can be determined and, therefore, Eq. (A.3a) may be expressed alternately as:

$$A_o(T) = A_o(T_{ref})\ (T/T_{ref})^{1/2}. \tag{A.4}$$

Equation (A.4) is a convenient form to compare its results with experimental values.

By noting that $\Gamma^2 \left(\frac{3}{4}\right) = [\Gamma\ (3/4)]^2$ and substituting values for c, h, and k, Eq. (A.3) can be expressed as:

$$A_o(T) = 1.59313\ (B_e T)^{1/2} \tag{A.5}$$

where A_o and B_e have units of cm^{-1} and T is in degrees Kelvin. For a particular gas, $A_o\ (T_{ref})$ can be obtained from Eq. (A.5) and then Eq. (A.4) can be used to determine $A_o(T)$ at other temperatures. For example, for CO the rotational constant is 1.931 cm^{-1} and at a reference temperature of 300 K, $A_o(T_{ref} = 300\ K) = 38.344\ cm^{-1}$. This compares very well with the experimental value of 38.1 given if Refs. 7 and 9 and presented in Table A.1. Similarly, for the 4.3 μ band of CO_2, the equivalent rotational constant is 0.3906 cm^{-1} and, therefore, $A_o(T_{ref} = 300\ K) = 17.246\ cm^{-1}$; the experimental value of 19.9 cm^{-1} given in Table A.1 for this band is slightly higher.

Spectral Information for OH

For the fundamental band of OH, the following information is obtained from Ref. 33:

$$\text{Band center, } \omega_c = 3570\ cm^{-1},$$

$$\text{Band strength at STP, } S(T_o) = 110\ cm^{-2}\ atm^{-1}$$

Also, from Ref. 33 the information on equilibrium rotational constant for OH is obtained as:

$$A\ ^2\Sigma^+ \rightarrow 17.355\ cm^{-1}$$

$$X\ ^2\Pi_i \rightarrow 18.871\ cm^{-1}$$

Thus, it is suggested to use a value for the equilibrium rotational constant for OH as $B_e = 18\ cm^{-1}$. Using this, a value of A_o (T_{ref}= 300 K) is found as

$$A_o\ (T_{ref} = 300) = 1.59313\ (B_e T_{ref})^{1/2} = 117.0707. \qquad (A.6)$$

Considering the value of $A_o(T_{ref}) = 117\ cm^{-1}$, the relation for $A_o(T)$ for OH is given as:

$$A_o(T) = 117\ (T/300)^{1/2}. \qquad (A.7)$$

By knowing ω_c, S (T_o), and $A_o(T)$, other required spectral information for OH can be evaluated.

Table A.1 Exponential Band Model Correlation Quantities**

Molecule	Band μ	Band Center cm^{-1}	Pressure Parameters		$A_o(T)$ cm^{-1}	$C_o^2(T)$ $atm^{-1}\ cm^{-1}$	B^2 (T) dimensionless
			b	n			
CO	4.7	2143	1.1	0.8	38.1 $K_1(T)$	6.24 $K_2(T)$	0.314 $\delta_1(T)$
	2.35	4260	1.0	0.8	38.1 $K_1(T)$	0.042 $K_2(T)$	0.300 $\delta_1(T)$
CO_2	15	667	1.3	0.7	22.3 $K_1(T)$	15.2 $K_2(T)$	0.084 K_1 (T)
	4.3*	2350	1.3	0.8	19.9 $K_1(T)$	98.7 $K_2(T)$	0.329 $K_1(T)$
	2.7	3715	1.3	0.65	41.6 $K_1(T)$	1.72 $K_2T)\phi_2(T)$	0.111$\delta_2(T)$
H_2O	I.R	500	5.0	1.0	49.4 $K_1(T)$	771 $K_2(T)\phi_7(T)$	0.073/$K_1(T)$
	6.3	1600	5.0	1.0	90.1 $K_1(T)$	3.35 $K_2(T)$	0.130/$K_1(T)$
	2.7	3750	5.0	1.0	112.6 $K_1(T)$	1.52 $K_2(T)$	0.145/K_1 (T)
	1.87	5350	5.0	1.0	79.7 $K_1(T)$	0.276 $K_2(T)\phi_{101}(T)$	0.118/$K_1(T)$
	1.38	7250	5.0	1.0	79.7 $K_1(T)$	0.230 $K_2(T)\phi_{101}(T)$	0.201/$K_1(T)$
CH_4	7.6	1310	1.3	0.8	39.8 $K_1(T)$	4.58 $K_2(T)$	0.067 $K_1(T)$
	3.3	3020	1.3	0.8	95.3 $K_1(T)$	3.15 $K_2(T)$	0.036 $K_1(T)$

**Notes on Table A.1. (See next page)

1. Correlation quantities are based on the results of reference [9]. The intensity of the band marked with * was taken from the reference [7].

2. Notations: $K_1(T) = (T/300)^{1/2}$, $K_2(T) = (300/T)^{3/2}$,

$\delta_1 = [\phi_1{}^2(T)/K_1(T)] \times 10^{-3}$, $\delta_2 = \phi_3{}^2(T)/[\phi_2(T)K_1(T)]$

$h = 6.625 \times 10^{-27}$ erg-sec, $C = 2.998 \times 10^{10}$ cm/sec,

$k = 1.380 \times 10^{-16}$ erg/K , $hC/k \approx 1.44$ cm - K

3. Temperature range: $300\ K < T < T_{max}$. For CO, $T_{max} = 1800$ K.

For CO_2, $T_{max} = 1400$ K. For H_2O, $T_{max} = 1100$ K. For CH_4,

$T_{max} = 830$ K.

4. For CO, $\omega = 2143\ cm^{-1}$ and

$\phi_1(T) = [15.15 + 0.22\ (T/T_o)^{3/2}]\ [1-\exp\ (-hC\omega/kT)]$, $T_o = 100$ K

5. For CO_2, $\omega_1 = 1351\ cm^{-1}$, $\omega_2 = 667\ cm^{-1}$, $\omega_3 = 2396\ cm^{-1}$

$\phi_2(T) = \{1 - \exp\ [(\ -\ hC/KT\ )\ (\omega_1 + \omega_3)]\}x$

$\{[1 - \exp\ (\ -\ hC\omega_1/kT)]\ [1 - \exp\ (-hC\omega_3/kT)]\}^{-1}$, $\phi_3(T) = 1 +$

$0.053\ (T/100)^{3/2}$

6. For H_2O, $\omega_1 = 3652\ cm^{-1}$, $\omega_2 = 1595\ cm^{-1}$, $\omega_3 = 3756\ cm^{-1}$

$$\phi_{v_1\ v_2\ v_3}(T) = \{1 - \exp[-hC(v_1\ \omega_1 + v_2\ \omega_2 + v_3\ \omega_3)/kT]\} \times$$

$$\{[1-\exp(-hC\omega_1/kT)]\ [1-\exp(-hC\omega_2/kT]\ [1-\exp(-hC\omega_3/kT]\}^{-1}$$

$$\phi_7(T) = \exp[-17.6\ (T/100)^{-1/2}]$$

APPENDIX B

RESULTS OF THE QUARTIC FORMULATION

Extensive results of the quartic formulation are presented in this appendix. The order of presentation of results is θ vs. τ, θ vs. ζ, and θ_b vs. L. The order of results for the four species considered is OH, CO, CO_2, and H_2O. Information on other physical conditions is provided on each figure. The notations used in these figures correspond to the notations used in the main text according to the following relations:

LARGE PATH = LARGE PATH LENGTH

OPT THIN = OPTICALLY THIN

TBULK = $\theta_b = (T_w - T_b)/(q_w L/K)$

THETA = $\theta = (T_w - T)/q_w L/K)$

T = τ

TW = T_w

Z = ζ

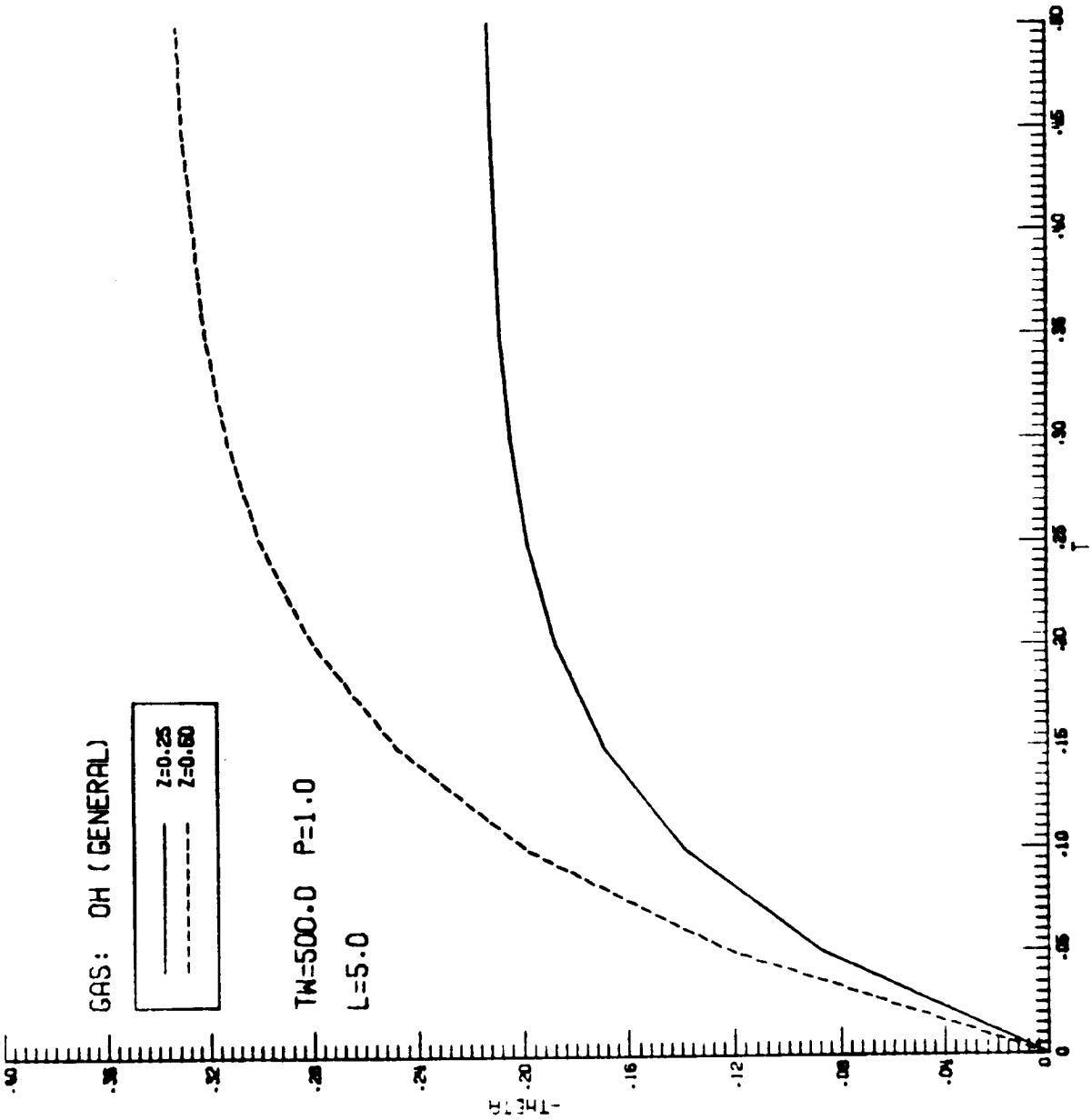

Figure B.1. Results for temperature variation with time (θ vs. τ) for OH.

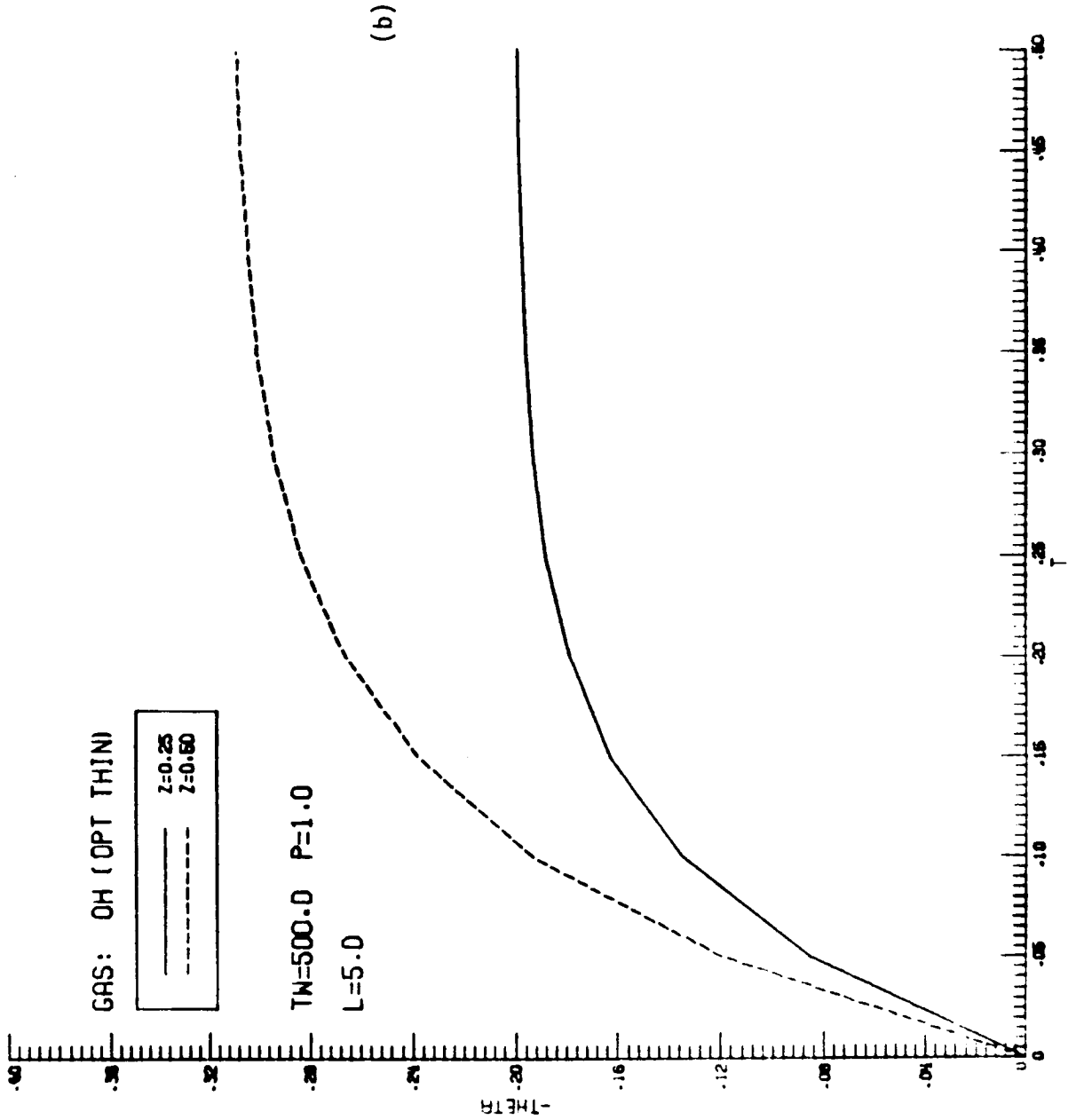

Figure B.1. (continued)

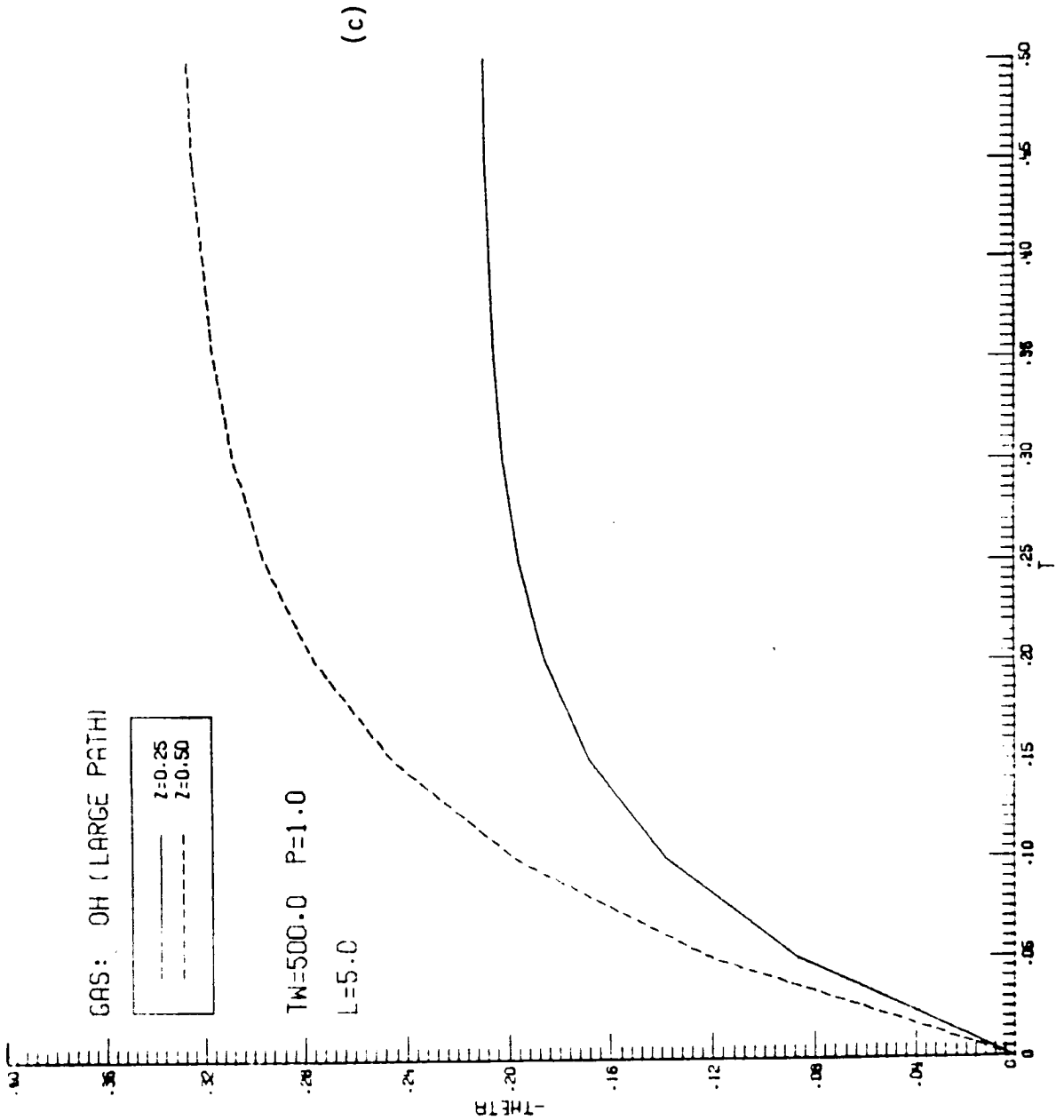

Figure B.1. (continued)

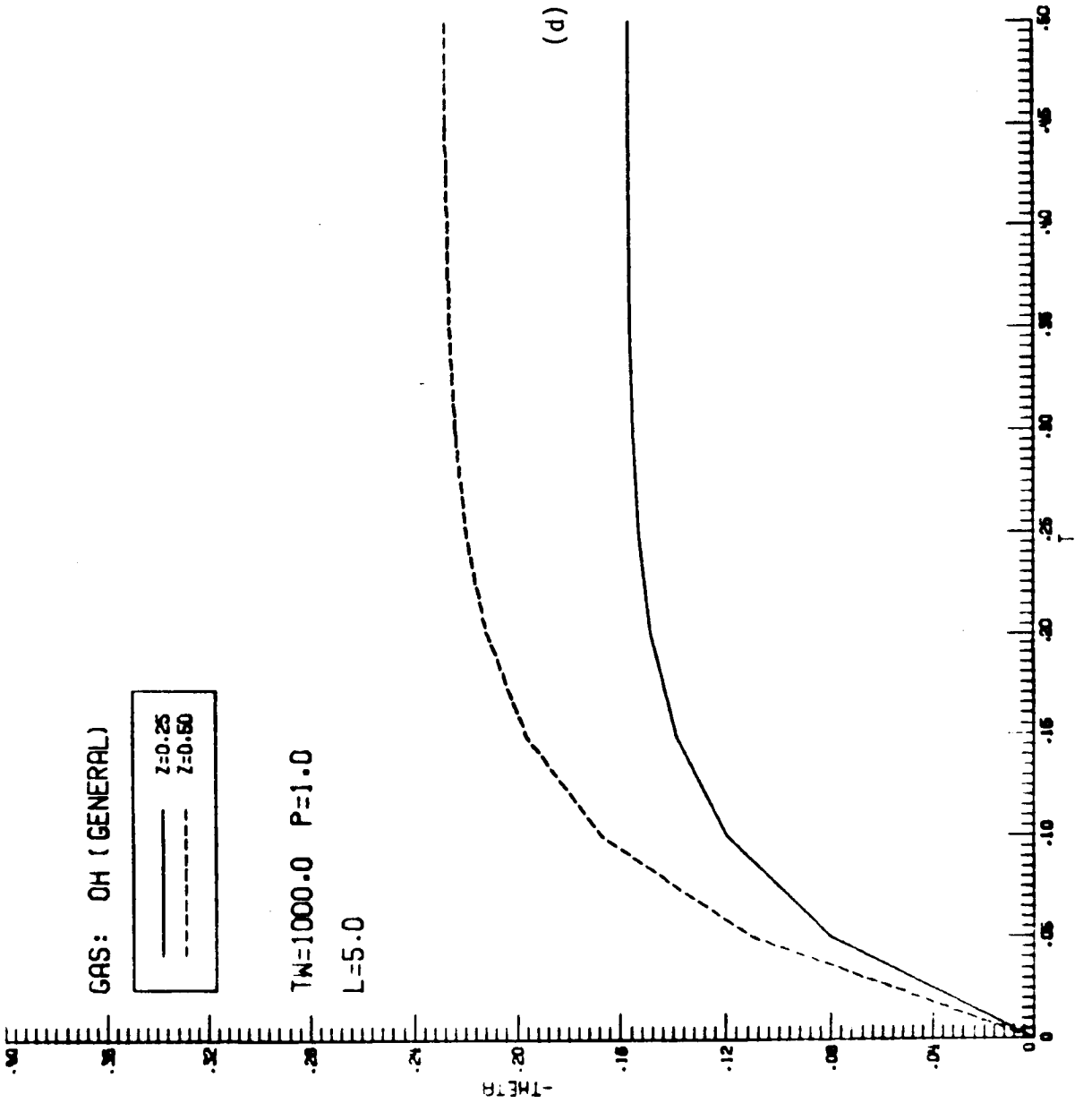

Figure B.1. (continued)

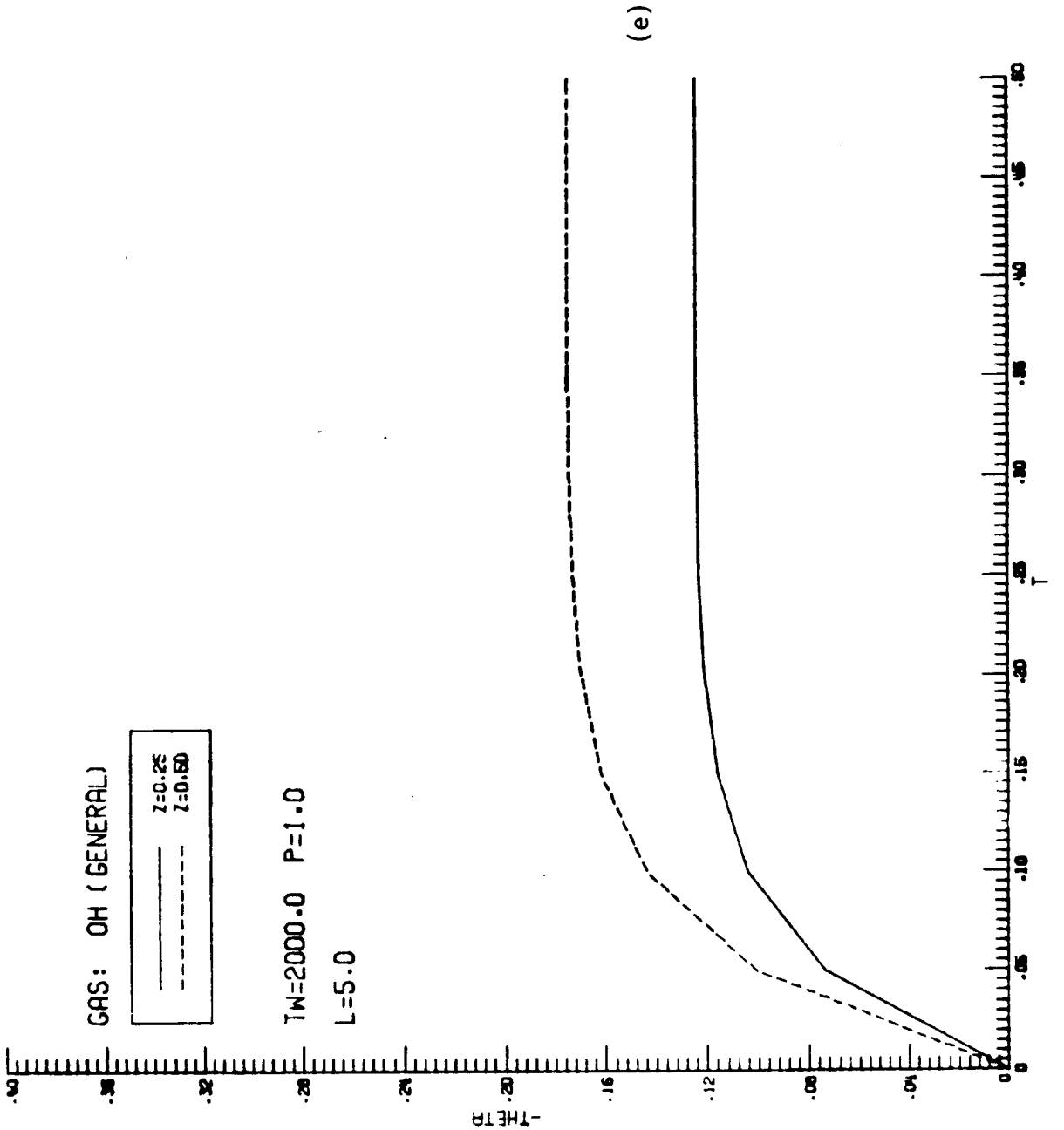

Figure B.1. (continued)

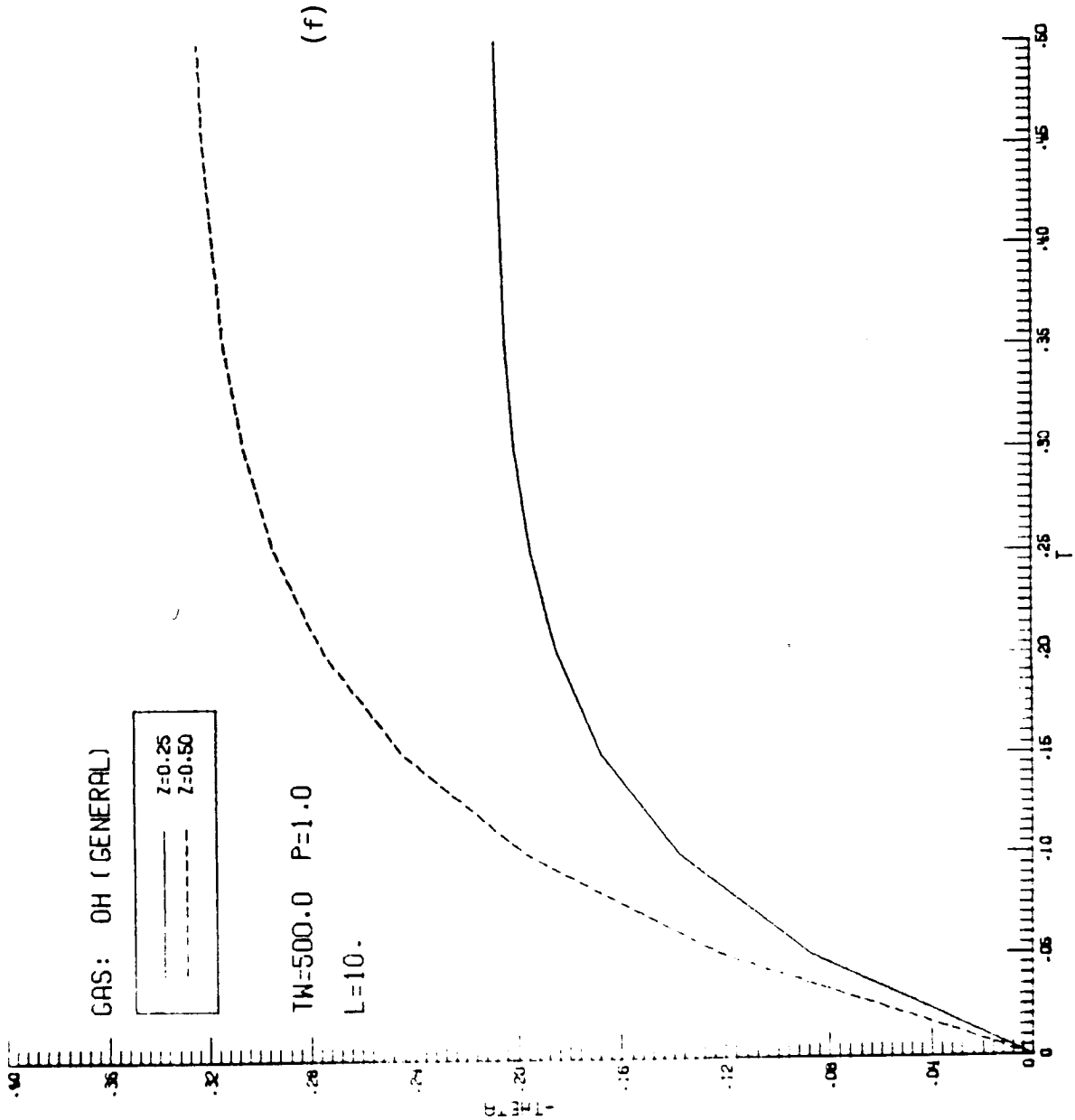

Figure B.1. (continued)

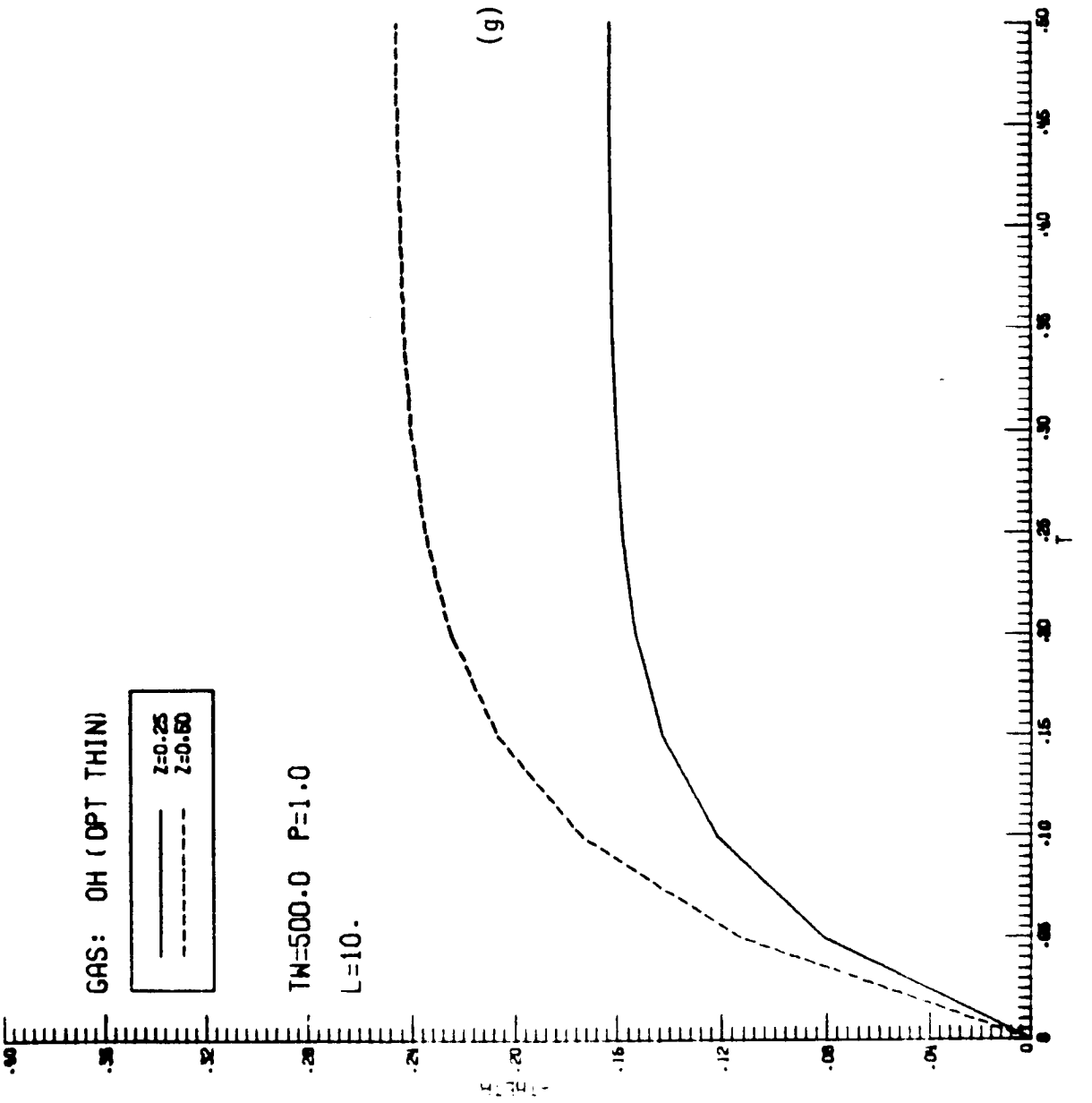

Figure B.1. (continued)

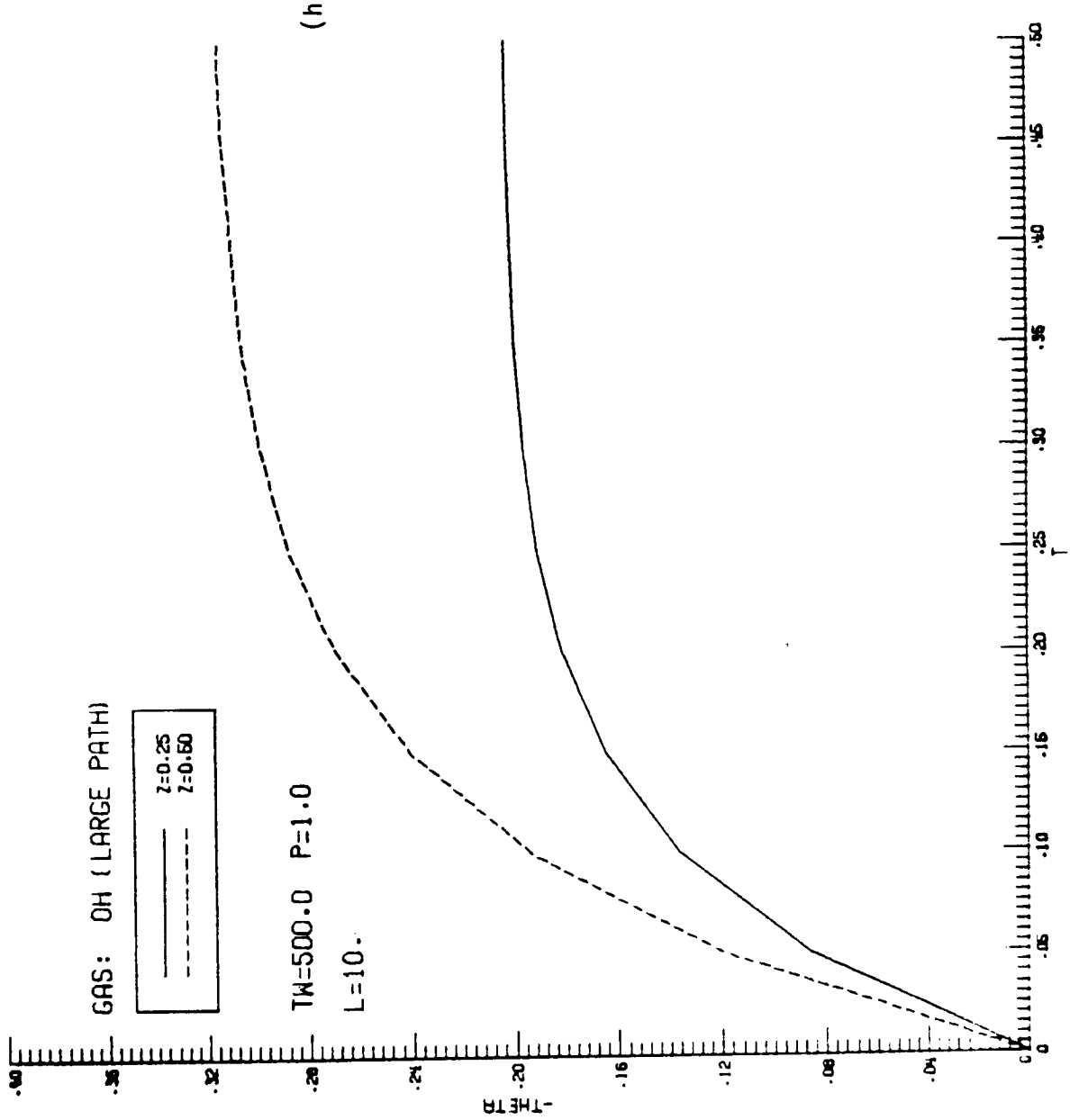

Figure B.1. (continued)

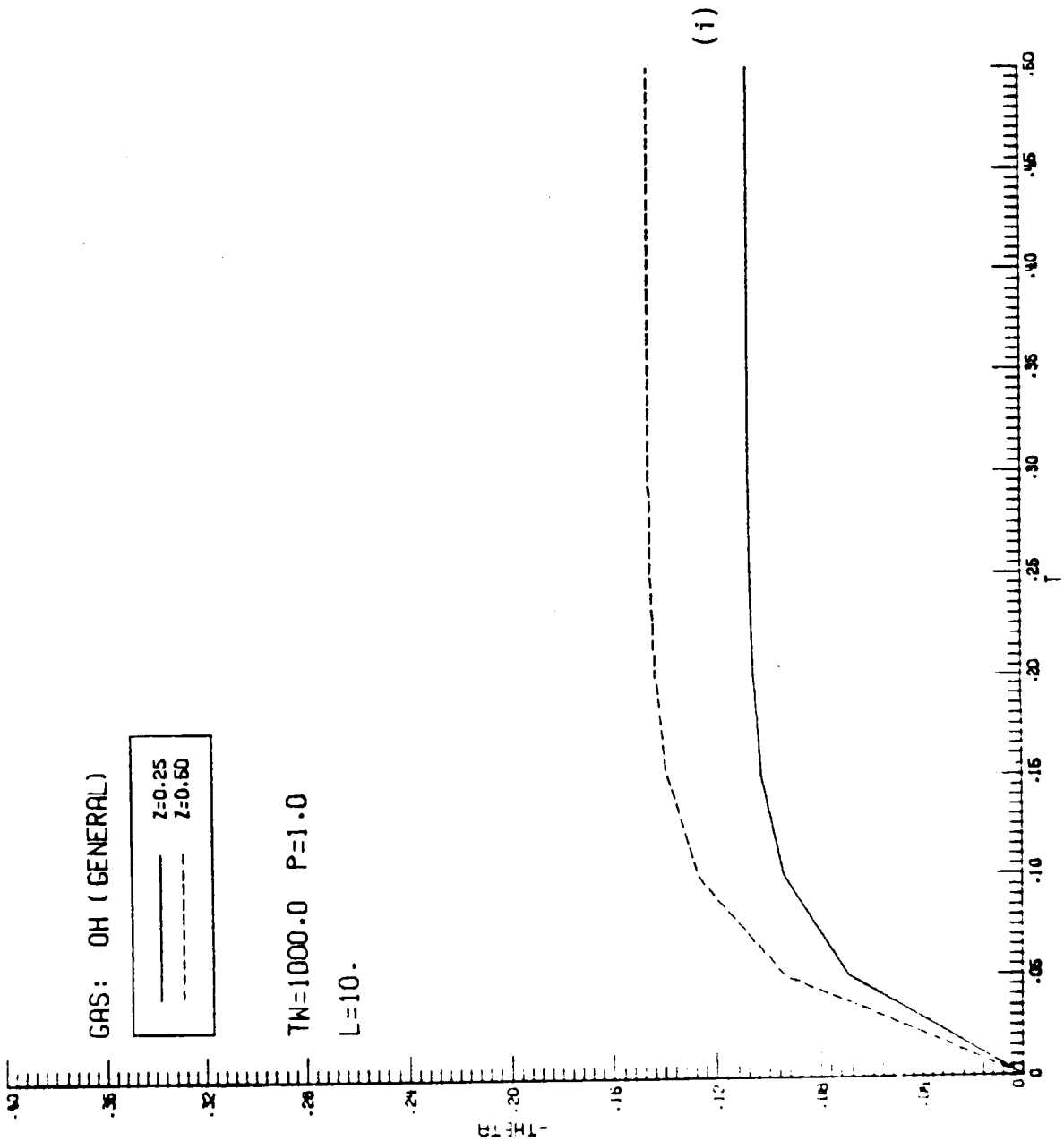

Figure B.1. (continued)

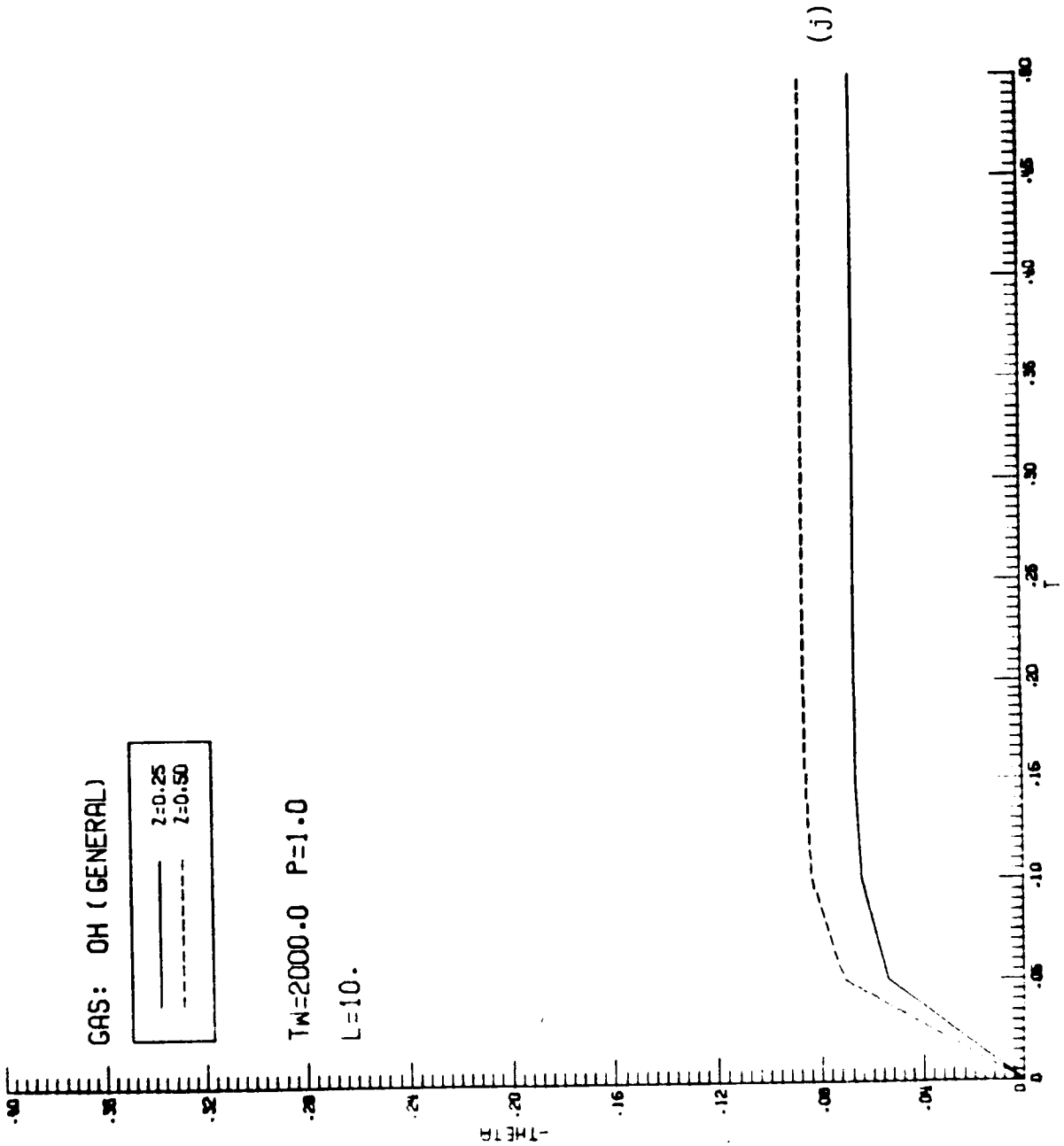

Figure B.1. (continued)

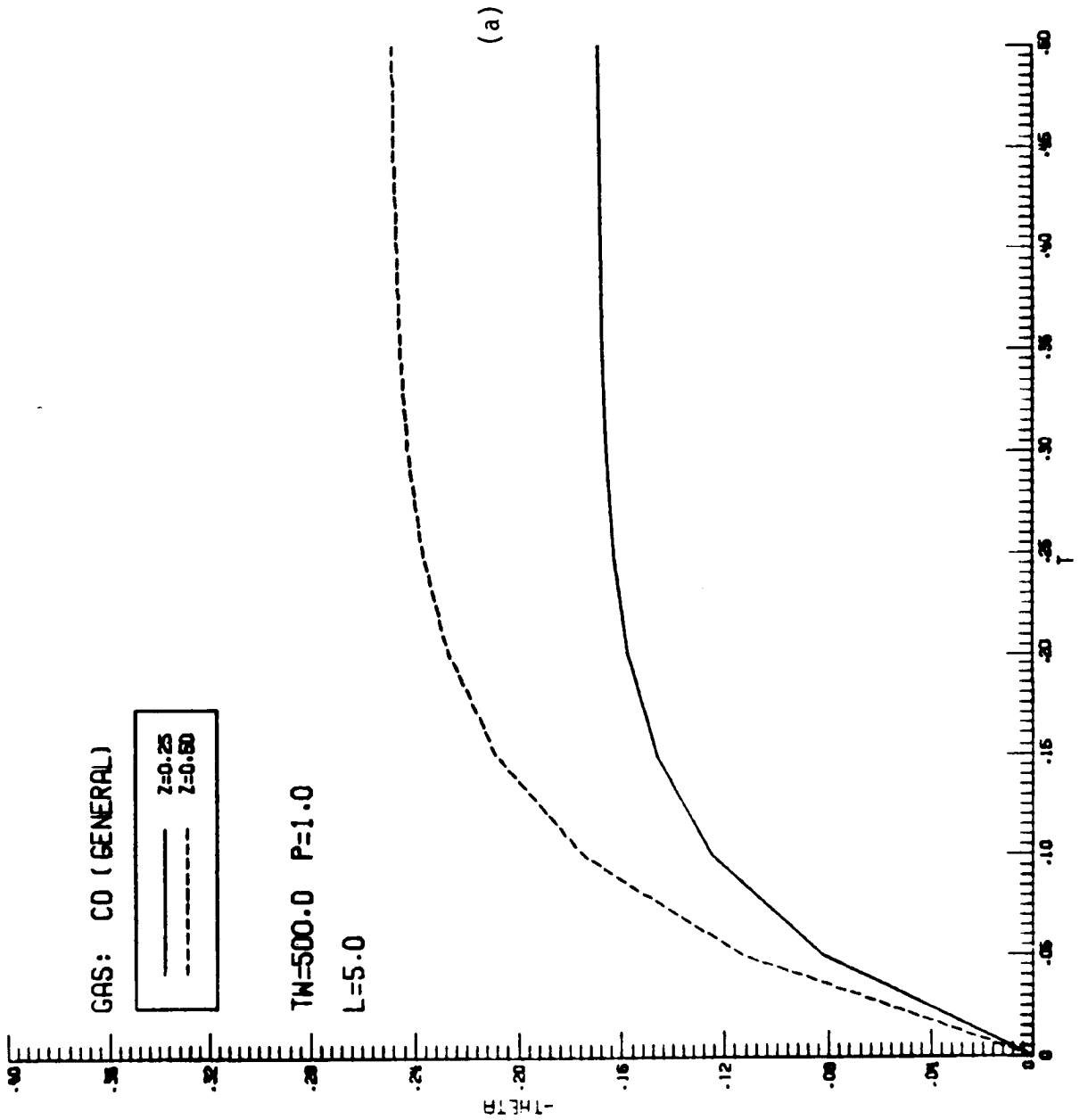

Figure B.2. Results for temperature variation with time (θ vs. τ) for CO.

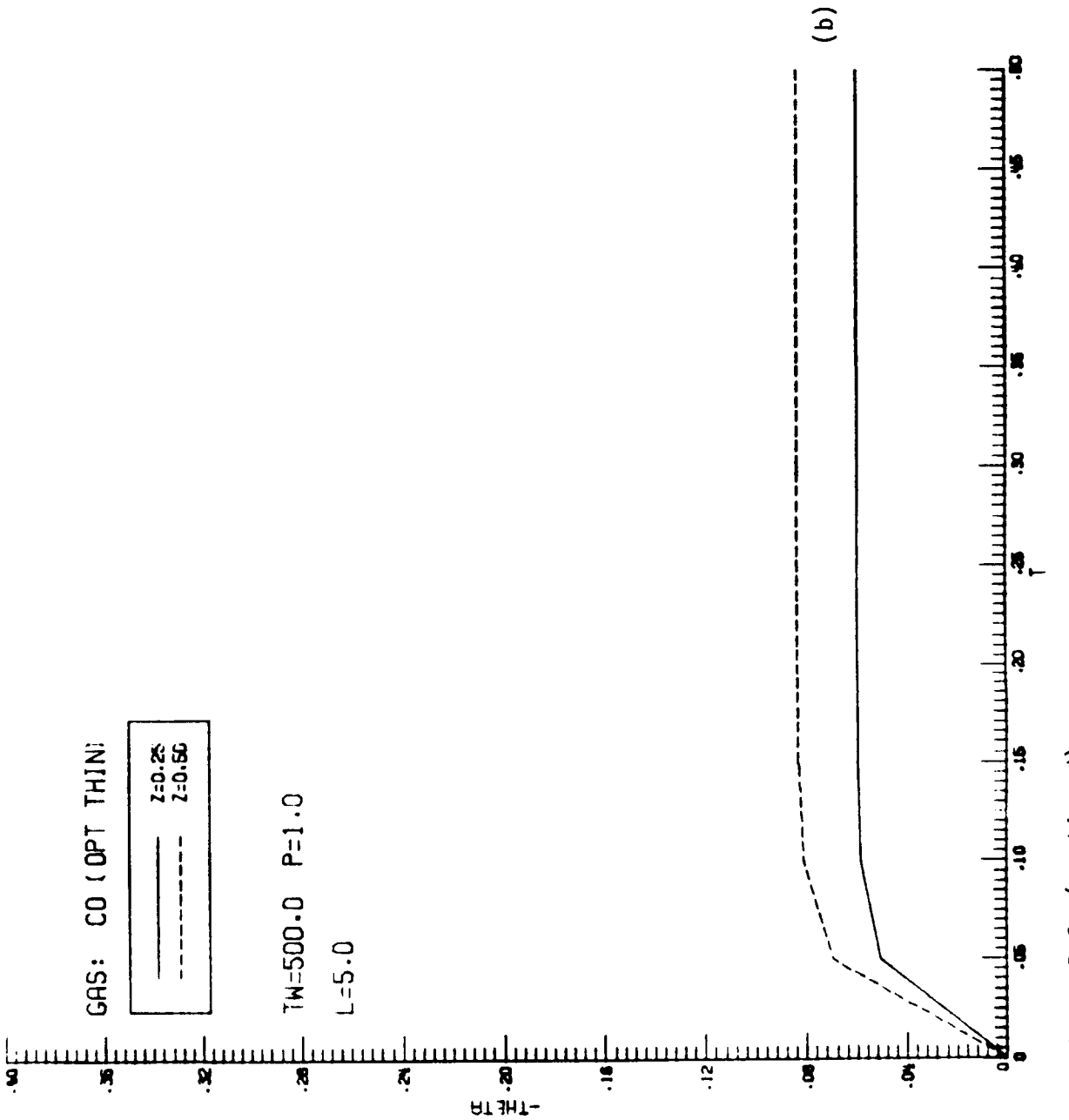

Figure B.2. (continued)

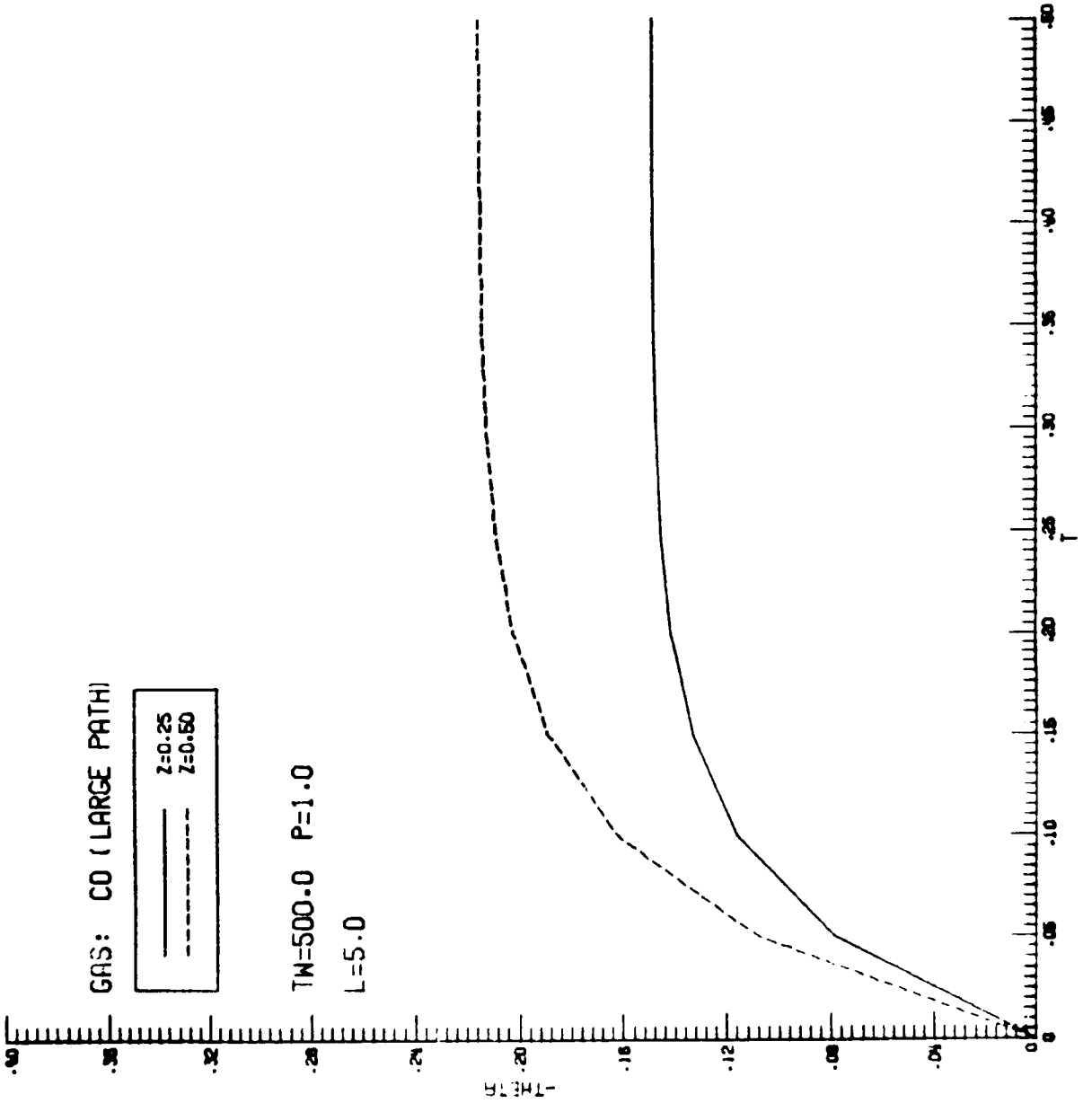

(c)

Figure B.2. (continued)

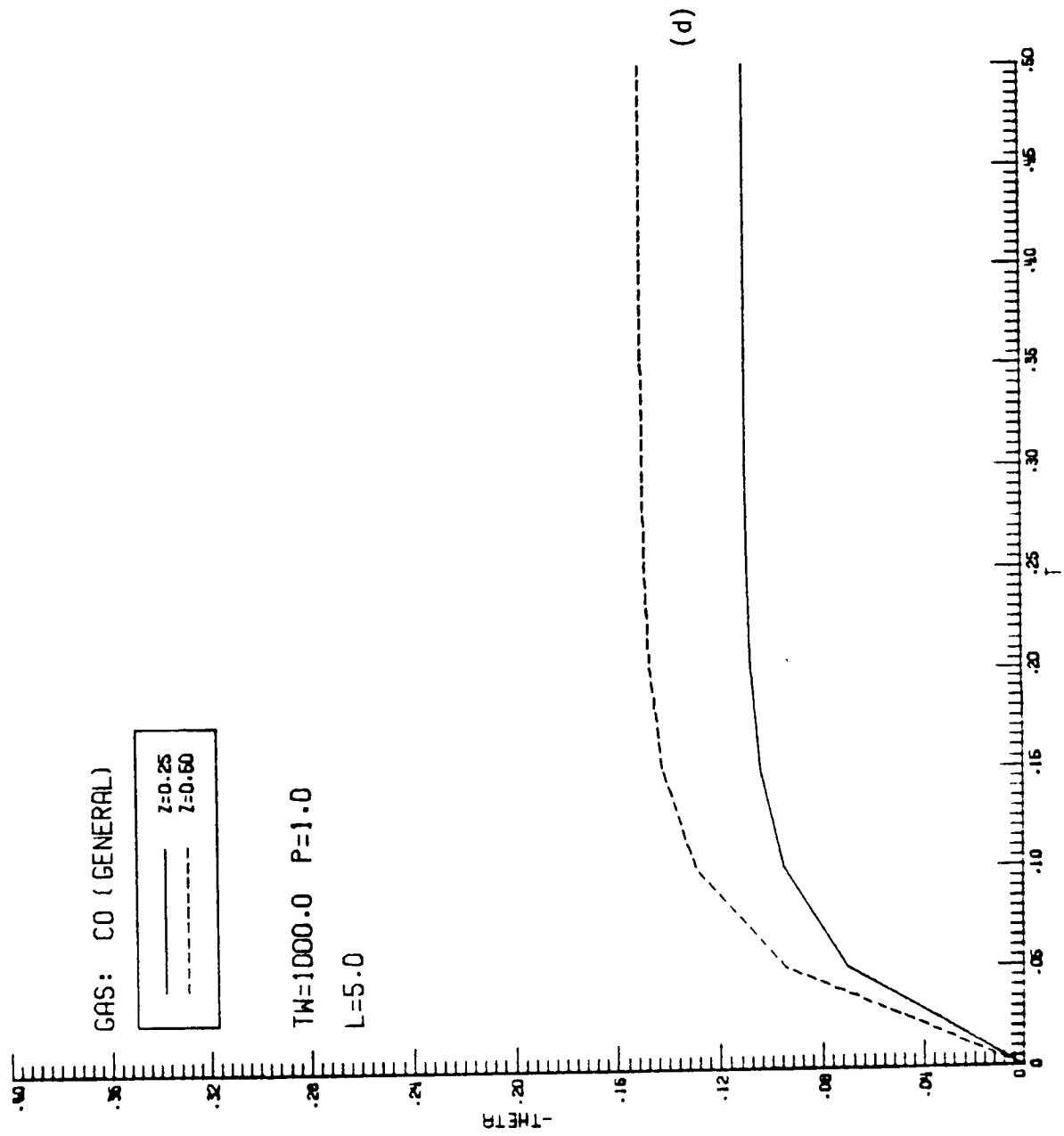

Figure B.2 (continued)

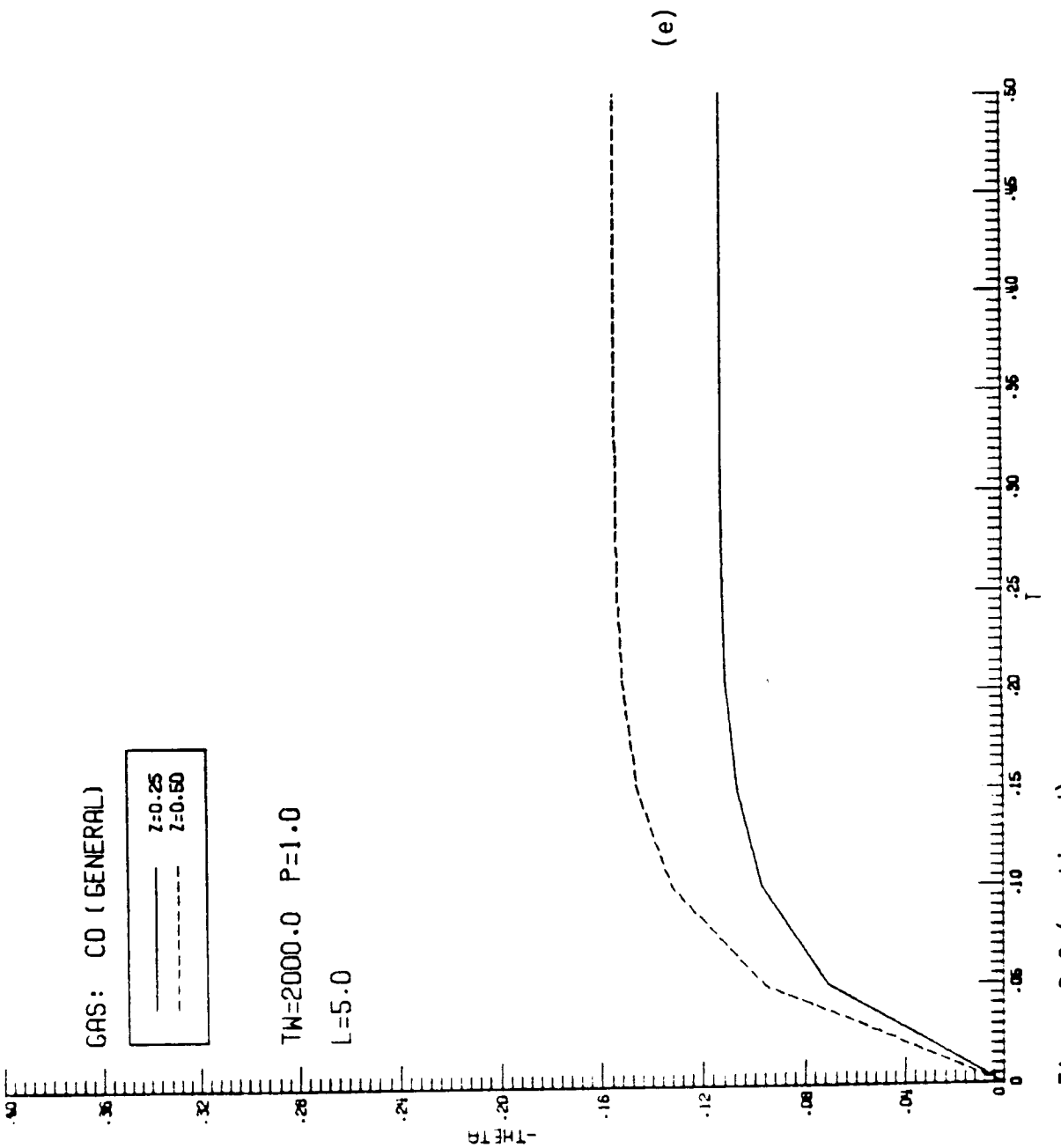

Figure B.2 (continued)

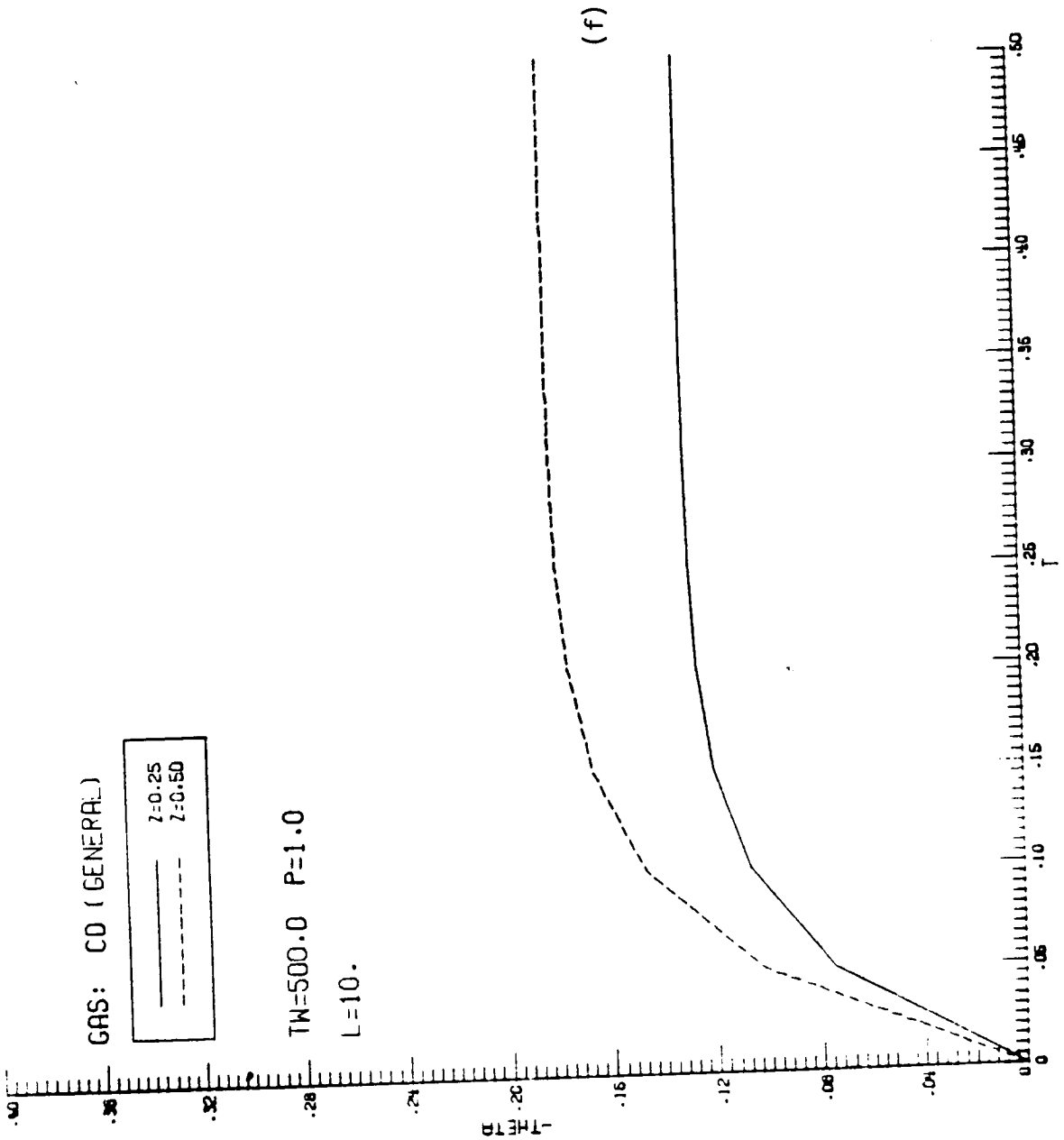

Figure B.2 (continued)

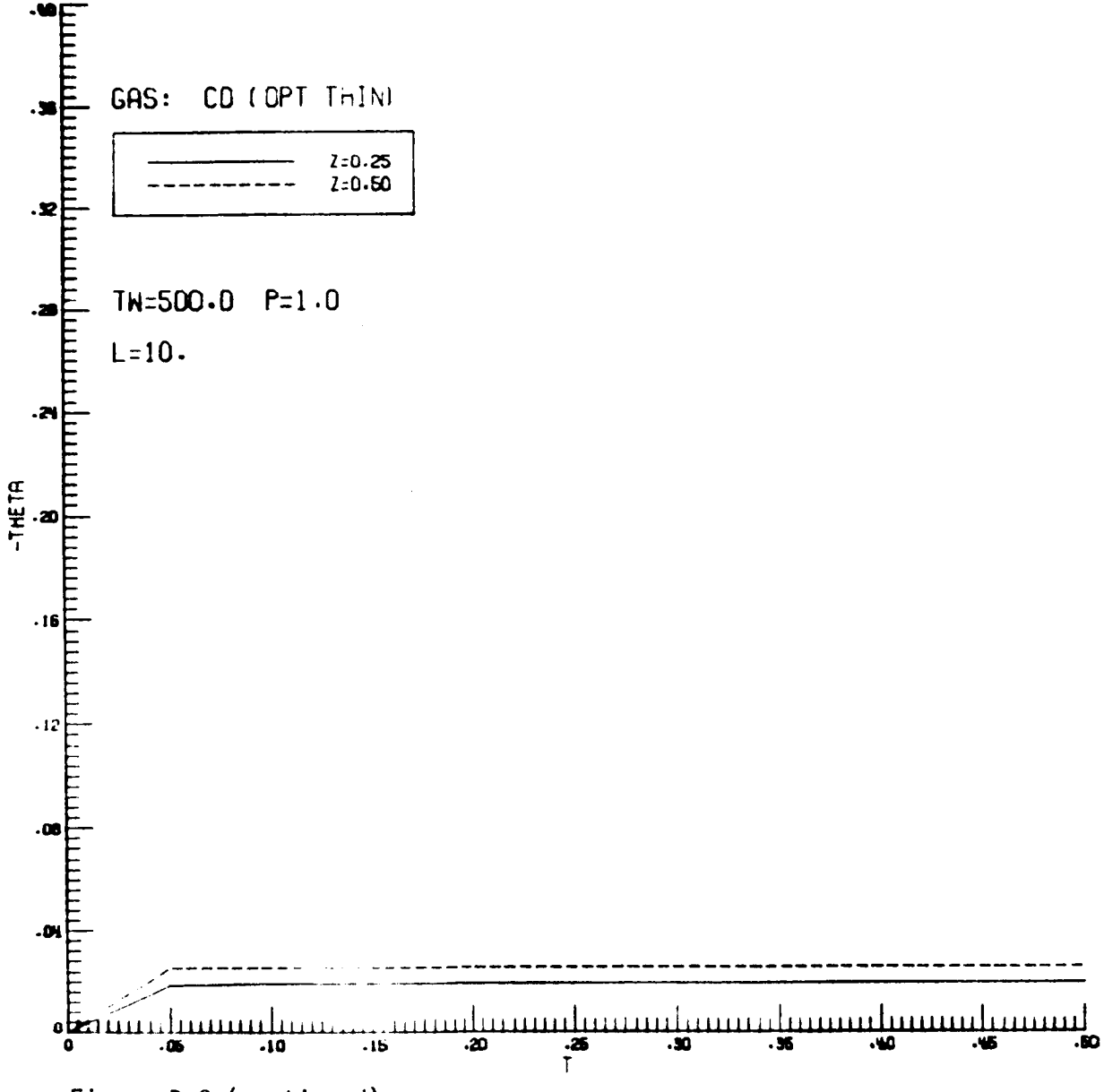

(g)

Figure B.2 (continued)

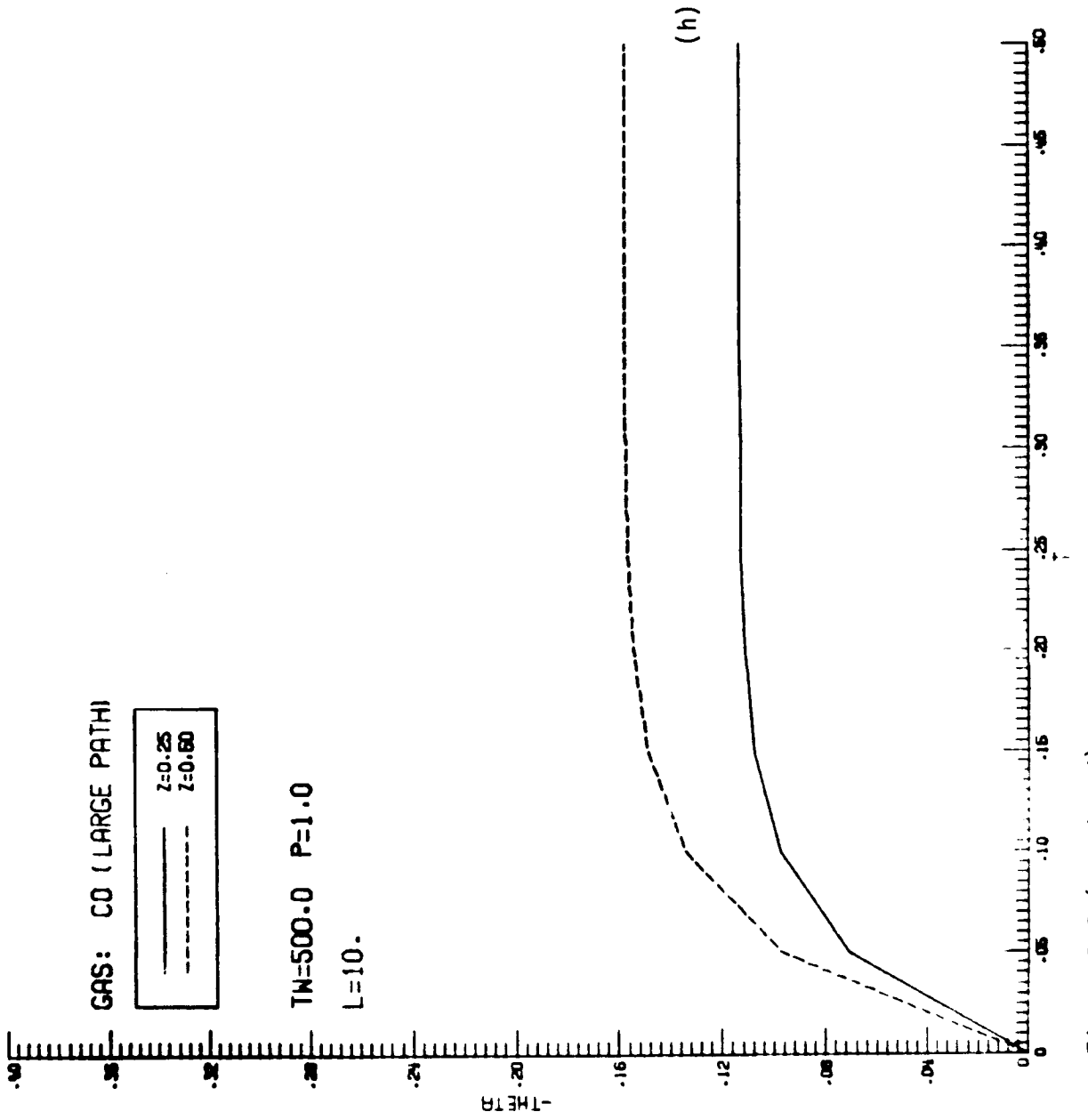

Figure B.2 (continued)

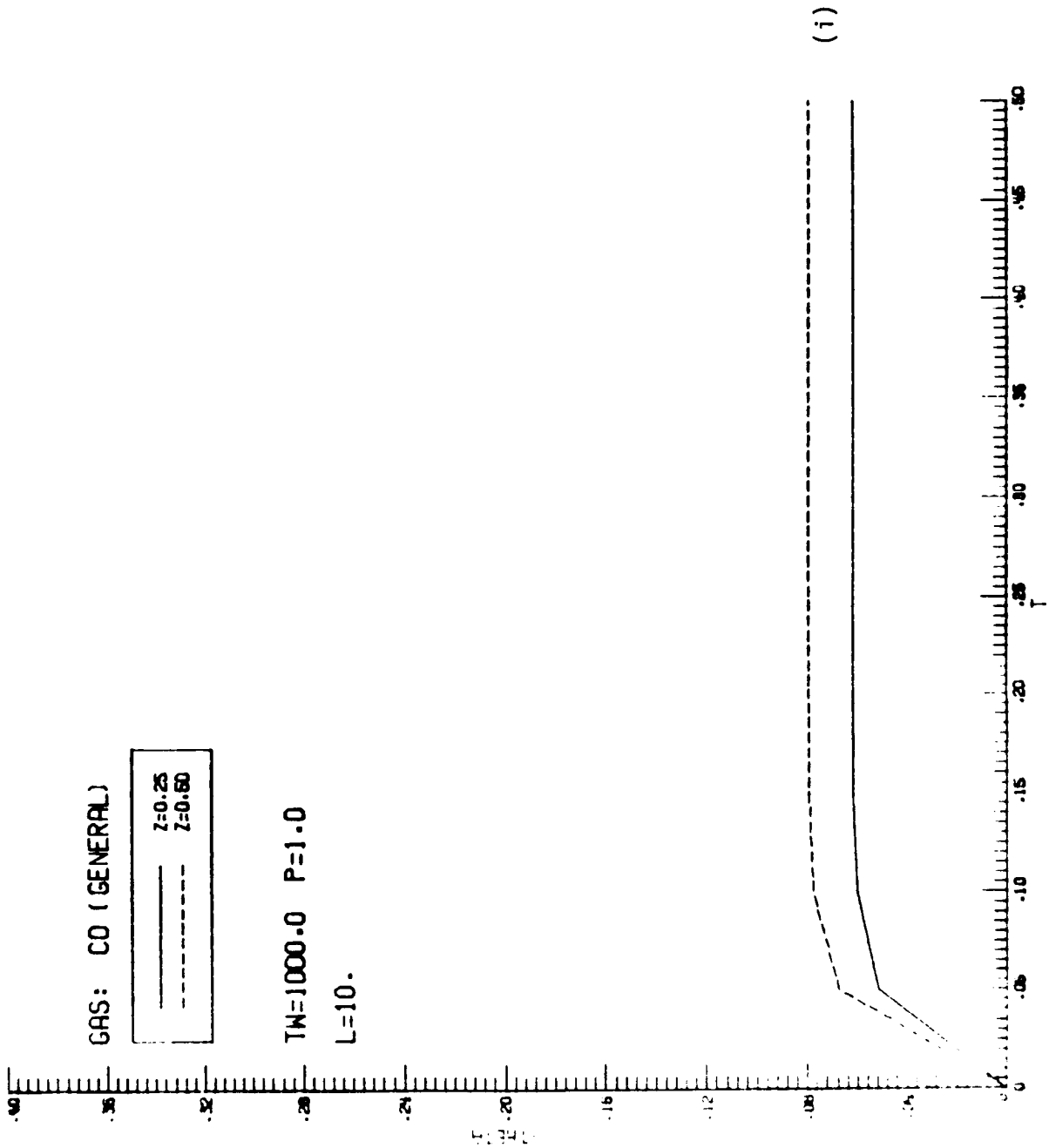

Figure B.2 (continued)

C-2

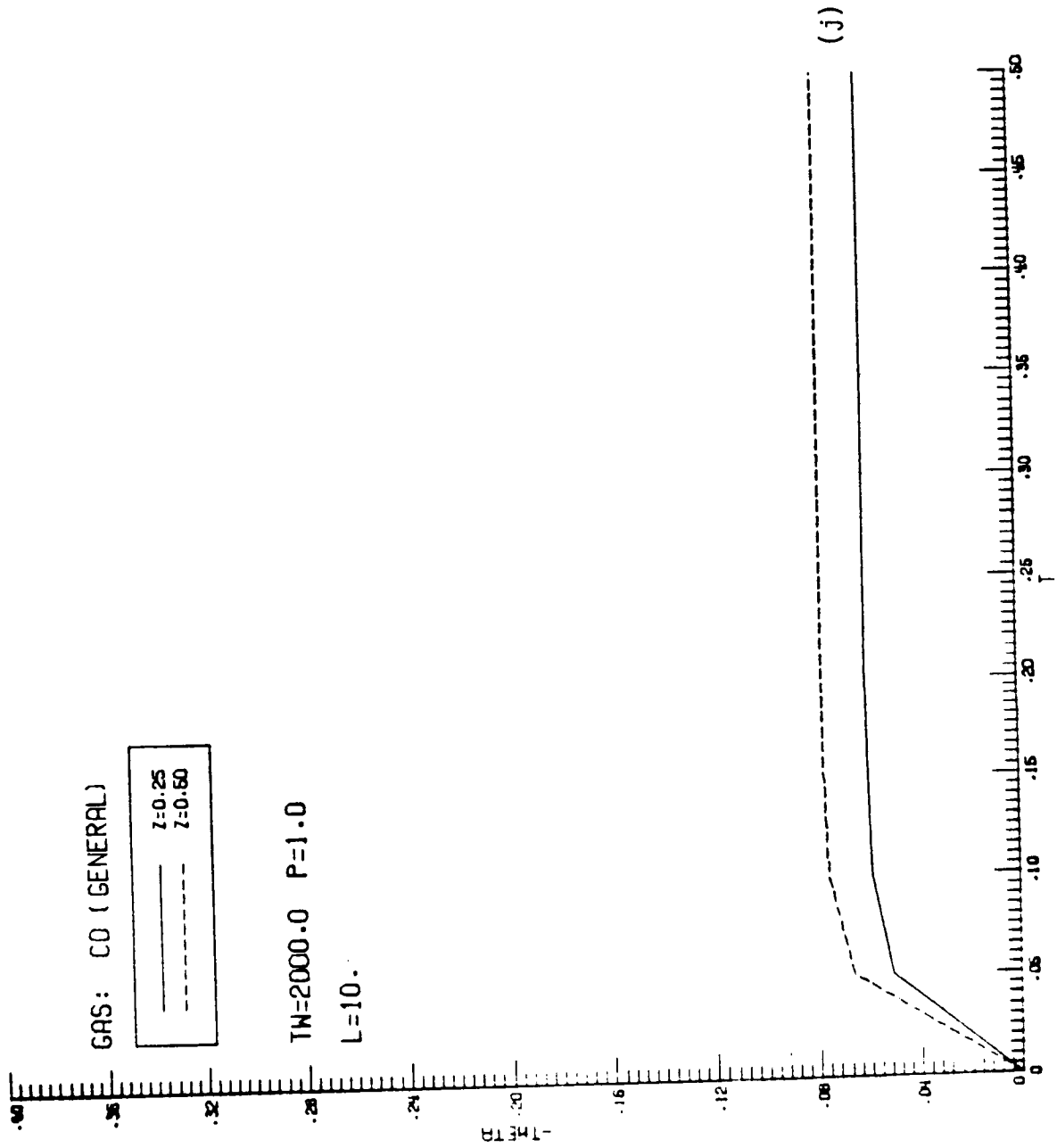

Figure B.2 (continued)

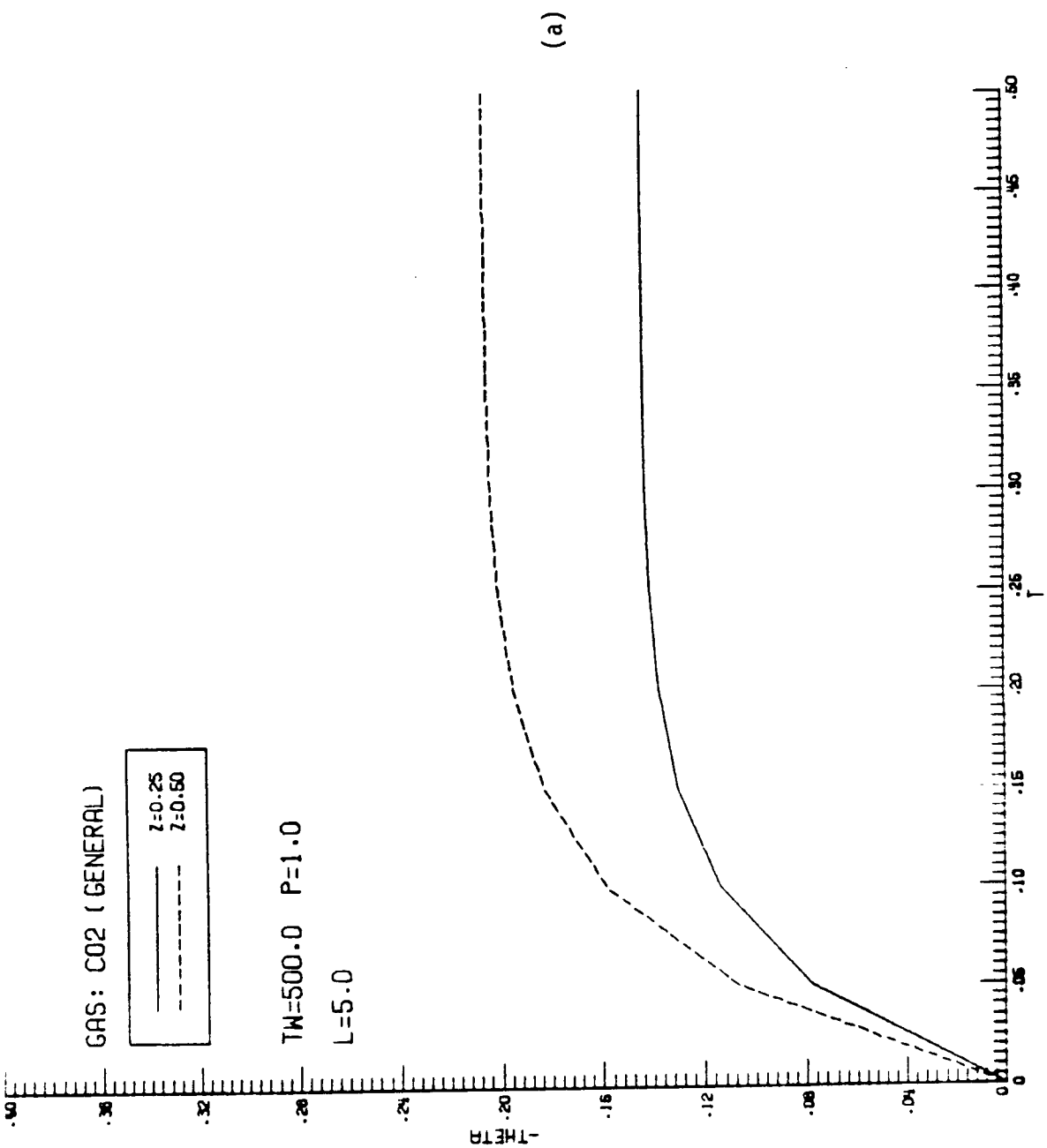

Figure B.3. Results for temperature variation (θ vs. τ) for CO_2.

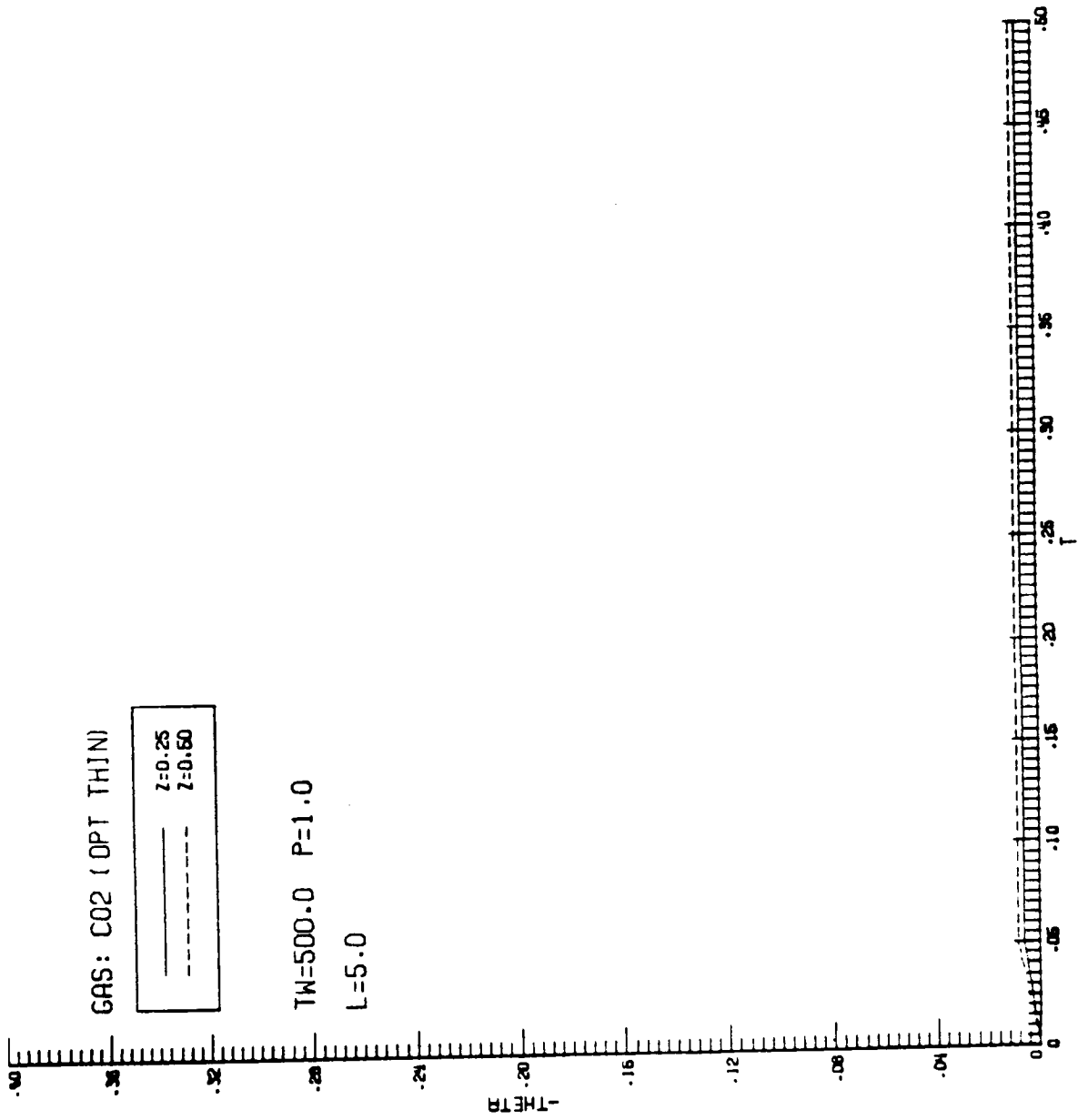

(b)

Figure B.3 (continued)

The results for temperature variations within the plates are presented in Figs. 10-14 for different conditions. Since the temperature profiles are symmetric, most of these results are illustrated only for $\xi = 0$ to $\xi = 0.5$. The stady-state solutions for various species are compared in Fig. 10 for P = 1 atm, L = 10 cm, and different wall temperatures. Results again demonstrate the relative importance of different species for energy transfer. It is noted that the results for CO_2 at T_w = 500 K are exactly the same as for OH at T_w = 1,000 K, and the results for CO and H_2O are about the same at T_w = 1,000 K and 2,000 K. This obviously is a coincidence for the physical case considered. The general and limiting solutions for OH, CO, CO_2, and H_2O are presented, respectively, in Figs. 11 through 14a for T_w = 500 K, P = 1 atm, and L = 10 cm. These results also show that the steady-state conditions reach earlier for H_2O and CO_2 than for CO and OH. In general, the differences between limiting and general solutions are found to be small at earlier times; the maximum difference occurs at the steady-state conditions. In each case, the large path length solutions are closer to the general solutions, but the optically thin solutions are found to deviate considerably. This is because for P = 1 atm and L = 10 cm, the pressure path length is sufficiently high and the optically thin limit is not the correct limit for the physical case considered. It should be noted that for CO, CO_2, and H_2O, the optically thin solutions are identical for $\tau > 0.05$. Additional results given in Appendix B reveal that the differences between general and large path length solutions are insignificant at higher temperatures for all species. The general solutions for the temperature variation across the entire duct are illustrated in Fig. 14b for H_2O for the physical conditions of T_w = 1,000 K, P = 1 atm, and L = 5 cm. The parabolic nature of the transient profiles is clearly evident and, in this case, the steady-state is reached at $\tau > 0.5$.

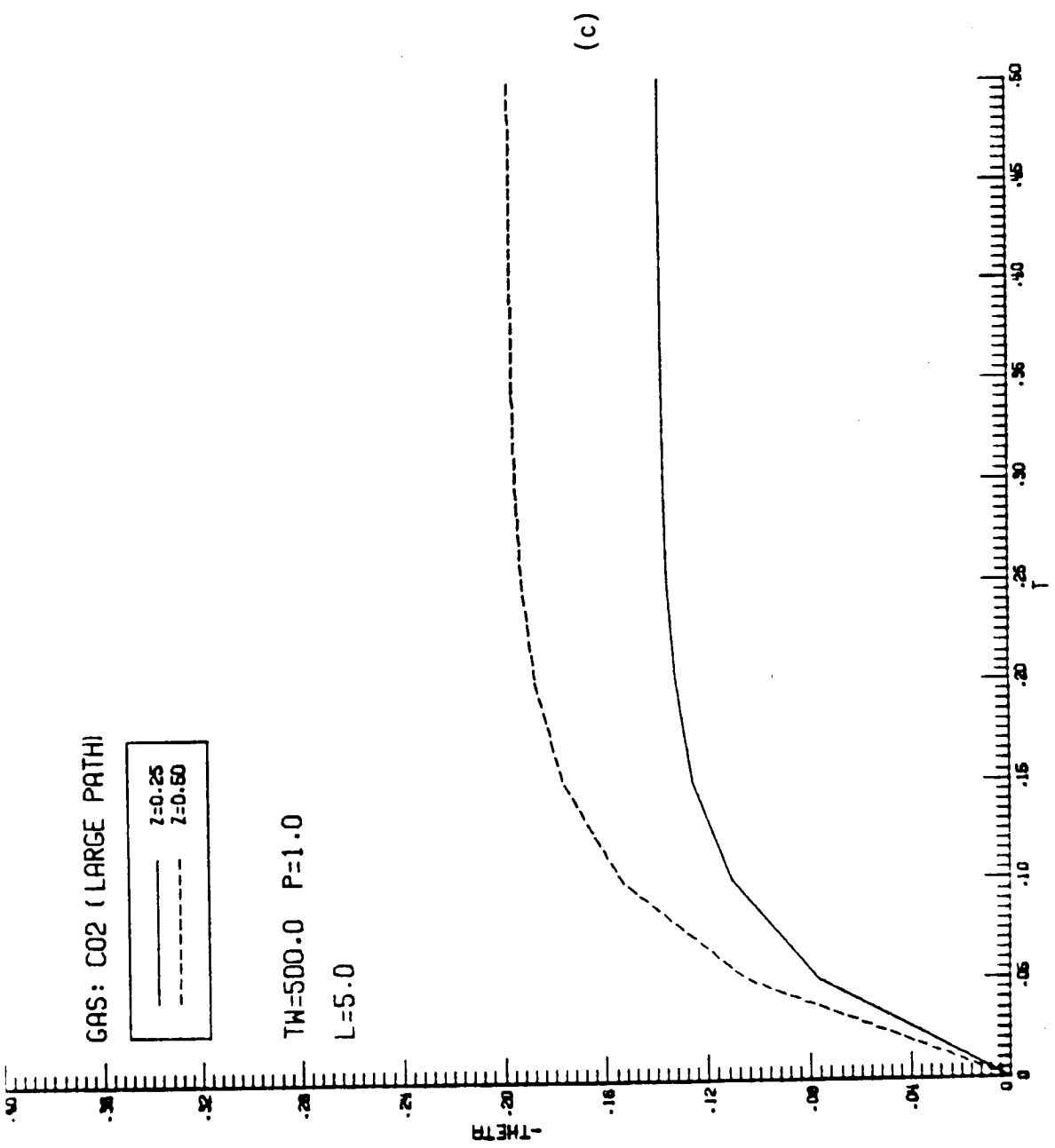

Figure B.3 (continued)

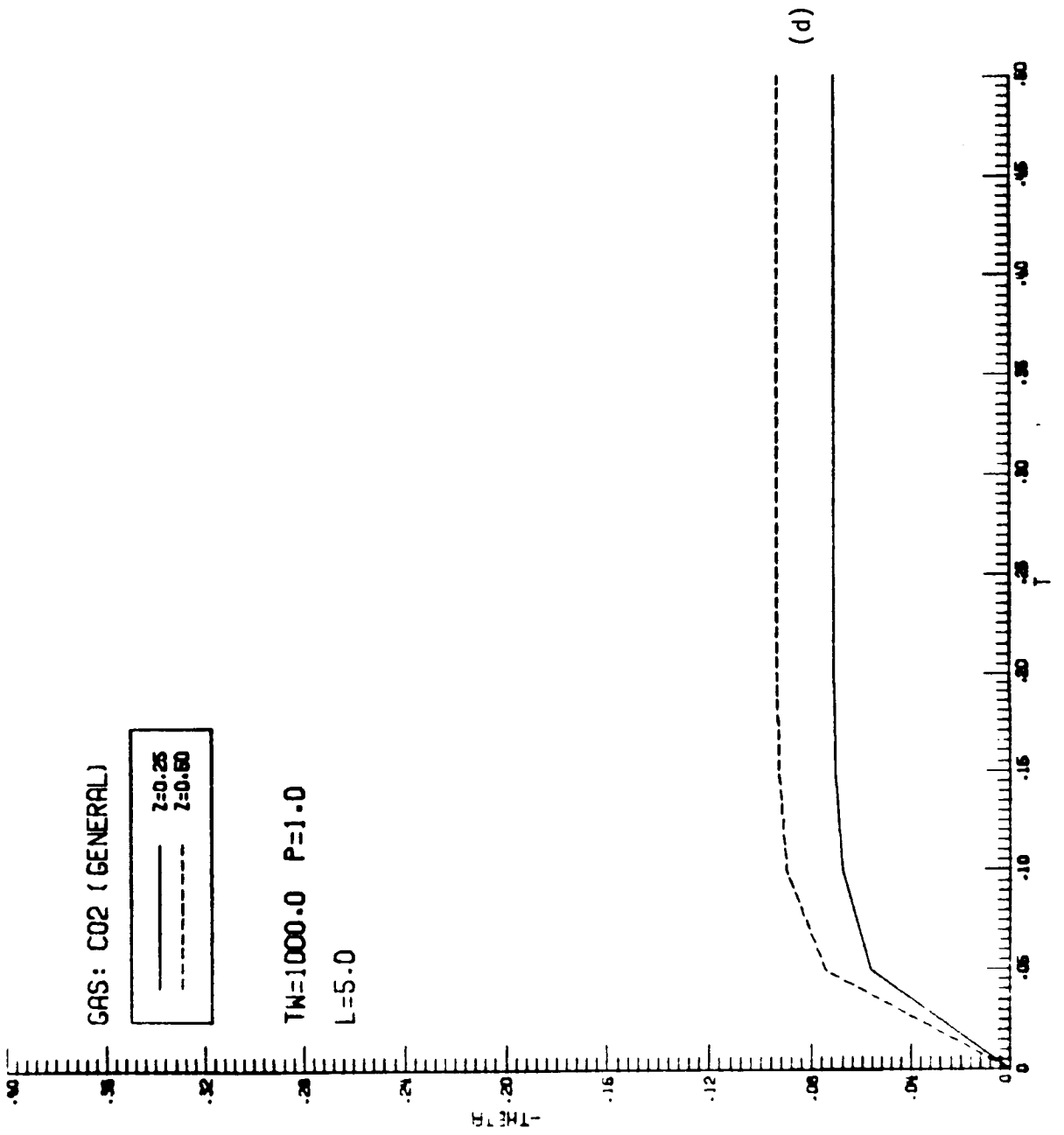

Figure B.3 (continued)

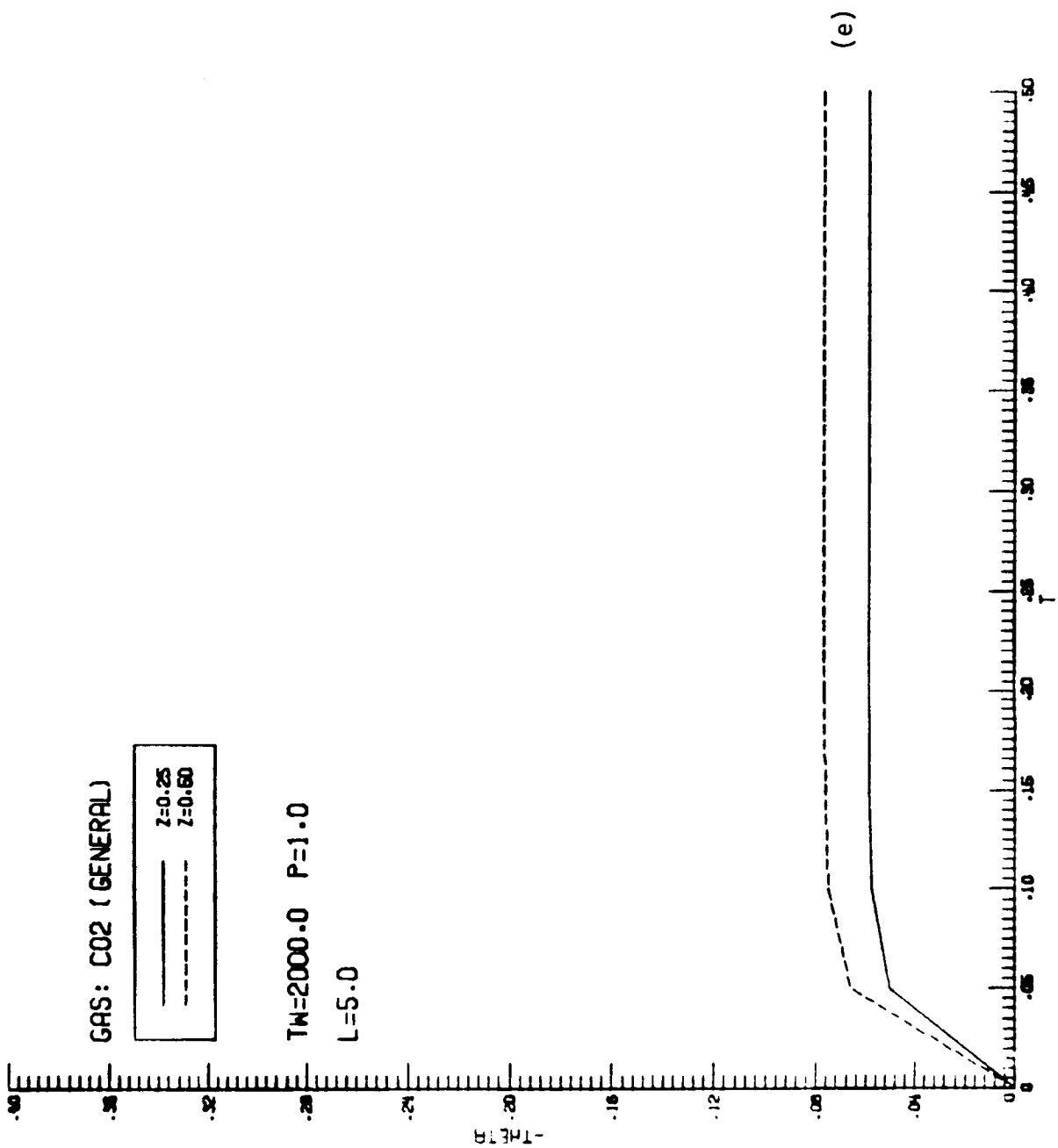

Figure B.3 (continued)

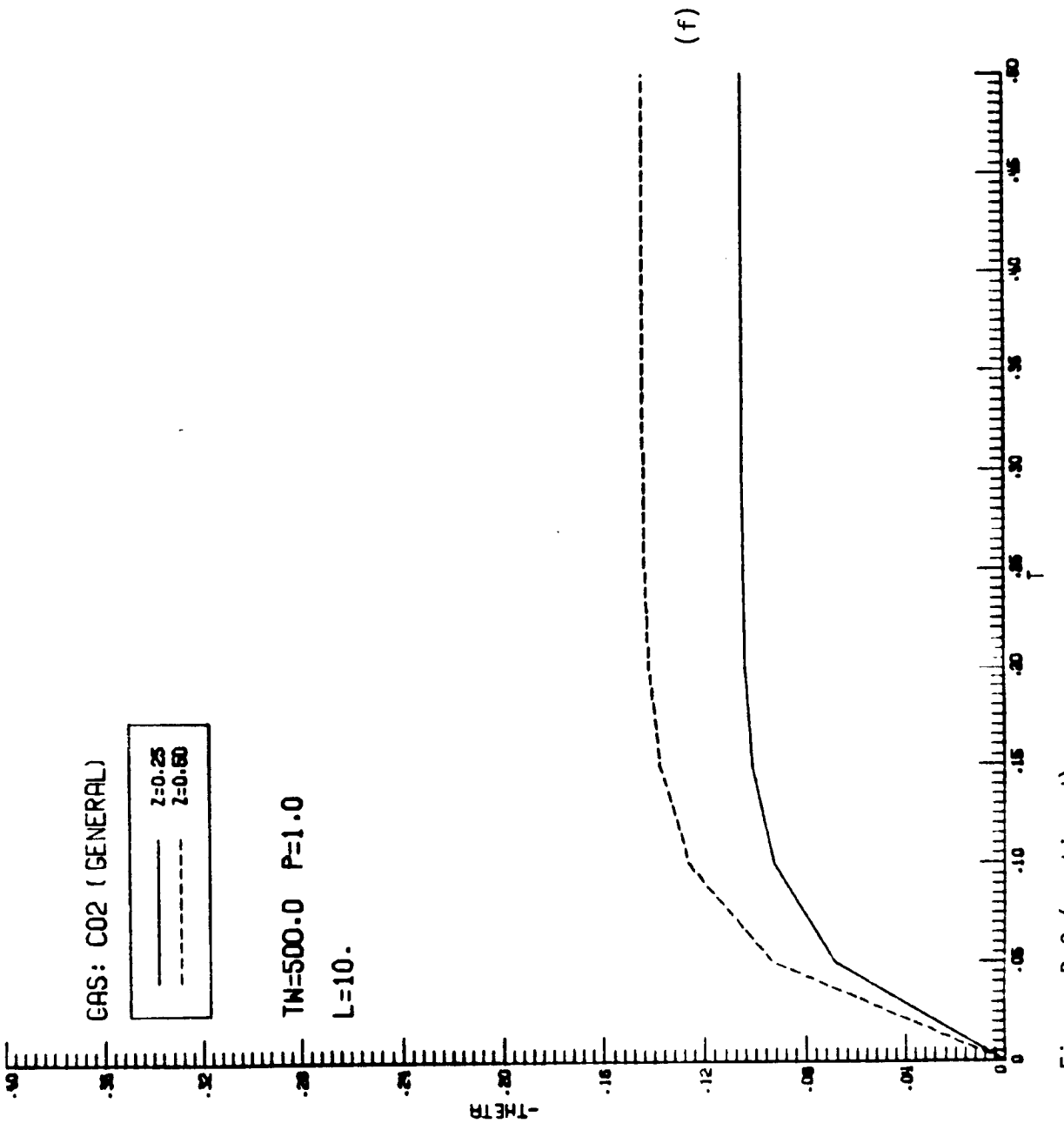

Figure B.3 (continued)

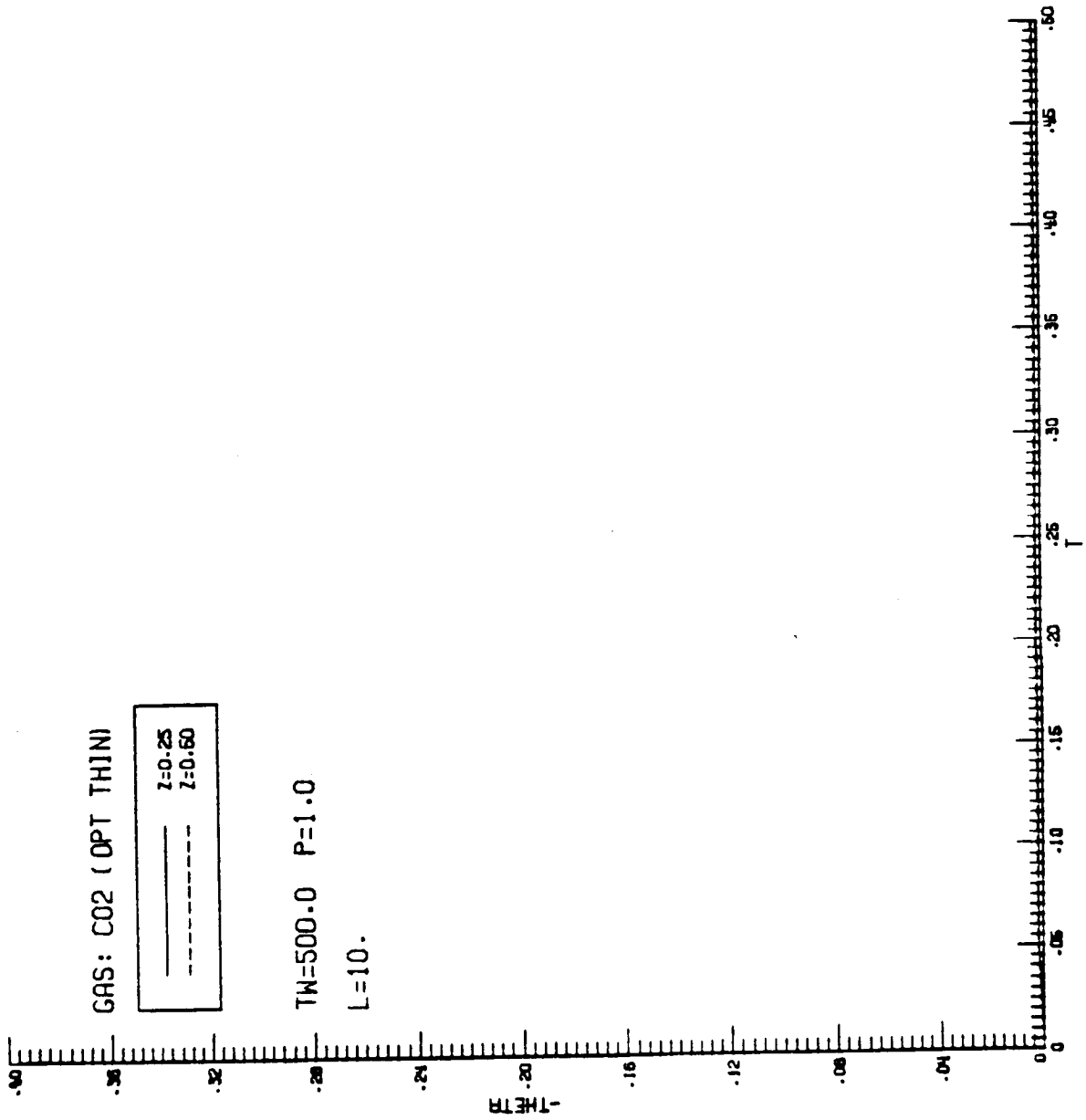

(g)

Figure B.3 (continued)

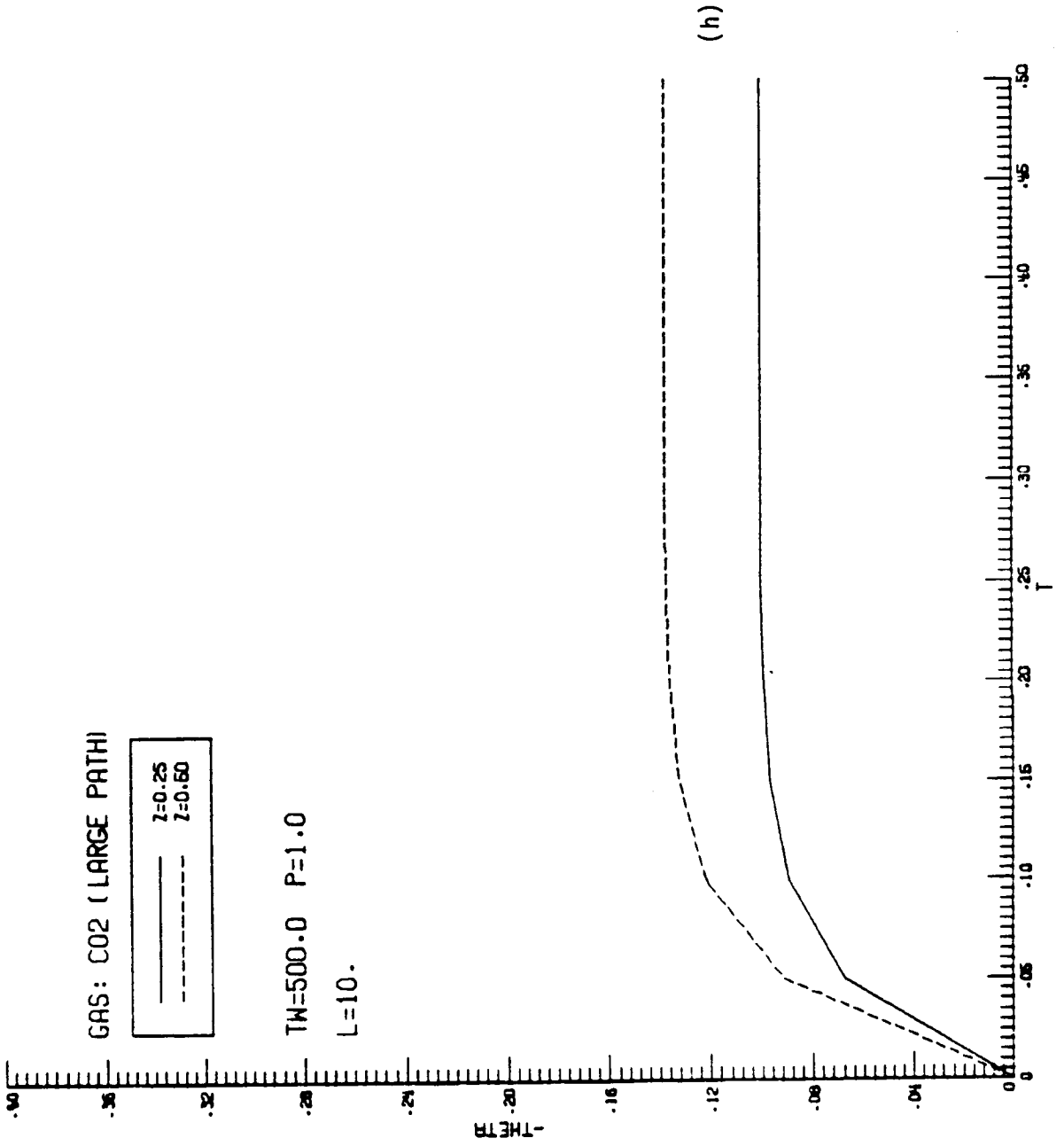

Figure B.3 (continued)

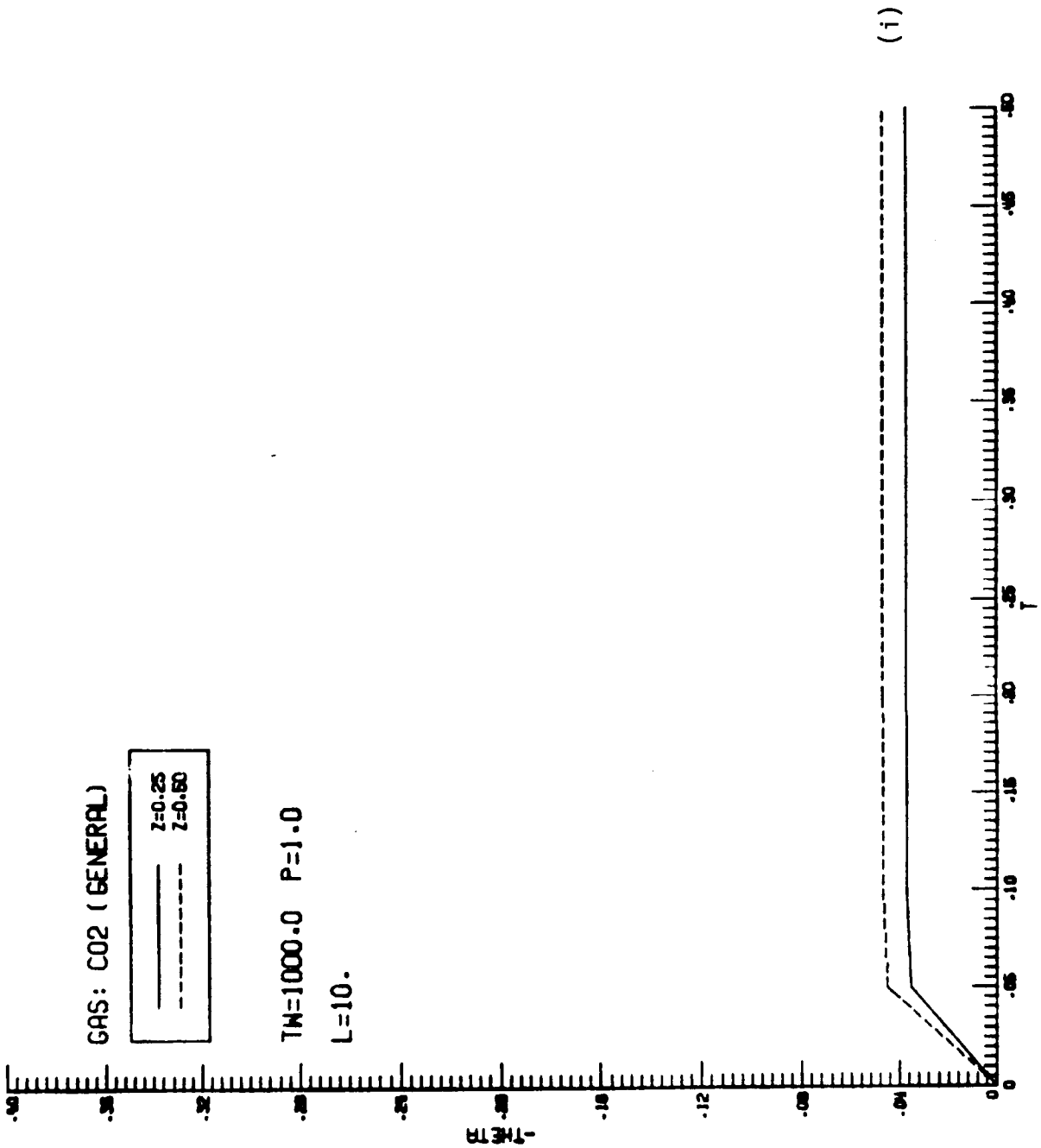

Figure B.3 (continued)

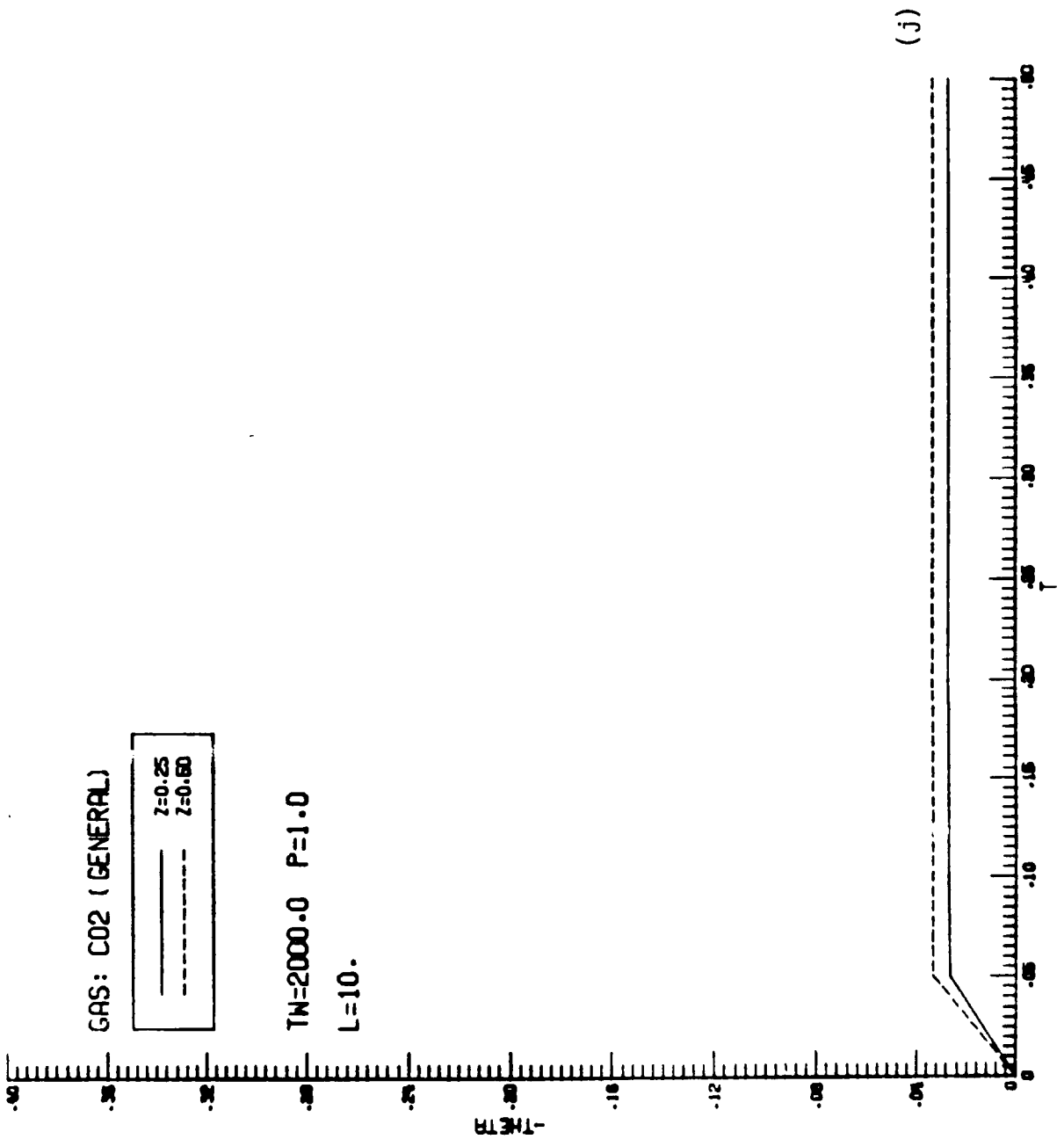

Figure B.3 (continued)

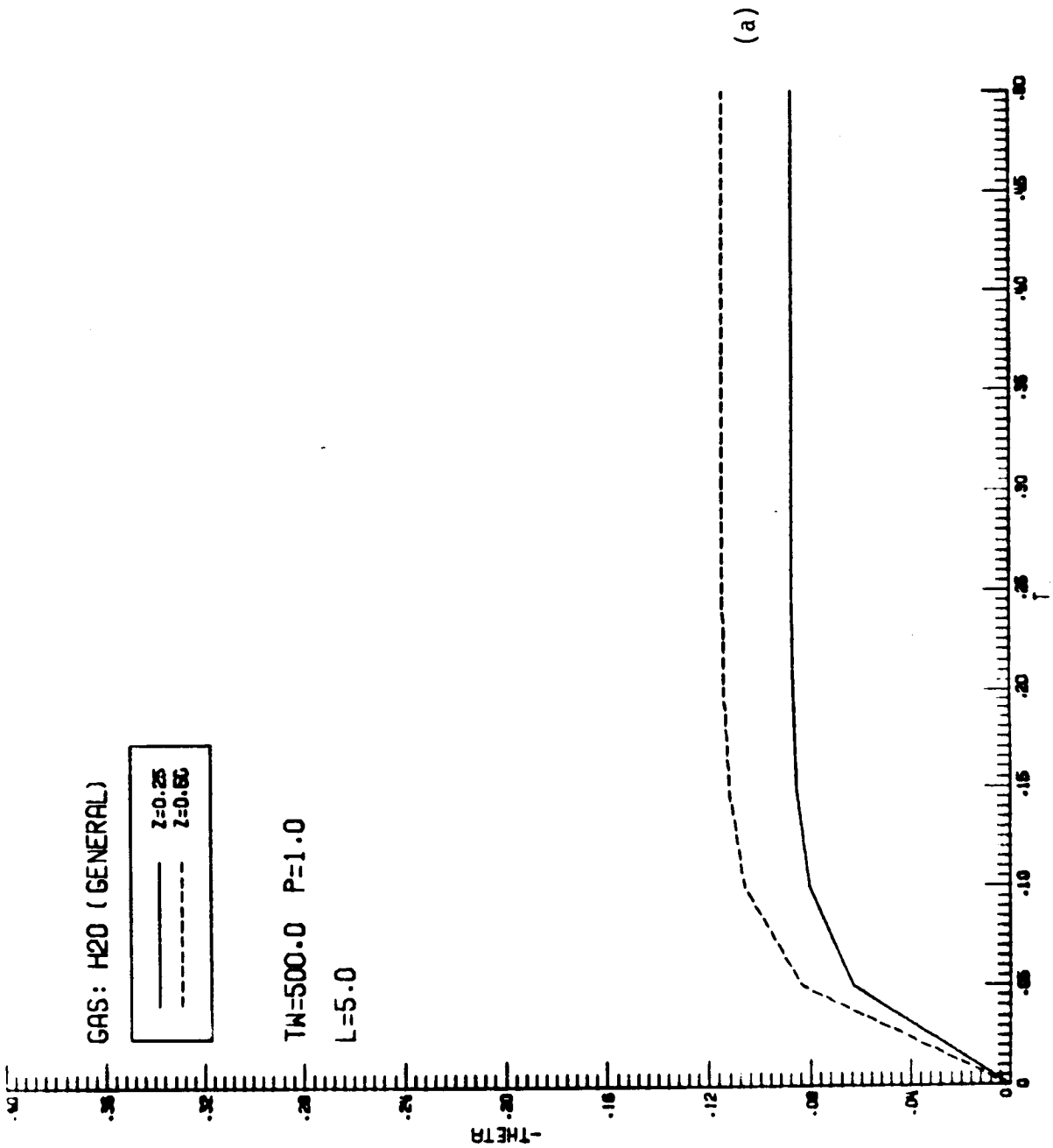

Figure B.4. Results for temperature variation with time (θ vs. τ) for H_2O.

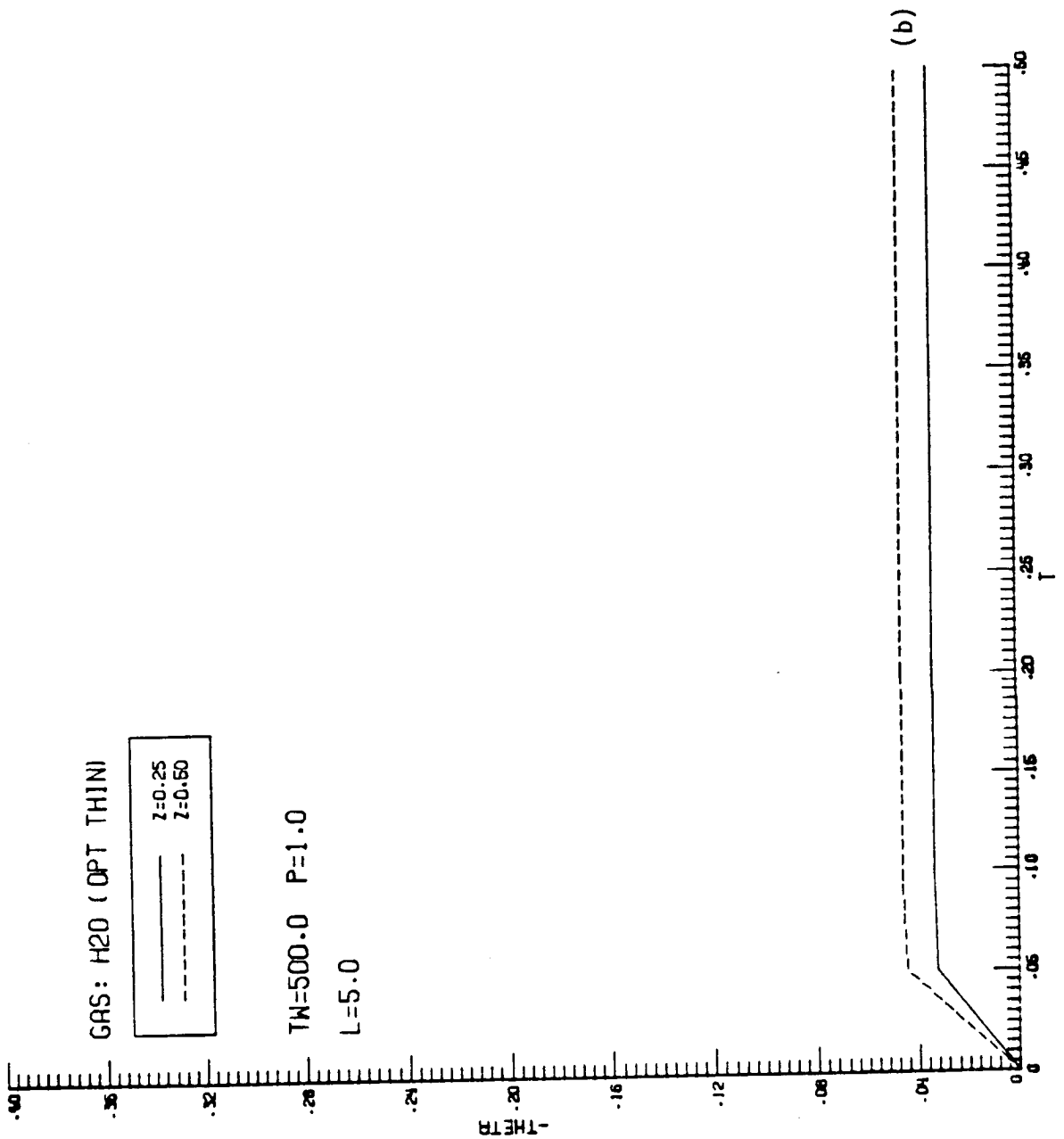

Figure B.4 (continued)

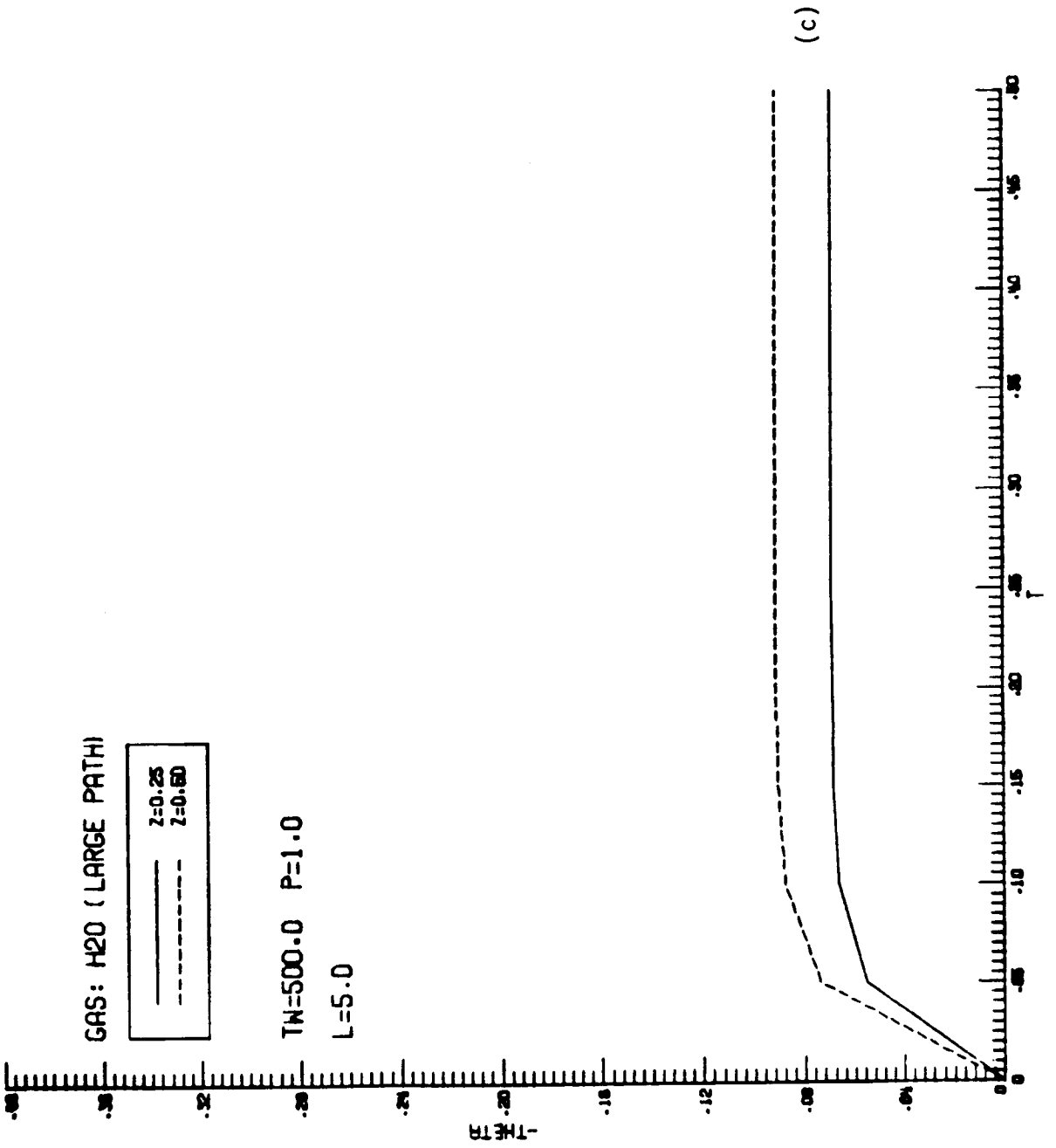

Figure B.4 (continued)

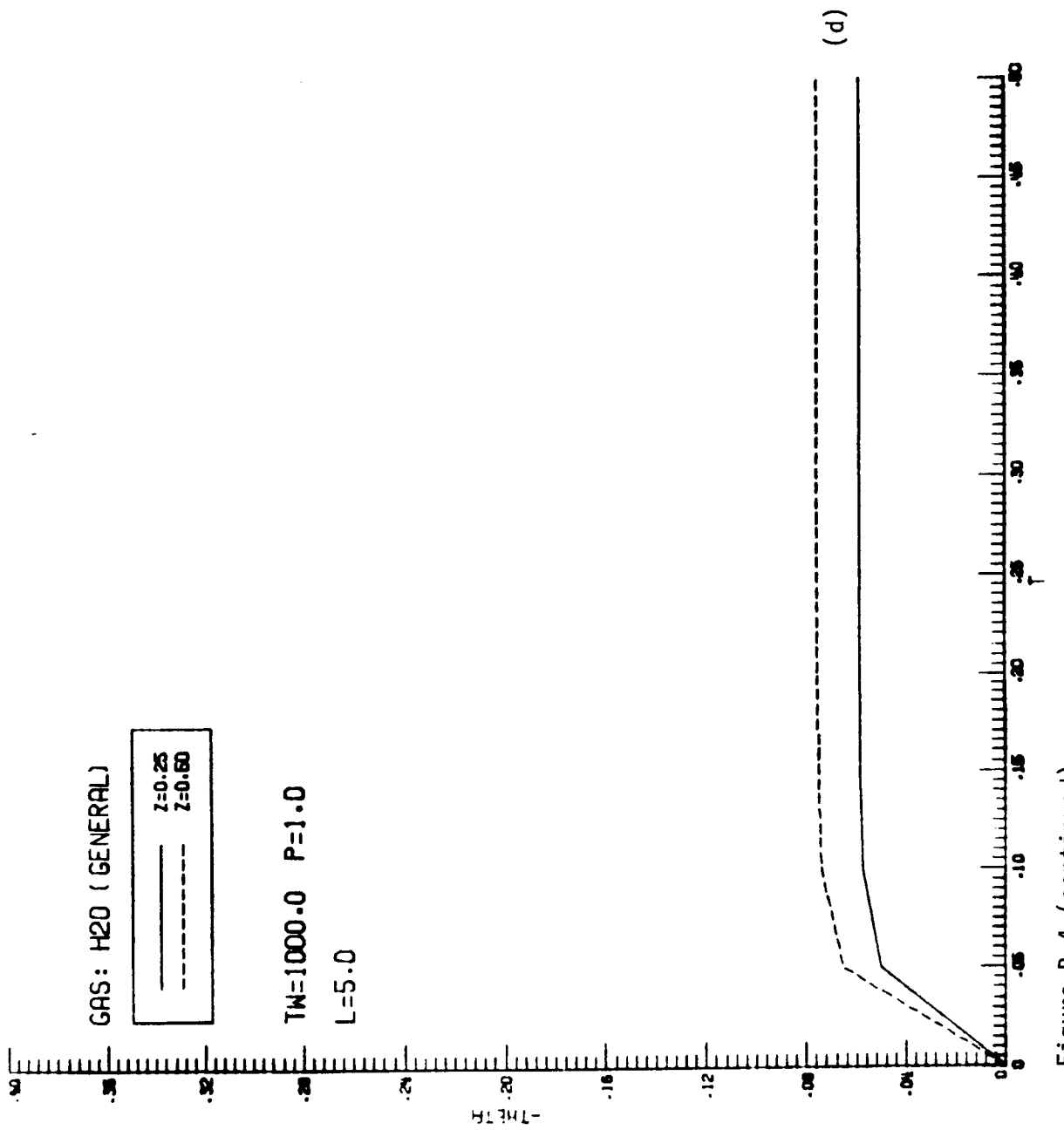

Figure B.4 (continued)

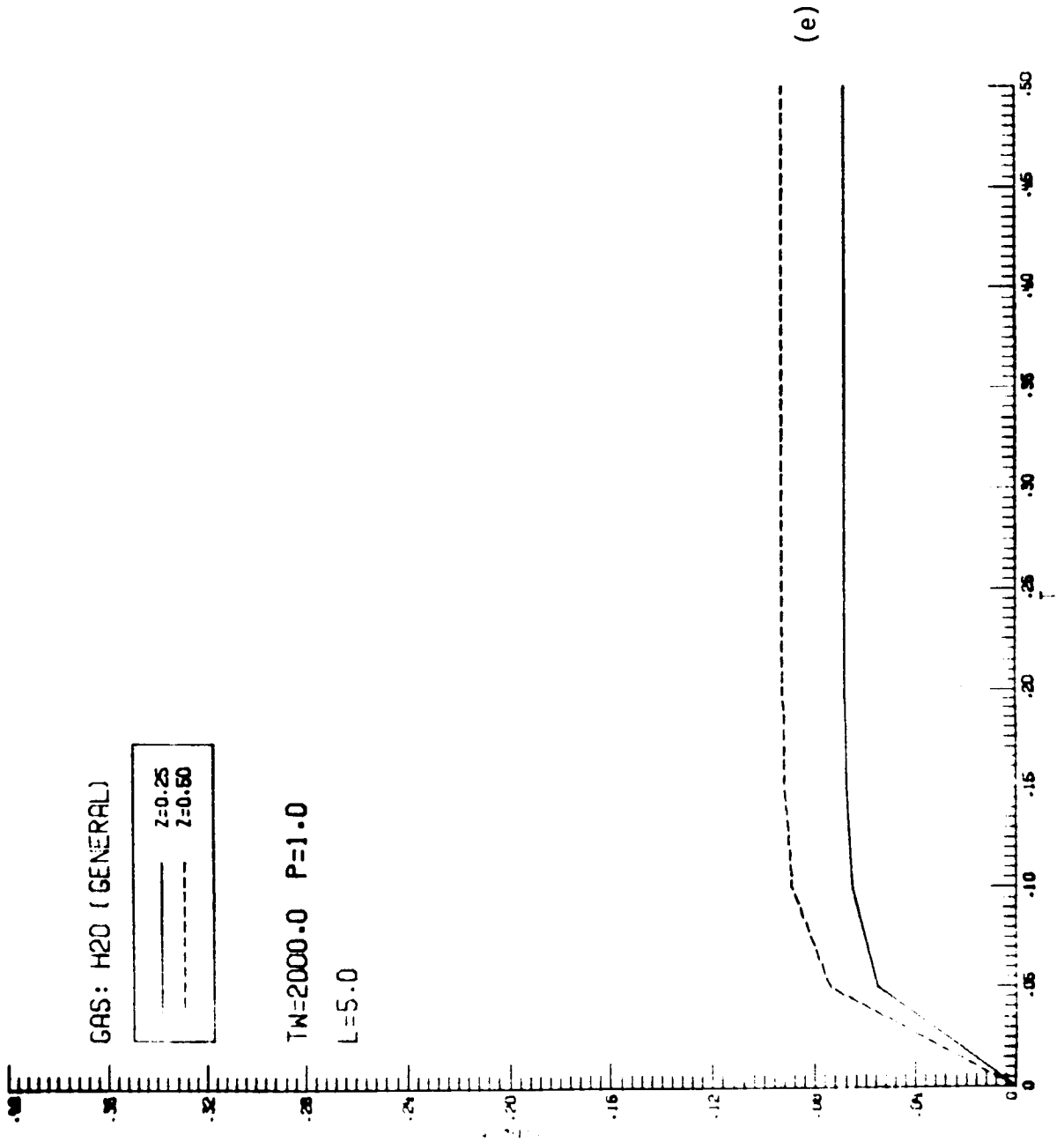

Figure B.4 (continued)

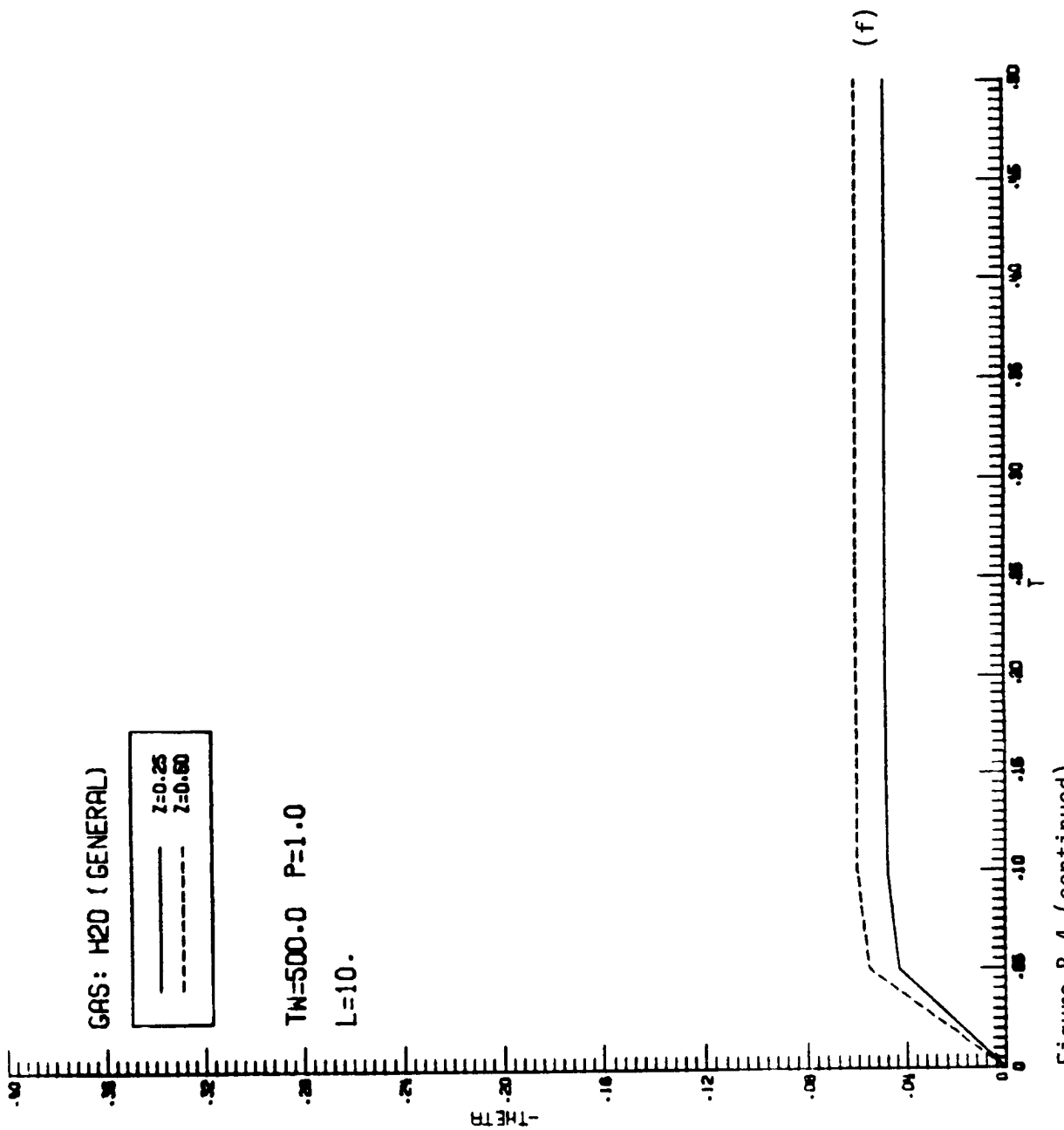

Figure B.4 (continued)

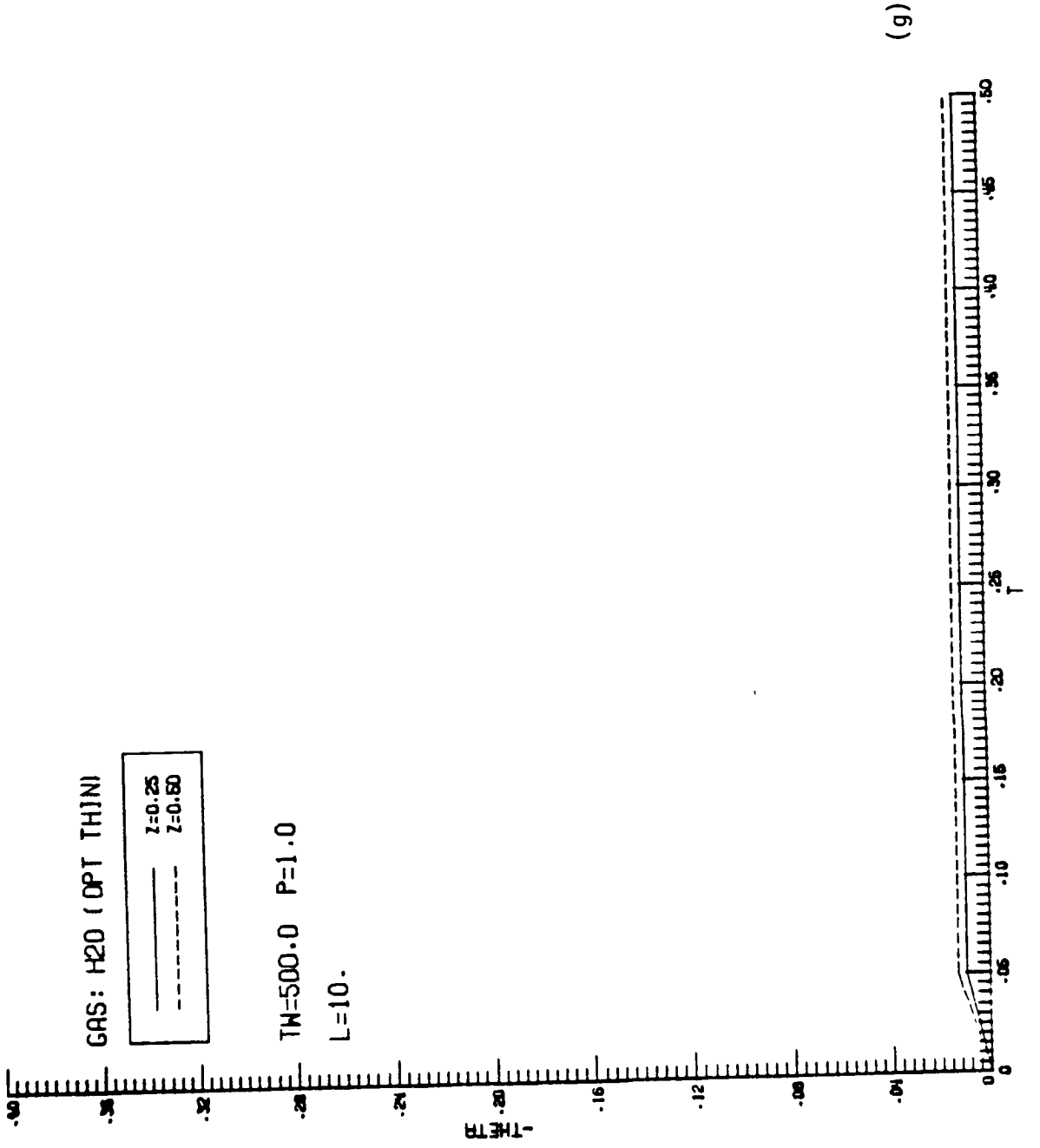

Figure B.4 (continued)

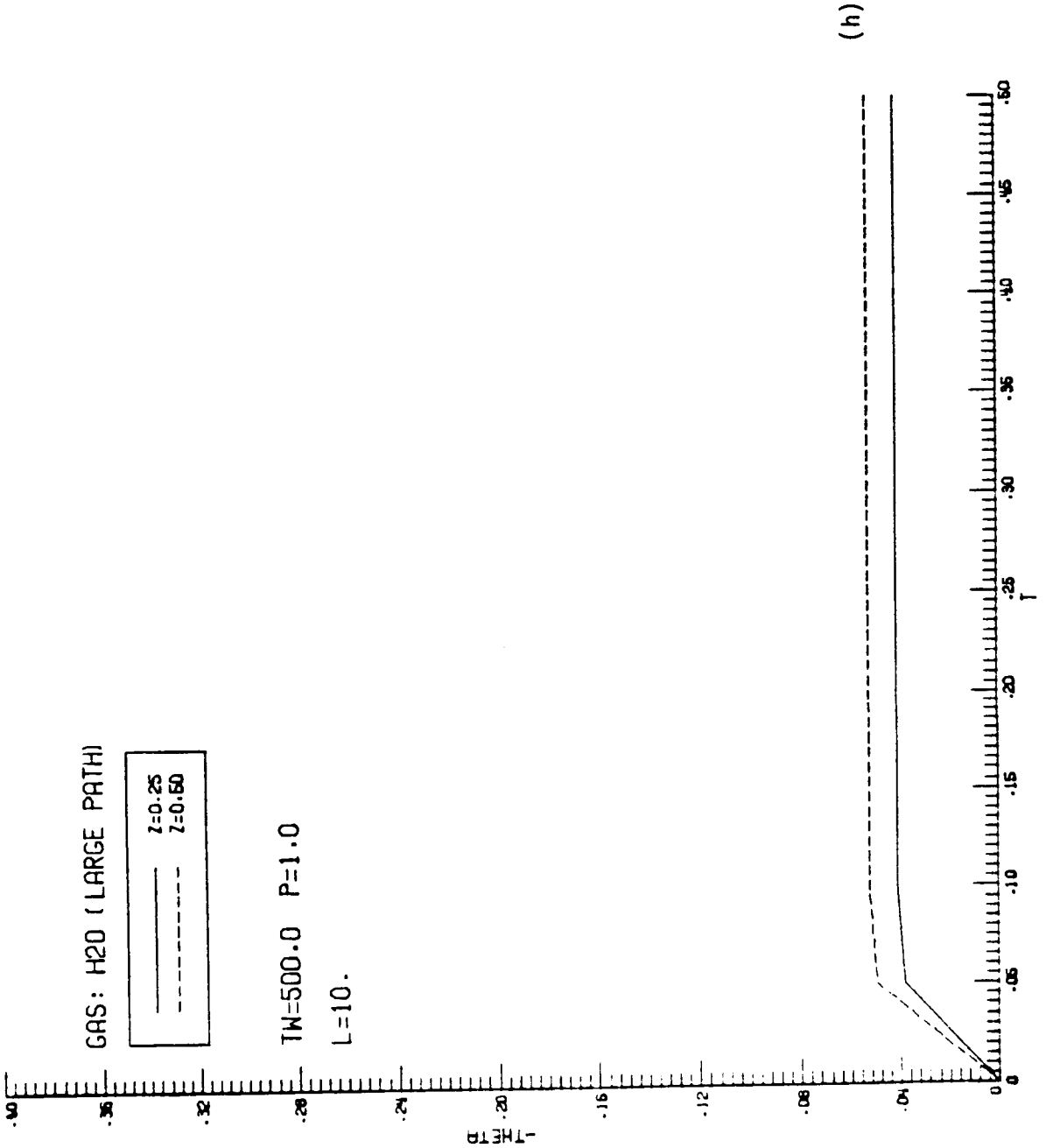

Figure B.4 (continued)

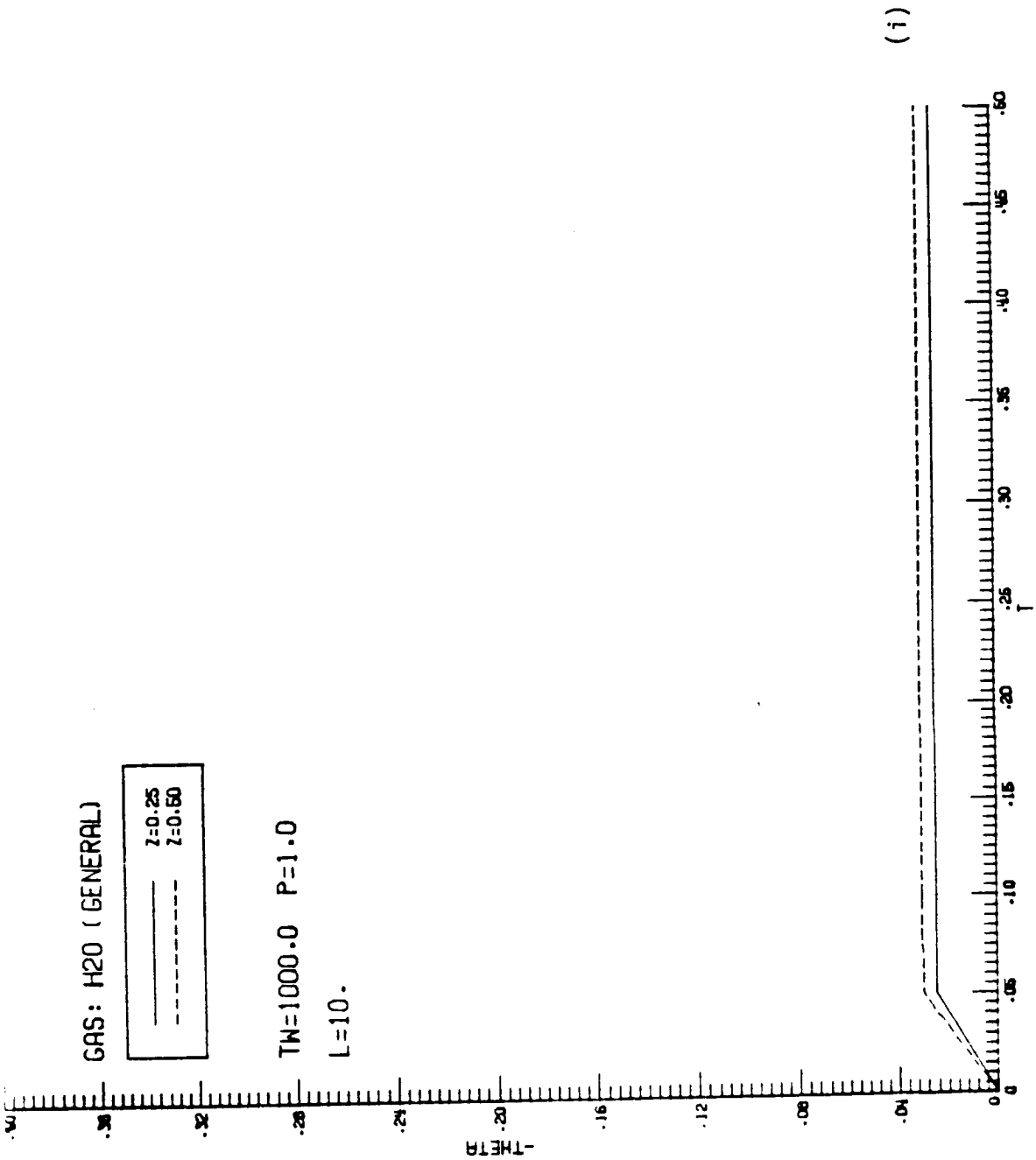

Figure B.4 (continued)

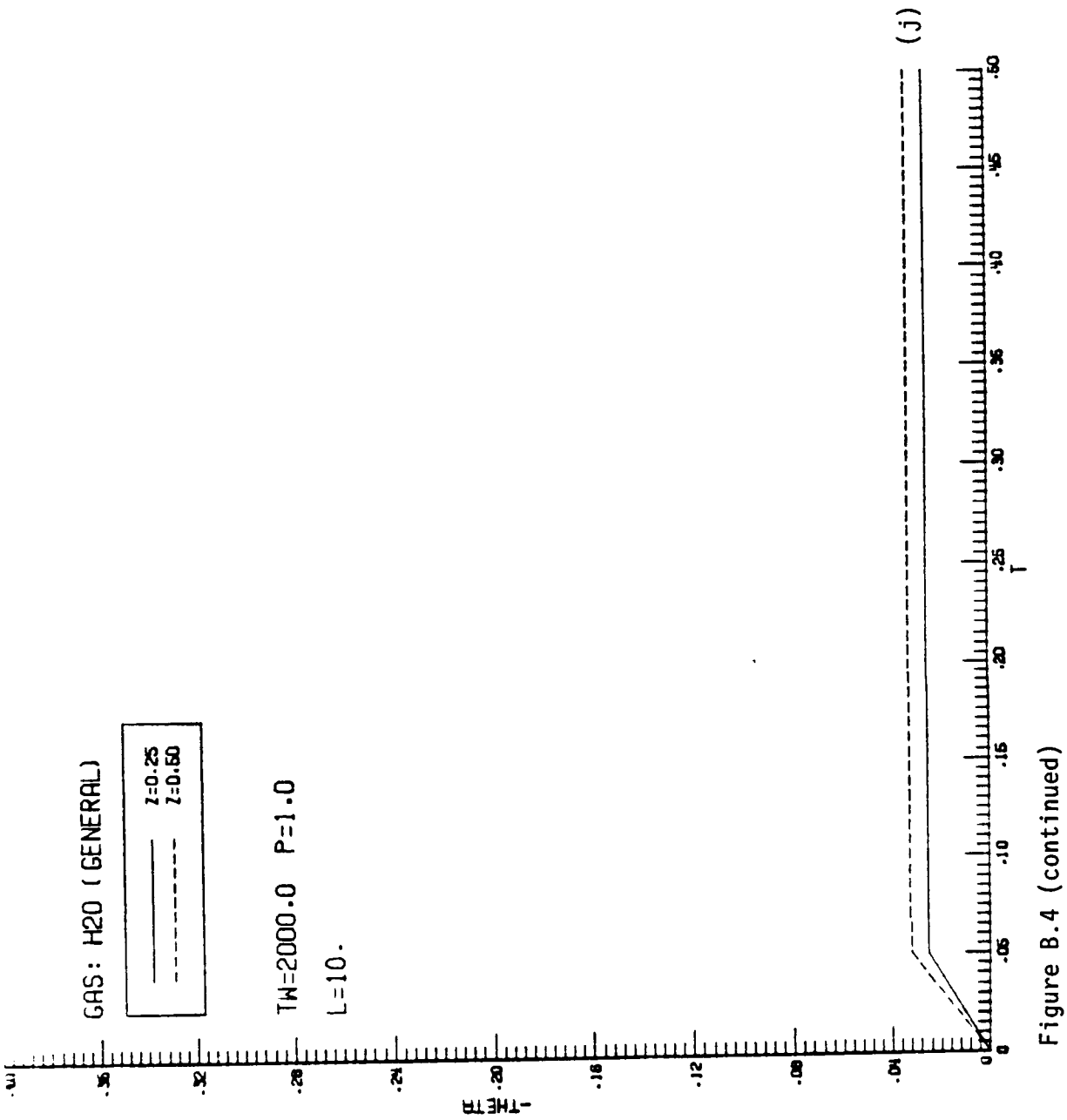

Figure B.4 (continued)

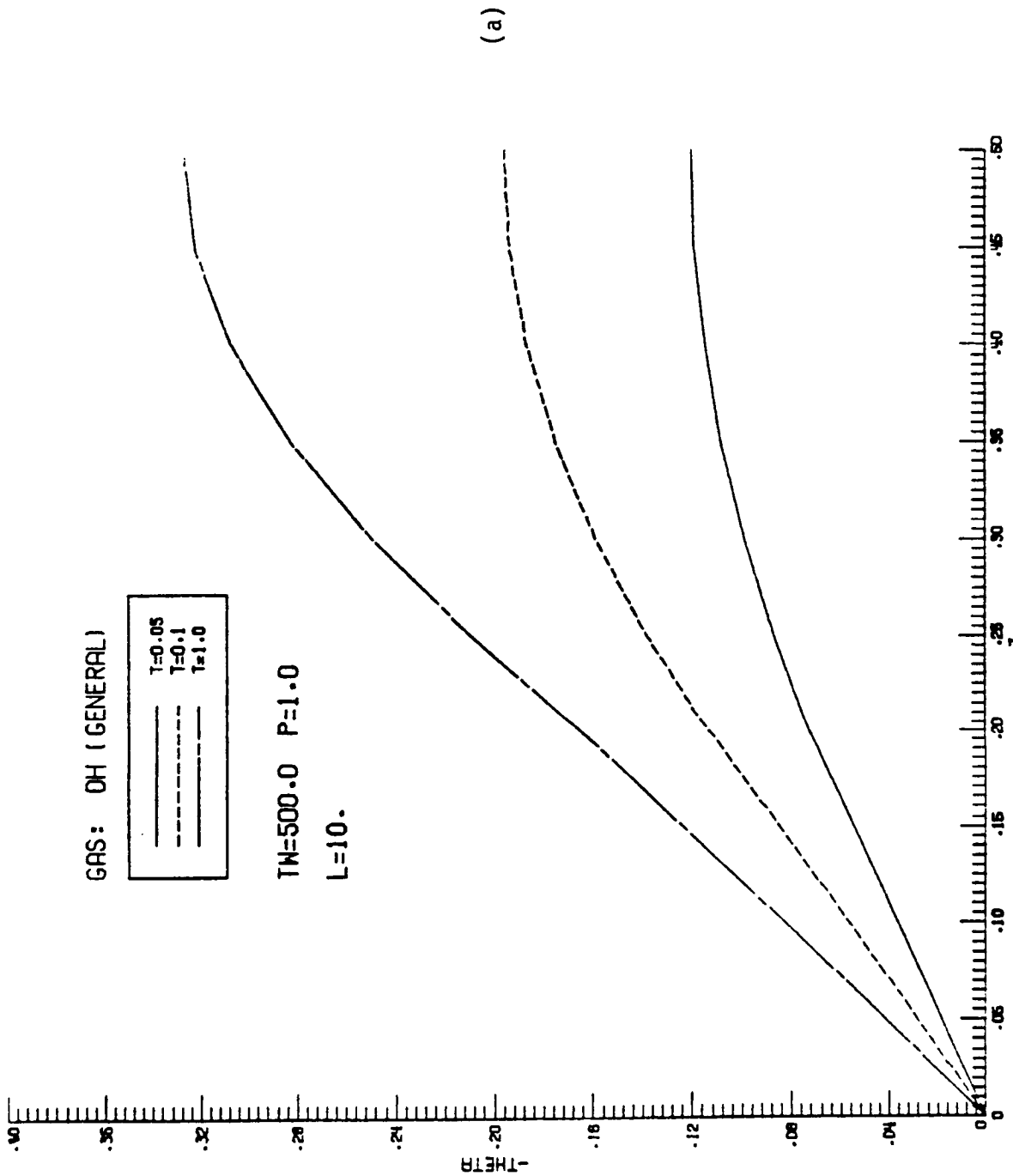

Figure B.5. Results for temperature variation across the duct (θ vs. ξ) for OH.

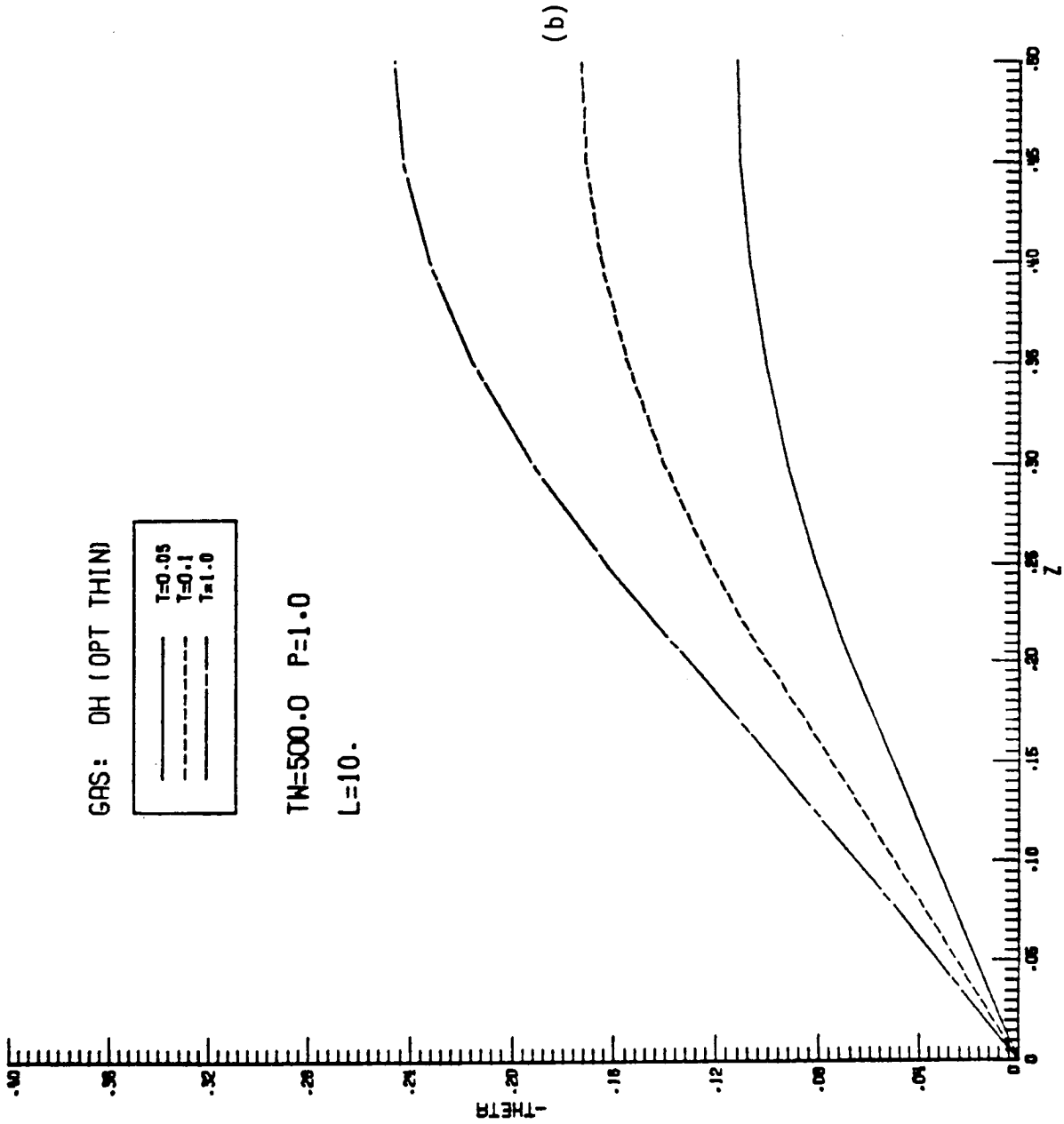

Figure B.5 (continued)

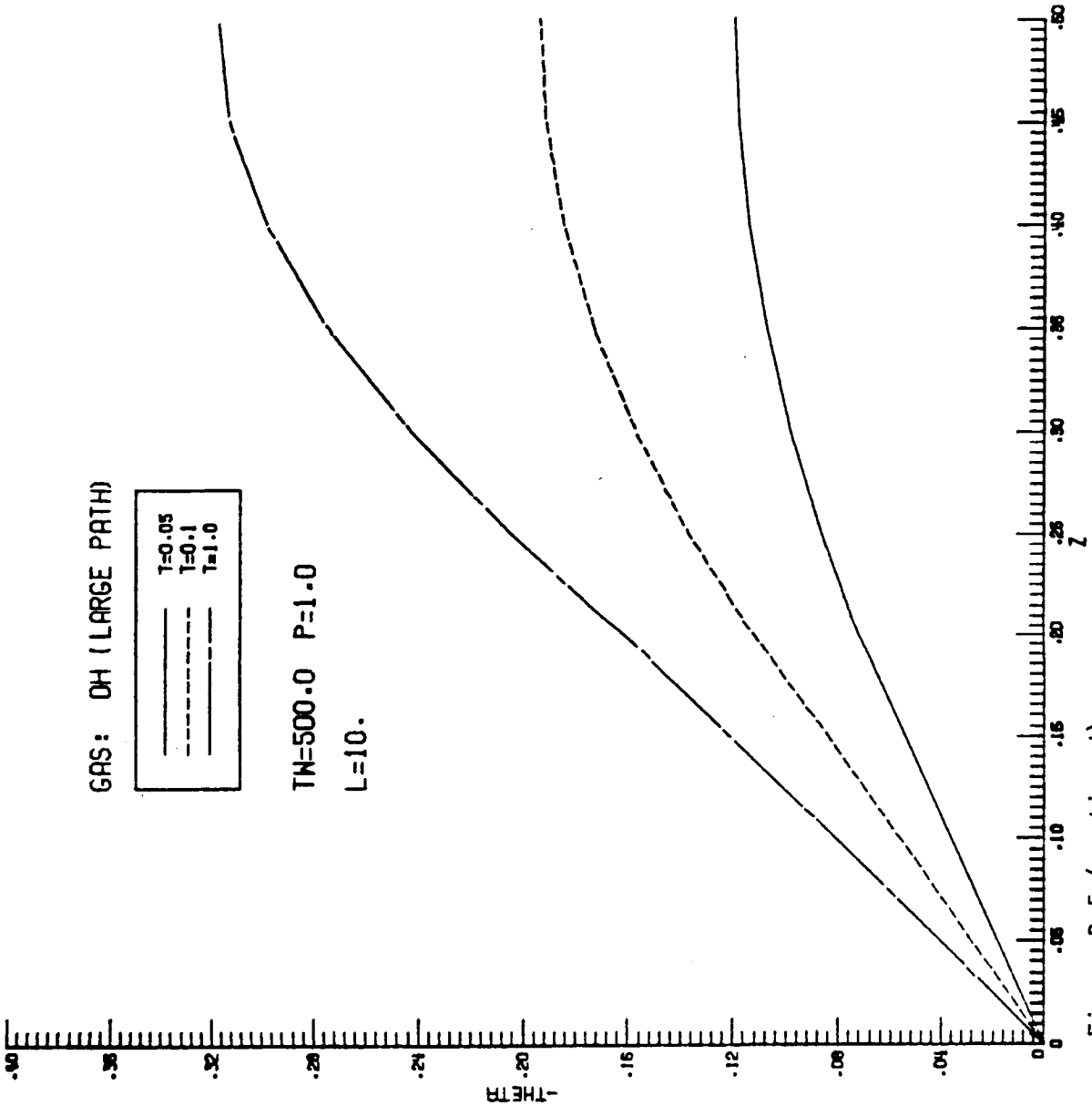

Figure B.5 (continued)

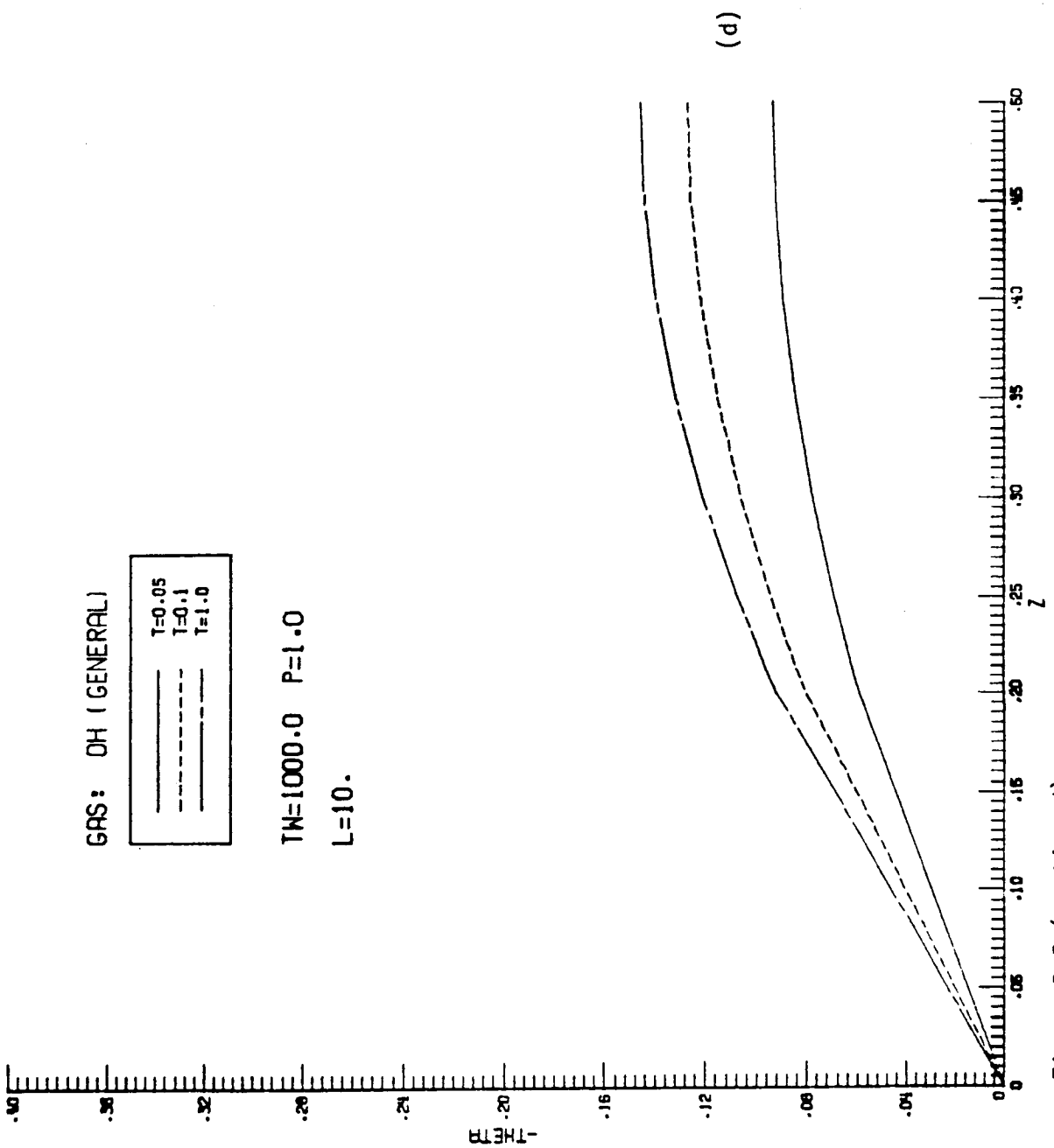

Figure B.5 (continued)

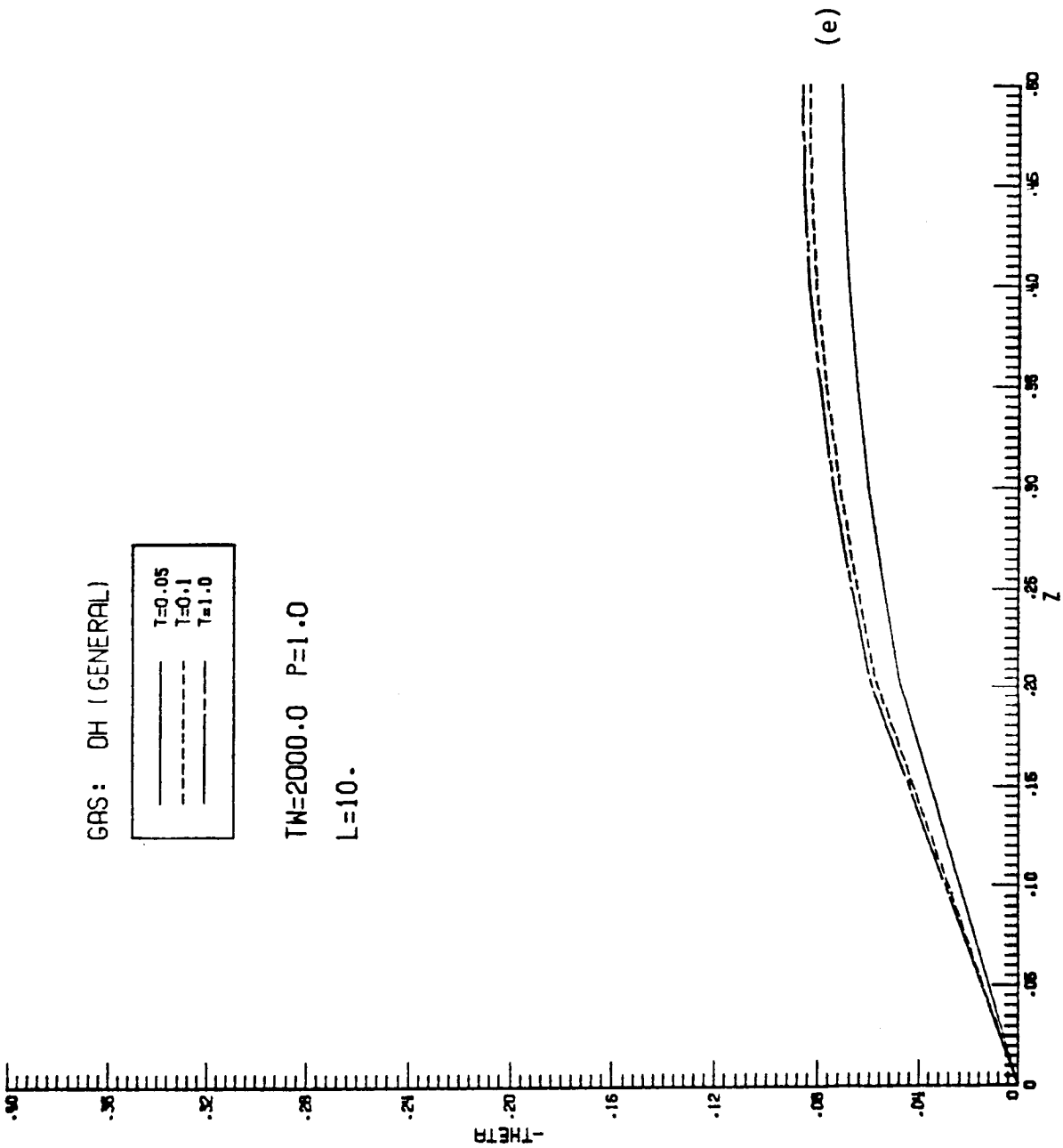

Figure B.5 (continued)

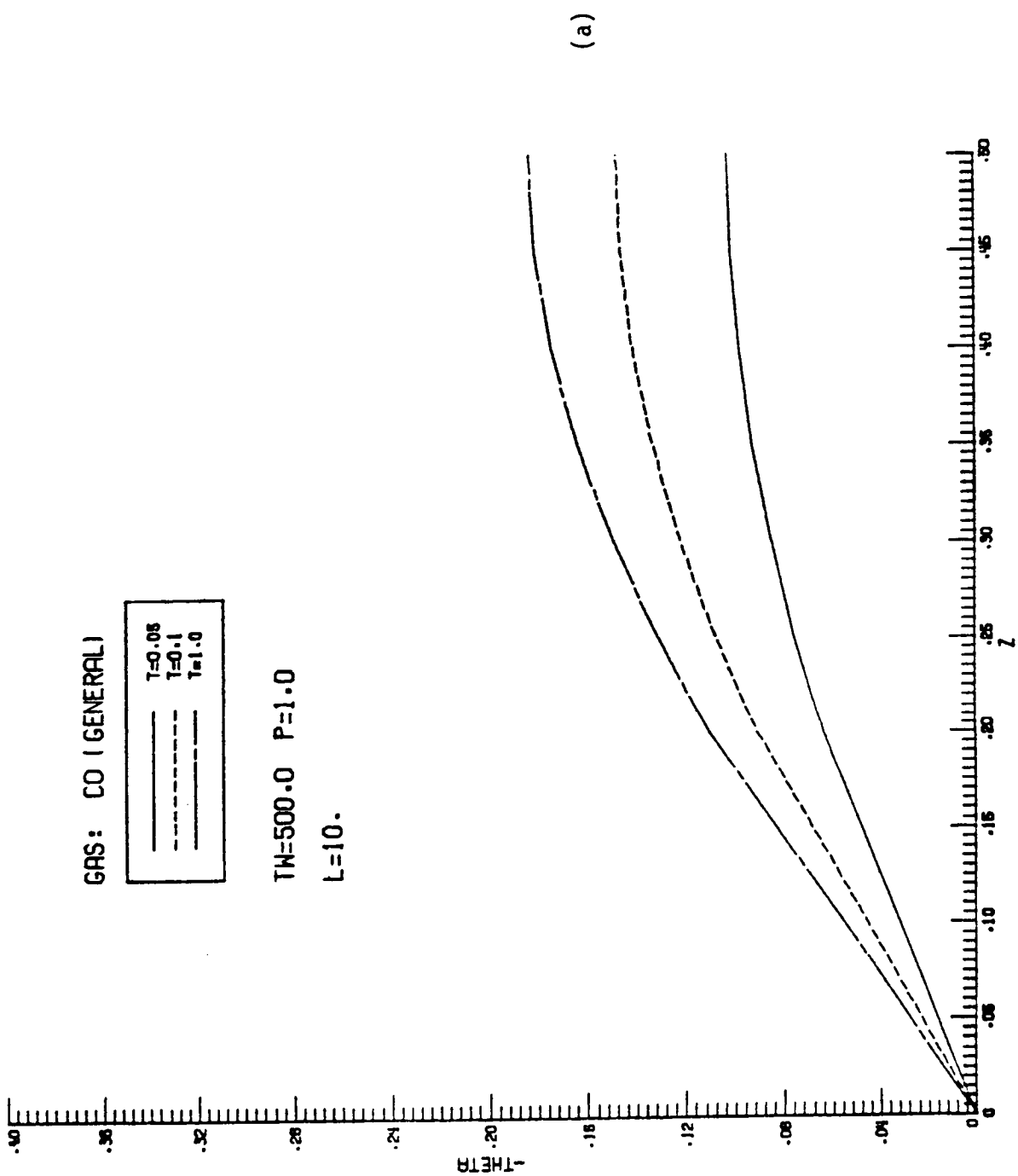

Figure B.6. Results for temperature vatiation across the duct (θ vs. ξ) for CO.

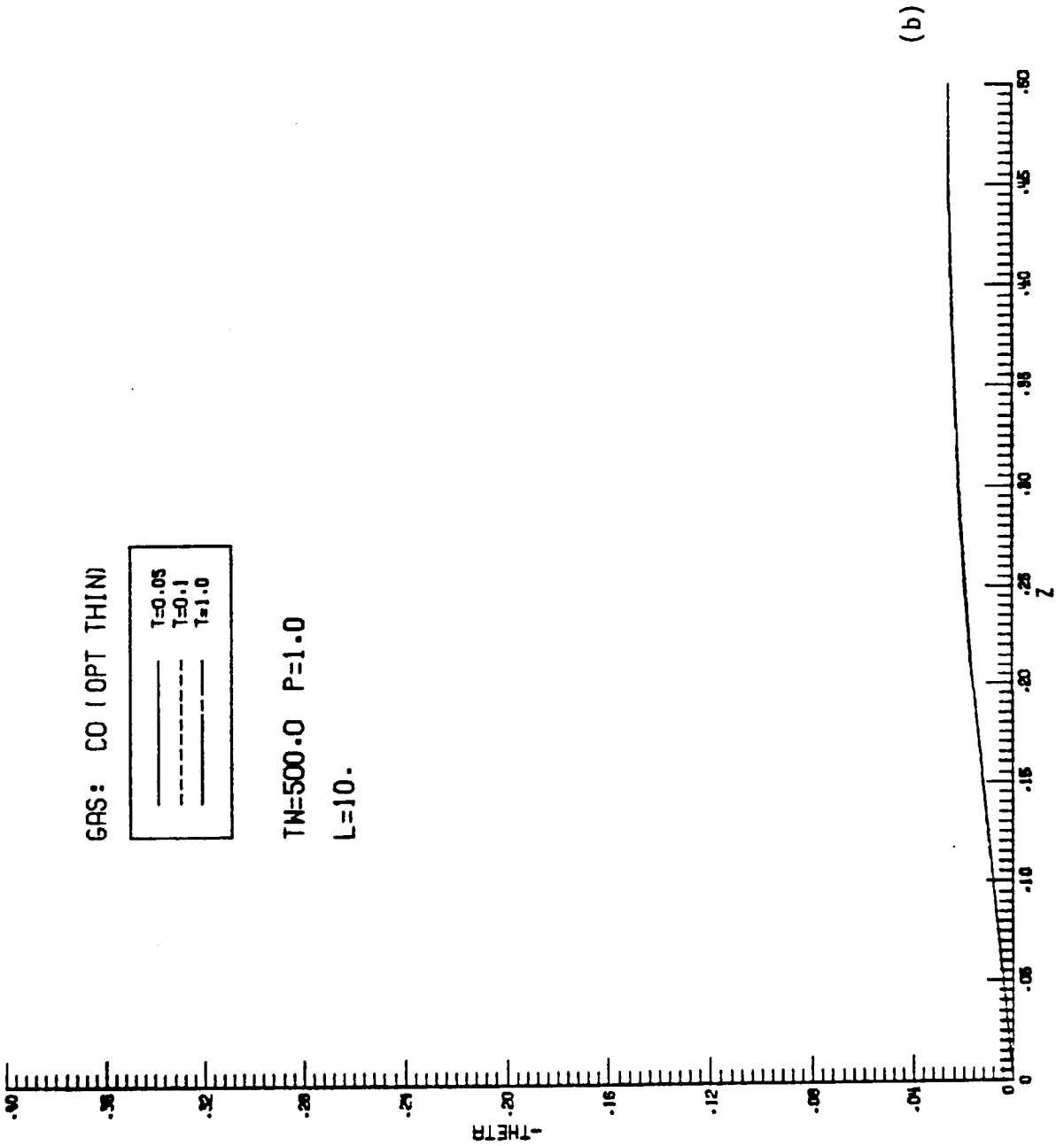

(b)

Figure B.6 (continued)

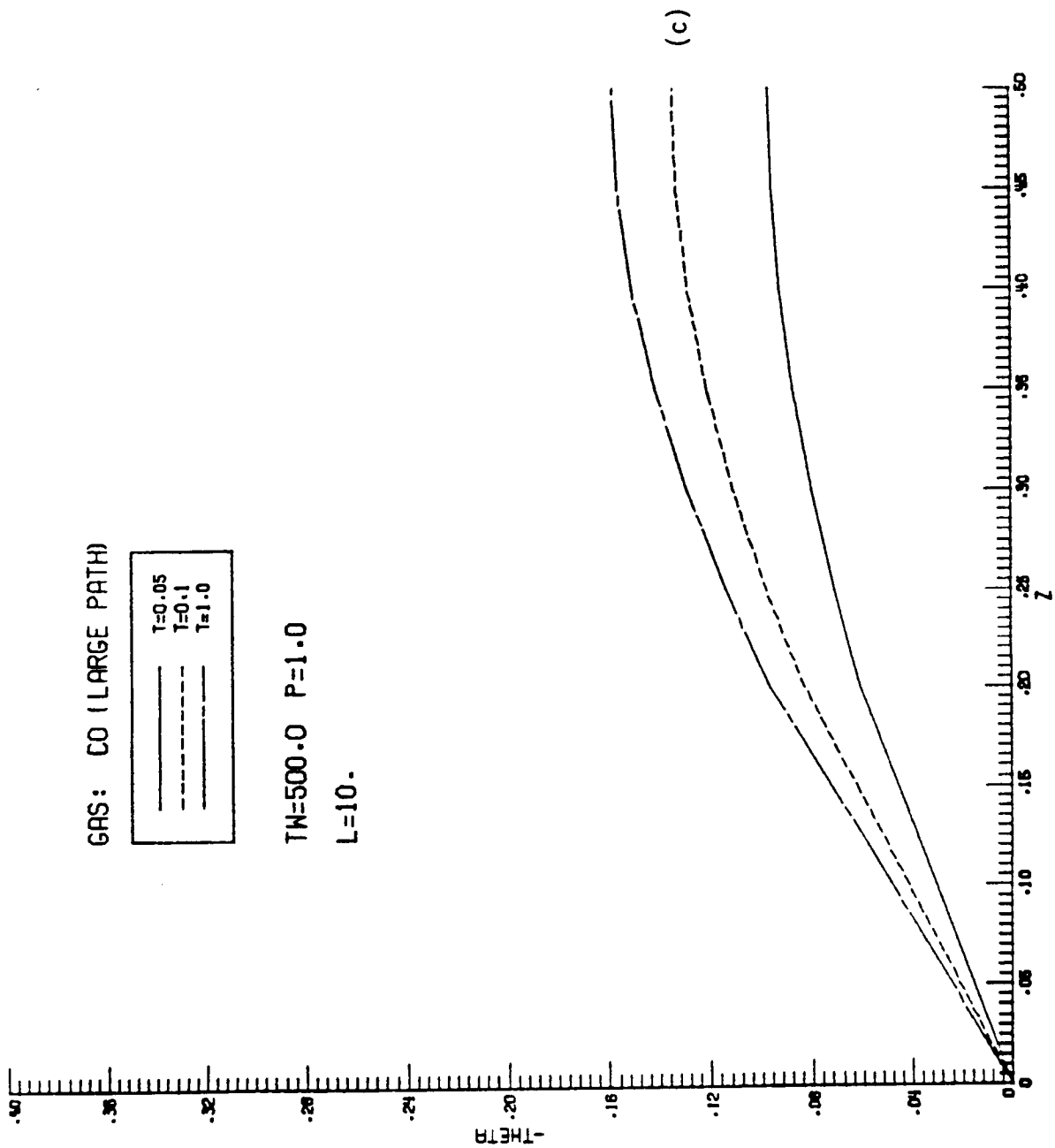

Figure B.6 (continued)

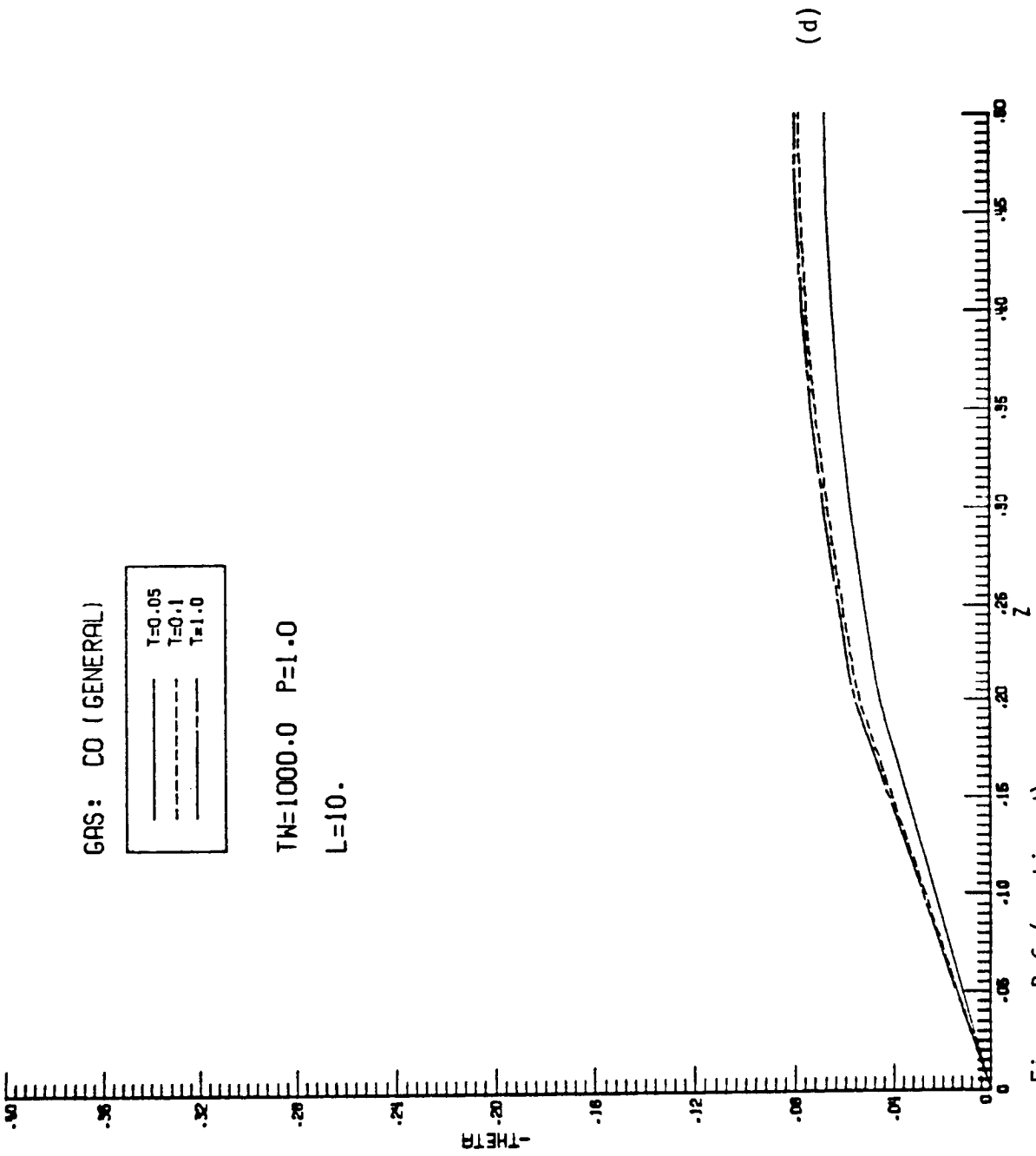

Figure B.6 (continued)

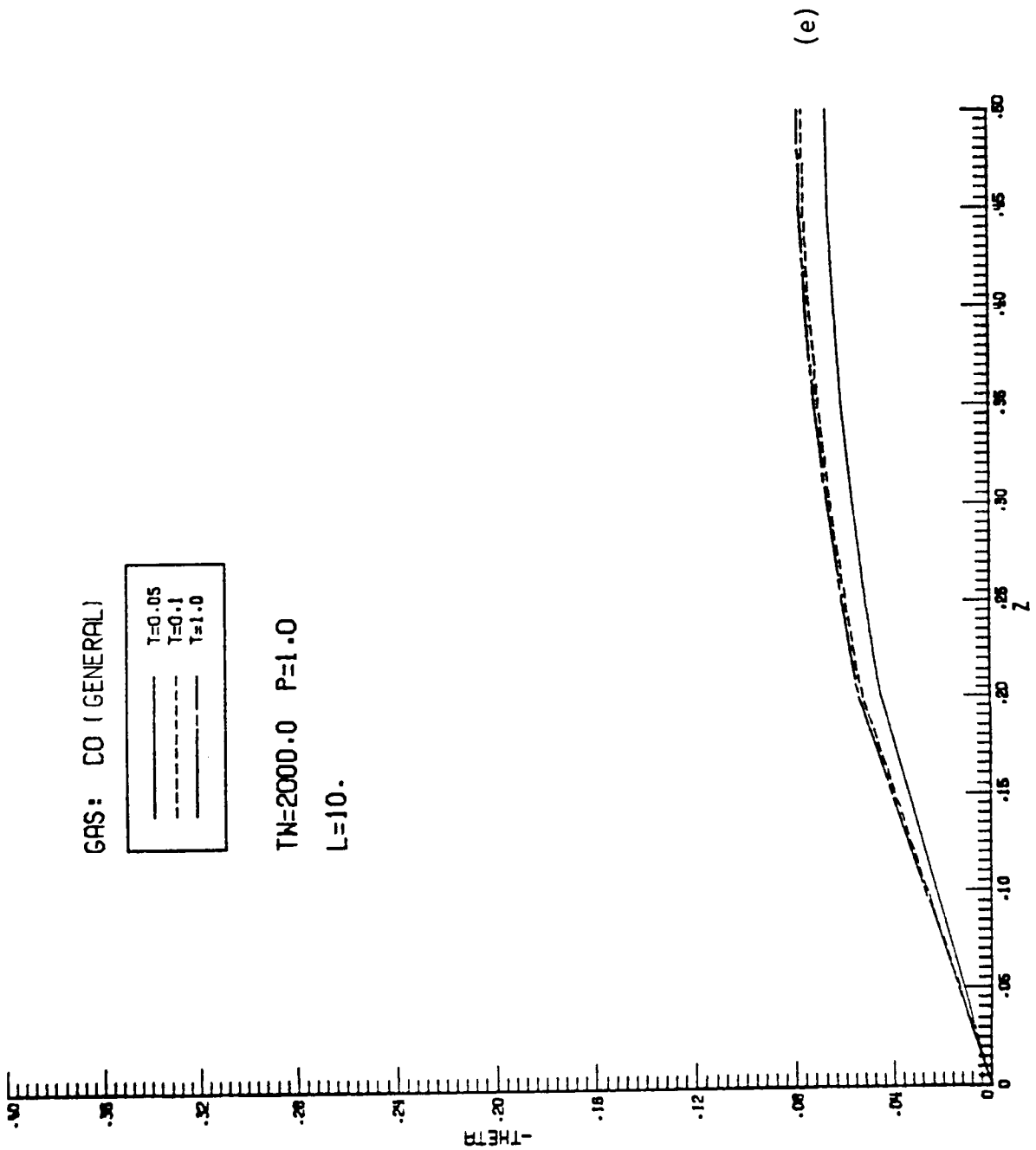

Figure B.6 (continued)

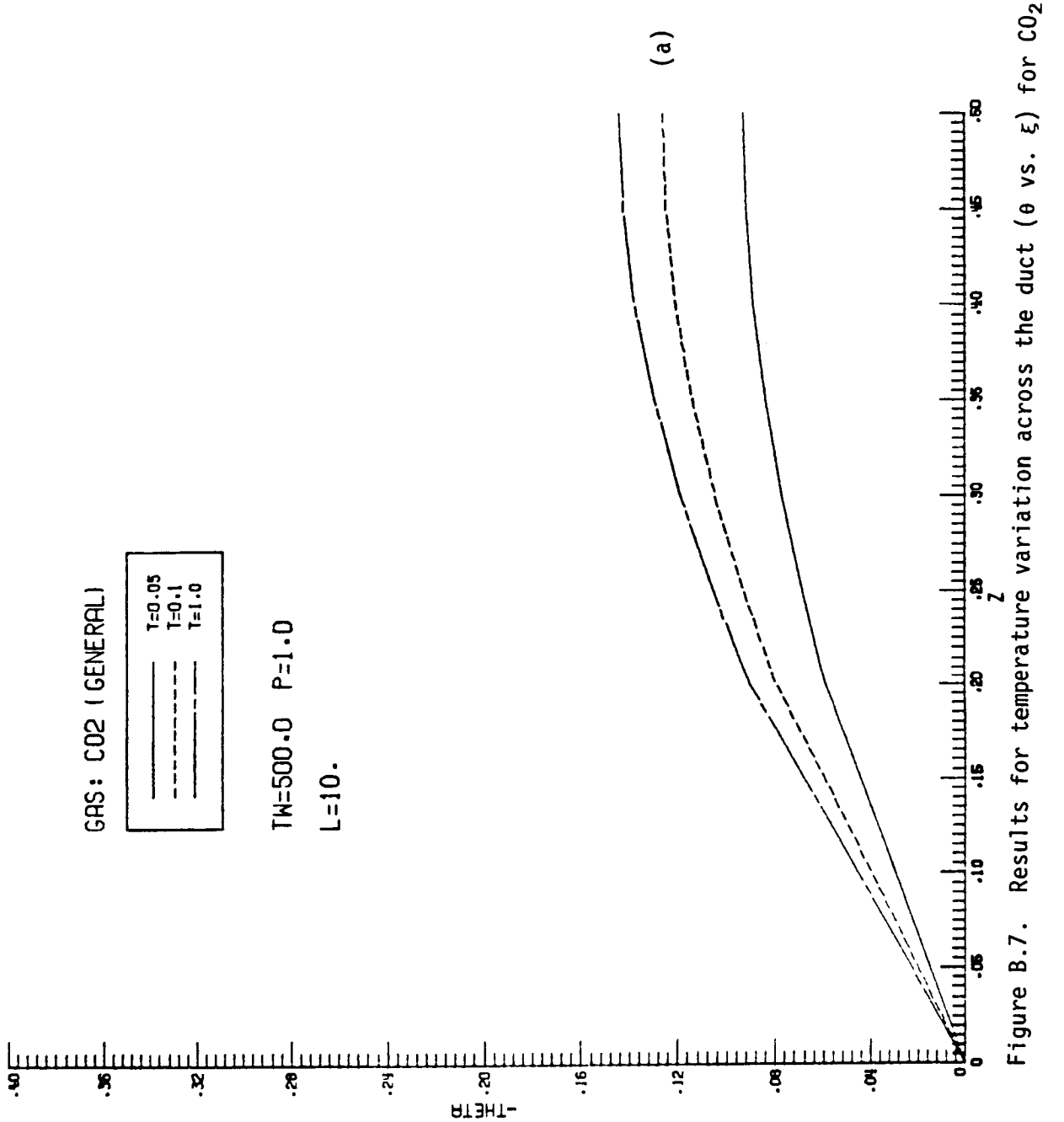

Figure B.7. Results for temperature variation across the duct (θ vs. ξ) for CO_2.

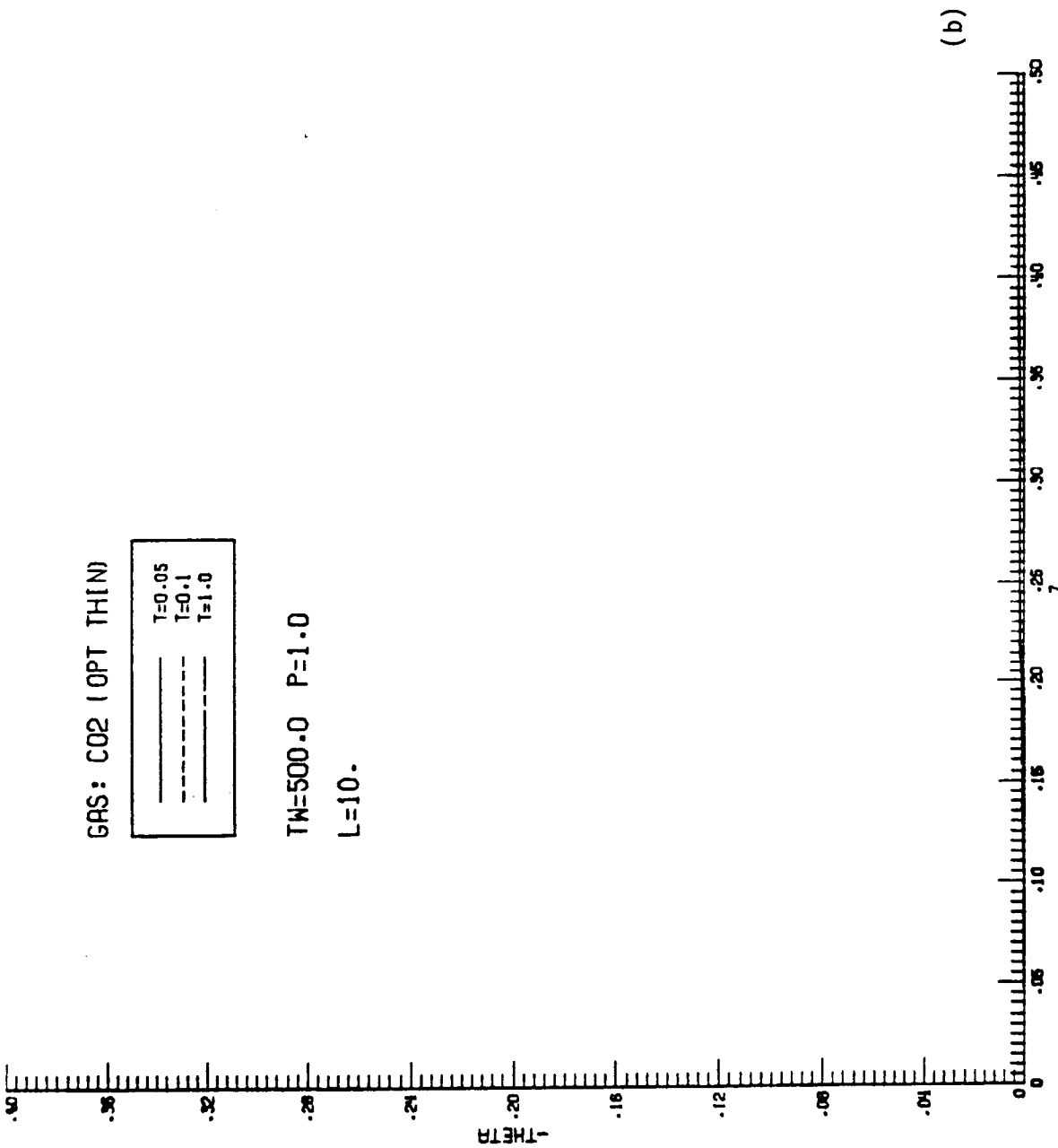

(b)

Figure B.7 (continued)

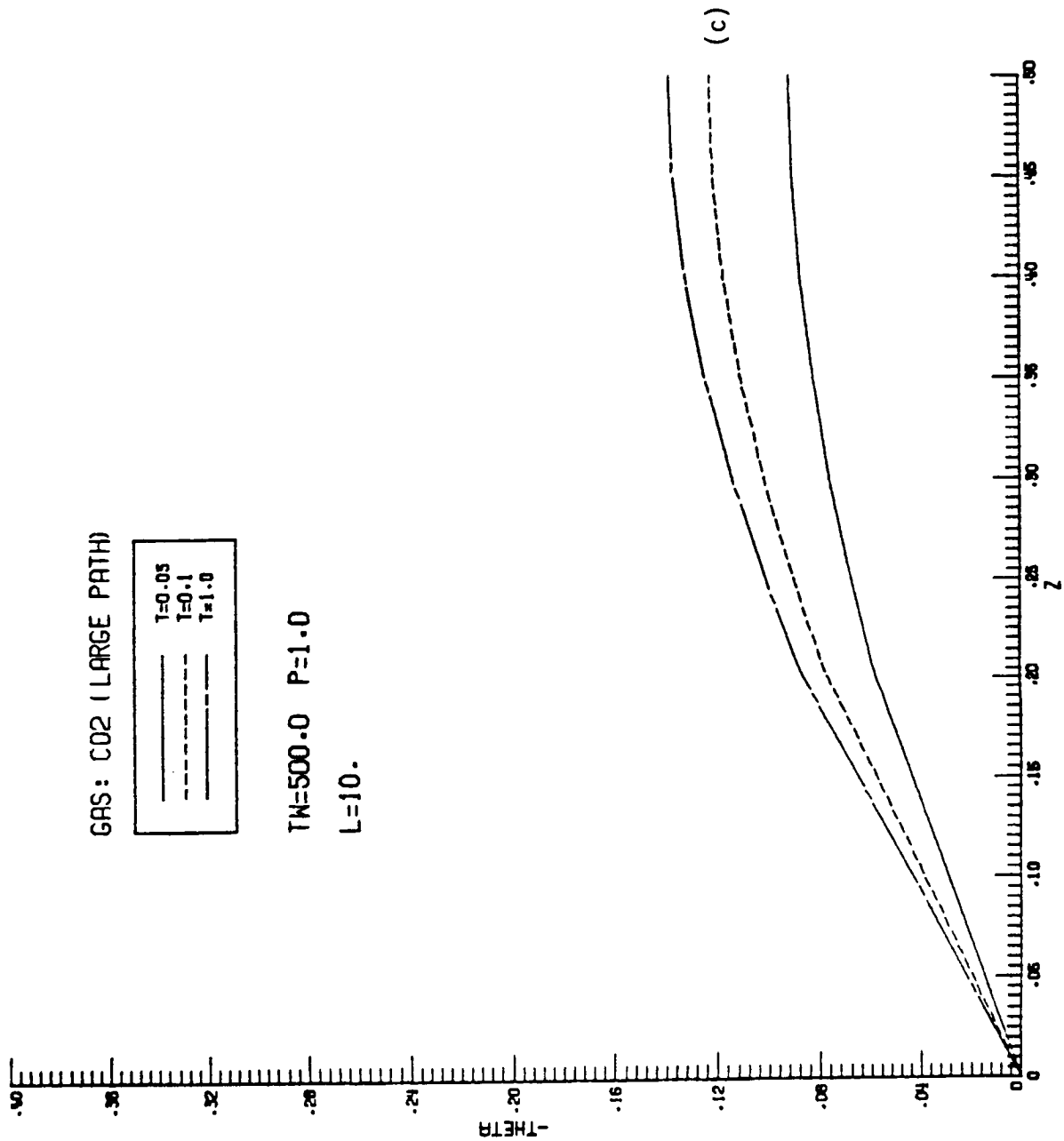

Figure B.7 (continued)

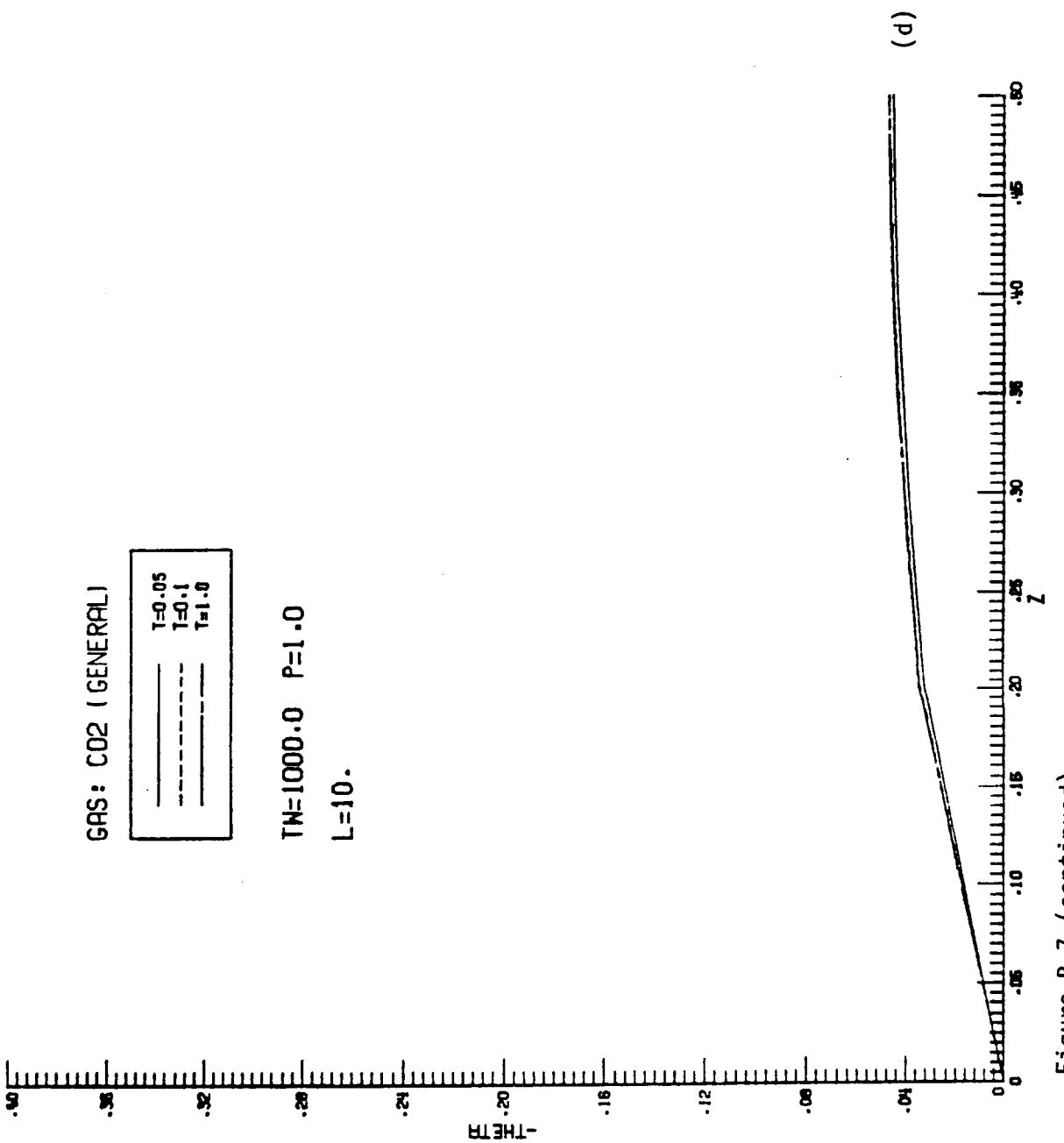

Figure B.7 (continued)

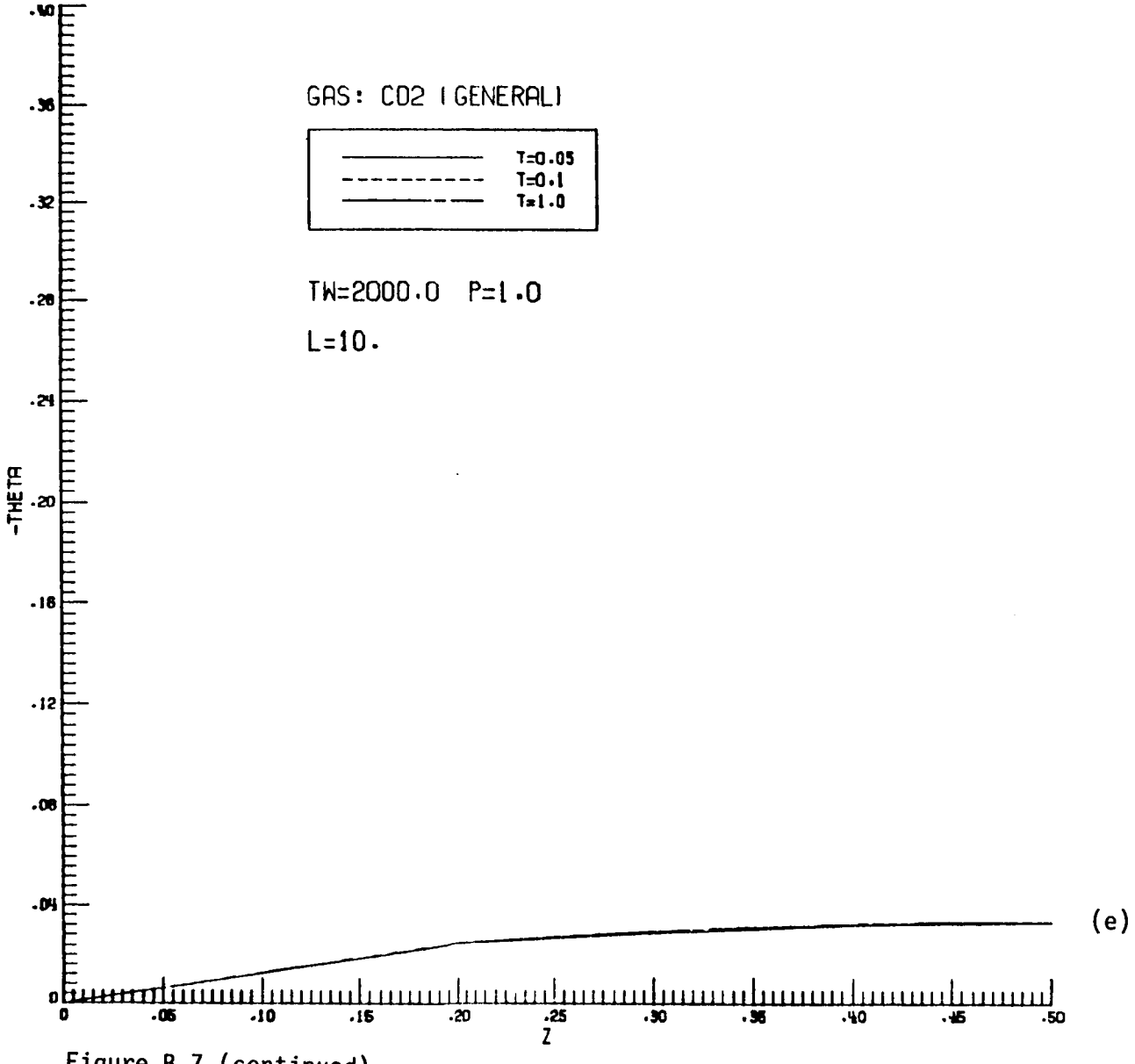

(e)

Figure B.7 (continued)

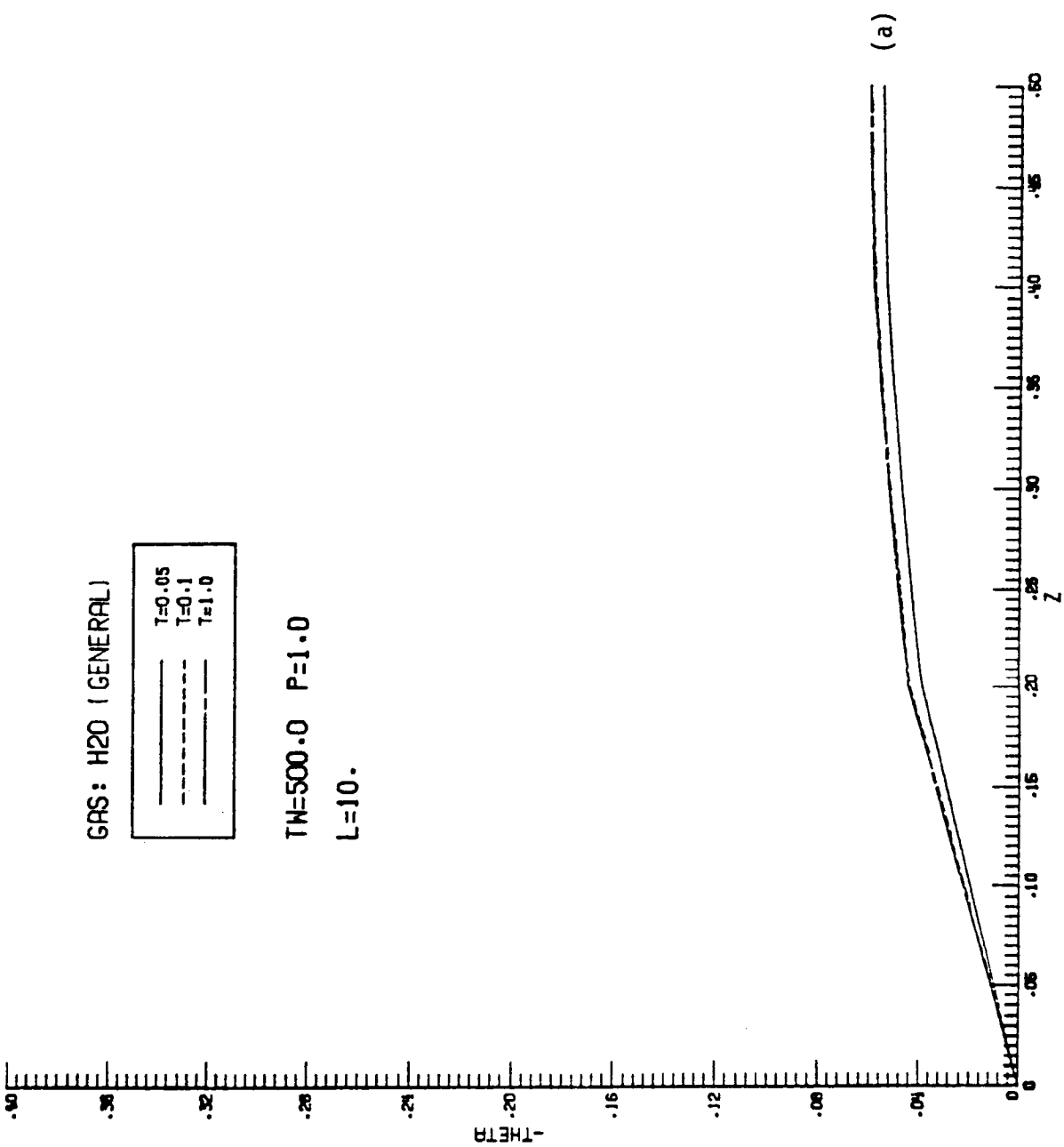

Figure B.8. Results for temperature variation across the duct (θ vs. ξ) for H_2O.

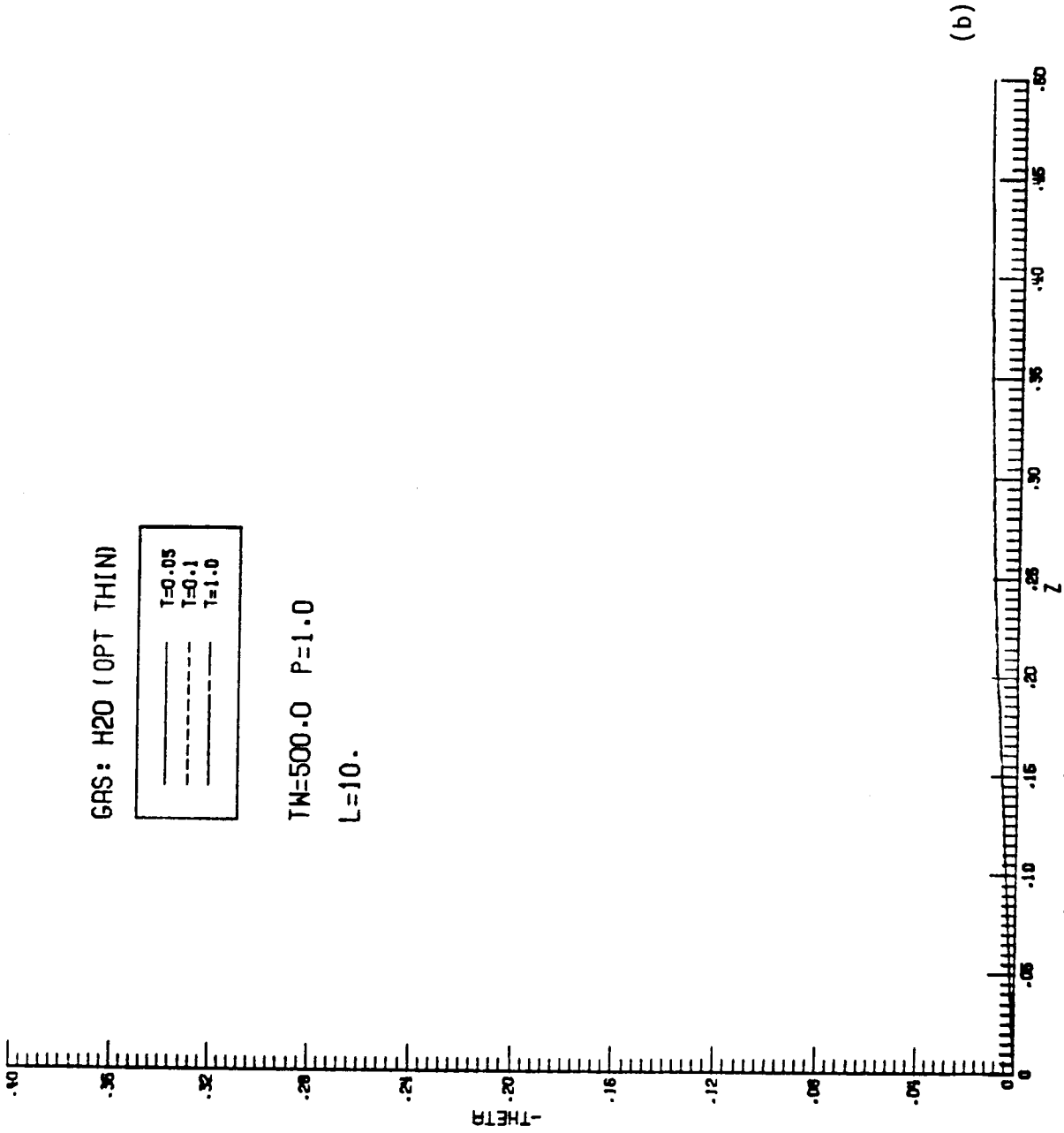

Figure B.8 (continued)

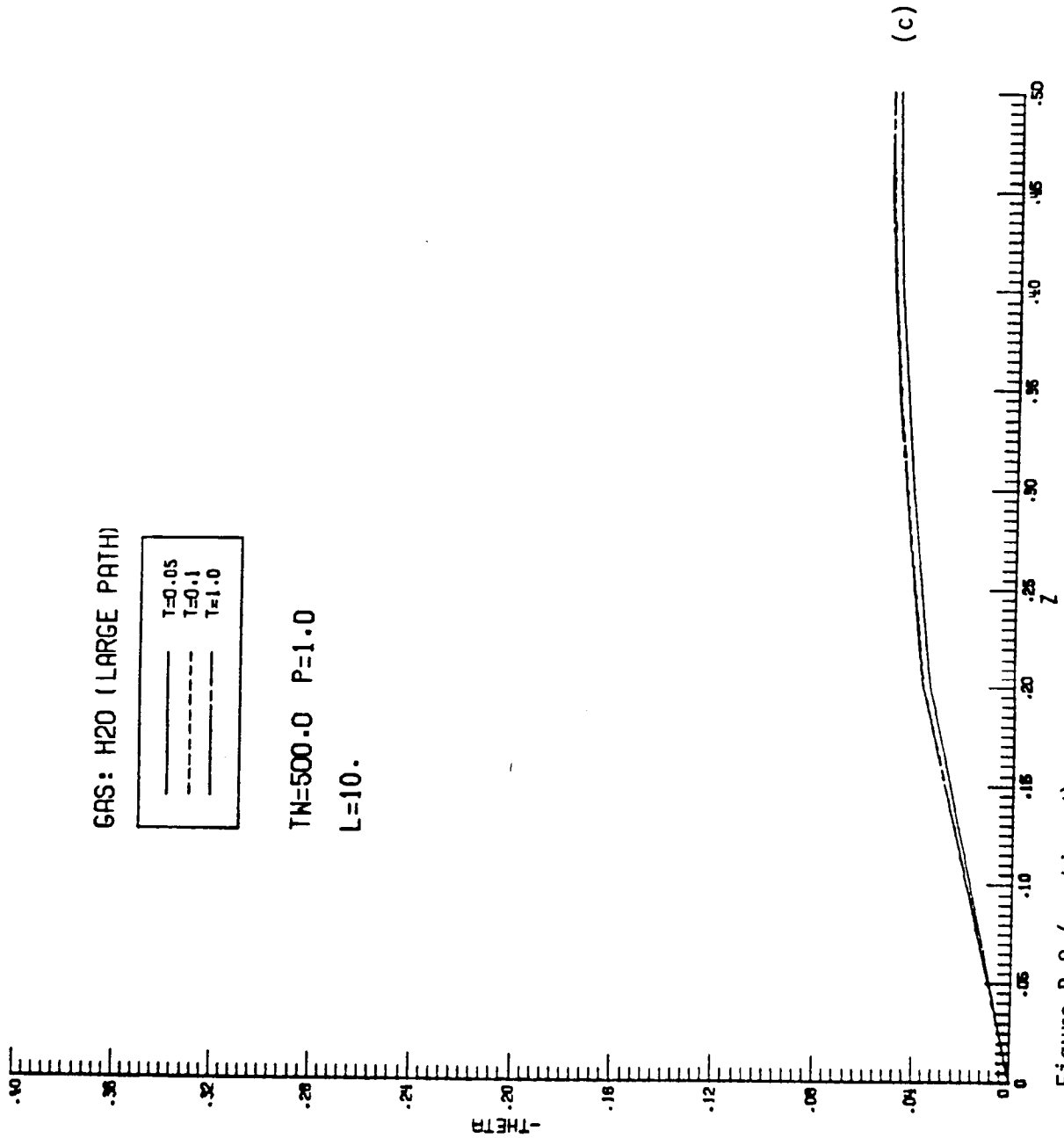

Figure B.8 (continued)

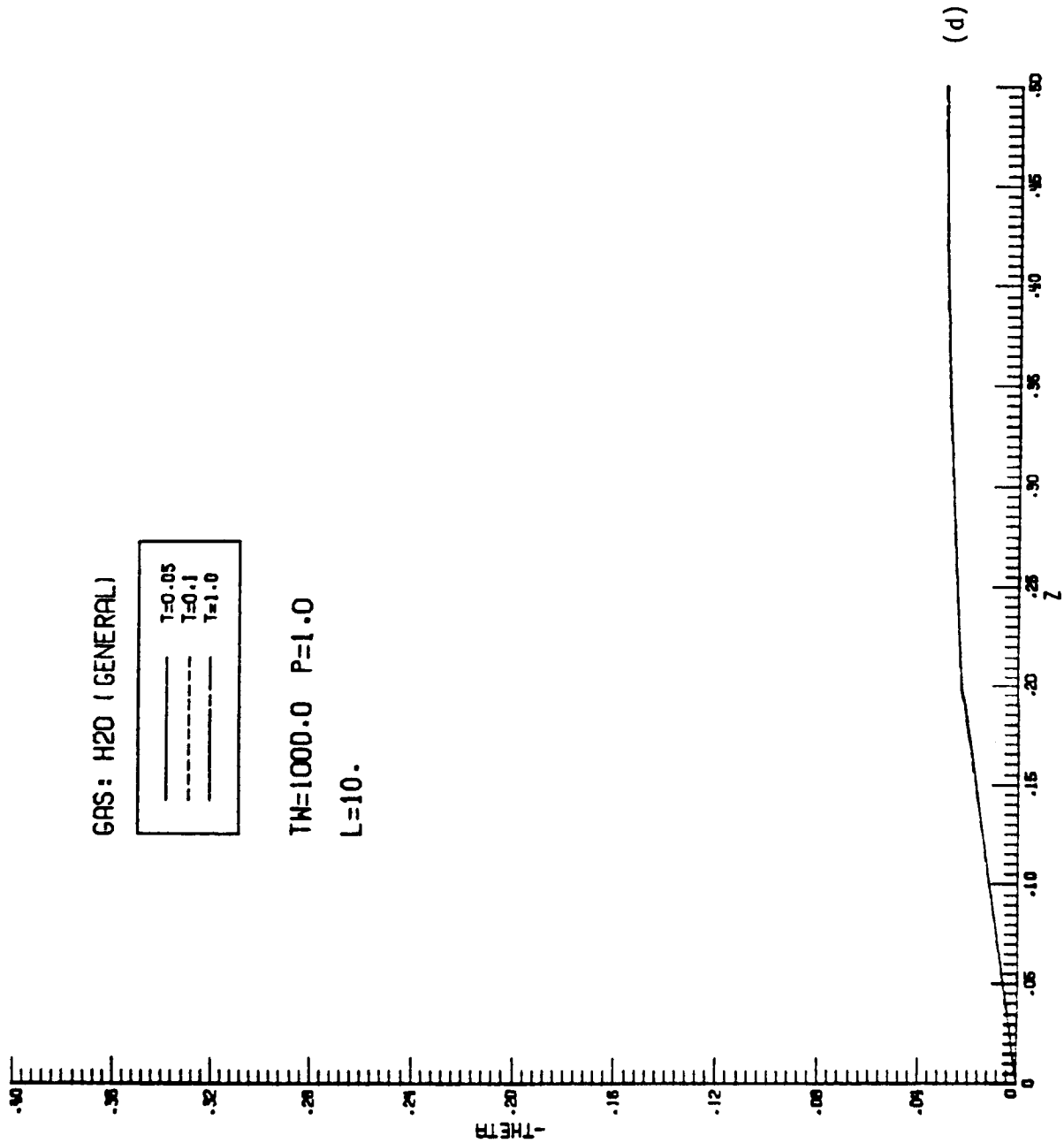

Figure B.8 (continued)

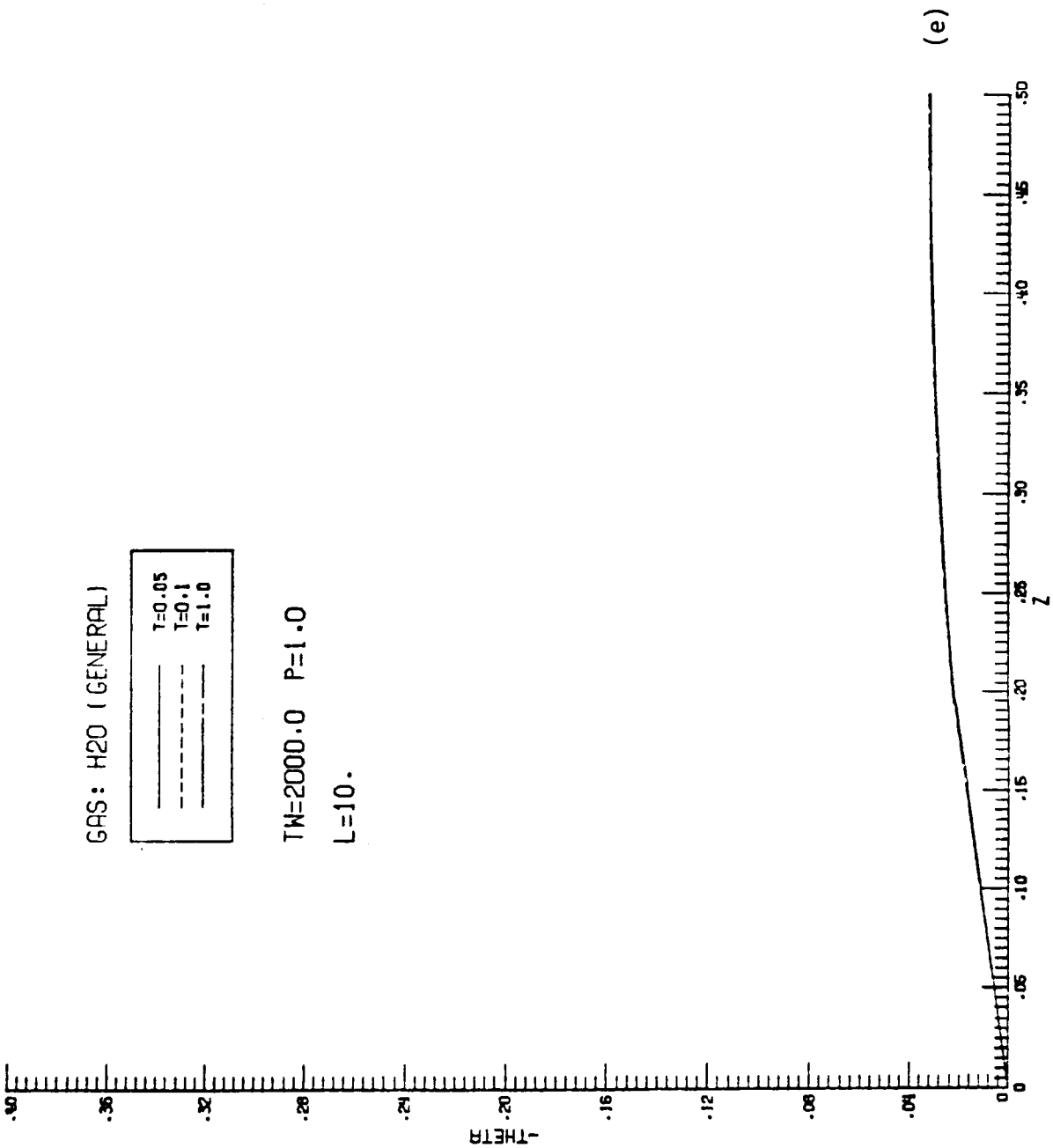

Figure B.8 (continued)

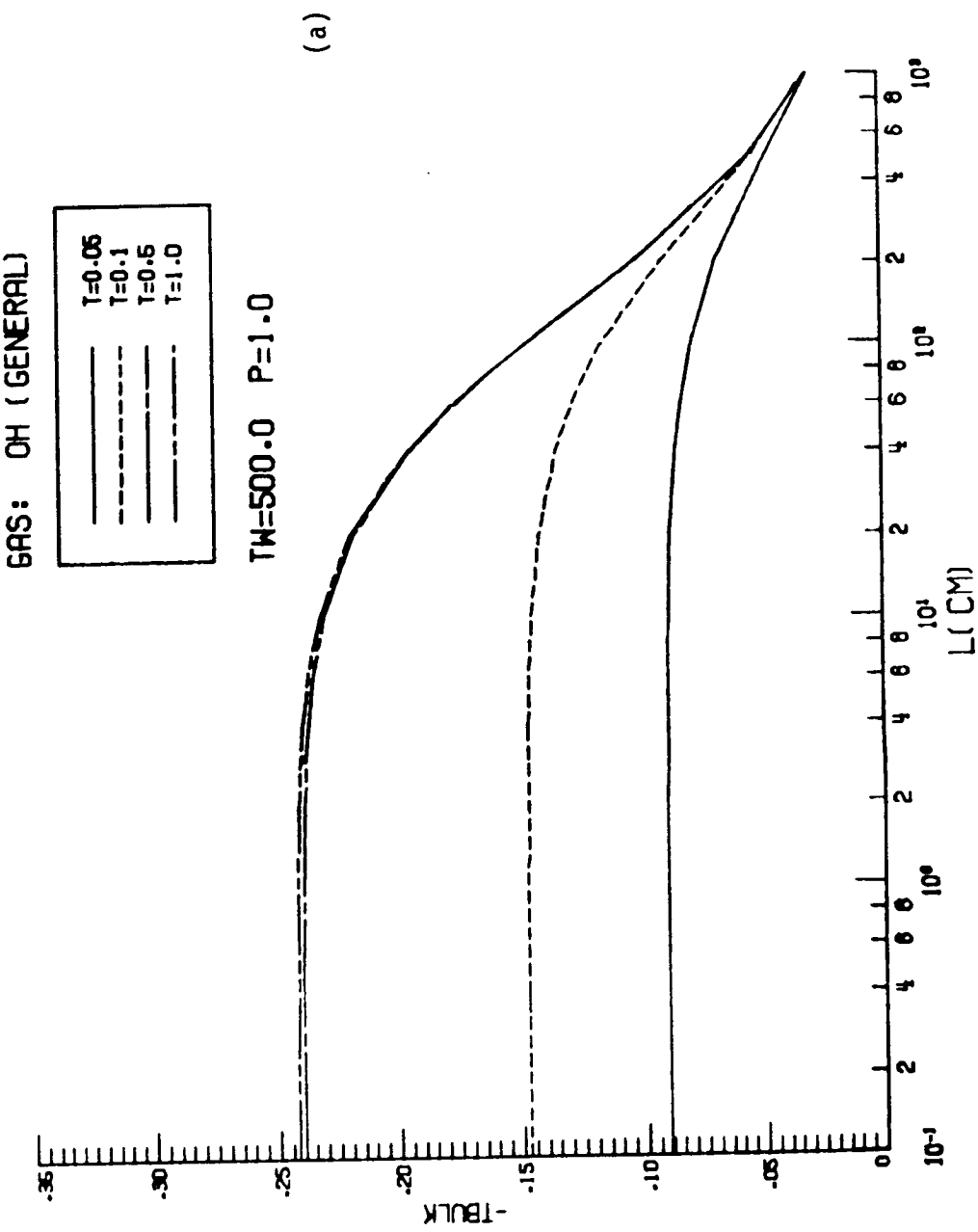

Figure B.9. Results for bulk temperature variation with plate spacing (θ_b vs. L) for OH.

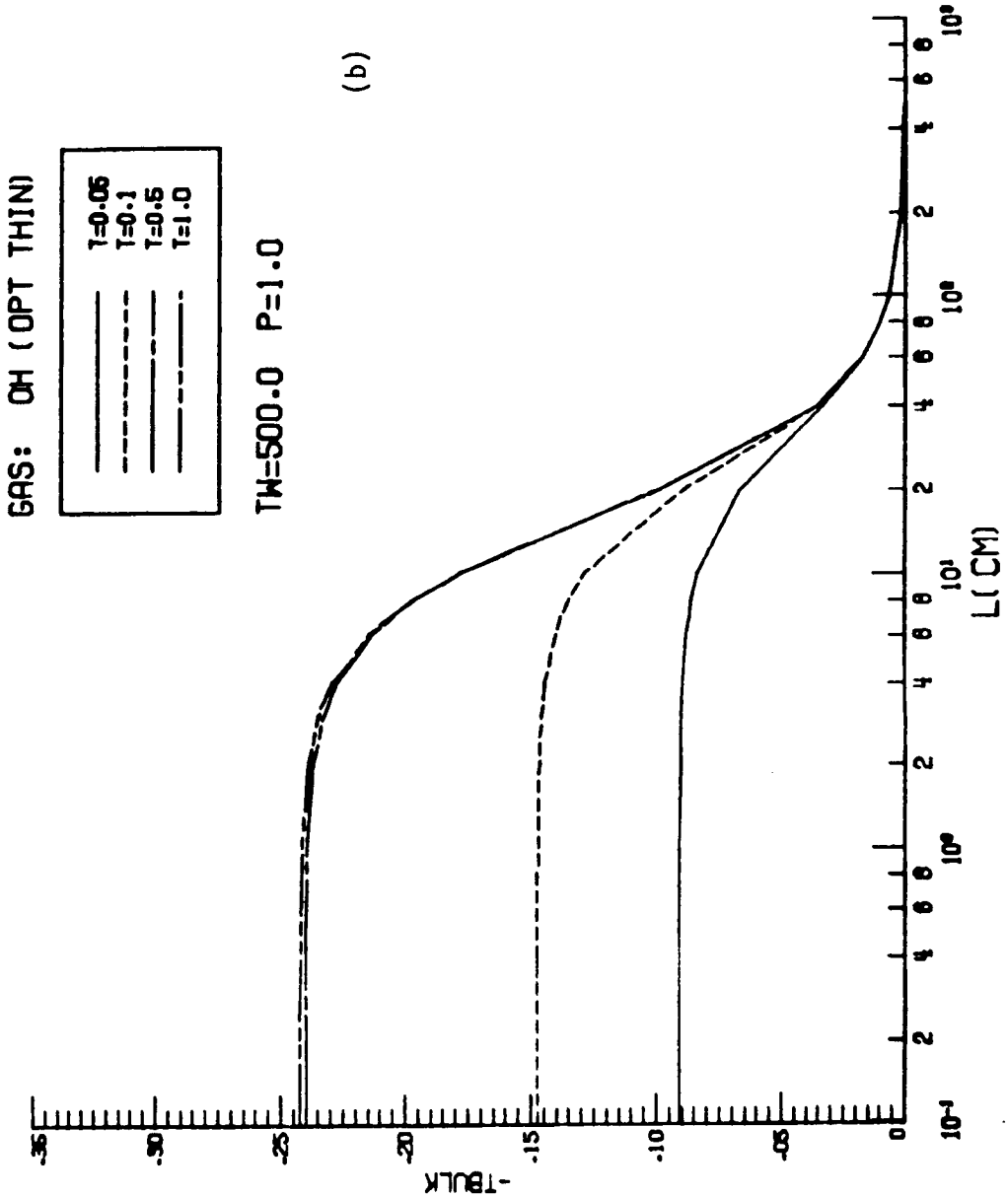

Figure B.9 (continued)

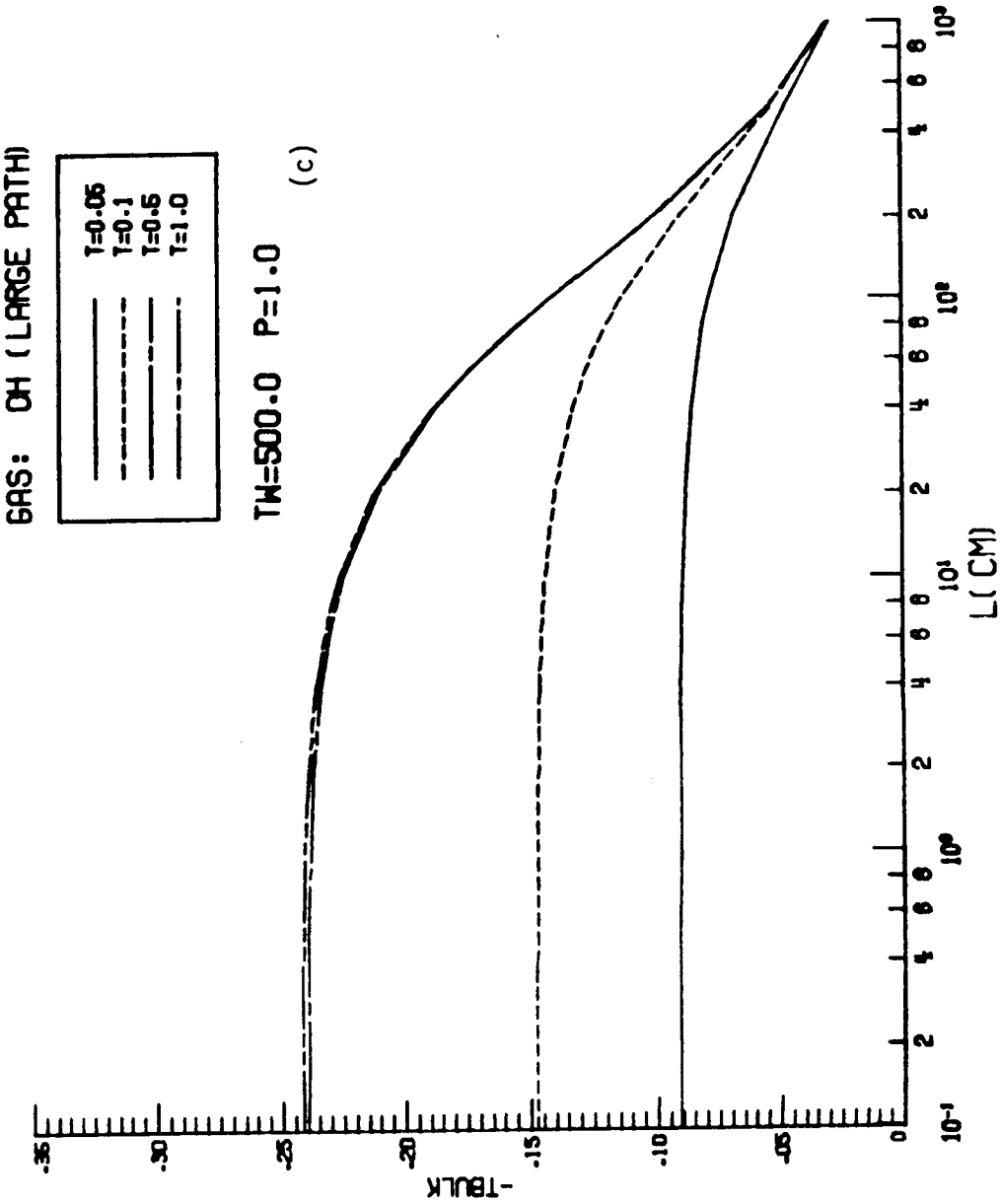

Figure B.9 (continued)

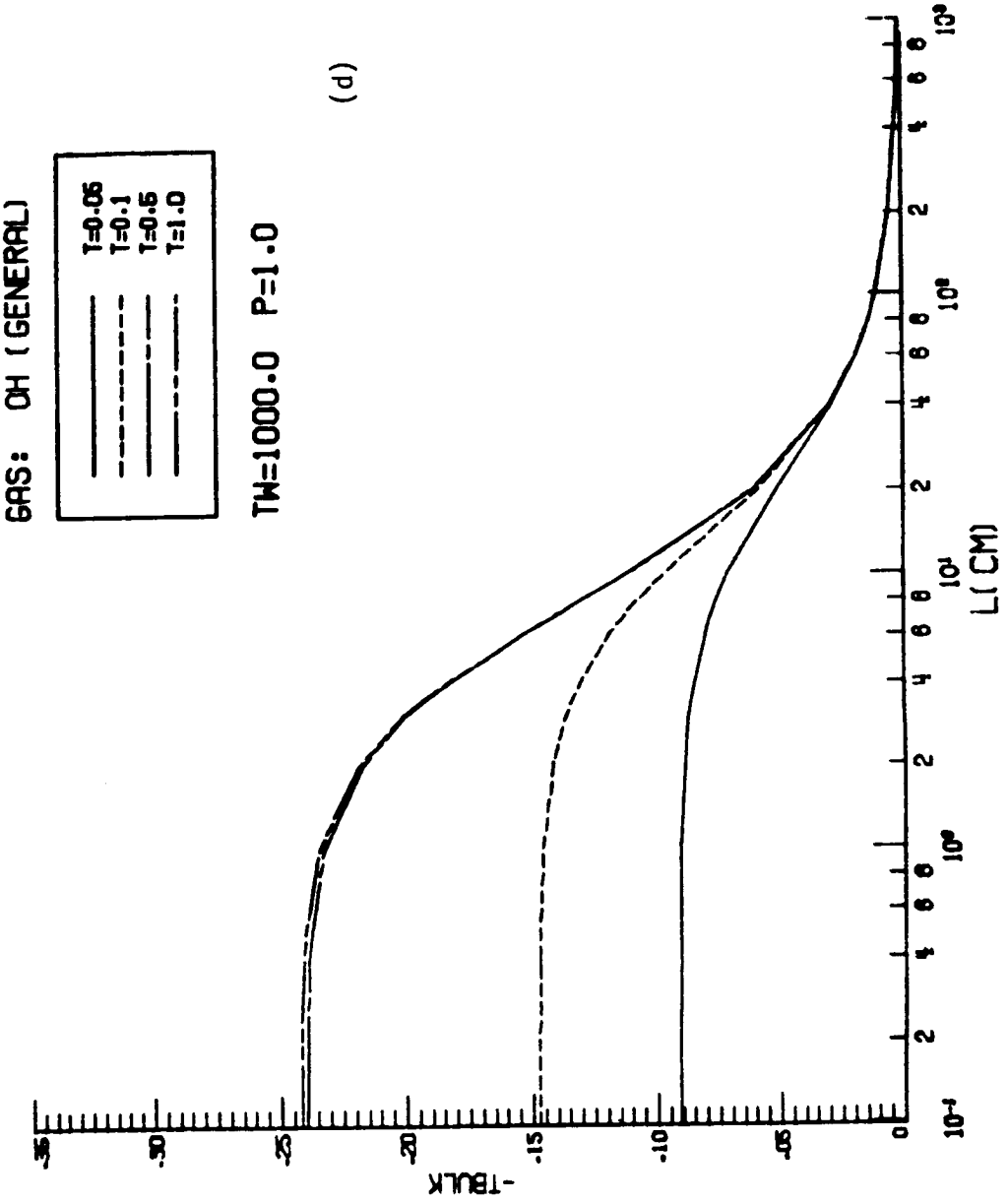

Figure B.9 (continued)

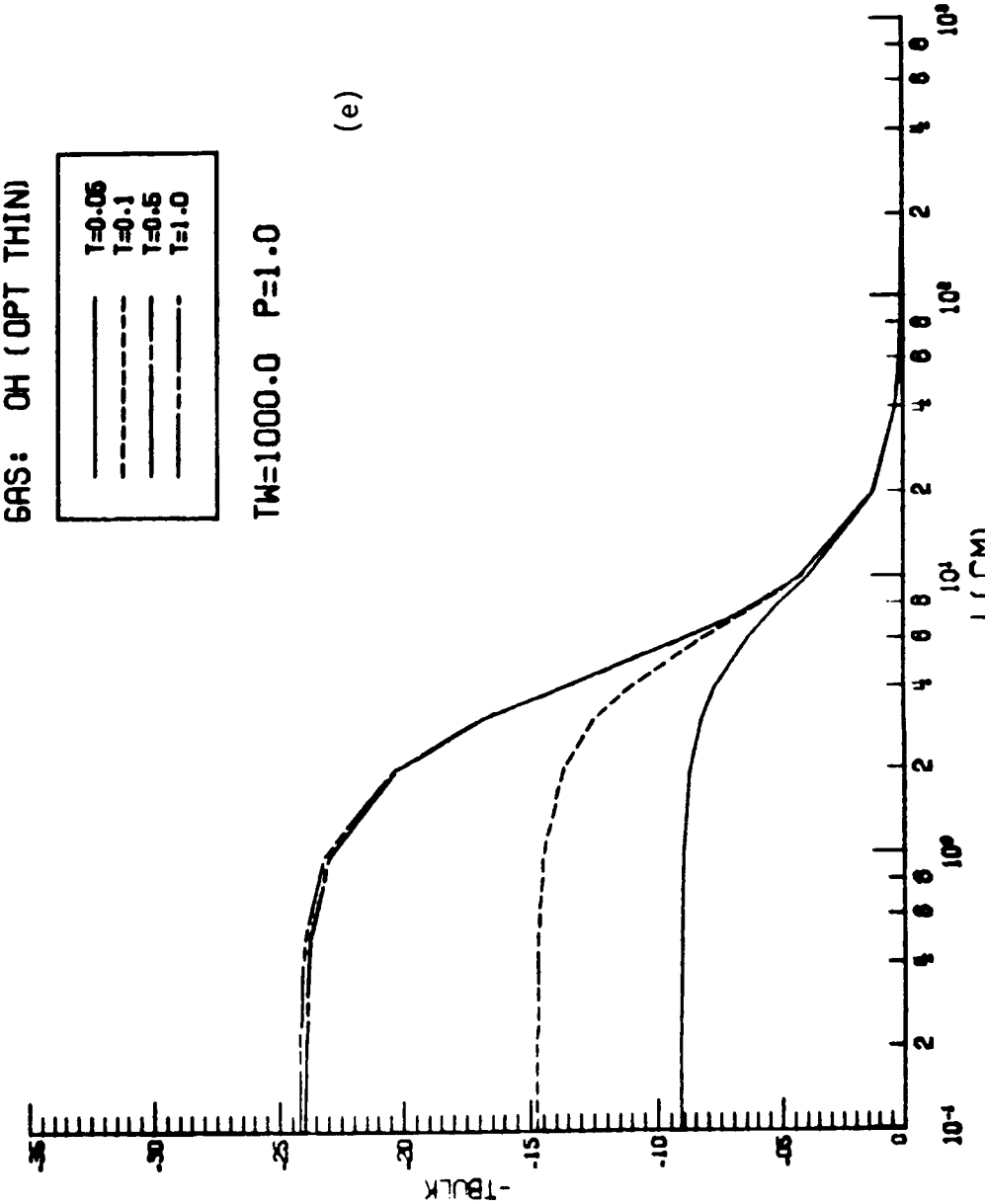

Figure B.9 (continued)

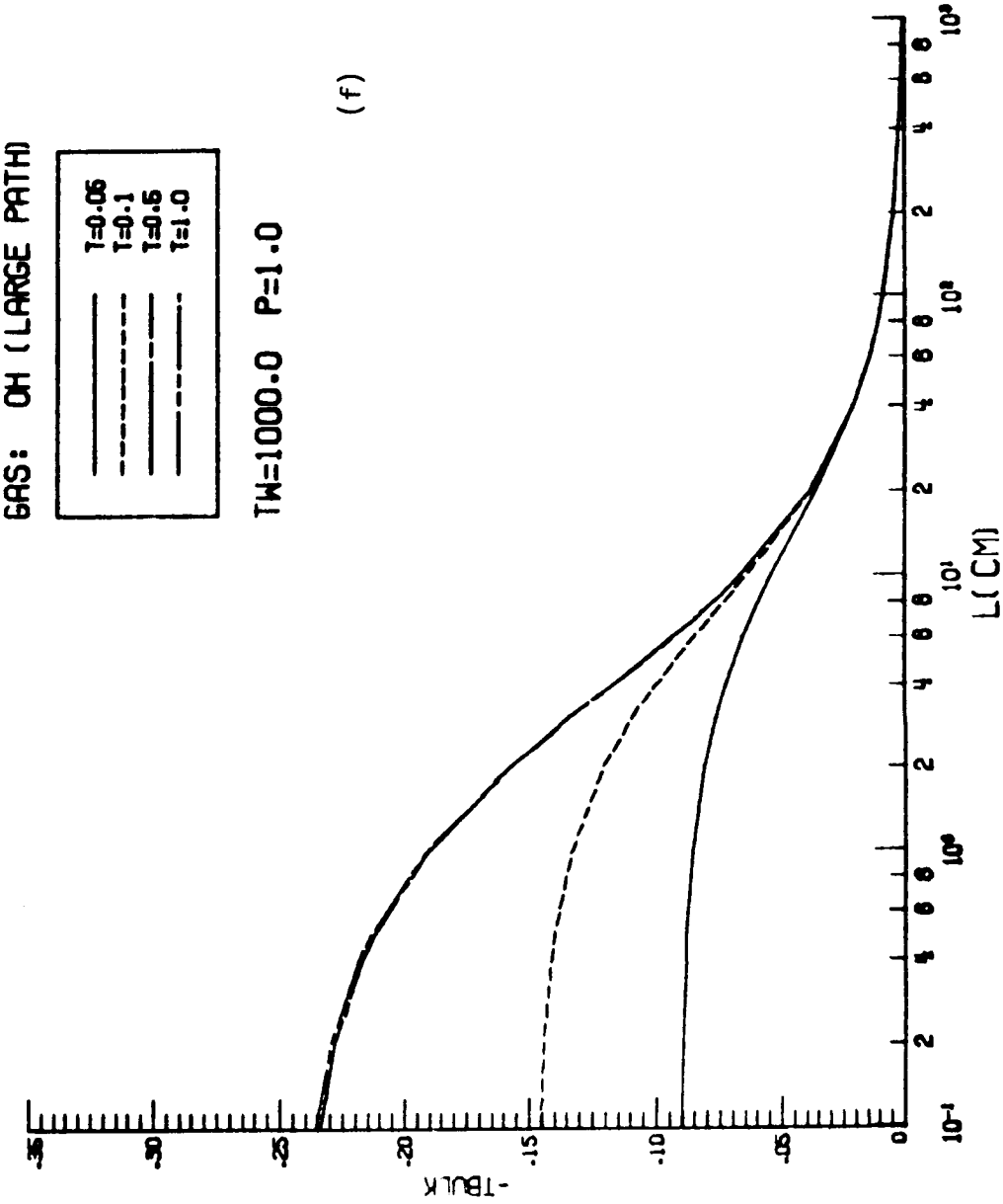

Figure B.9 (continued)

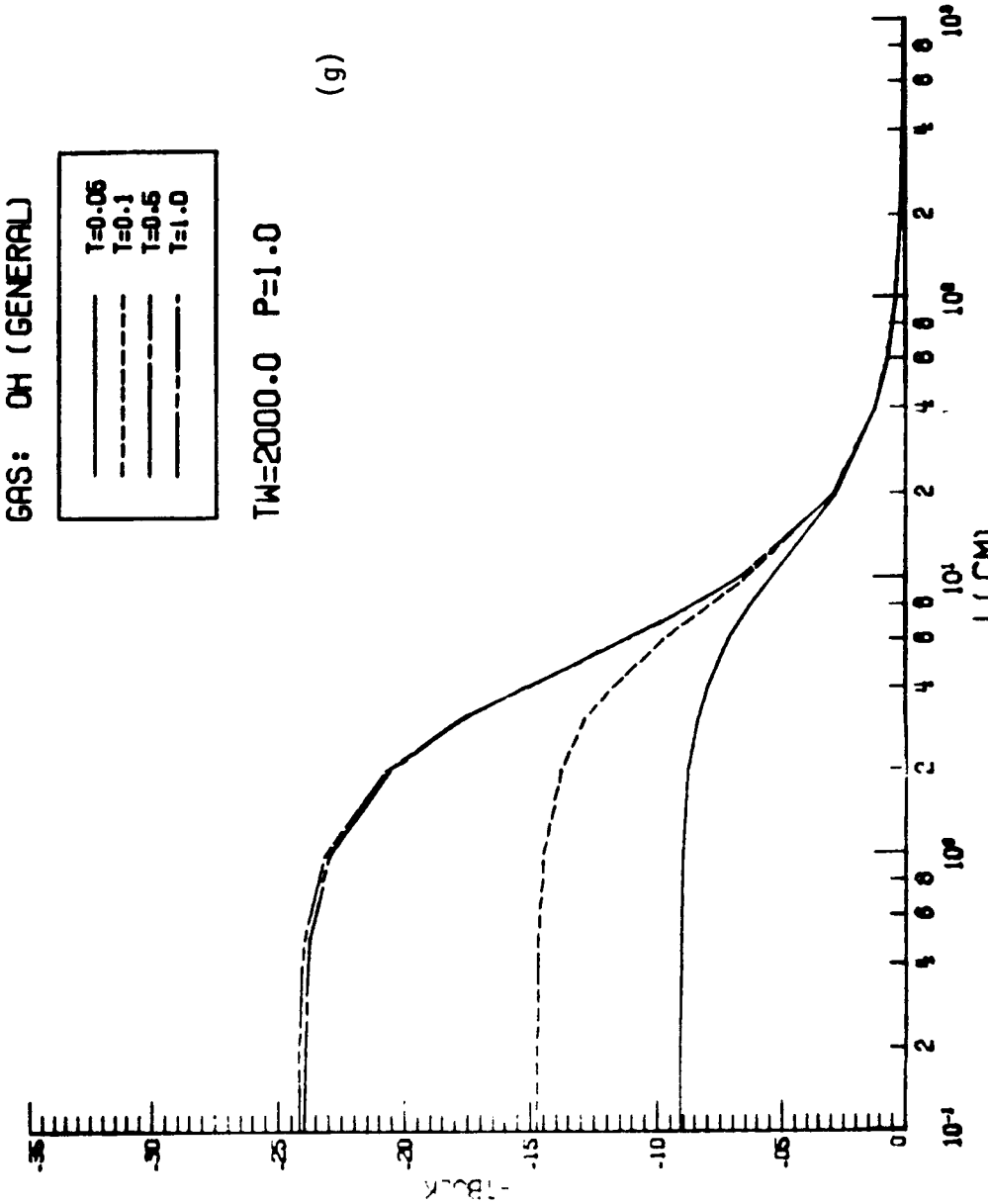

Figure B.9 (continued)

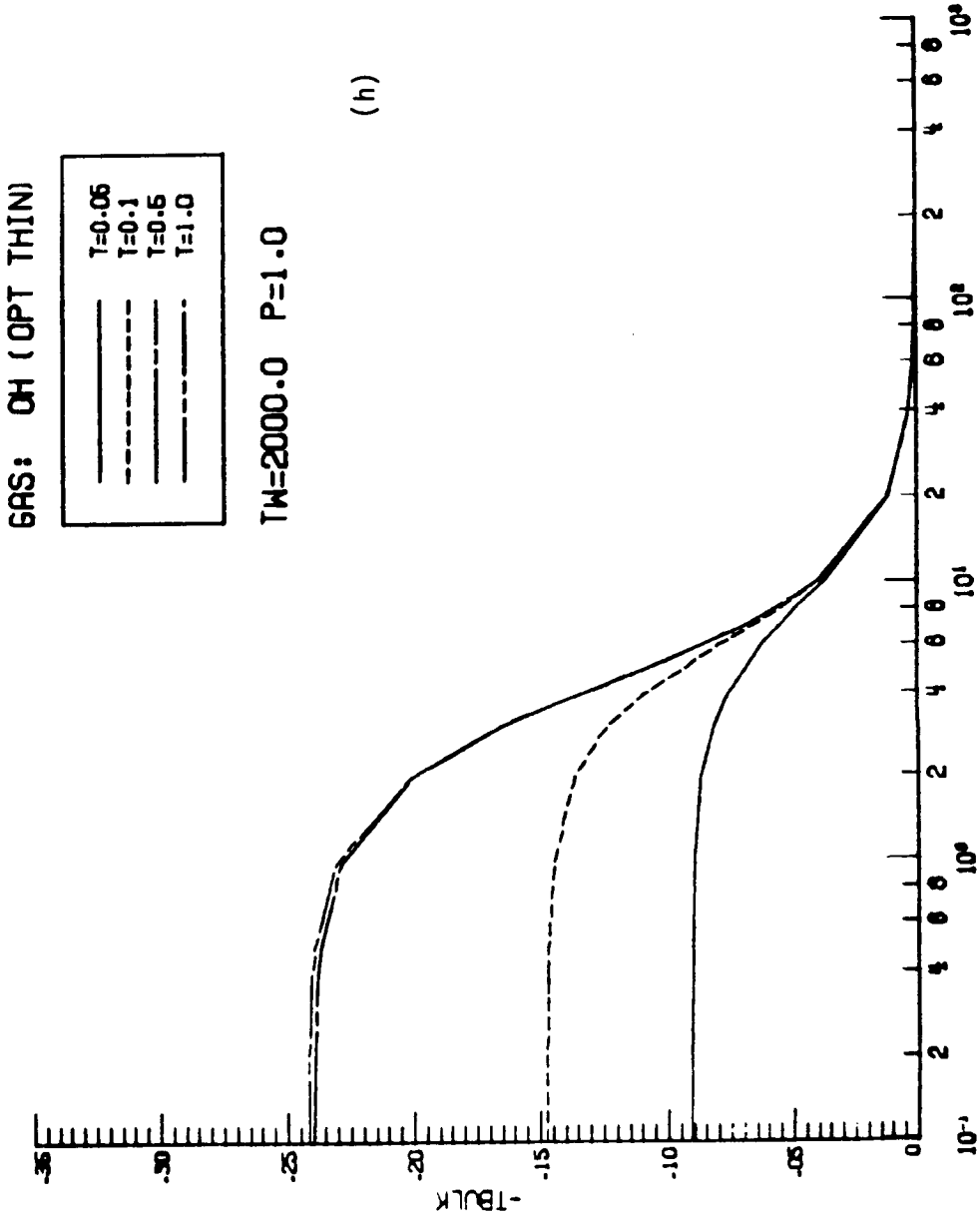

Figure B.9 (continued)

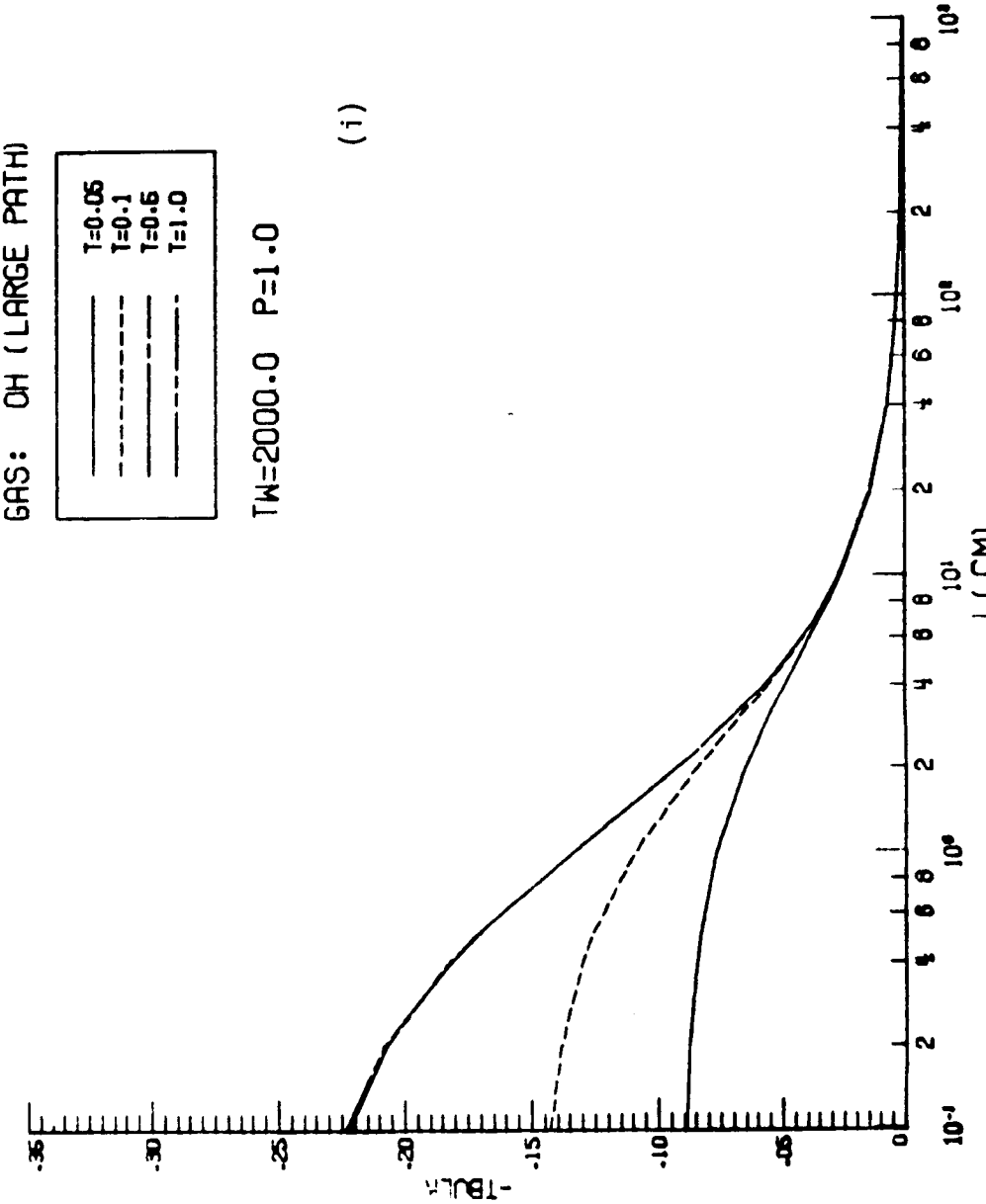

Figure B.9 (continued)

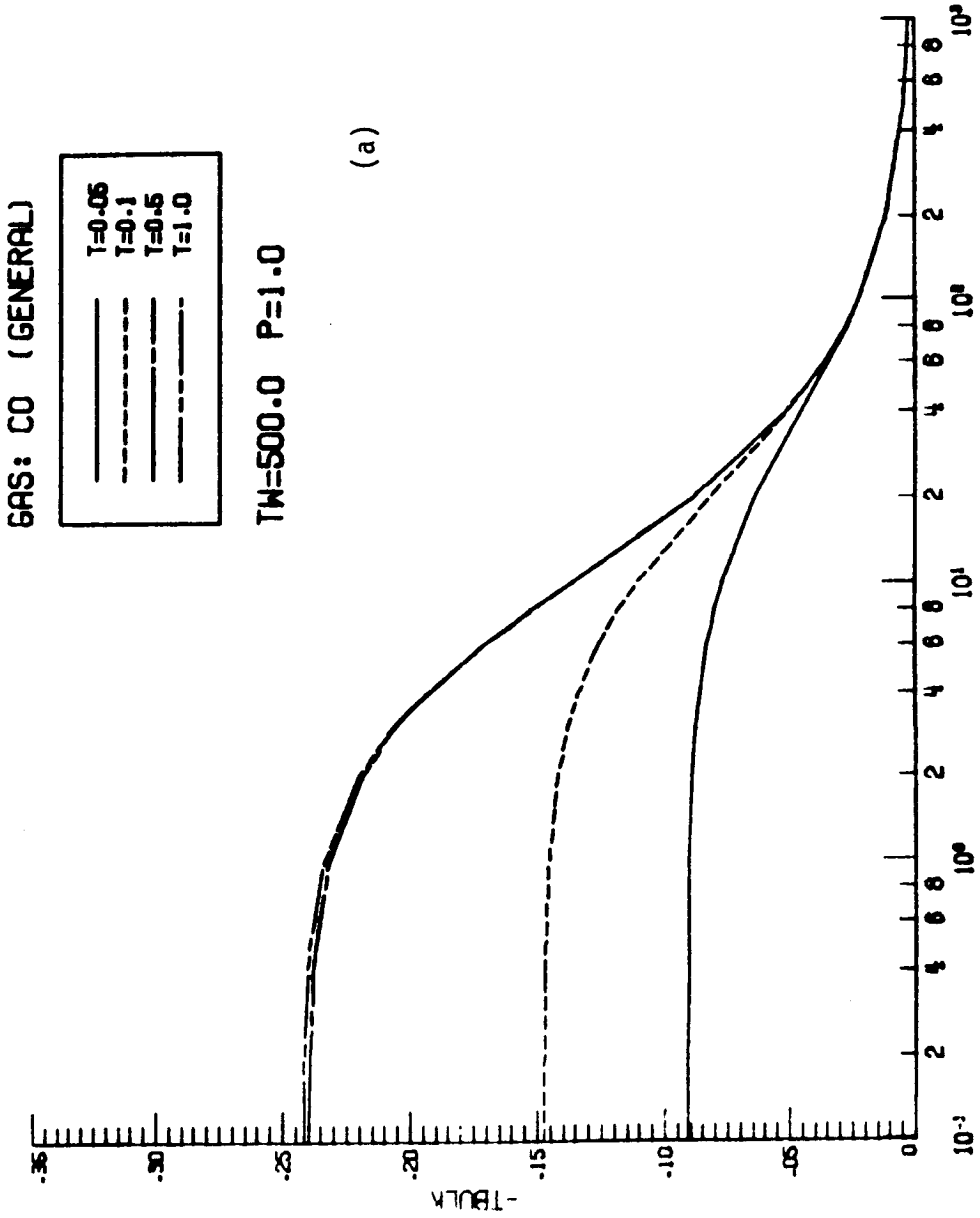

Figure B.10. Results for bulk temperature variation with plate spacing (θ_b vs. L) for CO.

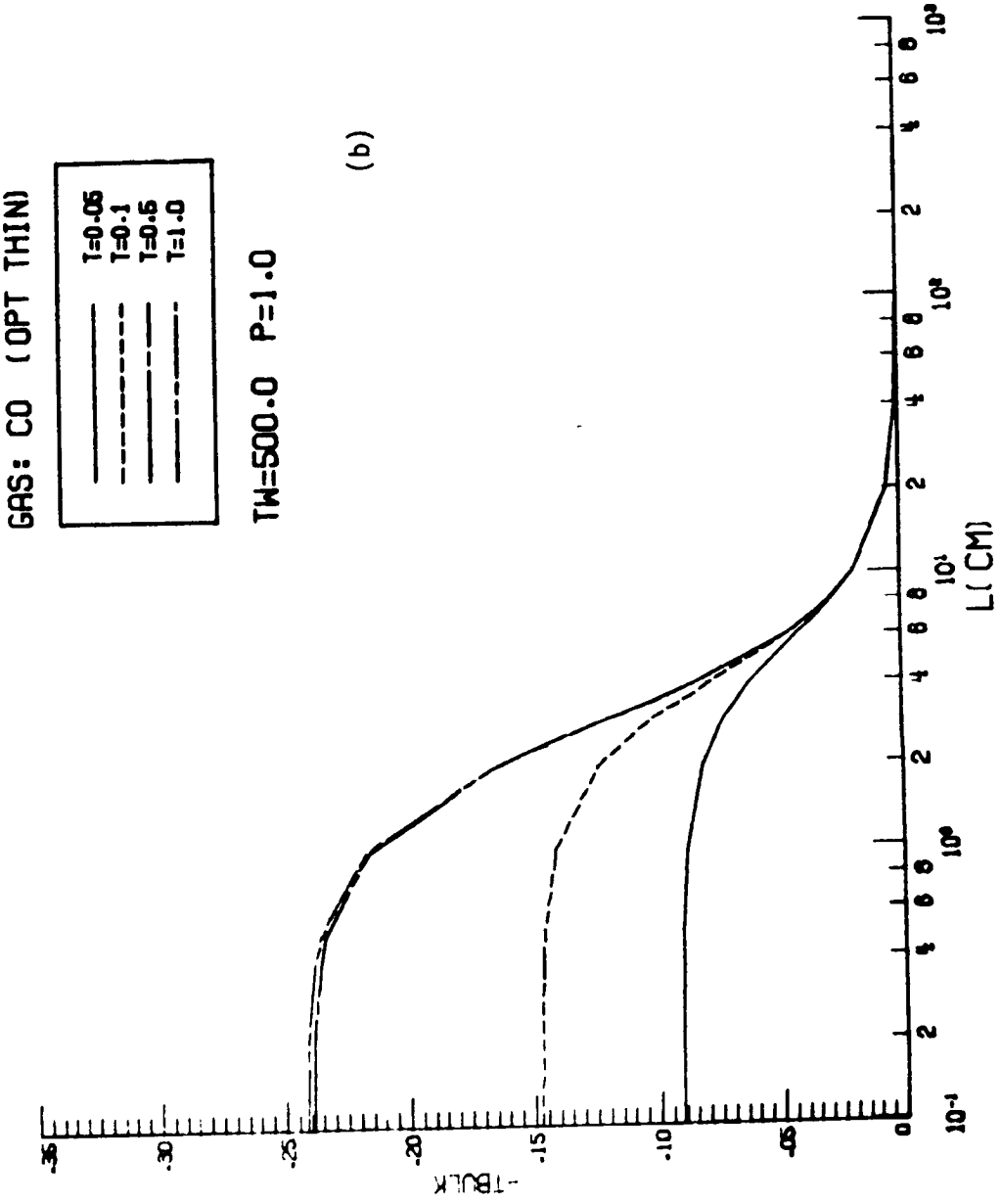

Figure B.10 (continued)

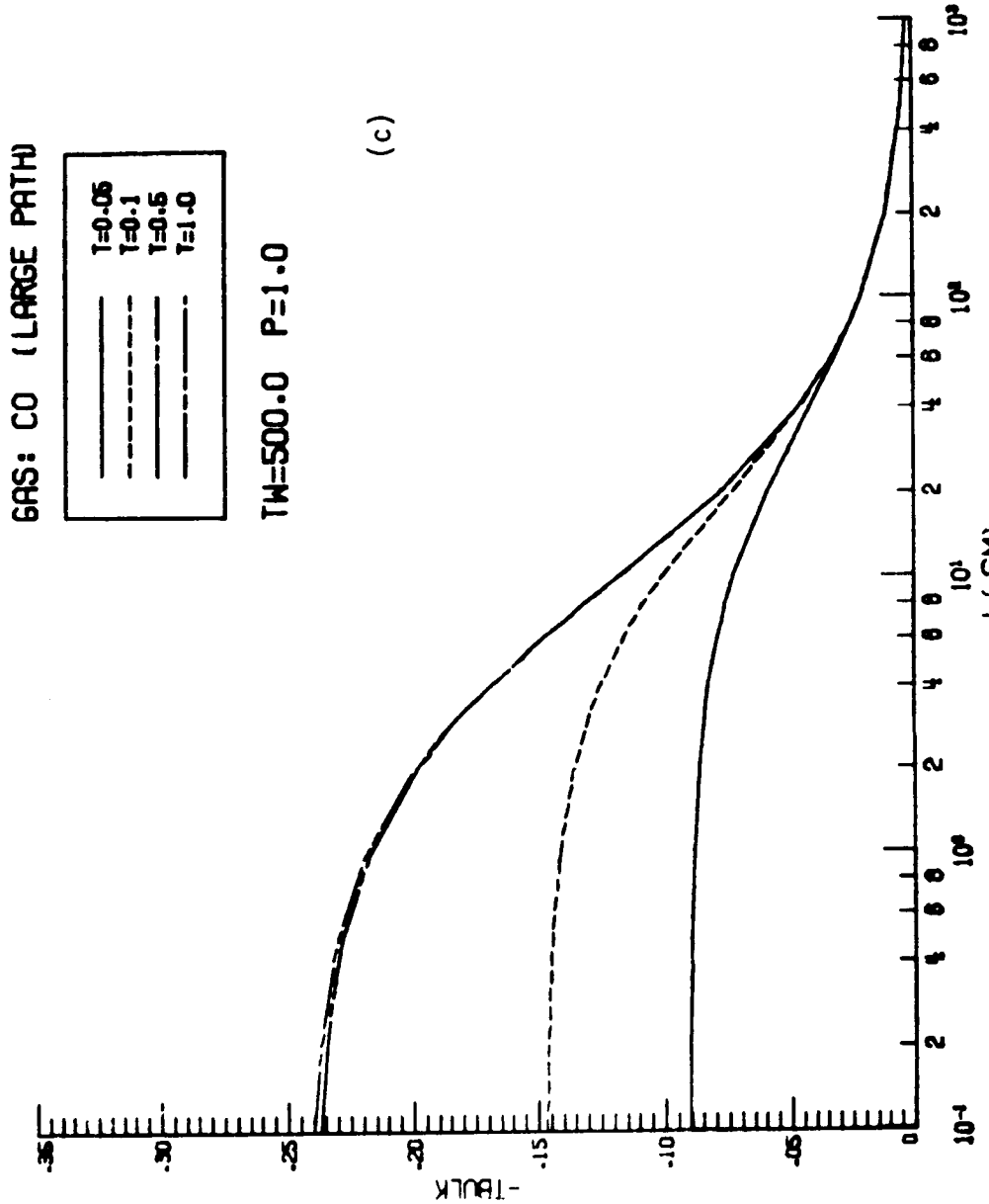

Figure B.10 (continued)

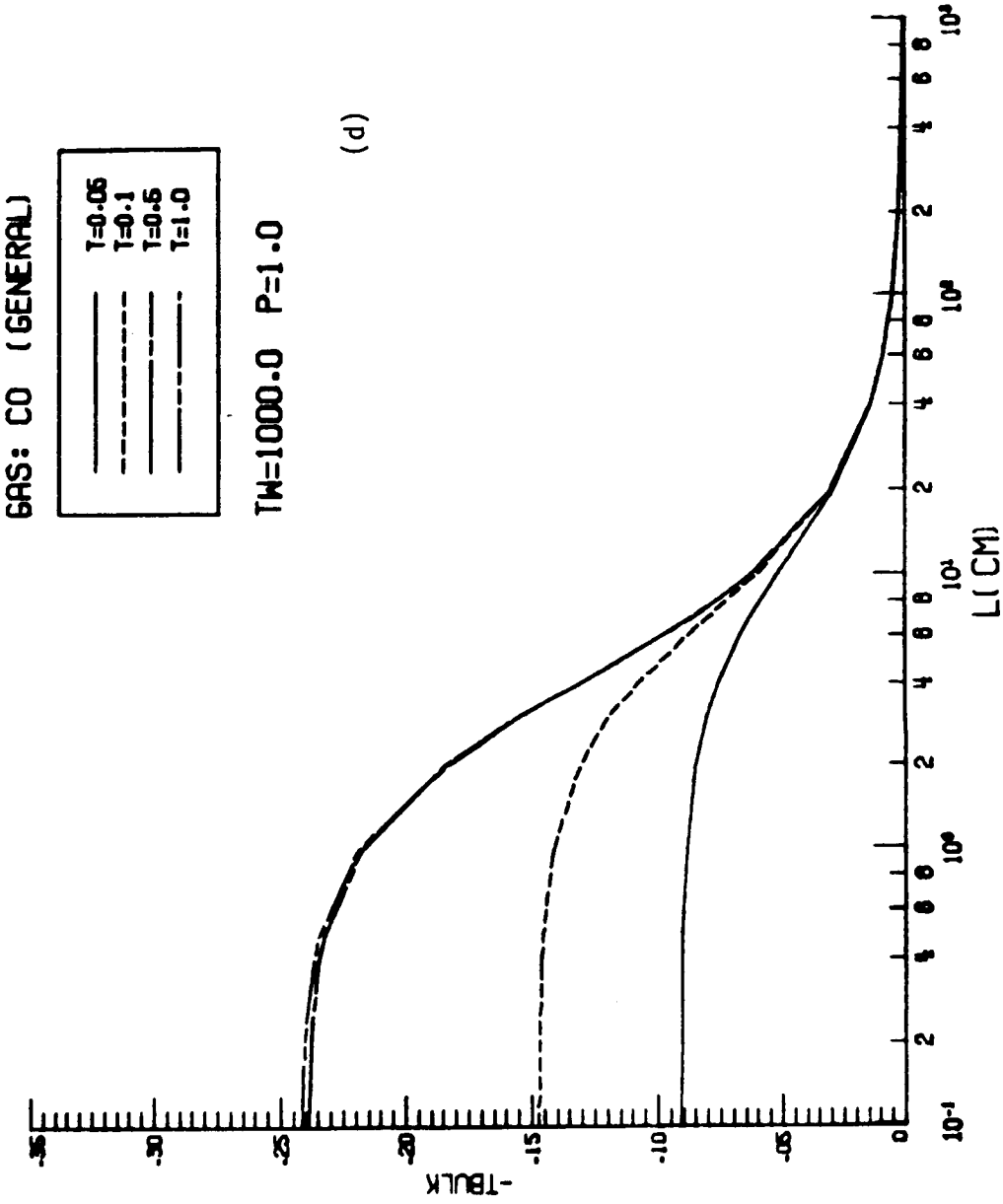

Figure B.10 (continued)

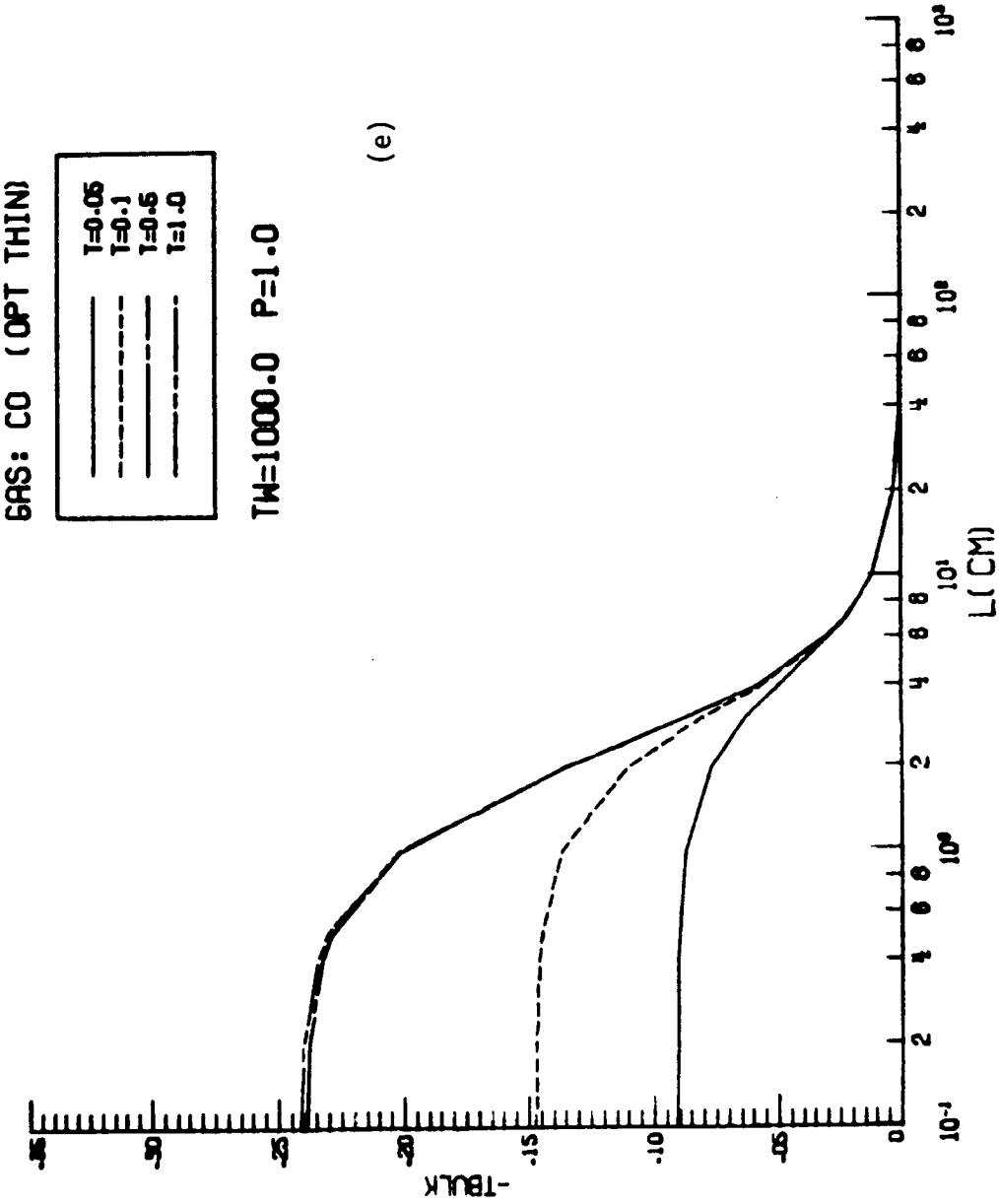

Figure B.10 (continued)

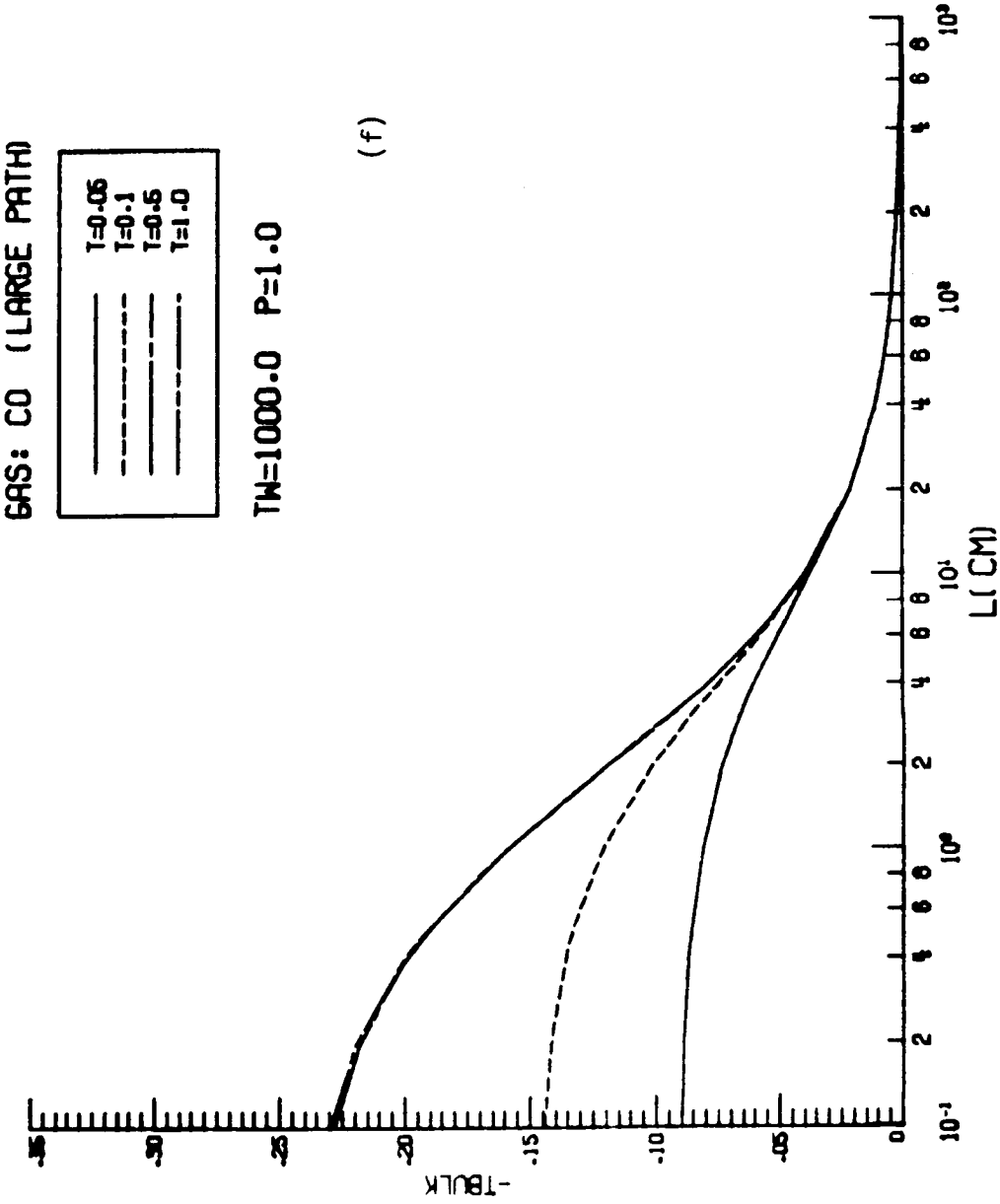

Figure B.10 (continued)

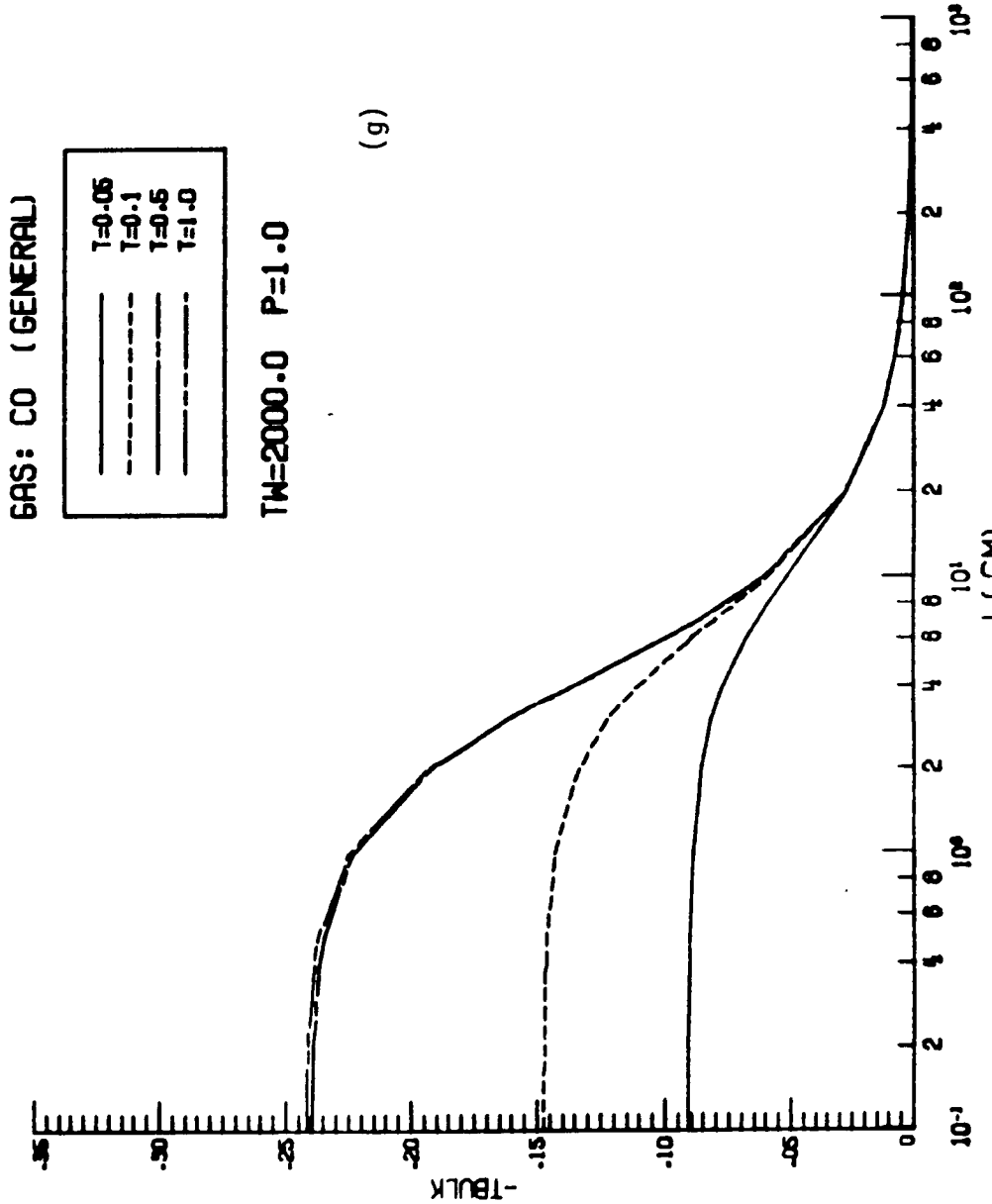

Figure B.10 (continued)

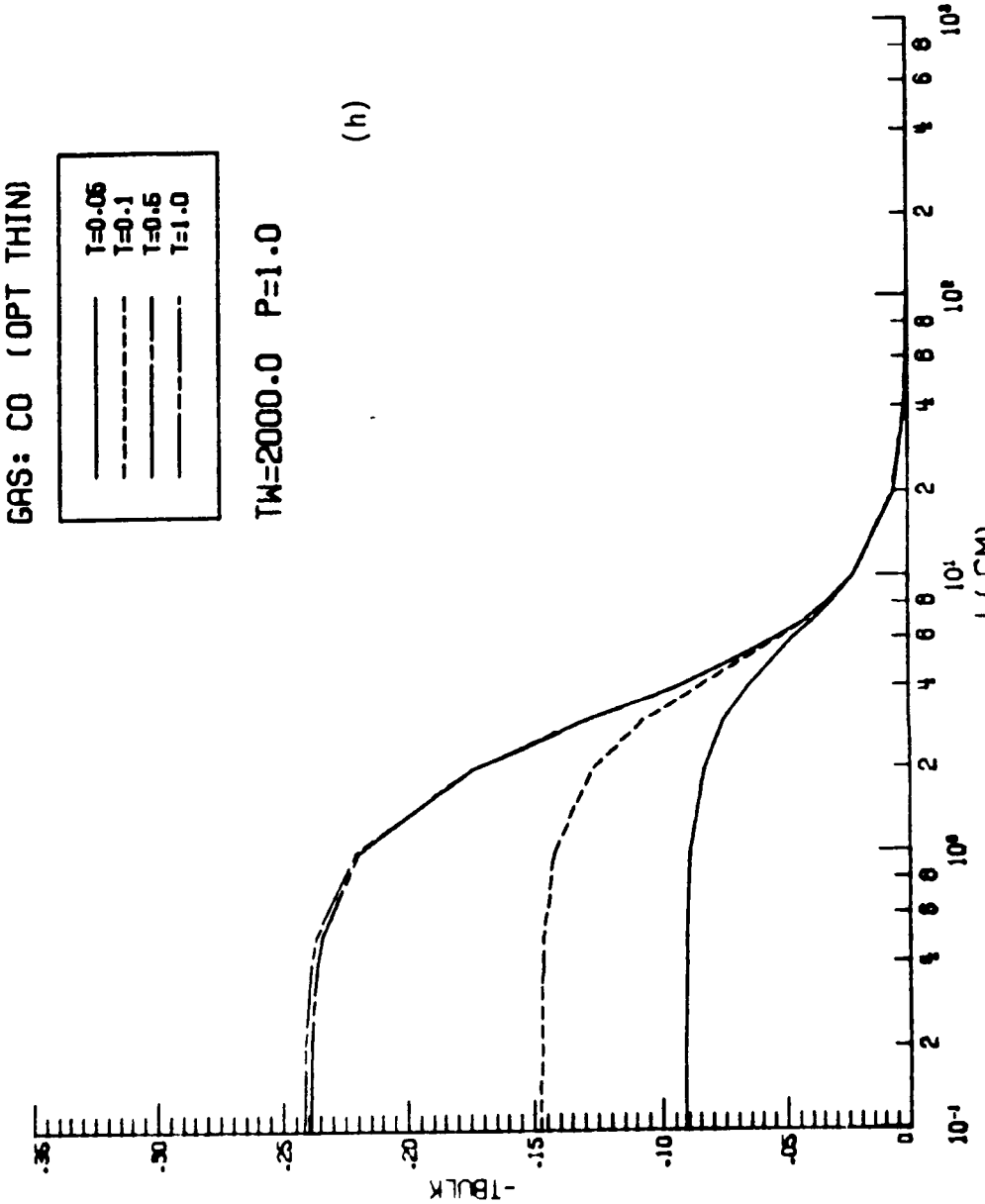

Figure B.10 (continued)

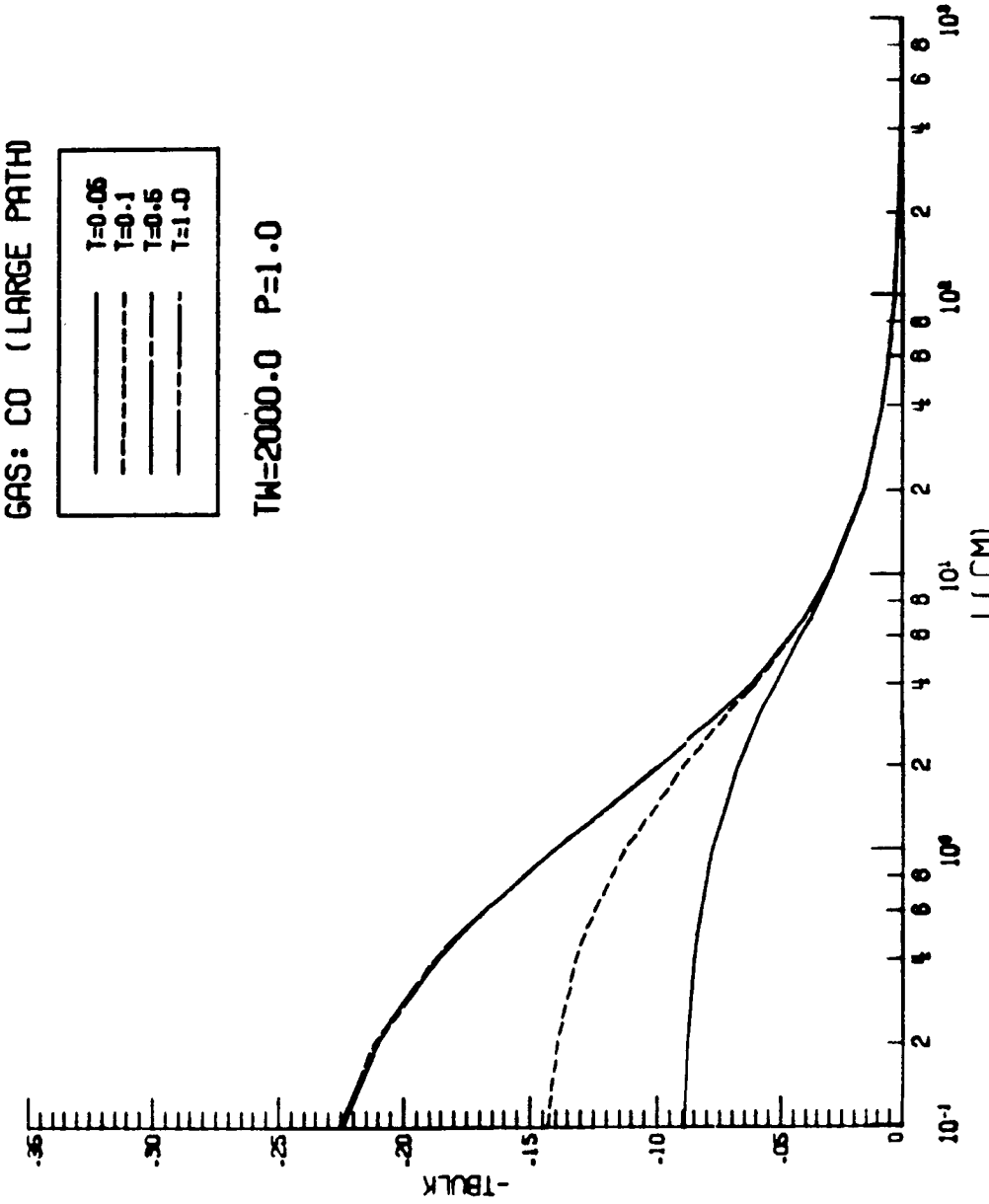

Figure B.10 (continued)

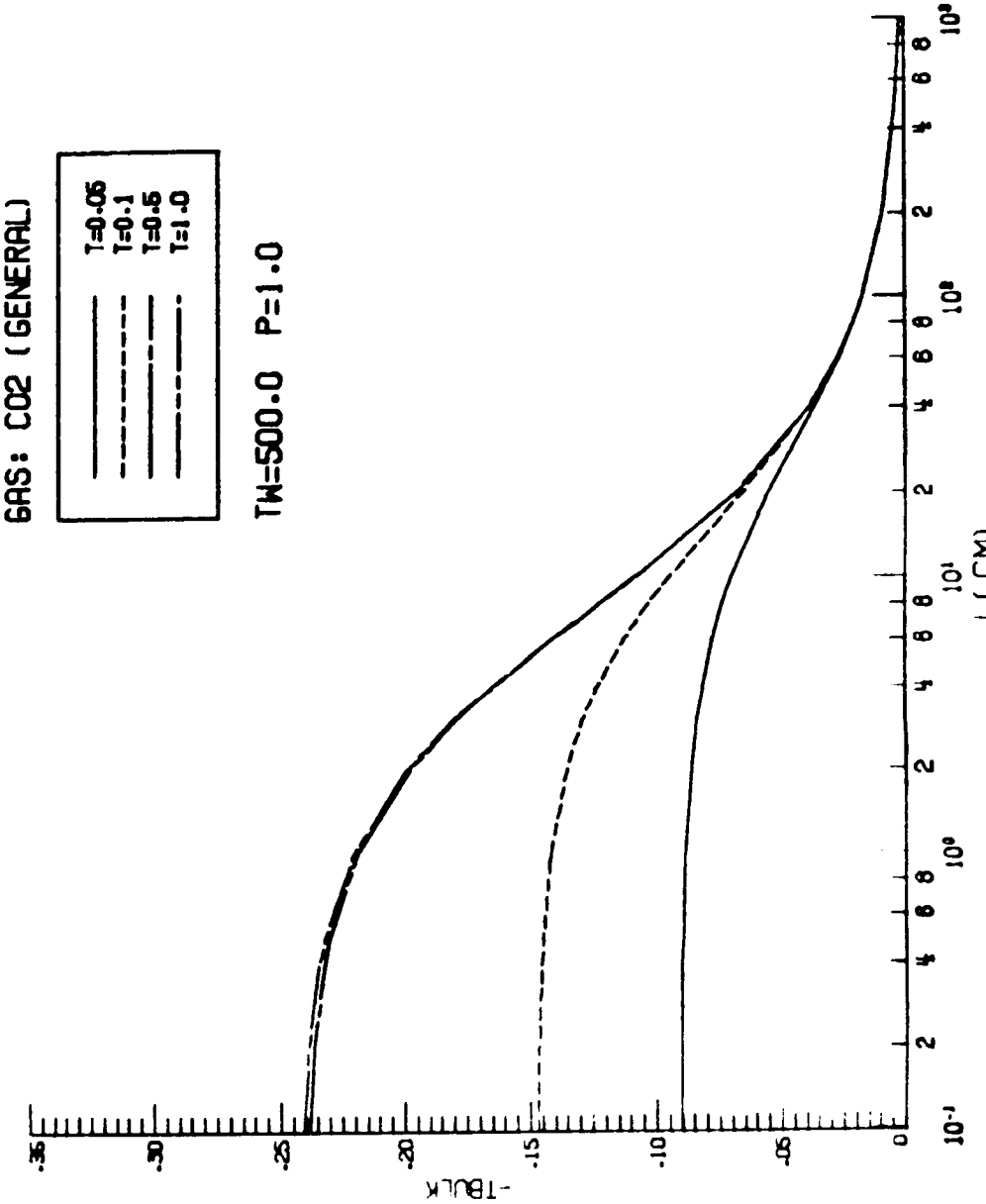

Figure B.11. Results for bulk temperature variation with plate spacing (θ_b vs. L) for CO_2.

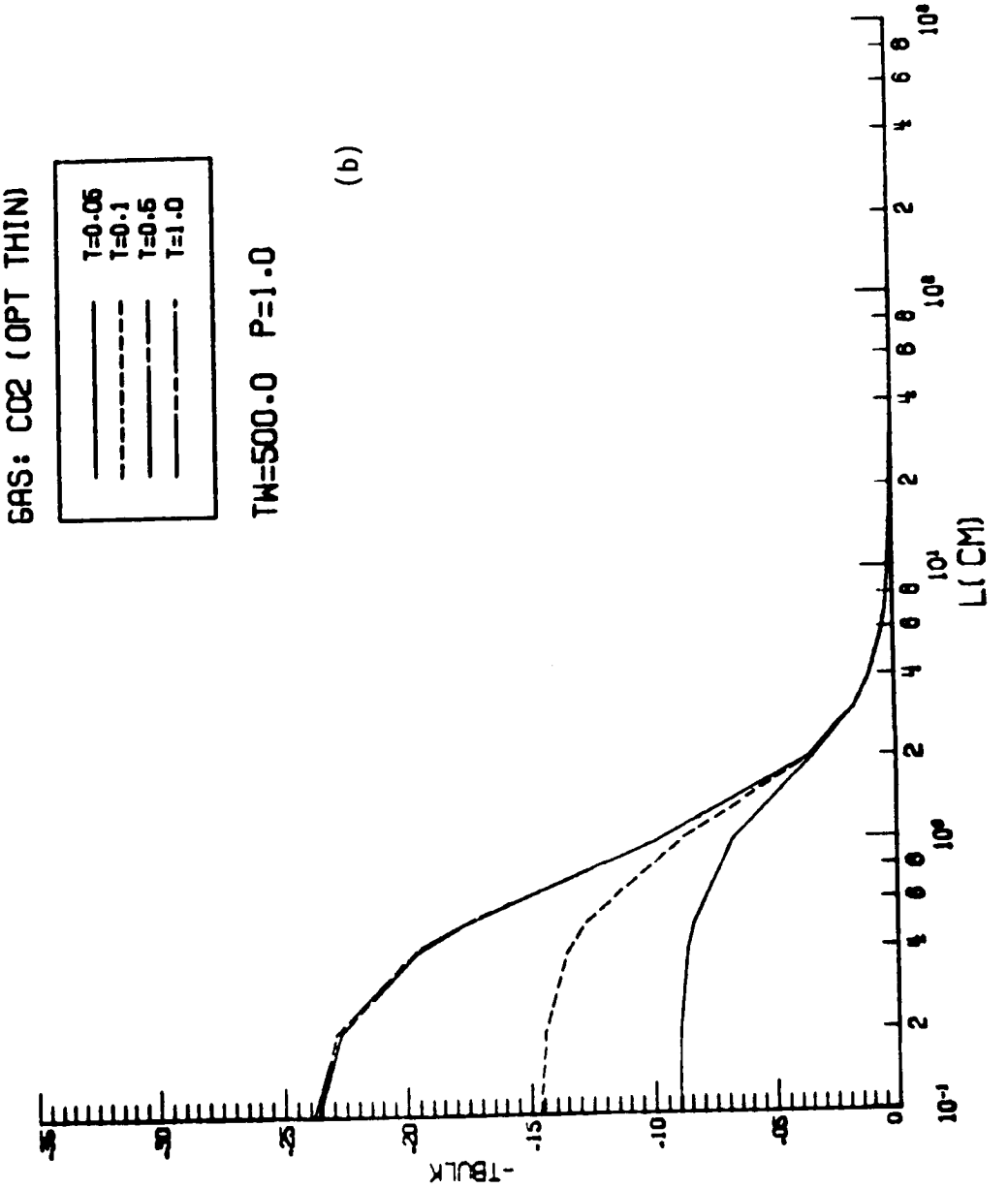

Figure B.11 (continued)

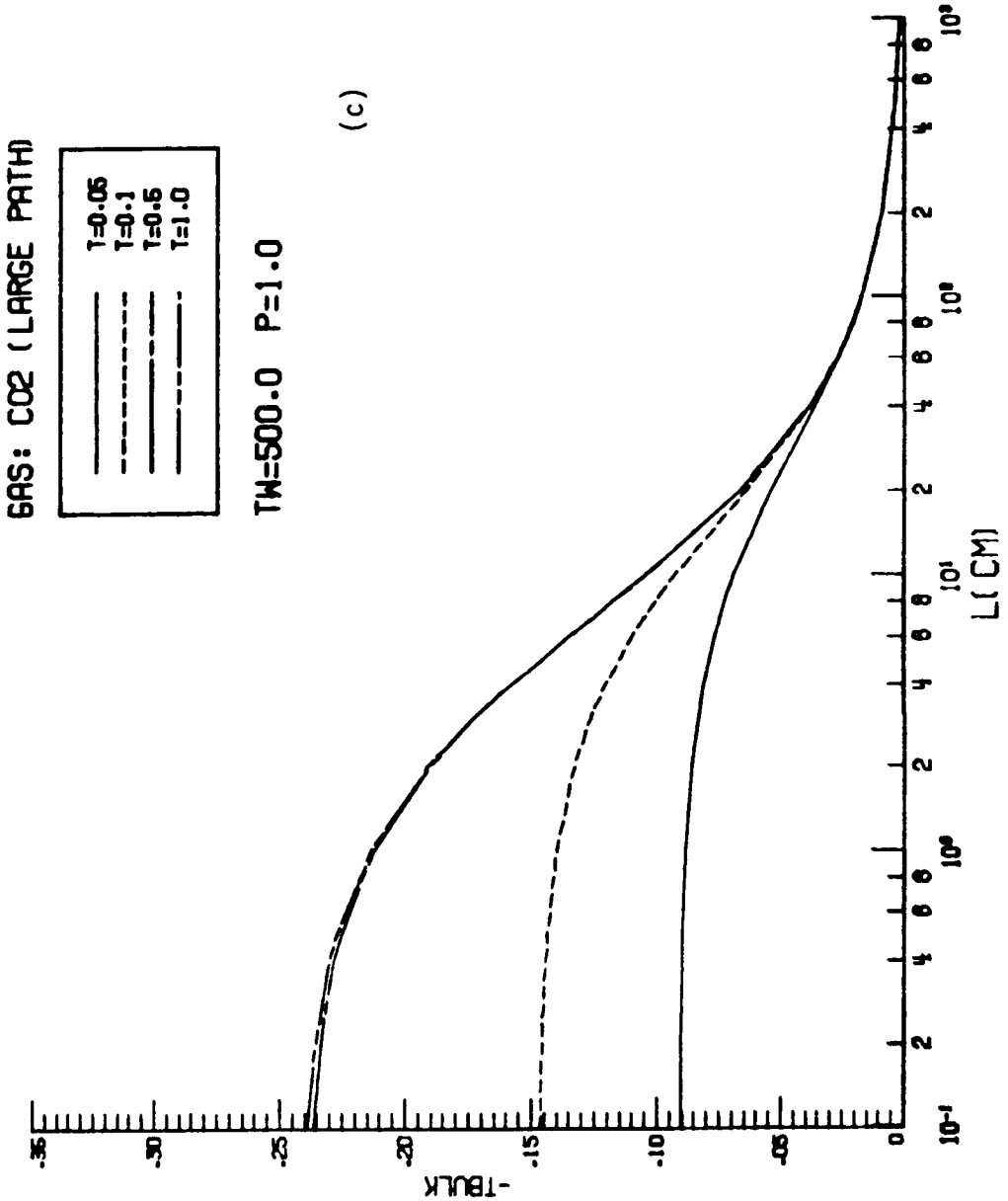

Figure B.11 (continued)

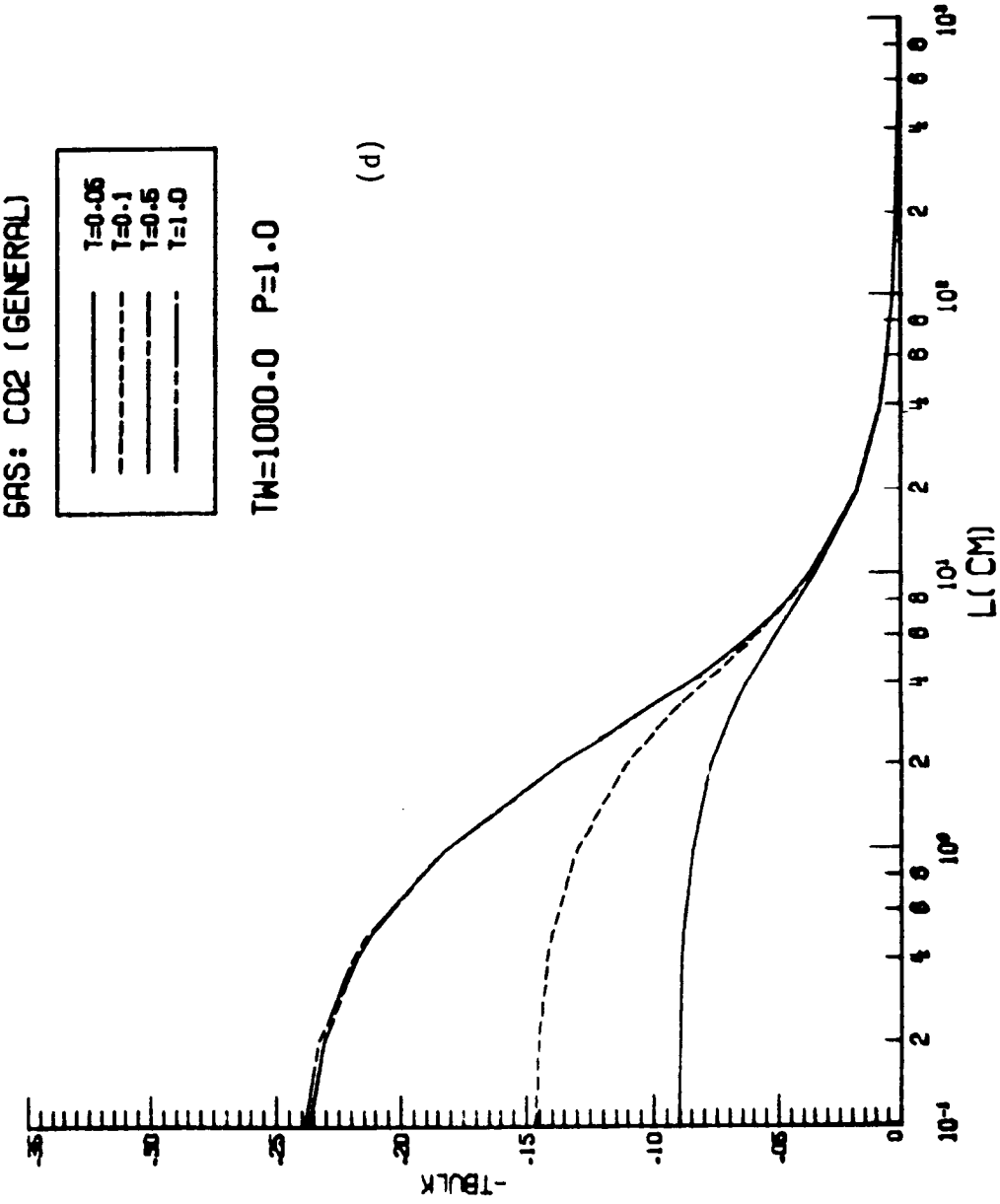

Figure B.11 (continued)

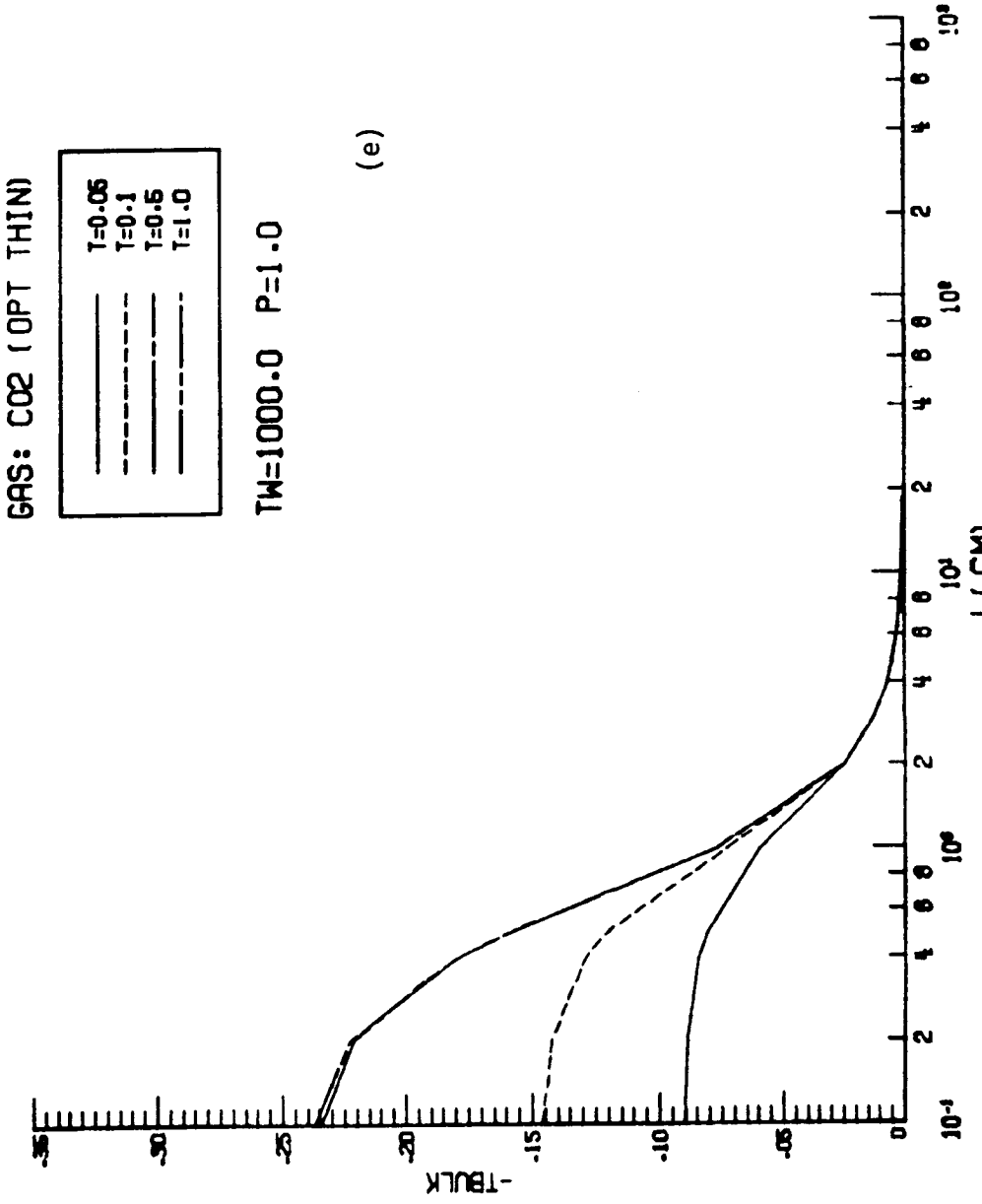

Figure B.11 (continued)

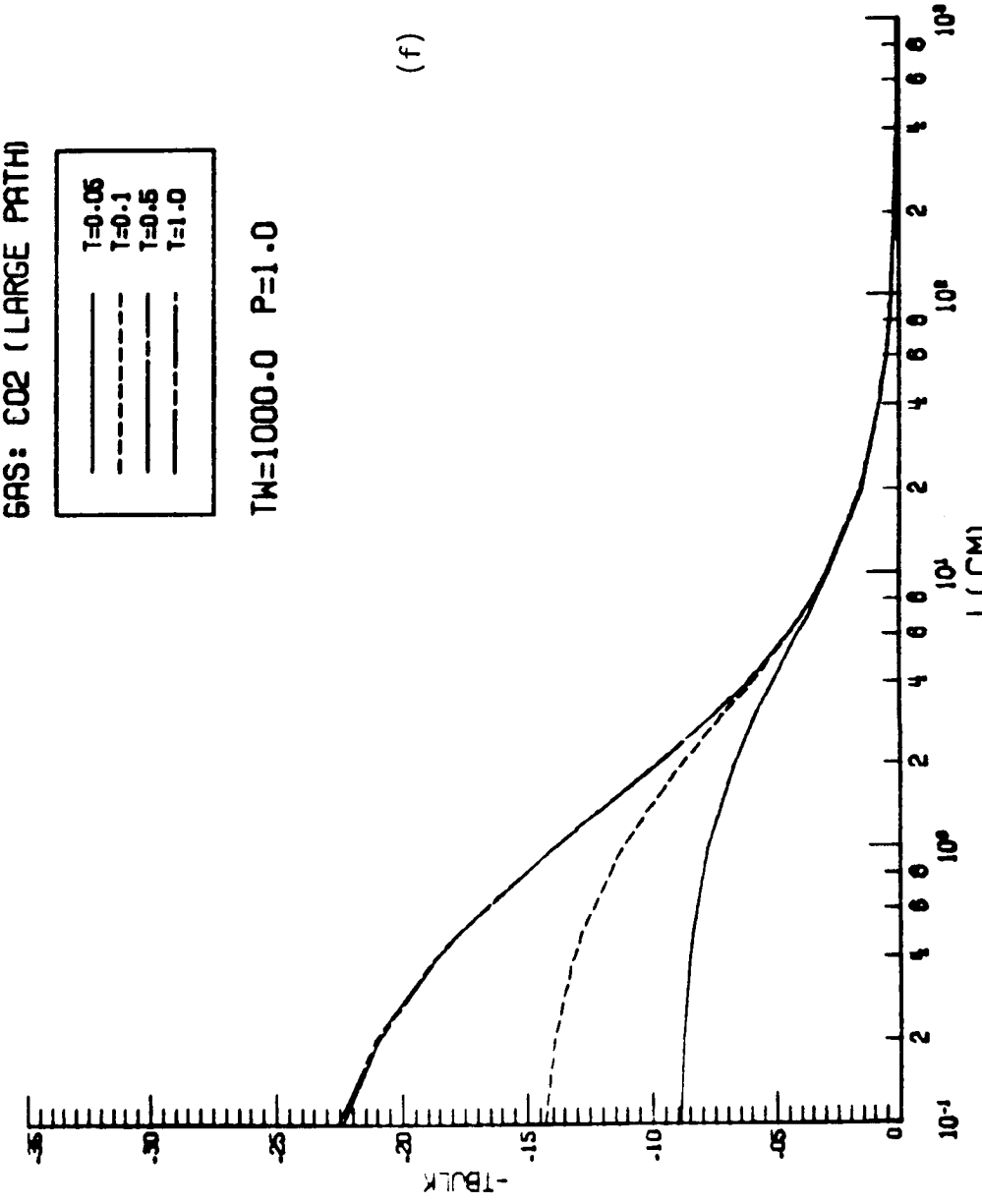

Figure B.11 (continued)

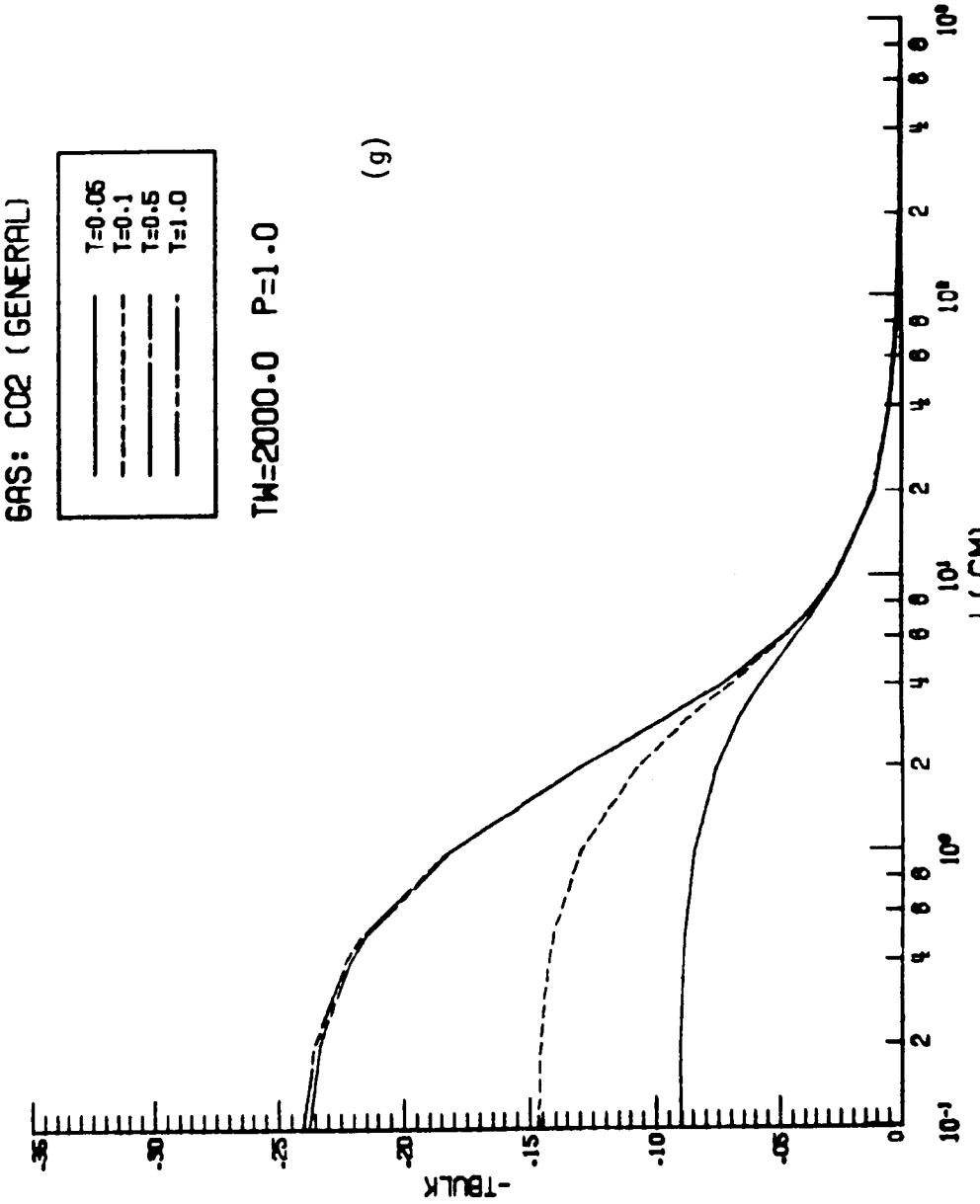

Figure B.11 (continued)

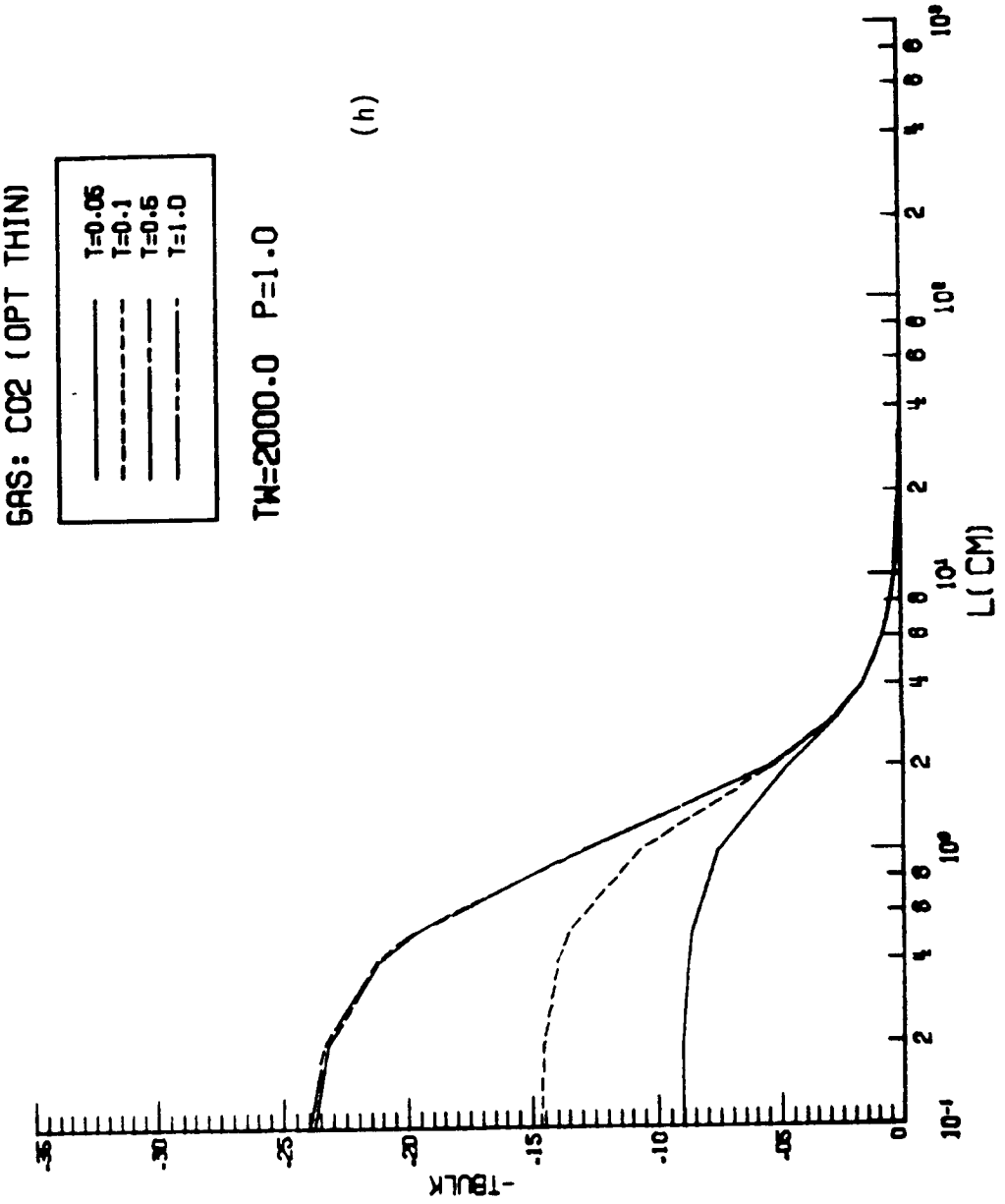

Figure B.11 (continued)

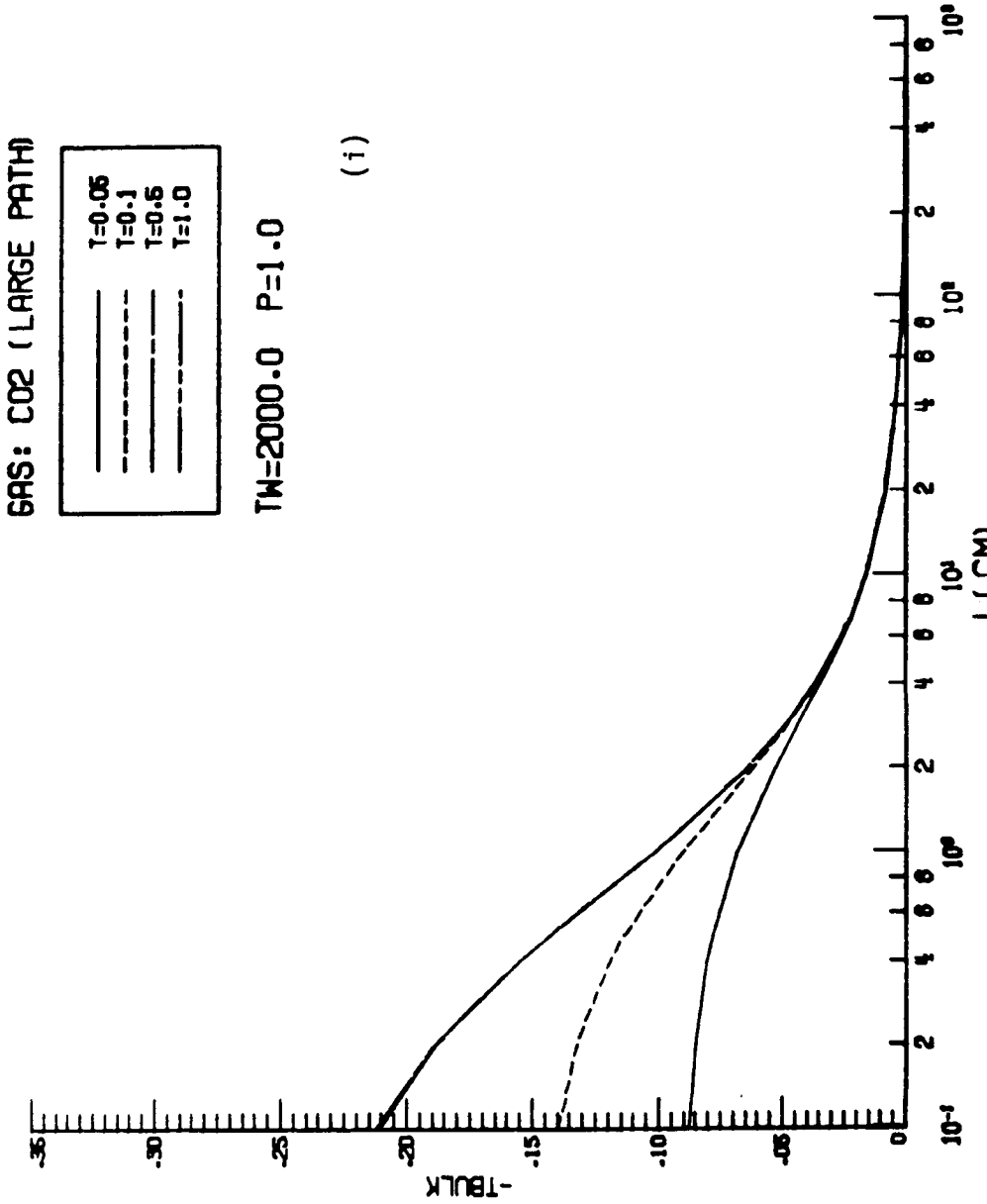

Figure B.11 (continued)

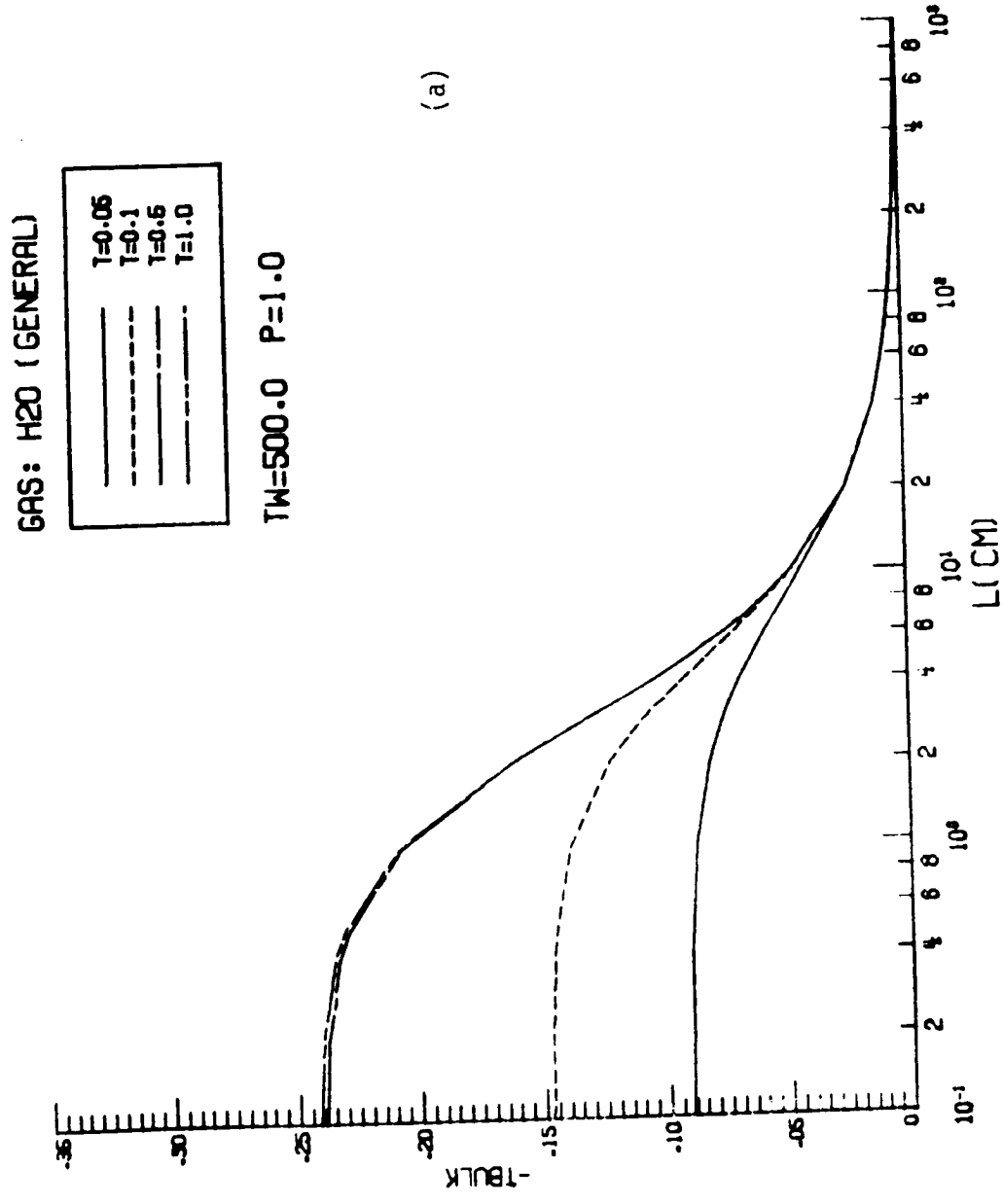

Figure B.12 Results for bulk temperature variation with plate spacing (θ_b vs. L) for H_2O.

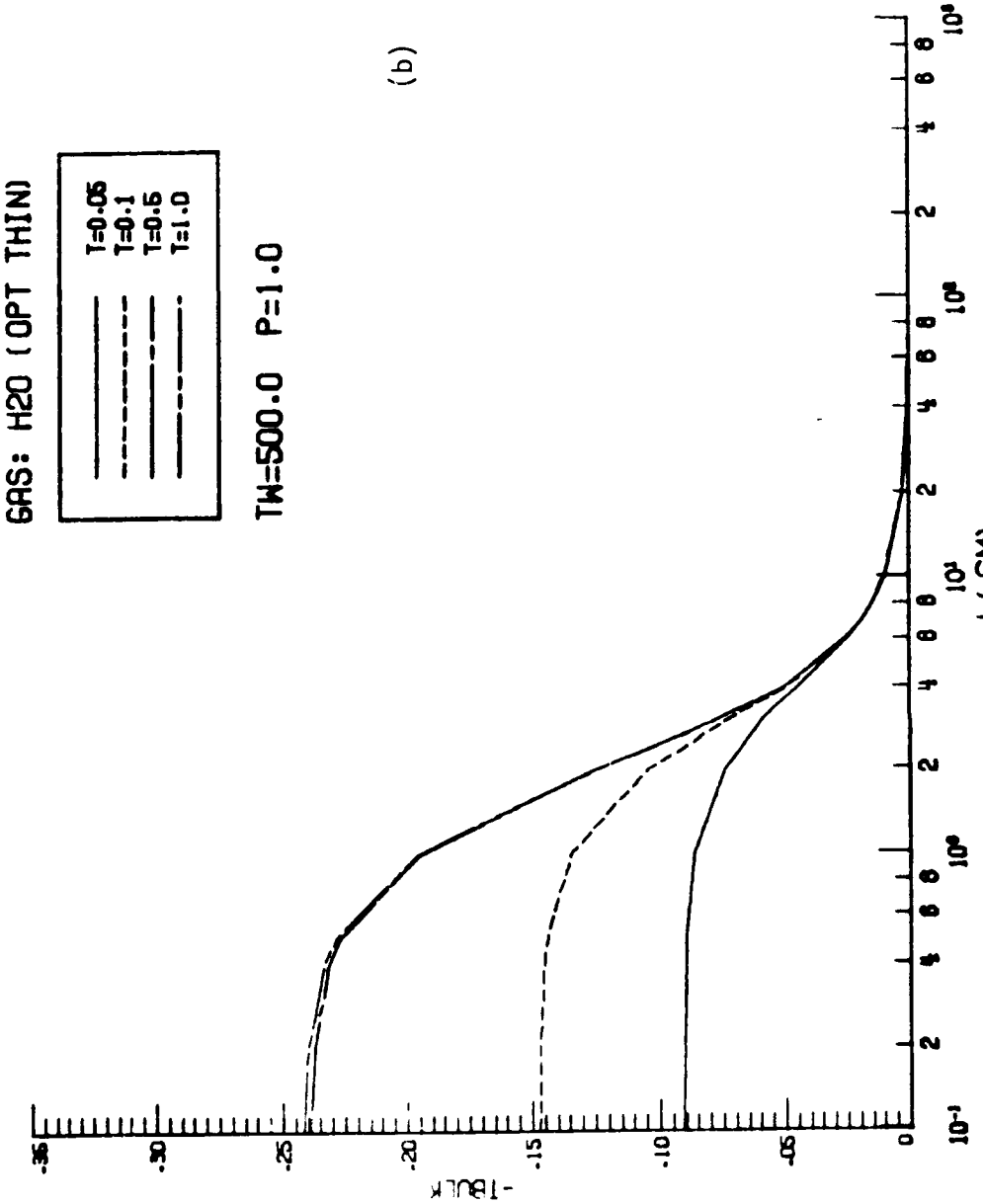

Figure B.12 (continued)

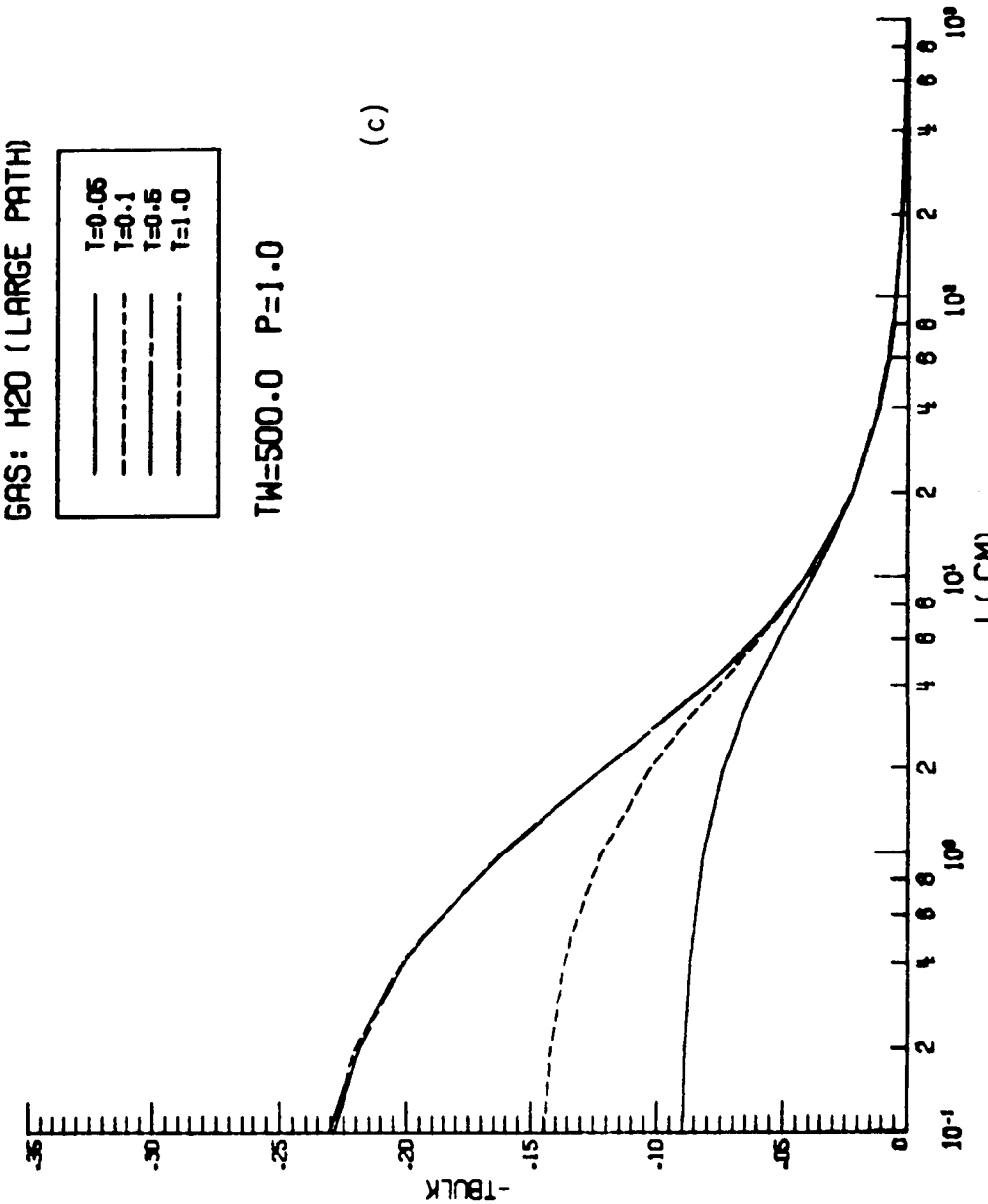

Figure B.12 (continued)

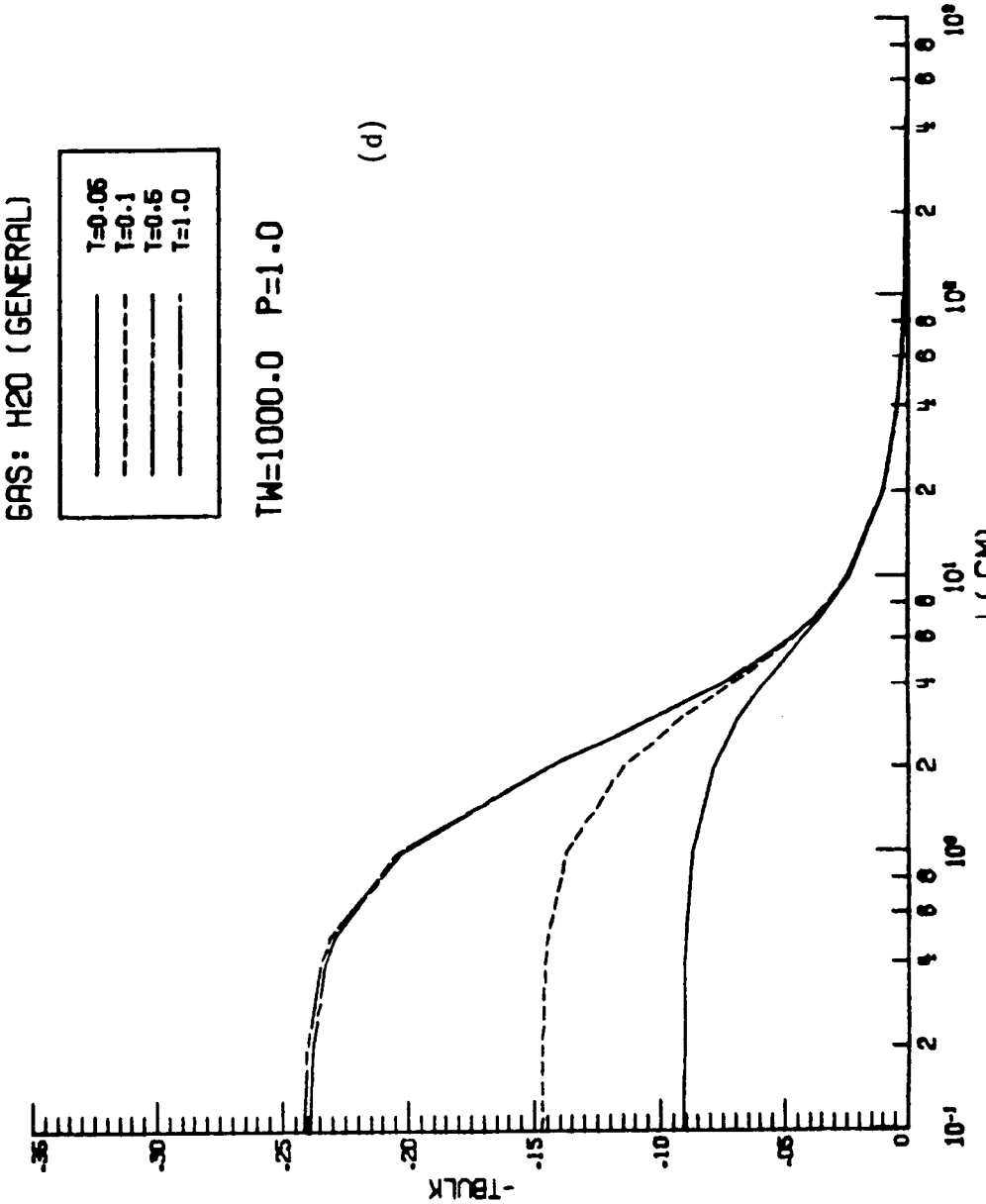

Figure B.12 (continued)

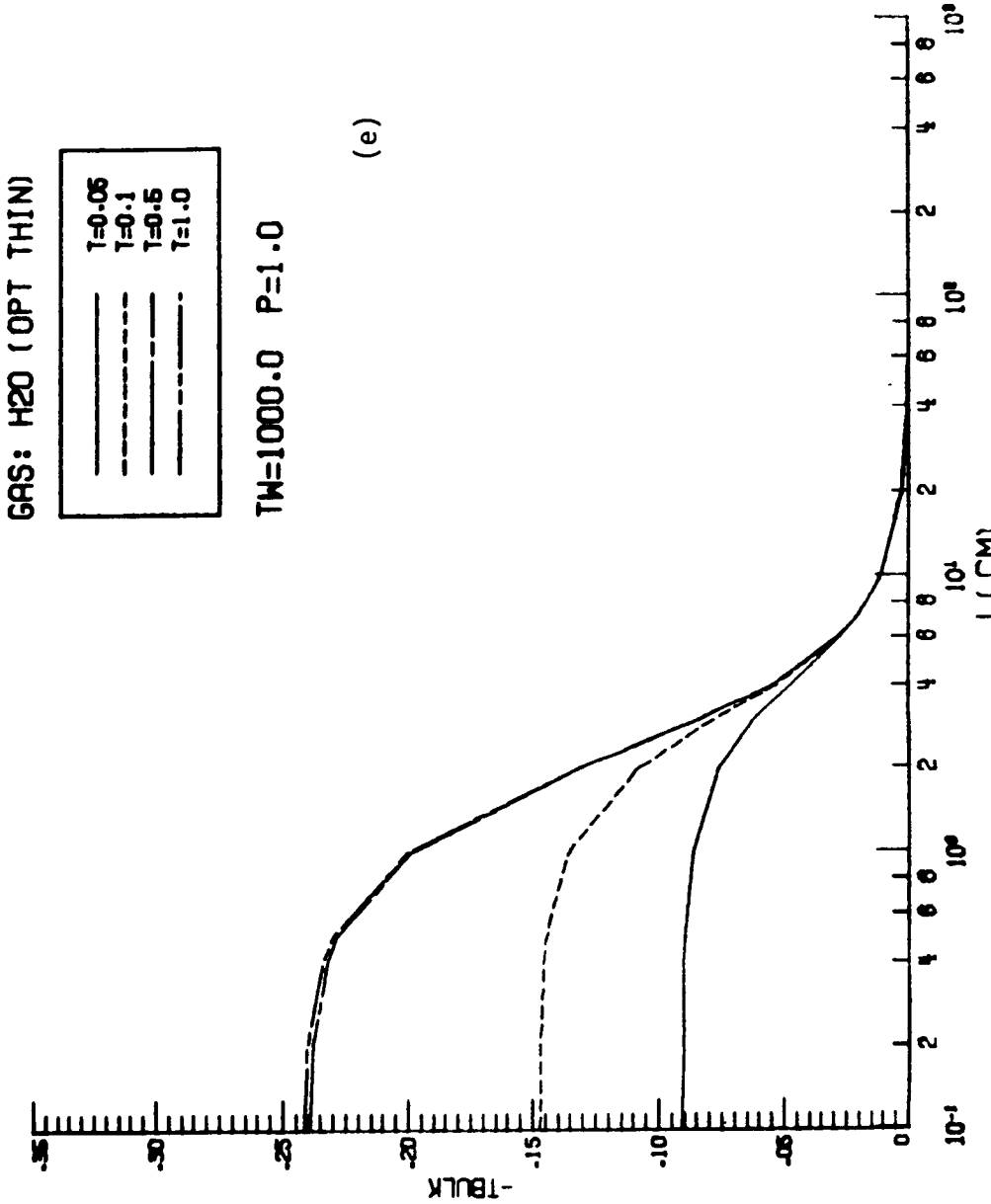

Figure B.12 (continued)

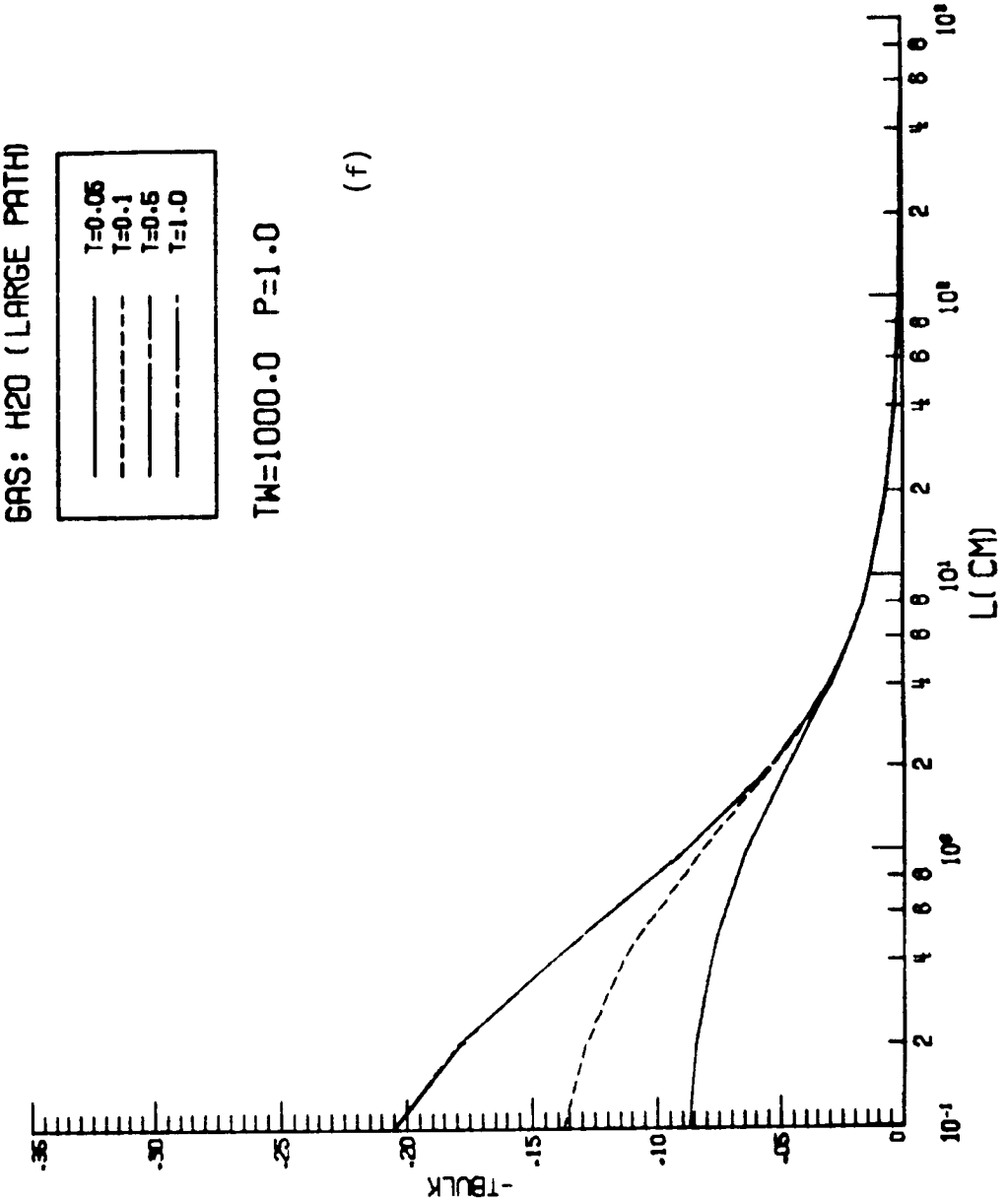

Figure B.12 (continued)

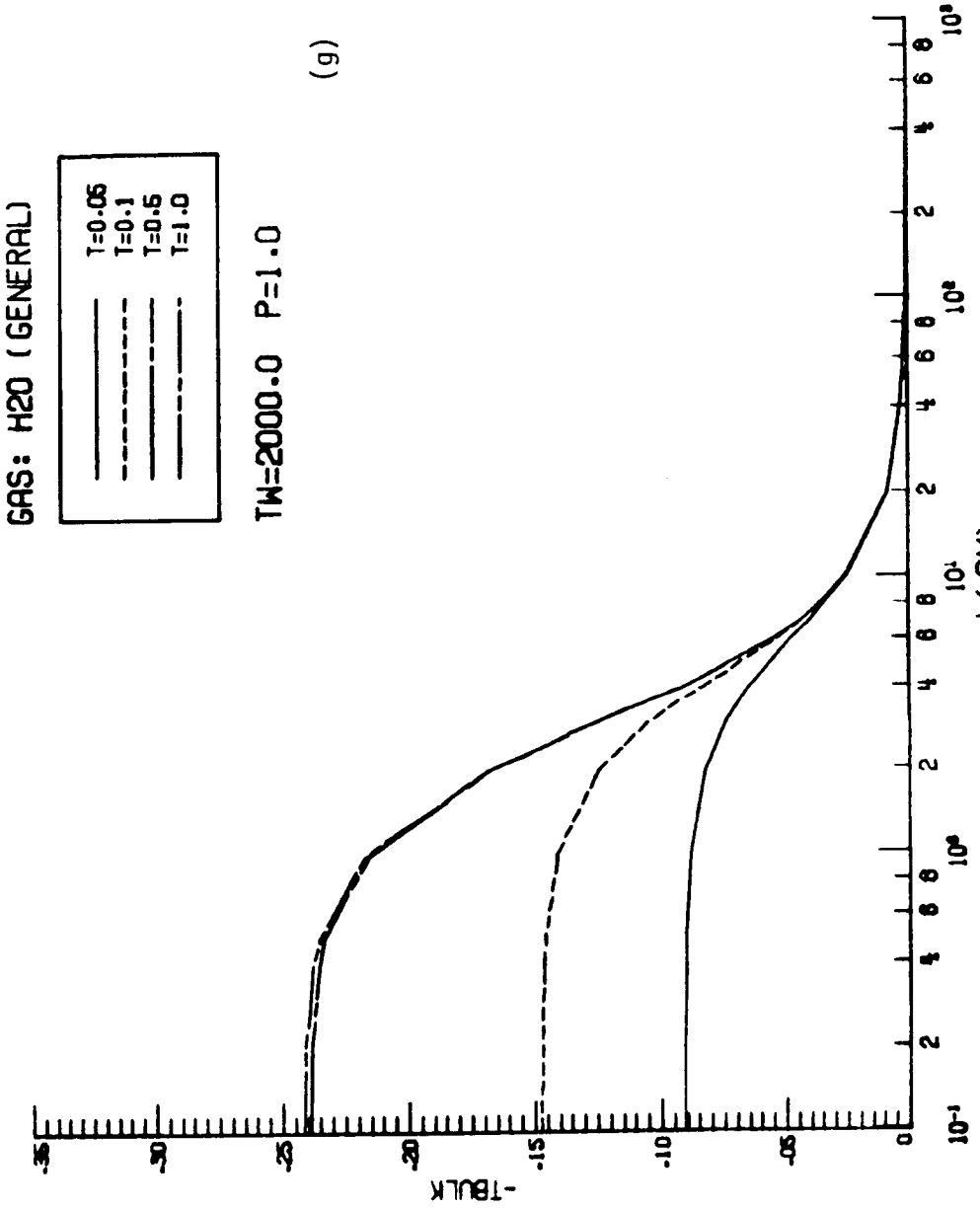

Figure B.12 (continued)

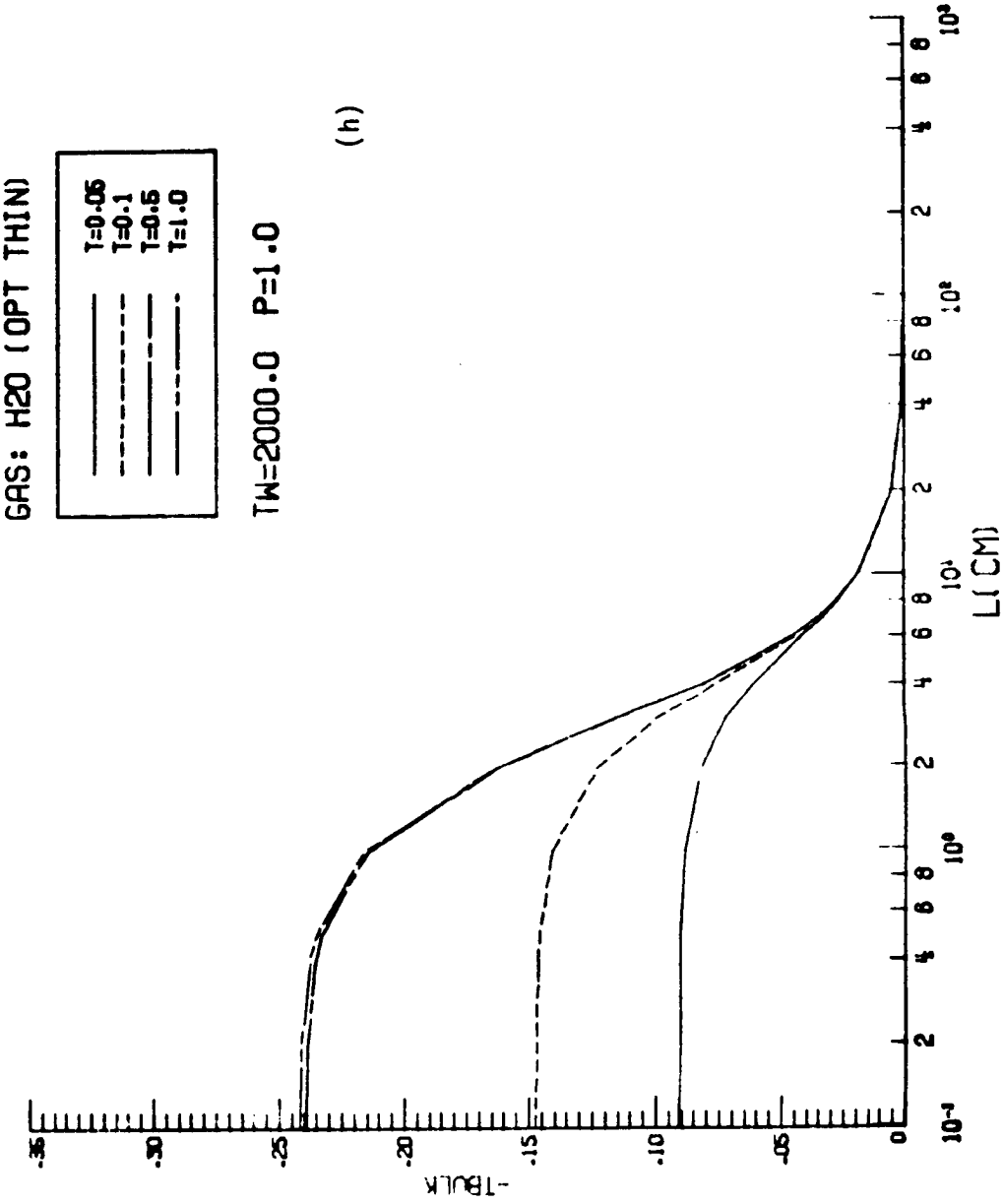

Figure B.12 (continued)

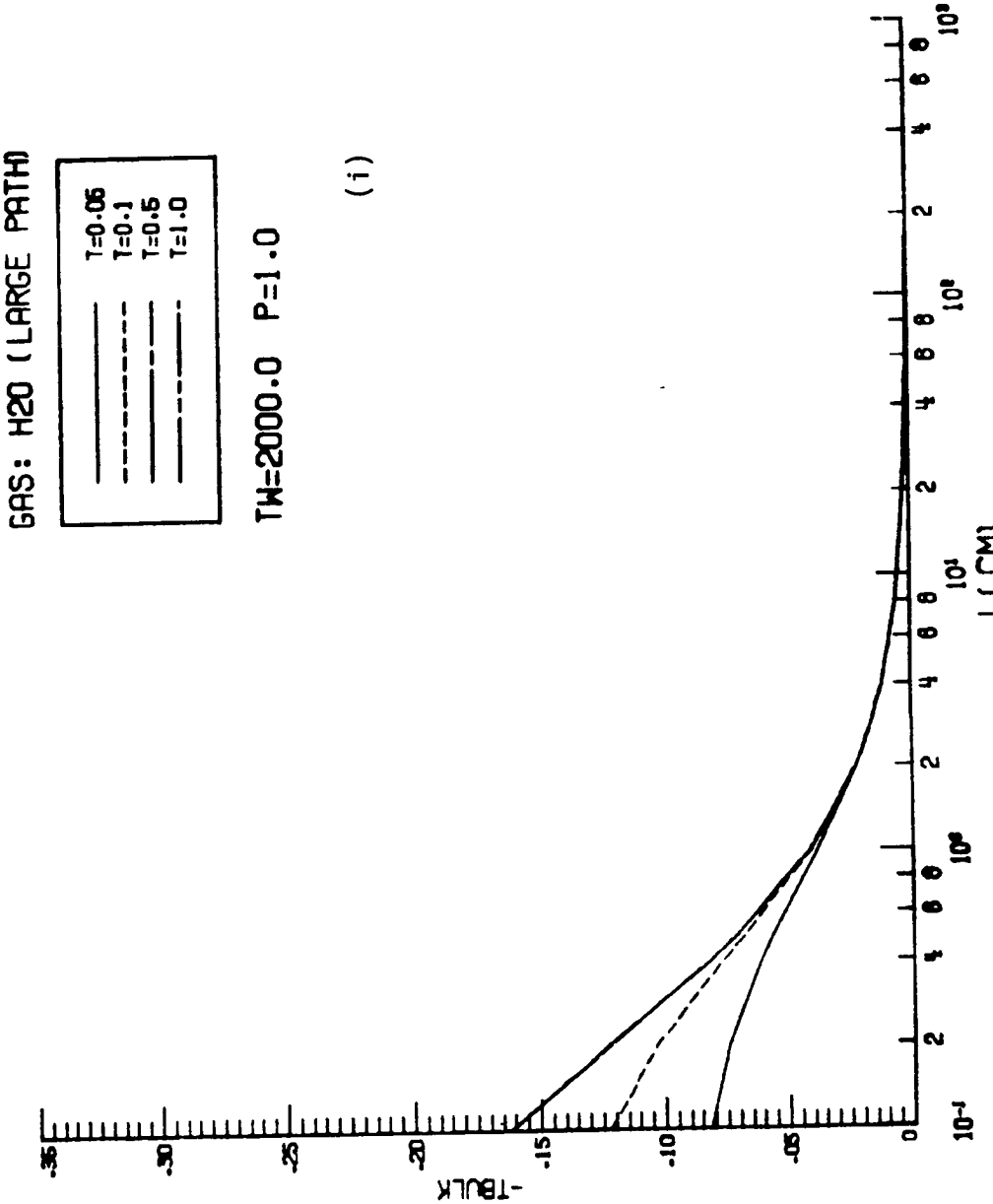

Figure B.12 (continued)

APPENDIX C

COMPUTER CODE FOR TRANSIENT ENERGY TRANSFER IN INCOMPRESSIBLE LAMINAR FLOWS

Following the numerical procedure discussed under the section "Method of Solution," a general computer program is developed to calculate the temperature variation and bulk temperature for a fully-developed laminar flow between two parallel plates having uniform wall heat flux. The program provides the general solution as well as the limiting (optically thin and large path length) solutions. The program is written for the three-band CO_2 gas, but can be used for any gas by employing appropriate thermophysical and radiative properties.

```
      PROGRAM TRAN(OUTPUT=65,TAPE6,TAPE11,TAPE15,TAPE10,TAPE1,TAPE2,
     &TAPE3)
C*********************************************************************
C
C     THIS PROGRAM CALCULATES THE TRANSIENT RADIATIVE
C     INTERACTION IN FULLY DEVELOPED LAMINAR FLOW OF
C     CO2 BETWEEN TWO PARALLEL BLACK WALLS WITH CONSTANT
C     HEAT FLUX.
C     IT IS BASED ON REPORT BY DR. S.N. TIWARI(REPORT NO 1-NAG 432)
C
C*********************************************************************
C
C
C     L  DISTANCE BETWEEN PLATES (IN CM)
C     TW  WALL TEMPRATURE ( K)
C     P  PRESSURE (ATM)
C     TT  TIME (NON DIMENSIONAL)
C     Z  NON DIMENSIONAL DISTANCE BETWEEN THE PLATES
C     Z = 0.0 AT LOWER WALL
C     Z = 1.0 AT UPPER WALL
C
      EXTERNAL F211,F212,F213,F221,F222,F223,F511,F512,F513,F611,F612,
     &F613,F521,F522,F523,F621,F622,F623
      REAL L,KFB
      DIMENSION U(60),EPS(3),PRES(10),TEMP(8),ZZ(60),TT(60),TB(65)
     &,TBO(65),TBL(65),DZZ(20)
      COMMON F1,F2,F3,B1,B2,B3,Z
      DATA U/0.1,0.2,0.4,0.5,1.0,2.,3.,4.,6.,7.,8.,10.,20.,40.,60.,80.
     &,100.,200.,500.,1000./
      DATA PRES/0.01,0.1,1.0,10.0/
      DATA TEMP/500.0,1000.0,2000.0,3000.0/
      DATA TT/0.05,0.1,0.5,1.0/
      DATA DZZ/0.2,0.3,0.4,.5,.6,.7,.8/
      WRITE(6,110)
      WRITE(10,120)
      WRITE(15,130)
      NP=20
      NT=4
C
C     TIME MARCHING
C
      DO 22 ITT=1,NT
      T=TT(ITT)
      IB=1
C     SET IB=0 FOR CALCULTING BULK TEMPRATURE,OTHERWISE IB=0
      IM=1
C     SET IM=1 FOR QUARTIC AND IM=2 FOR QUADRATIC
      IF(IB.EQ.1) GOTO 108
      WRITE(6,150)
      WRITE(10,150)
      WRITE(15,150)
      GOTO 109
108   WRITE(6,118)
      WRITE(10,118)
109   WRITE(15,118)
```

```
      WRITE(6,140)T
      WRITE(15,140) T
      WRITE(10,140) T
      DO 44 IT=1,3
      TW=TEMP(IT)
      DO 55 KK=3,3
      P=PRES(KK)
      DO 66 I=1,NP
      L=U(I)
C
      N11=7
      DZ=0.1
      DO 77 IZ=1,N11
      Z=DZZ(IZ)
C     CALCULATION OF PLANCK FUNCTION AND ITS DERIVATIVE
C
C     WNB BAND CENTER (1/CM)
C     HCK  CONSTANT (K CM)
C     CCC  C1*C2 (ERG-K-CM**3/SEC)
C     PFDBI PLANCK FUNCTION DERIVATIVE FOR I BAND
C
      CESS=TW**2
      STU=TW**0.5
      SNT=TW/273.0
      HCK=1.439257246
      CCC=0.000053847734
C
C     SPECTROSCOPIC PROPERTIES OF CO2
C     HERE WE HAVE CONSIDERED ONLY THREE BANDS(15,4.3 & 2.7 MICRONS)
C     WNBI  BAND CENTER (1/CM)
C
      WNB1=667.0
      WNB2=2347.0
      WNB3=3716.0
      C2B1=HCK*WNB1
      C2B2=HCK*WNB2
      C2B3=HCK*WNB3
      CCC=0.000053847734
      CCB1=CCC*(WNB1**4)
      CCB2=CCC*(WNB2**4)
      CCB3=CCC*(WNB3**4)
      TB1=C2B1/TW
      TB2=C2B2/TW
      TB3=C2B3/TW
      TEB1=EXP(TB1)
      TEB2=EXP(TB2)
      TEB3=EXP(TB3)
      SNTB1=CESS*((TEB1-1.0)**2.0)
      SNTB2=CESS*((TEB2-1.0)**2.0)
      SNTB3=CESS*((TEB3-1.0)**2.0)
      PFDB1=(CCB1*TEB1)/SNTB1
      PFDB2=(CCB2*TEB2)/SNTB2
      PFDB3=(CCB3*TEB3)/SNTB3
C
C     BAND MODEL CORRELATIONS (TIEN & LOWDER WIDE BAND MODEL)
```

```
C     AZI   AOI (1/CM)
C     CZSI   COI**2 (1/(ATM-CM))
C     BSI   B**2 (NON DIMENSIONAL)
C     OMGI  WAVE NUMBER(1/CM)
C     SI  INTEGRATED BAND INTENSITY (1/(ATM CM**2))
C
      AK1=(TW/300.0)**0.5
      AK2=(300.0/TW)**1.5
      AZ1=1.29*STU
      AZ2=1.15*STU
      AZ3=2.4*STU
C
C     KFB THERMAL CONDUCTIVITY (ERG/CM-SEC-K)
C
      KFB=(1488.365171)*(SNT**1.23)
      OMG1=1351.0
      OMG2=667.0
      OMG3=2396.0
      TX=-(HCK/TW)
      TX1=TX*OMG1
      TX2=TX*OMG2
      TX3=TX*OMG3
      ETX1=EXP(TX1)
      ETX2=EXP(TX2)
      ETX3=EXP(TX3)
      C1=1.0-ETX1
      C2=1.0-ETX2
      C3=1.0-ETX3
      BRKT=TX*(OMG1+OMG3)
      PHI2=(1.0-EXP(BRKT))/(C1*C3)
      TS=300.0/TW
      S1=339.685*TS
      S2=2702.7*TS
      S3=71.497*TS*PHI2
      CZS1=S1/AZ1
      CZS2=S2/AZ2
      CZS3=S3/AZ3
C
C     PL  PRESSURE PATH LENGTH (ATM-CM)
C
      PL=P*L
      UZ1=CZS1*PL
      UZ2=CZS2*PL
      UZ3=CZS3*PL
      BS1=0.0841*AK1
      BS2=0.32895*AK1
      PHI3=1.0+0.053*((TW/100.0)**1.5)
      DEL2=(PHI3**2.0)/(PHI2*AK1)
      BS3=0.1112*DEL2
C
C     PEI EFFECTIVE PRESSURE FOR EACH BAND (NON DIMENSIONAL)
C
      PE1=(1.3*P)**0.7
      PE2=(1.3*P)**0.8
      PE3=(1.3*P)**0.65
```

```
C
C     BETAI LINE STRUCTURE PARAMETER
C
      BETA1=BS1*PE1
      BETA2=BS2*PE2
      BETA3=BS3*PE3
C
C     CORRELATION FOR EACH BAND
C
      F1=2.94*(1.0-EXP(-(2.60*BETA1)))
      F2=2.94*(1.0-EXP(-(2.60*BETA2)))
      F3=2.94*(1.0-EXP(-(2.60*BETA3)))
      B1=1.5*UZ1
      B2=1.5*UZ2
      B3=1.5*UZ3
      H1=AZ1*PFDB1
      H2=AZ2*PFDB2
      H3=AZ3*PFDB3
      Z2=Z*Z
      CZ=1./(Z-Z2)
C
C     NUMERICAL INTEGRATION
C     FOR DETAILS OF INTEGRATION REFER MATHEMATICAL LIBRARY
C     AT NASA LANGLEY (DOCUMENT N-3)
C
      EPS(1)=1E-12
      EPS(2)=1E-12
      X=0.0
      IF(IM.EQ.1)  GOTO 678
      CALL CADRE(X,Z,F211,EPS,ITEXT,G211,IERR)
      CALL CADRE(X,Z,F212,EPS,ITEXT,G212,IERR)
      CALL CADRE(X,Z,F213,EPS,ITEXT,G213,IERR)
      CALL CADRE(Z,1.,F221,EPS,ITEXT,G221,IERR)
      CALL CADRE(Z,1.,F222,EPS,ITEXT,G222,IERR)
      CALL CADRE(Z,1.,F223,EPS,ITEXT,G223,IERR)
      SUM21=(G211-G221)
      SUM22=(G212-G222)
      SUM23=(G213-G223)
      BR1=H1*UZ1*SUM21
      BR2=H2*UZ2*SUM22
      BR3=H3*UZ3*SUM23
      BR=BR1+BR2+BR3
      AJ2=CZ*(2+1.5*L/KFB*BR )
      GT2=12*(EXP(-AJ2*T)-1)/AJ2
      THETA=GT2*(Z-Z2)
      GOTO 679
678   CONTINUE
      CALL CADRE(X,Z,F511,EPS,ITEXT,G511,IERR)
      CALL CADRE(X,Z,F512,EPS,ITEXT,G512,IERR)
      CALL CADRE(X,Z,F513,EPS,ITEXT,G513,IERR)
      CALL CADRE(Z,1.,F521,EPS,ITEXT,G521,IERR)
      CALL CADRE(Z,1.,F522,EPS,ITEXT,G522,IERR)
      CALL CADRE(Z,1.,F523,EPS,ITEXT,G523,IERR)
      CALL CADRE(X,Z,F611,EPS,ITEXT,G611,IERR)
      CALL CADRE(X,Z,F612,EPS,ITEXT,G612,IERR)
```

```
      CALL CADRE(X,Z,F613,EPS,ITEXT,G613,IERR)
      CALL CADRE(Z,1.,F621,EPS,ITEXT,G621,IERR)
      CALL CADRE(Z,1.,F622,EPS,ITEXT,G622,IERR)
      CALL CADRE(Z,1.,F623,EPS,ITEXT,G623,IERR)
      SUM51=G511-G521
      SUM52=G512-G522
      SUM53=G513-G523
      SUM61=G611-G621
      SUM62=G612-G622
      SUM63=G613-G623
      BR51=H1*UZ1*SUM51
      BR52=H2*UZ2*SUM52
      BR53=H3*UZ3*SUM53
      BR61=H1*UZ1*SUM61
      BR62=H2*UZ2*SUM62
      BR63=H3*UZ3*SUM63
      XZ=Z-2*Z**3.+Z**4.
      YZ=Z**2-Z
      ZZ=12*(Z-Z**2)
      AJ5=ZZ+1.5*L/KFB*(BR51+BR52+BR53)
      AJ6=-2.+1.5*L/KFB*(BR61+BR62+BR63)
      DAL=AJ5*T/XZ
      DAL1=AJ6*T/YZ
      DS=EXP(-DAL)
      DS1=EXP(-DAL1)
      GT=ZZ/(2.*AJ5)*(DS-1)
      HT=ZZ/(2.*AJ6)*(DS1-1)
      THETA=GT*XZ+HT*YZ
679   TB(IZ)=THETA*(Z-Z2)
      IF(IB.EQ.1) GOTO 207
      WRITE(6,160) TW,P,L,THETA,Z
207   CONTINUE
C
C     LARGE PATH LENGTH
C
      IF(IM.EQ.1) GOTO 801
      DS=ABS(Z/(Z-1))
      AJ=ALOG(DS)+ALOG(-2/Z+1/Z**2+1)*Z+2
      H=H1+H2+H3
      AJL=CZ*(2+H*L*AJ/KFB)
      GL=12*(EXP(-AJL*T)-1)/AJL
      THEL=GL*(Z-Z2)
      GOTO 802
801   CONTINUE
      Z1=Z-1
      AL1=Z1**3./3.-3.*Z*Z1**2./2.+3.*Z*Z*Z1-Z**3.*ALOG(1-Z)-Z**3.
     &*(11./6.-ALOG(Z))
      AL2=-(Z1**2./2.-2.*Z*Z1+Z**2*ALOG(1-Z)+Z*Z*(1.5-ALOG(Z)))
      AL3=-(ALOG(1-Z)-ALOG(Z))
      AL=4.*AL1-6.*AL2+AL3
      AJ5=ZZ+L/KFB*AL*(H1+H2+H3)
      ALL1=-1.-Z*ALOG(1.-Z)+Z*ALOG(Z)
      ALL2=AL3
      ALL=2.*ALL1-ALL2
      AJ6=-2+L/KFB*ALL*(H1+H2+H3)
```

```
      DAL=AJ5*T/XZ
      DAL1=AJ6*T/YZ
      DS=EXP(-DAL)
      DS1=EXP(-DAL1)
      GT=ZZ/(2.*AJ5)*(DS-1)
      HT=ZZ/(2.*AJ6)*(DS1-1)
      THEL=GT*XZ+HT*YZ
802   TBL(IZ)=THEL*(Z-Z2)
      IF(IB.EQ.1) GOTO 208
      WRITE(10,160) TW,P,L,THEL,Z
208   CONTINUE
C
C     OPTICALLY THIN
C
      IF(IM.EQ.1) GOTO 701
      AN1=H1*UZ1
      AN2=H2*UZ2
      AN3=H3*UZ3
      AN=L/KFB*(AN1+AN2+AN3)
      AJO=2*CZ+3*AN
      GO=12*(EXP(-AJO*T)-1)/AJO
      THEO=GO*(Z-Z2)
      GOTO 702
701   CONTINUE
      AN1=P*L*L/KFB*(S1*PFDB1+S2*PFDB2+S3+PFDB3)
      EE=Z**4-2*Z**3+Z
      FF=Z**2-Z
      AJ5=ZZ+3.*AN1*EE
      AJ6=-2.+3.*AN1*FF
      DAL=AJ5*T/XZ
      DAL1=AJ6*T/YZ
      DS=EXP(-DAL)
      DS1=EXP(-DAL1)
      GT=ZZ/(2.*AJ5)*(DS-1)
      HT=ZZ/(2.*AJ6)*(DS1-1)
      THEO=GT*XZ+HT*YZ
702   TBO(IZ)=THEO*(Z-Z2)
      IF(IB.EQ.1) GOTO 209
      TBO(IZ)=THEO*(Z-Z2)
      IF(IB.EQ.1) GOTO 209
      WRITE(15,160) TW,P,L,THEO,Z
209   CONTINUE
77    CONTINUE
      IF(IB.EQ.0) GOTO 234
      TBUL=0.
      TBULL=0.
      TBULO=0.
      DO 10 JB=1,N11
      TBUL=TBUL+TB(JB)
      TBULL=TBULL+TBL(JB)
10    TBULO=TBULO+TBO(JB)
      BULK=6.*DZ*TBUL
      BULKL=6.*DZ*TBULL
      BULKO=6.*DZ*TBULO
      WRITE(6,160) TW,P,L,BULK
```

```
      WRITE(10,160) TW,P,L,BULKL
      WRITE(15,160) TW,P,L,BULKO
234   CONTINUE
66    CONTINUE
55    CONTINUE
44    CONTINUE
33    CONTINUE
22    CONTINUE
110   FORMAT(7X,*GENERAL SOLUTION FOR CO2 (CONSTANT FLUX CASE)*)
118   FORMAT(4X,*TW*,T18,*P*,T28,*L*,T38,*TBULK*)
120   FORMAT(7X,*LARGE PATH LENGTH FOR CO2 (CONSTANT FLUX CASE)*)
130   FORMAT(7X,*OPTICALLY THIN  FOR CO2 (CONSTANT FLUX CASE)*)
140   FORMAT(10X,*TIME=*,F8.3)
150   FORMAT(4X,*TW*,T18,*P*,T28,*L*,T38,*THETA*,T48,*Z*)
160   FORMAT(7(1X, F9.4))
      STOP
      END
      FUNCTION F211(ZB)
      COMMON F1,F2,F3,B1,B2,B3,Z
      XX=B1*(Z-ZB)
      DEN1=(F1*((XX**2.0)+(2.0*XX)+2.0)+XX)*(XX+2.0*F1)
      AUD1=(F1*((XX**2.0)+(4.0*XX*F1)+(4.0*F1)))/DEN1
      F211=(1-2*ZB)*AUD1
      RETURN
      END
      FUNCTION F212(ZB)
      COMMON F1,F2,F3,B1,B2,B3,Z
      XX=B2*(Z-ZB)
      DEN2=(F2*((XX**2.0)+(2.0*XX)+2.0)+XX)*(XX+2.0*F2)
      AUD2=(F2*((XX**2.0)+(4.0*XX*F2)+(4.0*F2)))/DEN2
      F212=(1-2*ZB)*AUD2
      RETURN
      END
      FUNCTION F213(ZB)
      COMMON F1,F2,F3,B1,B2,B3,Z
      XX=B3*(Z-ZB)
      DEN3=(F3*((XX**2.0)+(2.0*XX)+2.0)+XX)*(XX+2.0*F3)
      AUD3=(F3*((XX**2.0)+(4.0*XX*F3)+(4.0*F3)))/DEN3
      F213=(1-2*ZB)*AUD3
      RETURN
      END
      FUNCTION F221(ZB)
      COMMON F1,F2,F3,B1,B2,B3,Z
      XX=B1*(ZB-Z)
      DEN1=(F1*((XX**2.0)+(2.0*XX)+2.0)+XX)*(XX+2.0*F1)
      AUD1=(F1*((XX**2.0)+(4.0*XX*F1)+(4.0*F1)))/DEN1
      F221=(1-2*ZB)*AUD1
      RETURN
      END
      FUNCTION F222(ZB)
      COMMON F1,F2,F3,B1,B2,B3,Z
      XX=B2*(ZB-Z)
      DEN2=(F2*((XX**2.0)+(2.0*XX)+2.0)+XX)*(XX+2.0*F2)
      AUD2=(F2*((XX**2.0)+(4.0*XX*F2)+(4.0*F2)))/DEN2
      F222=(1-2*ZB)*AUD2
```

```
      RETURN
      END
      FUNCTION F223(ZB)
      COMMON F1,F2,F3,B1,B2,B3,Z
      XX=B3*(ZB-Z)
      DEN3=(F3*((XX**2.0)+(2.0*XX)+2.0)+XX)*(XX+2.0*F3)
      AUD3=(F3*((XX**2.0)+(4.0*XX*F3)+(4.0*F3)))/DEN3
      F223=(1-2*ZB)*AUD3
      RETURN
      END
      FUNCTION F511(ZB)
      COMMON F1,F2,F3,B1,B2,B3,Z
      XX=B1*(Z-ZB)
      DEN1=(F1*((XX**2.0)+(2.0*XX)+2.0)+XX)*(XX+2.0*F1)
      AUD1=(F1*((XX**2.0)+(4.0*XX*F1)+(4.0*F1)))/DEN1
      F511=(1-6*ZB*ZB+4*ZB**3)*AUD1
      RETURN
      END
      FUNCTION F512(ZB)
      COMMON F1,F2,F3,B1,B2,B3,Z
      XX=B2*(Z-ZB)
      DEN2=(F2*((XX**2.0)+(2.0*XX)+2.0)+XX)*(XX+2.0*F2)
      AUD2=(F2*((XX**2.0)+(4.0*XX*F2)+(4.0*F2)))/DEN2
      F512=(1-6*ZB*ZB+4*ZB**3)*AUD2
      RETURN
      END
      FUNCTION F513(ZB)
      COMMON F1,F2,F3,B1,B2,B3,Z
      XX=B3*(Z-ZB)
      DEN3=(F3*((XX**2.0)+(2.0*XX)+2.0)+XX)*(XX+2.0*F3)
      AUD3=(F3*((XX**2.0)+(4.0*XX*F3)+(4.0*F3)))/DEN3
      F513=(1-6*ZB*ZB+4*ZB**3)*AUD3
      RETURN
      END
      FUNCTION F521(ZB)
      COMMON F1,F2,F3,B1,B2,B3,Z
      XX=B1*(ZB-Z)
      DEN1=(F1*((XX**2.0)+(2.0*XX)+2.0)+XX)*(XX+2.0*F1)
      AUD1=(F1*((XX**2.0)+(4.0*XX*F1)+(4.0*F1)))/DEN1
      F521=(1-6*ZB*ZB+4*ZB**3)*AUD1
      RETURN
      END
      FUNCTION F522(ZB)
      COMMON F1,F2,F3,B1,B2,B3,Z
      XX=B2*(ZB-Z)
      DEN2=(F2*((XX**2.0)+(2.0*XX)+2.0)+XX)*(XX+2.0*F2)
      AUD2=(F2*((XX**2.0)+(4.0*XX*F2)+(4.0*F2)))/DEN2
      F522=(1-6*ZB*ZB+4*ZB**3)*AUD2
      RETURN
      END
      FUNCTION F523(ZB)
      COMMON F1,F2,F3,B1,B2,B3,Z
      XX=B3*(ZB-Z)
      DEN3=(F3*((XX**2.0)+(2.0*XX)+2.0)+XX)*(XX+2.0*F3)
      AUD3=(F3*((XX**2.0)+(4.0*XX*F3)+(4.0*F3)))/DEN3
```

```
F523=(1-6*ZB*ZB+4*ZB**3)*AUD3
RETURN
END
FUNCTION F611(ZB)
COMMON F1,F2,F3,B1,B2,B3,Z
XX=B1*(Z-ZB)
DEN1=(F1*((XX**2.0)+(2.0*XX)+2.0)+XX)*(XX+2.0*F1)
AUD1=(F1*((XX**2.0)+(4.0*XX*F1)+(4.0*F1)))/DEN1
F611=(2*ZB-1)*AUD1
RETURN
END
FUNCTION F612(ZB)
COMMON F1,F2,F3,B1,B2,B3,Z
XX=B2*(Z-ZB)
DEN2=(F2*((XX**2.0)+(2.0*XX)+2.0)+XX)*(XX+2.0*F2)
AUD2=(F2*((XX**2.0)+(4.0*XX*F2)+(4.0*F2)))/DEN2
F612=(2*ZB-1)*AUD2
RETURN
END
FUNCTION F613(ZB)
COMMON F1,F2,F3,B1,B2,B3,Z
XX=B3*(Z-ZB)
DEN3=(F3*((XX**2.0)+(2.0*XX)+2.0)+XX)*(XX+2.0*F3)
AUD3=(F3*((XX**2.0)+(4.0*XX*F3)+(4.0*F3)))/DEN3
F613=(2*ZB-1)*AUD3
RETURN
END
FUNCTION F621(ZB)
COMMON F1,F2,F3,B1,B2,B3,Z
XX=B1*(ZB-Z)
DEN1=(F1*((XX**2.0)+(2.0*XX)+2.0)+XX)*(XX+2.0*F1)
AUD1=(F1*((XX**2.0)+(4.0*XX*F1)+(4.0*F1)))/DEN1
F621=(2*ZB-1)*AUD1
RETURN
END
FUNCTION F622(ZB)
COMMON F1,F2,F3,B1,B2,B3,Z
XX=B2*(ZB-Z)
DEN2=(F2*((XX**2.0)+(2.0*XX)+2.0)+XX)*(XX+2.0*F2)
AUD2=(F2*((XX**2.0)+(4.0*XX*F2)+(4.0*F2)))/DEN2
F622=(2*ZB-1)*AUD2
RETURN
END
FUNCTION F623(ZB)
COMMON F1,F2,F3,B1,B2,B3,Z
XX=B3*(ZB-Z)
DEN3=(F3*((XX**2.0)+(2.0*XX)+2.0)+XX)*(XX+2.0*F3)
AUD3=(F3*((XX**2.0)+(4.0*XX*F3)+(4.0*F3)))/DEN3
F623=(2*ZB-1)*AUD3
RETURN
END
```